DE GRUYTER

Kirsten Heimann,
Christos Katsaros (Eds.)

ADVANCES IN ALGAL CELL BIOLOGY

MARINE AND FRESHWATER BOTANY

DE G

Also of Interest

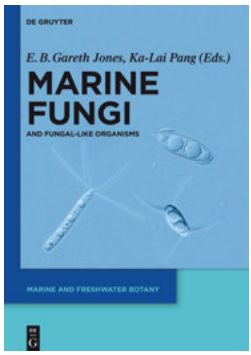

Marine Fungi and Fungal-like Organisms
Edited by E. B. Gareth Jones and Ka-Lai Pang, 2012
ISBN 978-3-11-026406-7
e-ISBN 978-3-11-026398-5

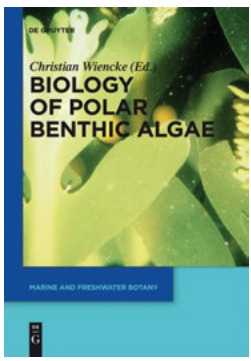

Biology of Polar Benthic Algae
Edited by Christian Wiencke, 2011
ISBN 978-3-11-022970-7
e-ISBN 978-3-11-022971-4

Botanica Marina
Editor-in-Chief: Anthony R. O. Chapman
ISSN 1437-4323
e-ISSN 1437-4323

Advances in Algal Cell Biology

Edited by Kirsten Heimann
and Christos Katsaros

DE GRUYTER

Editors
Prof. Dr. Kirsten Heimann
Director of NQAIF
School of Marine and Tropical Biology
James Cook University
Douglas Campus
Townsville QLD 4811
Australia
E-mail: kirsten.heimann@jcu.edu.au

Prof. Christos Katsaros
University of Athens
Faculty of Biology
Department of Botany
Panepistimiopolis
157 84 Athens
Greece
E-mail: christos.katsaros@biol.uoa.gr

ISBN 978-3-11-022960-8
e-ISBN 978-3-11-022961-5

Library of Congress Cataloging-in-Publication Data
A CIP catalog record for this book has been applied for at the Library of Congress.

Bibliographic information published by the Deutsche Nationalbibliothek
The Deutsche Nationalbibliothek lists this publication in the Deutsche Nationalbibliografie; detailed bibliographic data are available in the Internet at http://dnb.dnb.de.

Typesetting: Compuscript Ltd., Shannon, Ireland
Printing: Hubert & Co. GmbH & Co. KG, Göttingen

♾ Printed on acid-free paper
Printed in Germany
www.degruyter.com

Preface

Almost every algal textbook starts by underlining the fundamental importance of algae. It is true that they are key primary producers in marine and freshwater environments and represent a relatively untapped resource for food, bioenergy and biopharmaceuticals. Knowledge of algal cell biology is indeed the successful recipe for the current boom of biotechnological applications of micro- and macroalgae. Apart from these indisputable features, algae have attracted the interest of researchers since the first studies in the plant kingdom.

Algal research passed from different stages, reflecting not only the interest of the scientists, but also the dynamics and the facilities available in each of these time periods. External morphology was completed by (light and electron) microscopy, chemistry by biochemistry and finally molecular biology. The tremendous progress of biological research during the last decades of the 20th century, which has made biology the most important science of the 21st century, has been extended to algal research by giving the tools for specialized studies which provided deep insights into algal structural and functional organization. In this way, the application of modern techniques and sophisticated tools contributed drastically not only to the study of algal cell metabolism but also to algal evolution, the latter, in turn, contributing to species evolution in general.

These approaches were used not only to study the physiological mechanisms functioning during the life cycles of algae, but also to clarify the taxonomic and phylogenetic relationships between them.

However, despite the vast of information revealed from these studies and published in many scientific journals, there is a considerable lack of a book dealing with the structure and molecular biology of algae.

The publication of this book was the physical continuation of the publication of the Botanica Marina special issue entitled “Advances in algal cell biology and genomics”. The high quality of the articles included in this issue, revealed the tremendous progress in the field of the biology of algal cells.

Having the above accumulated information in hands and considering the necessity of a book in which scientists (students, phycologists, etc.) would find answers to questions and/or triggers for further research, we proceeded to this publication.

Apoptosis or programmed cell death is a fundamental mechanism for the development and repair of tissues. Indeed the process of apoptosis has even been realised in cyanobacteria where if functions in bloom control. Given the importance of programmed cell death, this book starts out with a review on programmed cell death in multicellular algae. This chapter investigates the implication of programmed cell death for algal development, such as spore germination, hair development, the development of reticulate thallus structures, cell surface cleaning mechanisms, reactions to parasites, senescence and abscission. These developmental patterns are compared to analogous processes in terrestrial plants. It can be concluded that programmed cell death is yet another unifying concept in biology.

Algal biodiversity is extremely high compared to other groups of organisms. Hence the second chapter reviews the mechanism by which this diversity was generated.

Current knowledge of endosymbiosis giving rise to the highly diverse plastids in the algae is placed into context with gene transfer and algal evolution.

The third chapter pays tribute to the unusual pennate diatom, *Phaeodactylum tricorunutum*. It summarises knowledge regarding factors and mechanisms involved in the polymorphism of this organism. It also investigates possible drivers for the conversion of one morphotype into the other and mechanisms that make such tremendous morphological changes possible.

The fourth chapter reviews cytological and cytochemical aspects of carrageenophytes, a group of red algae that are growing steadily in commercial applications.

The fifth chapter presents the findings of a desktop study using a molecular approach to unravel algal protein trafficking, specifically vacuolar protein sorting and provide strong evidence that such investigations can assist in the assembly of a holistic picture of protist evolution.

The sixth chapter presents data on the function of contractile vacuoles in green algae and places these into context with protists used as models for studies on contractile vacuole function and mechanisms, such as ciliates, slime moulds and the parasitic trypanosomes.

Chapter seven reviews advances in our understanding of the mechanisms and structures required for cytokinesis in brown algae. Particular focus has been given to the role of the cytoskeleton in cell wall morphogenesis, the deposition of wall materials, the role of the centrosome in the determination of the division site, and the formation of plasmodesmata, The techniques used in these studies include not only conventional microscopy, but also immunofluorescence and TEM as well as cryofixation – freeze-substitution and electron tomography.

Chapter eight provides new insight in the function of the cytoskeleton for sperm release in *Chara*. This study uses cytoskeletal drugs to modulate cytoskeletal function and demonstrates, using scanning laser confocal immunofluorescence microscopy, that sperm release in *Chara* is a highly dynamic process.

Chapter nine presents findings on the involvement of the cytoskeleton for the regulation of an important marine phenomenon – bioluminescence. Using cytoskeleton modulating drugs, evidence is presented that the cytoskeleton is involved in the reciprocal movement of chloroplasts and bioluminescent organelles at the transition of photoperiods in the marine dinoflagellate, *Pyrocystis lunula*.

Lastly, chapter 10 explores how the bioluminescent system of *Pyrocystis lunula* and specific signal modulators can be used to unravel potential signal transduction cascades required for eliciting the touch-induced bioluminescent response. It also provides insights into potential mechanisms involved in the reduction of bioluminescence when exposed to heavy metals and explores the use of the herbicide oxyfluorfen, which inhibits chlorophyll biosynthesis, for determining the biosynthetic origin of the bioluminescent substrate luciferin.

Kirsten Heimann
Christos Katsaros

List of contributing authors

John Archibald
Department of Biochemistry &
Molecular Biology
Dalhousie University
Halifax, Canada
e-mail: JMARCHIB@dal.ca
Chapter 2

Burkhard Becker
Biozentrum Köln, Botanik
Universität zu Köln
Köln, Germany
e-mail: b.becker@uni-koeln.de
Chapter 5, 6

Karin Komsic-Buchmann
Biozentrum Köln, Botanik
Universität zu Köln
Köln, Germany
e-mail: karin.buchmann@uni-koeln.de
Chapter 6

Moira E. Galway
Department of Biology
St. Francis Xavier University
Antigonish, Canada
e-mail: mgalway@stfx.ca
Chapter 1

David J. Garbary
Department of Biology
St. Francis Xavier University
Antigonish, Canada
e-mail: dgarbary@gmail.com
Chapter 1

Arunika Gunawardena
Biology Department
Dalhousie University,
Halifax, Canada
e-mail: arunika.gunawardena@dal.ca
Chapter 1

Karl H. Hasenstein
Department of Biology
University of Louisiana
Lafayette, LA, USA
e-mail: Hasenstein@louisiana.edu
Chapter 8, 9

Kirsten Heimann
NQAIF
School of Marine & Tropical Biology
James Cook University
Townsville, Australia
e-mail: kirsten.heimann@jcu.edu.au
Chapter 9, 10

Kerstin Hoef-Emden
Biozentrum Köln, Botanik
Universität zu Köln
Köln, Germany
e-mail: kerstin.hoef-emden@uni-koeln.de
Chapter 5

Véronique Martin-Jézéquel
Faculté des Sciences et Techniques
Université de Nantes
Nantes, France
e-mail: Veronique.Martin-Jezequel@
univ-nantes.fr
Chapter 3

Qiaojun Jin
Max-Planck Institute of terrestrial
Microbiology
Marburg, Germany
e-mail: jqiaojun@yahoo.com
Chapter 8

Christos Katsaros
Department of Botany
Faculty of Biology
University of Athens
Athens, Greece
e-mail: Christos.Katsaros@biol.uoa.gr
Chapter 7

Paul L. Klerks
Department of Biology
University of Louisiana
Lafayette, LA, USA
e-mail: klerks@louisiana.edu
Chapter 9

Christina E. Lord
Biology Department
Dalhousie University
Halifax, Canada
e-mail: celord@dal.ca
Chapter 1

Shinichiro Maruyama
Department of Biochemistry & Molecular Biology
Dalhousie University
Halifax, Canada
e-mail: maruyama@dal.ca
Chapter 2

Taizo Motomura
Muroran Marine Station
Field Science Center for Northern Biosphere
Hokkaido University
Muroran 051-0013, Japan
e-mail: motomura@fsc.hokudai.ac.jp
Chapter 7

Chikako Nagasato
Muroran Marine Station
Field Science Center for Northern Biosphere
Hokkaido University
Muroran 051-0013, Japan
e-mail: nagasato@bio.sci.hokudai.ac.jp
Chapter 7

Leonel Pereira
Department of Life Sciences
Faculty of Sciences and Technology
University of Coimbra
Coimbra, Portugal
e-mail: leonel@bot.uc.pt
Chapter 4

Makoto Terauchi
Muroran Marine Station
Field Science Center for Northern Biosphere
Hokkaido University
Muroran 051-0013, Japan
e-mail: yellowplanterauchi@fsc.hokudai.ac.jp
Chapter 7

Benoit Tesson
University of California
San Diego, CA, USA
e-mail: btesson@ucsd.edu
Chapter 3

Contents

1 Programmed cell death in multicellular algae

David J. Garbary, Moira E. Galway, Christina E. Lord and Arunika N. Gunawardena

Introduction

Growth and differentiation of multicellular organisms typically involves the addition of new cells through cell division; unicellular organisms may undergo cell enlargement to accomplish similar ends. In addition, many aspects of morphogenesis and differentiation are associated with cell death. While regularized patterns of cell death have been recognized in the animals and plants, such cell death has rarely been the focus of developmental studies or cell biology in multicellular algae. Cell death resulting from trauma, severe injury or acute physiological stress has been classified as necrosis (Reape et al. 2008; Palavan-Unsal et al. 2005, but see discussion in Kroemer et al. 2009 and in the introduction to Noodén 2004). When localized and endogenously induced death of cells occurs, it may be considered under the general rubric of Programmed Cell Death (PCD) or Apoptosis (APO). The literature on PCD in plant and animal systems is extensive, and there is considerable controversy in defining the various forms of cell death based on processes of ultrastructural and biochemical changes (e.g., Morgan and Drew 2004; Noodén 2004; Reape et al. 2008; Kroemer et al. 2009). While APO and PCD were considered synonymous in much earlier literature, there is a general consensus that APO is a specialized case of PCD from which Apoptosis-Like (APL) phenomena and autophagy (AUT) also need to be distinguished (Reape et al. 2008; Reape and McCabe 2010). As a result of this state of flux, the umbrella term of programmed cell death or PCD will be used hereafter.

In plant (i.e., non-algal) and animal systems, cell death is also a basic feature of development (e.g., Noodén 2004; Bishop et al. 2011). In plants, PCD can be divided into two broad categories: environmentally induced or developmentally regulated (Greenberg 1996; Pennell and Lamb 1997; Palavan-Unsal et al. 2005; Gunawardena 2008; Reape et al. 2008; Williams and Dickman 2008). Environmentally induced PCD is an outcome of external biotic or abiotic factors. Examples of environmentally induced PCD include, but are not limited to, the hypoxia-triggered development of internal gas-filled spaces (lysigenous aerenchyma) (Gunawardena et al. 2001; Morgan and Drew 2004), and the hypersensitive response (HR) triggered by pathogen invasion (Heath 2000; Palavan-Unsal 2005; Khurana et al. 2005; Williams and Dickman 2008). The latter is an example of PCD for which an analogous process has been identified among multicellular algae (Wang et al. 2004; Weinberger 2007). Conversely, developmentally regulated PCD is a predictable event that occurs in response to internal signals. Developmentally regulated PCD typically removes cells to produce spaces (such as in xylem elements for water

transport, or the perforations in leaves of certain plants), or it removes mature cells, tissues and organs that have fulfilled their functions (Greenberg 1996; Pennell and Lam 1997; Palavan-Unsal et al. 2005; Gunwardena and Dengler 2006; Williams and Dickman 2008). Plant developmental processes that involve PCD for which analogous processes can be identified amongst the multicellular algae include the death and usually shedding of cells derived from root caps, root epidermis and trichomes (Greenberg 1996; Wang et al. 1996; Pennell and Lamb 1997; McCully 1999; Enstone et al. 2003; Palavan-Unsal et al. 2005; Hamamoto et al. 2006; Papini et al. 2010), leaf perforation formation (Gunawardena and Dengler 2006; Gunawardena et al. 2004, 2005), senescence and abscission (Greenberg 1996; Pennell and Lamb 1997; Taylor and Whitelaw 2001; Palavan-Unsal 2005; Lim et al. 2007).

With the exception of certain examples (for example, xylogenesis) in which PCD can be studied *in vitro* under controlled conditions, it is striking how little is actually known about developmentally regulated PCD in plants. Molecular details of plant PCD have been primarily obtained from cultured plant cells due to the difficulty in accessing and assessing cells in tissues of intact plants (Reape et al. 2008; Palavan-Unsal et al. 2005).

PCD has rarely been considered for multicellular algae. This is in spite of the occurrence of complex morphologies in which there may be very strict cell and tissue differentiation, and considerable cell death. Even in syntagmatic (i.e., pseudoparenchymatous) algal anatomies, with their fundamentally filamentous structure, cell differentiation is extensive. Thus multiple cell types occur that are specialized for photosynthesis, structural integrity and reproduction (e.g., Bold and Wynne 1985; Gabrielson and Garbary 1986). Development of these systems is often accompanied by cell death.

The purpose of this review is to demonstrate how multicellular (and unicellular – but functionally multicellular) algae provide a rich assemblage of developmental phenomena that would be appropriate as model systems for studies of PCD. While the modes of PCD in the sense of animal or terrestrial plant systems have been largely unstudied in algae, these developmental phenomena provide models that should be useful to cell biologists. Hence, the focus here is on endogenous, localized cell death that is associated with clearly defined morphogenetic patterns. We will consider these processes in the general context of PCD, and point out where additional evidence may suggest more specialized forms of PCD (e.g., APO or AUT). The relevant evidence to distinguish among the various forms of PCD include nuclear DNA fragmentation and laddering, occurrence of metacaspases and caspase-like enzyme activity, calcium ion flux, production of reactive oxygen species, specific changes in mitochondrial function and permeability, in organelle number and morphology and in cell vacuolation, as well as tonoplast rupture, plasmolysis and cell wall modification (Gunawardena et al. 2004, 2007; Morgan and Drew 2004; Reape et al. 2008; Reape and McCabe 2010). Since there are only two studies on macroalgae that considered even some of these syndromes (i.e., Garbary and Clarke 2001; Wang et al. 2004), we will refer to all of the algal developmental processes described here as simply PCD pending further study. Illustrations of the organisms, their authorities and many of the phenomena are available in the cited literature, and also on AlgaeBase (Guiry and Guiry 2011).

There is a literature on PCD and APO in diverse unicellular lineages. These include cyanobacteria (e.g., *Microcystis*, Ross et al. 2006), and various unicellular algae and protists (e.g., Gordeeva et al. 2004; Zuppini et al. 2007; Darehshouri et al. 2008; Affenzeller

et al. 2009). PCD has been considered an underlying regulatory process in phytoplankton populations (Franklin et al. 2006; Veldhuis and Brusard 2006). The cytology of cell death in these systems may be equivalent to those in multicellular organisms, and many of the same gene products and pathways may be involved. However, we largely exclude unicellular organisms from this review having rejected the analogy that a single free-living cell in a population is the equivalent of a single cell in a multicellular organism. Since PCD and APO were first identified and are best understood in multicellular organisms, evidence for these phenomena is best sought among analogous developmental processes in multicellular algae.

Thus this review deals with multicellular and macroscopic algae. Rather than being exhaustive, we provide selected examples of developmentally regulated cell death across the three primary assemblages of multicellular eukaryotic algae, i.e. Chlorophyta, Phaeophyceae and Rhodophyta. Unicellular forms such as *Acetabularia* will be considered only when differentiation produces structures that can be considered as clearly cell-like (e.g. hairs). Where possible, we will examine these developmental phenomena in the context of analogous features of plant systems (i.e., the terrestrial plant clade from bryophytes to flowering plants). Because of space constraints we have limited the discussion largely to vegetative processes and omit reproductive development. Where the plant systems have no apparent anatomical analogy in the algae (e.g., xylogenesis) we have not discussed them. Our review will provide a useful starting point for algal cell biologists to begin more definitive studies on these important and intriguing developmental patterns.

Spore germination

Spore germination has attracted the interest of phycologists because of its inherent importance in morphogenesis. While early 20th century phycologists lacked the media and technical expertise to complete the life histories of seaweeds, it became obvious that a variety of different ontogenies were present that could characterize different groups at a variety of taxonomic levels (e.g., Sauvageau 1918; Chemin 1937; Fritsch 1935, 1945). Thus various algae showed patterns of unipolar and bipolar germination as well as ontogenies in which cell walls were formed inside the original spore wall, the latter typically leading to a basal disc from which upright axes were formed. Of particular interest to this discussion are those forms with unipolar germination in which a single axis (typically a filament) is formed, and the original spore is left empty of cytoplasm, or if it retains cytoplasm, dies early in development.

Phaeophyceae

The spores of many groups of brown algae apparently undergo a process of empty spore germination (e.g. Sauvageau 1918; Fritsch 1945). In this process the spores settle onto the substratum, form a bulge on the side of the spore that develops into a germ tube into which cytoplasmic contents of the spore are extruded. This typically forms the first cell in a prostrate filament and, when all of the cytoplasm has been extruded into the germ tube, a septum is formed that cuts off the original spore wall from the initial filament (e.g., Hubbard et al. 2004). Accounts of spore germination in various taxa suggest that this germination and the formation of two cells may occur in the absence of mitosis.

In many species, the empty spore germination is associated with complete evacuation of the original spore. Even when complete evacuation of the spore cytoplasm does not occur (e.g., Toth 1976), the long-term survival of the original spore is doubtful.

Rhodophyta

Many red algae in diverse lineages have a developmental pattern in which spore germination proceeds by unipolar germination to form a filament (Chemin 1937). In some taxa all of the cytoplasm evacuates the original spore and forms the apical cell of the primary axis. This leaves behind an empty wall that usually breaks down over time. In other cases a mitotic division may occur and the spore is cut off from the developing filament. Here the original spore may or may not be long-lived, and often undergoes degeneration (e.g, Chemin 1937; Dixon 1973; Bouzon et al. 2005). Variation in the extent to which the original spore is evacuated is common at the infraspecific level, and cytoplasmic remnants may include a nucleus and some chloroplasts (e.g., Guiry et al. 1987).

Chlorophyta

The genus *Blidingia* shows several different zoospore germination patterns including empty spore germination in *B. minima* (Bliding 1963; Kornmann and Sahling 1978). In one form of *Blidingia minima*, i.e., *B. minima var. stolonifera* the empty spore development may be continued for several cells into the developing prostrate axis (Garbary and Tam 1989). The terminal cell can repeat the empty spore process several times to form a green terminal cell at the end of several 'empty' cells, or the apical cell may form a disc of cells. The later may generate one to several cells from the margin that grow along the substratum and produce further empty cells. These 'empty' cells have not been studied ultrastructurally, and it is unclear if there is any remaining cytoplasm in them when they are cut off, or if all of the cytoplasm is collected at the apical end prior to cytokinesis. Regardless, the formation of these anucleate cell wall remnants can be considered a form of PCD which may be unique to algae. This process can be interpreted as an ecological adaptation allowing the germinating spore to occupy a large basal area prior to the development of the erect axes (Garbary and Tam 1989).

Hairs

Algal hairs are extremely variable: they may be present or absent, unicellular or multicellular, secretory or absorptive, uninucleate, multinucleate or anucleate, photosynthetic or non-photosynthetic, produced once or many times from subtending cells, and they may be associated with either vegetative or reproductive development (Rosenvinge 1911; Feldmann-Mazoyer 1940; Fritsch 1945; Duckett et al. 1974; Whitton 1988; Pueschel 1990; Oates and Cole 1994; Delivopoulos 2002). Except for some specialized cases in which hairs have thick walls, hairs are typically short-lived and deciduous; hence they should provide excellent examples of developmental PCD. While unicellular hairs typically have tip growth like plant root hairs, multicellular hairs (e.g., trichoblasts in Rhodophyta) may grow by means of an apical cell or basal meristem (e.g., multicellular brown algal hairs); in the latter case the terminal cell is the oldest

in the hair. Multicellular hairs with a basal or intercalary meristem are typical of Phaeophyceae, and they are often associated with trichothallic growth in which vegetative tissues of fronds are added based on cell divisions at the base of the hairs (Graham and Wilcox 2000; Lee 2008). Terminal cells are often dead and this suggests that developmentally they are undergoing PCD. Because of their position at the ends or periphery of thalli, hairs are relatively easy to visualize and should provide simple model systems for study of algal cell death. A discussion of PCD in plant systems then follows the presentation of algal examples to provide a deeper context in cell biology.

Phaeophyceae

There are numerous examples of multicellular hairs in Phaeophyceae associated with the vegetative structure and morphogenesis of thalli from microscopic filaments (e.g. *Streblonema* species) to large fronds (e.g., *Desmarestia* species) (Fritsch 1945). In all cases, these hairs are deciduous and undergo PCD. While hairs in Phaeophyceae in general, and those in mature fronds of fucoids may function in nutrient uptake (e.g. Hurd et al. 1993; Steen 2003), here, we limit our discussion to the well-known case of hairs formed in fucoid embryogenesis. The formation of these apical hairs and their subsequent degeneration provides key landmarks in fucoid embryogenesis.

Following zygote germination to form a rhizoid cell and a thallus cell, the latter typically undergoes a series of cell divisions in which cells are undifferentiated and the embryo is merely a club-shaped mass of cells with basal rhizoids (McLachlan et al. 1971). After four to six days, a series of hairs have formed in an apical groove or pit. The hairs are multicellular and have basal meristems. Above the meristematic region, the hair cells undergo considerable elongation. After maturation, the entire hair is shed, although it is unclear if some or all or the cells in the hairs are already dead (about 10–15 days after zygote germination). Before being shed, one or more of these hairs are associated with an apical cell at the base of the apical groove. This indicates the completion of the meristematic differentiation and the end of embryogenesis. This process occurs in all fucoids, but has been described in numerous papers associated with differentiation of *Fucus*, *Ascophyllum*, *Himanthalia* and other genera (Moss 1969, 1970). Little is known about the cell biology of these hairs. Hair formation, development and abundance can be readily manipulated and modified based on a wide range of environmental characters, e.g., light, temperature, and medium composition (McLachlan 1974; McLachlan 1977; McLachlan and Bidwell 1983), indicating that they are a useful model system to study PCD.

Rhodophyta

In a comprehensive review of red algal hairs, Oates and Cole (1994) compare hair morphology and development across a wide range of red algae. They emphasize that these hairs are short-lived and deciduous. The single observation that might indicate PCD concerns the formation of a “large granular structure containing numerous longitudinally oriented striations” that form at the base of the hair in many species. The authors interpreted this structure as representing “degenerating cytoplasm” when the hair is no longer functional.

Hair morphogenesis in the filamentous red alga, *Audouinella hermannii* (Hymes and Cole 1983) is one of the best descriptions for this process. These uninucleate hairs are apoplastidic and have a large central vacuole with most of the cytoplasm, including the nucleus, near the hair tip. These thin-walled cells have an extensive endomembrane system with several layers of smooth and rough ER surrounding the nucleus. While the possibility of PCD was not specifically addressed, the altered morphology and staining of the nucleus in the most mature hairs is consistent with some reports of PCD in plant systems (Palavan-Unsal et al. 2005; Gunawardena et al. 2004).

Judson and Pueschel (2002) described the ontogeny of hairs and their associated cells (a trichocyte complex) in the coralline red alga, *Jania rubens*. This paper clarified the hair ontogeny in relation to the surface structure and anatomy described by Garbary and Johansen (1982) and Pueschel et al. (2002). Not only are the hairs deciduous in *J. rubens*, but during their ontogeny a specialized crown cell is formed at the thallus surface. The developing hair then grows through the crown cell and its remnants remain in place during subsequent hair formation from the underlying cortical cell. Judson and Pueschel (2002) do not describe the state of the nucleus in these cells although they contain abundant endoplasmic reticulum or were filled with "amorphous material". It is unclear whether these cells die before they are penetrated by the growing hair or as a consequence of that penetration.

Red algae in the family Rhodomelaceae often have multicellular, branched, hair-like structures termed trichoblasts. These branch systems (i.e. trichoblasts) are typically colourless, or at least poorly pigmented, and they are usually fragile structures that are deciduous. Like the unicellular hairs described above, trichoblasts have not been well studied. The most comprehensive ultrastructual study by Delivopoulos (2002) gives an account of morphogenesis in *Osmundea spectabilis*, although this account stops at trichoblast maturity and does not attempt to deal with degeneration or PCD. The only study of trichoblasts that examined these structures in the context of PCD is in *Polysiphonia harvei* (Garbary and Clarke 2001). Here the trichoblasts are formed as lateral systems just below the apex of each vegetative branch. They undergo rapid cell divisions to form all of the cells in the trichoblast. As the vegetative branch grows, cells in the trichoblast elongate. Thus there is a gradation of trichoblast age and developmental state in relation to a vegetative branch apex. Garbary and Clarke (2001) demonstrated that trichoblast cells were undergoing PCD. Following the mitotic and cytokinetic events that formed these cells close to the branch apex, the nuclear DNA was in fact degrading while the cells were undergoing enlargement. Indeed, in the largest cells, staining with DAPI (4´,6-diamidino-2-phenylindole) was unable to show that nuclei were even present. This paper used terminal deoxynucleotidyl transferase dUTP nick end labeling (TUNEL) to show that DNA fragmentation was in fact taking place.

Chlorophyta

Species of *Acetabularia* have been widely studied by developmental biologists, indeed whole volumes have been written on morphogenesis and cell biology of the genus (Puiseux-Dao 1970). *Acetabularia* is a unicellular alga (e.g. Bold and Wynne 1985; Mandoli 1998; Dumais et al. 2000; Graham and Wilcox 2000; Berger and Liddle 2003). This interpretation is based on the coenocytic nature of the stalk that makes up the vast proportion of the cytoplasmic contents, and the presence of a single nucleus located at the base prior to reproductive development. Such an interpretation ignores the

development of the whorls of hairs that are successively formed at the stalk apex and then shed, leaving scars on the thallus surface (Solms-Laubach 1895; Gibor 1973; Ngo et al. 2005). Thus the vegetative state of *Acetabularia* might be better characterized as being uninucleate and multicellular. *Acetabularia* hair growth and development has been extensively studied. The hairs are initially cytoplasmic extensions of the stalk apex but become separated by an incomplete wall septum which must become completely occluded prior to hair shedding (Ngo et al. 2005). The extent to which cytoplasmic contents remain in the hairs when they are shed is unclear. The formation and shedding of these anucleate hairs of *Acetabularia* and other dasycladalean algae, like the anucleate cell remnants in germinating zoospores of *Blidingia minima* var. *stolonifera,* involves the subdivision of a nucleated cell, essentially via cytokinesis in the absence of mitosis. As previously indicated, this may be a form of PCD unique to the algae.

Unlike the anucleate hairs of *Acetabularia* spp., the hairs of *Sporocladopsis jackii* are multicellular, unbranched and clearly nucleate, at least when first formed (Garbary et al. 2005a). The nuclei in the hairs are not apparent in the mature structures and they appear to degrade. The lifespan of the hairs is not known and while dehiscence has not been observed, this is their likely end state.

Plant hairs

Like algae, plants also have hair-like structures known as trichomes. Trichomes are outgrowths or extensions of the epidermis and are generally found on leaves, stems and roots, where they are referred to as root hairs (Pennel and Lamb 1997; Evert 2006). Trichomes on shoots may be living or dead at maturity (Greenberg 1996; Evert 2006). Dead trichomes may protect plants from high intensity light or reduce water loss (Greenberg 1996). Trichome death may also be environmentally induced, for example by a pathogen (Wang et al. 2009). Papini et al. (2010) have investigated the ultrastructural development of *Tillandsia* spp. (Bromeliaceae) of the multicellular shoot epidermal trichomes. These are commonly used for the absorption of atmospheric water, minerals and organic nutrients. Water coming from outside can pass through the distal trichome cells via a symplastic route and subsequently reach mesophyll cells. Within the last stage of trichome ontogeny, when the hair is reaching maturity, the distal trichome cells die via what appears to be PCD.

In contrast to shoot trichomes, all root hairs are considered to be short-lived under natural growing conditions (Evert 2006), although there is surprisingly little data on root hair death, apart from the presumed death of hairs in roots in which there is developmental shedding of the epidermis (see section on epidermal shedding). One exception is a report of developmental PCD in root hairs and root cap cells found in the determinate primary roots of certain cacti using the TUNEL assay for DNA fragmentation (Shiskova and Dubrovsky 2005).

Perforations

Perforation formation in plants

The development of complex leaf shapes during leaf morphogenesis includes the formation of holes or perforations, and this forms a rare and unique type of developmentally

regulated PCD. There are only two families of vascular plants that produce perforations in their leaves via PCD, the Araceae and Aponogetonaceae (Gunawardena et al. 2004, 2005; Gunawardena and Dengler 2006). Functions suggested for plant leaf perforations include herbivore deterrence and thermoregulation (Gunawardena and Dengler 2006). Early in the development of *Monstera* spp. (Araceae) leaf blades, cell death occurs simultaneously in discrete patches of cells. These minute pinprick size perforations will increase more than 10,000 times in area as the leaf expands, inevitably forming large prominent holes within the mature leaf. Neighbouring ground meristem and protoderm cells are unaffected, and the ground meristem cells at the rim of the perforation, which were once mesophyll cells, transdifferentiate to become epidermal cells. The dying cells within these perforation sites display many of the key characteristics of PCD, including chromatin condensation, DNA fragmentation, tonoplast disruption, as well as cytoplasmic shrinkage. One characteristic of PCD that is absent within the *Monstera* system is the degradation of cell walls within the dying cells (Gunawardena et al. 2005). Although this system of developmentally regulated PCD has been well characterized, the adaptive significance of the perforations is unknown (Gunawardena et al. 2005).

The lace plant (*Aponogeton madagascariensis*) is one of forty species in the monogeneric family Aponogetonaceae, and is the only species in the family that produces leaf perforations through PCD. Within the leaf, longitudinal and transverse veins form a network of small, roughly square segments known as areoles within which PCD is initiated. The perforations radiate outward until cell death is halted four to five cells from the perimeter veins, creating a lattice-like pattern over the entire leaf surface (Gunawardena et al. 2004, 2007; Gunawardena and Dengler 2006). Common characteristics of PCD in the lace plant include: the loss of anthocyanin and chlorophyll, chloroplast degradation, alteration in mitochondrial dynamics, cessation of cytoplasmic streaming, increased vesicle formation and transvacuolar strands, and plasma membrane blebbing. The lace plant is an extremely attractive system for the study of PCD due to the accessibility and predictability of perforation formation, the perfection of a protocol for both sterile plant propagation and protoplast isolation, along with the thin nature of the leaf which makes it ideal for live cell imaging (Gunawardena et al. 2004, 2007; Gunawardena and Dengler 2006; Lord and Gunawardena 2010, 2011; Wright et al. 2009).

These perforations in flowering plants provide model systems against which analogous algal morphogenesis can be evaluated.

Phaeophyceae

Agarum (Costariaceae) is a subtidal kelp genus in which fronds develop a complex series of perforations. These holes develop initially at the base of the blade near the intercalary meristem and are about 1 mm in diameter. As the frond grows, the perforations enlarge and may reach several cm in diameter in older parts of the frond. The adaptive significance of the holes is unknown, although it may be associated with increasing water turbulence on the frond surface to allow for nutrient absorption. An early account of perforation development in *Agarum* by Humphrey (1887) suggested inward growth of meristoderm around a patch of tissue that is cut away when the meristoderm from the two sides of the frond join. Preliminary observations (Garbary unpublished) show that the thallus region where the holes develop have great concentrations of physodes (i.e. tannins consisting

of polymers of phloroglucinol). Schoenwaelder (2008) provided an extensive review of phlorotannins; however, their potential role in PCD was not considered. As the holes enlarge as a consequence of cell death, the cells around the holes continue to show high concentrations of tannins. These observations are consistent with the holes developing through an AUT mode of PCD, although phenolic compounds also accumulate in plants undergoing HR-mediated PCD (Heath 2000).

There is a second genus in Costariaceae, i.e., *Thalassiophyllum*, that also has well-developed perforations in its blades (see Fritsch 1945; Guiry and Guiry 2011). The development of the holes in the single species, *T. clathrus* has not been studied. All species of *Hydroclathrus* also form holes in their thalli as a part of normal development but there is no information as to how these holes form.

Rhodophyta

Diverse red algae form blades in which holes are a regular feature of morphogenesis. These include *Sparlingia pertusa*, several species of *Kallymenia* (e.g., *K. perforata*, *K. pertusa* and *K. thompsonii*, see Abbott and McDermid 2002 for summary) and *Martensia australis* (Svedelius 1908). In *S. pertusa* the perforations vary from 1 to about 20 mm in diameter and are scattered over the blade surface except at the blade base and tips (Guiry and Guiry 2011). No information is available on the mechanism of their formation. In *Kallymenia* perforation size is highly variable with larger holes resulting from the fusion of smaller ones (Norris and Norris 1973).

Martensia is a genus that superficially forms a regular pattern of window-like perforations similar to the lace plant, *Aponogeton madagascariensis*. In *Martensia,* however, they form through the separations of cell files and cell proliferation rather than through localized cell death (e.g., Svedelius 1908). Accordingly, the thallus perforations in *Martensia* enlarge without the loss of cells around the periphery of each perforation as occurs in *A. madagascariensis*. Although this is not an example of PCD, the separation of cells to form the open spaces may be analogous to cell separation in the plant abscission process.

Epidermal shedding

Root cap cells and root epidermis

The developing roots of flowering plants shed cells, and in some cases, entire portions of the epidermis. The developmentally regulated death and loss of the root epidermis is best known from soil-grown *Zea mays* (maize) as well as from *Allium cepa* (onion) and the model plant *Arabidopsis thaliana* growing in soil-free conditions (Enstone et al. 2003; McCully 1999, Dolan and Robert 1995), but the process of cell death has not been examined.

In roots, a cap of cells protects the root apical meristem during germination and seedling development. These root cap cells are formed in the meristem as initials and are continuously displaced to the periphery during root growth by new cells (Hamamoto et al. 2006). The displaced cells separate individually or in groups, and may die before or after separation. The death of root cap cells in some species grown under soil-free growing conditions (for example the monocot *Allium cepa* (onion), or the dicot *Brassica napus*), provides evidence that death is developmentally regulated and is not a consequence of mechanical damage instigated by soil penetration (Wang et al. 1996; Pennell and Lamb

1997; Hamamoto et al. 2006). Onion root cap cells that die via PCD exhibit condensed membranes, cytoplasm and nuclei, as well as DNA with 3'-OH nick ends detected via TUNEL staining (Wang et al. 1996). Similar observations were made in 2–4 week root cap cells of the dicot *Arabidopsis thaliana* (Zhu and Rost 2000). At a morphological level, this PCD is similar to the irregular sloughing of surface layers in the non-calcified, crustose red alga *Hildenbrandia* described below.

Epidermal shedding in Phaeophyceae

The process of epidermal shedding was initially described in *Ascophyllum nodosum* by Filion-Myklebust and Norton (1981). They determined that a layer of cells was being shed at regular intervals. The proposed function of this shedding was the removal of epiphytes that could land on the surface and grow. Epiphyte shedding removes potential constraints of light and nutrient absorption. It also provides a way of avoiding drag that could negatively impact whole fronds, which can live up to 20 years. Filion-Myklebust and Norton (1981) suggested that epidermal shedding occurred in *A. nodosum* at intervals as short as two weeks. Given that the thickness of these sheets of cells is about 20 μm and that they may be shed at least 20 times per year, this results in a substantial loss of biomass. Epidermal shedding was subsequently described in other fucoids (Moss 1982; Russell and Veltkamp 1984), and this form of PCD may be a general phenomenon in these brown algae.

Garbary et al. (2009) studied epidermal shedding in *A. nodosum* in the context of morphogenesis of the meristoderm cells. They demonstrated that the meristoderm cells expanded and formed a periclinal cell wall that cut off the apical portion of the cell. The resulting epidermal cell was devoid of nuclei and chloroplasts. Ultrastructure of the predivision meristoderm cells (Xu et al. 2008) showed that the bulk of the cytoplasm in the distal cell portions consisted of numerous small vacuoles and physodes. Numerous small mitochondria lined the cell membrane adjacent to the outer wall of the cell. The proximal cell portions contained chloroplasts, typically a single nucleus, larger mitochondria and fewer physodes. Nuclei in these cells did undergo mitosis as a prelude to cytokinesis to form either tangential walls (allowing for branch elongation, see Eckersley and Garbary 2007), or to form a cortical cell to the interior of the thallus (allowing for branch thickening). In any case, the nuclei always remained in the proximal portions of the meristoderm cells, and there was never any evidence of nuclear breakdown that might be associated with DNA degradation (Garbary et al. 2009).

Garbary et al. (2009) concluded that the epidermal shedding represented a previously undescribed mechanism of PCD. This phenomenon, along with the formation and shedding of anucleate *Acetabularia* hairs and the formation of anucleate cell remnants in *Blidingia* germinating zoospores, could represent a form of PCD unique to the algae.

Given the abundance of *A. nodosum*, this organism could be a particularly useful model system for investigating the homology between the molecular mechanisms of cell death in macroalgae and terrestrial plants. This is especially the case as the cell death is occurring in the absence of apparent nuclear involvement.

Rhodophyta

Most multicellular red algae are characterized ontogenetically by having one or more apical cells, the products of which may form complex thalli through the production

of filaments that differentiate to form cortical and medullary regions. Members of calcified order Corallinales have an alternative developmental system in which an intercalary meristem below the surface of the crust produces an epithallus of one to many cell layers. Cells senesce at the surface and are replaced by cell divisions of the intercalary meristem. This is interpreted as an adaptation to resist the ravages of herbivory in these slow growing organisms. Thus, when molluscs rasp the surface layers, they do not remove the meristematic cells needed to regenerate the surface. The system may also facilitate the removal of epiphytes as the surface cells can be shed along with epiphytic and epizoic organisms that have settled (Johansen 1981; Keats et al. 1997).

The development and senescence of the epithallial cells of Corallinaceae was best described in a series of genera by Pueschel et al. (1996) and Wegeberg and Pueschel (2002). The most conspicuous early changes in *Lithophyllum impressum* were associated with dedifferentiation of chloroplasts and development of specialized wall ingrowths along with overall cytoplasmic deterioration. Later, cytoplasmic disintegration and chloroplast degeneration occurs. Chloroplast degradation is a feature of developmental and environmental PCD in lace plant cells (Gunawardena et al. 2004; Lord and Gunawardena 2011) and in plant leaf senescence (Lim et al. 2007). Changes in mitochondria of the corallines were not identified, and changes in nuclei were not well characterized, although in *Corallina* they became irregular in outline and located peripherally; in all species, nuclei were absent in late developmental stages. Pueschel et al. (1996) concluded: "Epithallial cells are programmed for a stereotypic patterns of differentiation, isolation and senescence." The diversity of these systems ranging from single to multiple epithallial cell layers means that Corallinales may contribute multiple model systems for characterization of PCD in the red algae.

Pueschel (1988) described the death of surface cells in the non-calcified, crustose red alga *Hildenbrandia rubra*. The living crust consists of multiple cell layers from which the dead cells are eventually shed from the surface. The crusts retain the remnant cell walls that become infected with bacteria. Chloroplasts of mature or dying cells have unusual inclusions, visible even with light microscopy, that are sometimes associated with phytoferritin granules. Cells below the zone of PCD often re-establish new apices that had resumed apical cell division. Pueschel (1988) concluded that this process was not associated with mechanical damage or predation, and that the bacteria were a result of, rather than a cause of, cell death. Further studies on this system need to determine the cellular processes leading to cell death, and the extent to which this is an internally regulated phenomenon.

Senescence and abscission

Plants and leaf senescence and abscission

As the name indicates, senescence is an aging process ending in the death of an organism, or specific organs and tissues, while abscission is the separation and shedding of an organ that may occur at the end of senescence (Taylor and Whitelaw 2001). Leaf senescence has been recognized as a highly ordered process that characterizes the last phase of this organ's development (Noodén 2004; Lim et al. 2007). The process of leaf senescence is age-dependent, and associated with characteristic changes in chloroplasts and

mitochondria. This degradation marks the switch from anabolic to catabolic metabolism. The nutrients that accumulated through the life of the leaf are exported to other parts of the plant. Leaf senescence is accompanied by a number of cellular morphological features characteristic of other types of PCD, including chromatin condensation, mitochondrial degradation, loss of tonoplast integrity and plasma membrane (PM) collapse. Consequently, most authors consider leaf senescence to be a type of PCD, characterized by its slowness, whole organ involvement, and the need for cell function during nutrient mobilization and export (Noodén 2004; Lim et al. 2007). Other authors argue that leaf senescence involves suppression of PCD, and that PCD is simply the terminal event (Reape and McCabe 2008). PCD in senescence also shares some similarities, but is distinct from PCD induced by pathogens (HR) (Khurana et al. 2005; Lim et al. 2007; Reape and McCabe 2008). A combination of internal and external cues, resulting in auxin and ethylene production, and the activation of senescence-associated genes (SAGS) are thought to play a role in leaf senescence (Lim et al. 2007). The final stage of leaf senescence is abscission, a complex, poorly-understood process that involves schizogeny (Gunawardena and Dengler 2006; Noodén 2004) and cell death (Noodén 2004). This process occurs in the abscission zone of the petiole attaching the leaf to the plant body. The abscission zone features morphologically distinct small cells organized into up to 50 layers such that cell separation can occur between the cells of two adjacent layers, or between cells in multiple layers (Taylor and Whitelaw 2001).

Algal systems

In *Ascophyllum nodosum* there is an annual production of receptacles. These structures are formed as lateral branches on vegetative axes, and hundreds to thousands of receptacles are formed on each male or female frond. Following gamete maturation and release over a period of several weeks to a month in a given population, the receptacles are shed from the parent frond. There is some degradation of the tissues following gamete release that is associated with receptacle shrinkage and loss of colour. This process may involve senescence-like PCD, while the region at the base of the receptacle where it is attached to the vegetative axis may be undergoing a leaf-like abscission process that could involve PCD. Here the cells must undergo considerable changes to form an abscission zone. Furthermore, following abscission, the cells at the abscission site must differentiate, such that exposed cortical cells form scar tissue that remains at the surface of the axis well into the subsequent growth season. Receptacle abscission in *A. nodosum* appears analogous to plant leaf abscission. Since indole-3-acetic acid (IAA) is present in fucoids at similar concentrations to that in terrestrial plant systems (Augier 1977; Tarakhovskaya et al. 2007), IAA could be part of an equivalent regulatory process in *Ascophyllum* as it is in leaf senescence and abscission (Taylor and Whitelaw 2001; Lim et al. 2007). The formation of the abscission zone and scar tissue may therefore provide another PCD system.

In many algae individual fronds may detach from common holdfasts that can have dozens to hundreds of fronds. For example, reproductive, spore-producing thalli of *Chondrus crispus* detach from their holdfasts leaving non-reproductive fronds (McLachlan et al. 1989). Whether this detachment occurs as a result of increased drag that preferentially removes large thalli, or by development of specific abscission zones at the base of fronds that is a form of PCD, remains to be determined.

Pathogen infection and hypersensitive responses (HRs)

Hypersensitive response in plants

The HR is the rapid death of cells within a plant following pathogen infection by fungi, bacteria, viruses or nematodes (Khurana et al. 2005). This death is a mechanism used by plants to prevent the spread of pathogens to neighboring cells (Greenberg 1996; Pennell and Lamb 1997; Heath 2000; Khurana et al. 2005). Cells that have undergone the HR display some key characteristics of PCD including cessation of cytoplasmic streaming, protoplasm shrinkage, cytoplasmic condensation and vacuolization, plasma membrane blebbing, tonoplast disruption, altered mitochondrial structure and function, and cleavage of nuclear DNA into oligonucleosomal fragments (Greenberg 1996; Pennell and Lamb 1997; Heath 2000; Khurana et al. 2005).

Algae – response to pathogens

PCD also occurs in algal responses to pathogen invasion (e.g., Pontier et al. 2004; Hao et al. 2007). A similar process forms the basis of one of the few explicit invocations of PCD in a multicellular alga, *Laminaria japonica* (Wang et al. 2004; Weinberger 2007).

Wang et al. (2004) characterized PCD in vegetative tissue of *Laminaria japonica* responding to an infection of an alginic acid decomposing bacterium. The authors detected TUNEL positive nuclei, and caspase-3 activity. They observed rapid cell death following infection of the pathogen. While there was no DNA laddering, the authors considered this equivalent to the HR of higher plants. A HR was also suggested by Garbary et al. (2005b) following the penetration of host *Ascophyllum nodosum* by the rhizoids of the red algal epiphyte *Vertebrata lanosa*, although no attempt was made to examine cell death from the perspective of PCD.

Conclusions and future prospects

Similarities in PCD in terrestrial plants and multicellular algae are apparent. In both systems, cell death can result in conspicuous perforations in thalli or leaves. In both plants and algae, PCD may accompany the shedding of hairs (trichomes). A key difference between these systems is that in algae there are no real analogues to the sclerenchyma cells of plants. Thus plants form thick walled, dead cells that have important transport (e.g., tracheids) or supportive (e.g. fibers) functions. While not a widely occurring developmental system, it appears that only brown and green algae form anucleate (empty) cells by cytokinesis in the absence of mitosis.

This review has emphasized the morphological/anatomical features of multicellular algae that are potentially involved with PCD. There is a virtual absence of knowledge of biochemical mechanisms of PCD in multicellular algae. This is despite the fact that macroalgae may have novel systems for PCD that are both interesting in their own right, and may provide insight into the origins and mechanisms of PCD in non-algal taxa.

There are numerous studies in which extracts from both microalgae and macroalgae are able to induce PCD or apoptosis in animal cell lines (e.g. Cornish and Garbary 2010). There are also numerous studies where these extracts or purified compounds are able to prevent PCD or apoptosis. Perhaps such effects could provide clues to the cell signaling

pathways that induce or restrict PCD in the algae. However, at present there is no evidence that these compounds induce PCD within the organisms that produce the compounds.

Rhodophyta, Chlorophyta and Phaeophyceae include multicellular forms that provide important sources of such bioactive compounds that could have medical applications for regulating animal cell PCD. Thus from species of green algae in the genera *Capsosiphon* and *Halimeda* (Huang et al. 2005; Kwon and Nam 2007), from the brown algae in *Colpomenia* (Huang et al. 2005) and from the red algae *Symphyocladia*, *Porphyra*, *Ptilota*, *Corallina* and *Galaxaura* (Huang et al. 2005; Tsuzuki et al. 2005; Kwon and Nam 2006; Kwon et al. 2007; Lee et al. 2007; Cornish and Garbary 2010) compounds have been extracted that induce apoptosis in animal models involving various types of cancer cells.

The morphogenetic systems highlighted in this review show that a knowledge of algal PCD will be fundamental to fully understand the development of the multicellular algae. Moreover, this knowledge will ultimately provide new insights into the origins of, and variations in, the process of PCD as it occurs in multicellular plants and algae.

Acknowledgements

This work was supported by grants from the Natural Sciences and Engineering Research Council of Canada to DG and AG.

References

Abbott, I. A. and K.J. McDermid. 2002. On two species of *Kallymenia* (Rhodophyta: Gigartinales: Kallymeniaceae) from the Hawaiian Islands, Central Pacific. *Pac. Sci. 56*: 149–162.

Affenzeller, M.J., A. Darehshouri, A. Andosch, C. Lutz and U. Lutz-Meindl. 2009. Salt stress induced cell death in the unicellular green alga *Micrasterias denticulata*. *J. Exp. Bot. 60*: 939–954.

Augier, H. 1977. Les hormones des algues. Etat actuel des connaissances. V. Index alphabétique par espèces des travaux de caractérisation des hormones endogens. *Bot. Mar. 20*: 187–203.

Berger, S. and L.B. Liddle. 2003. The life cycle of *Acetabularia* (Dasycladales, Chlorophyta): textbook accounts are wrong (commentary). *Phycologia 42*: 204–207.

Bishop, C.D., M.E. Galway and D.J. Garbary. 2011. Architecture and design among plants and animals: convergent and divergent developmental mechanisms. *In:* (R.L. Gordon, S. Stillwaggon, and J. Seckbach, eds) *Origins of design in nature*. Springer, Dordrecht. pp. 325–341.

Bliding, C. 1963. A critical survey of European taxa in Ulvales. Part 1. *Capsosiphon, Percursaria, Blidingia, Enteromorpha. Opera Botanica* 8(3): 1–160.

Bold, H.C. and M.J. Wynne. 1985. *Introduction to the algae*, 2nd ed. Prentice-Hall, Englewood Cliffs, NJ. pp. 720.

Bouzon, Z.L., L.C. Ouriques and E.C. Oliveira. 2005. Ultrastructure of tetraspore germination in the agar-producing seaweed *Gelidium floridanum* (Gelidiales, Rhodophyta). *Phycologia 44*: 409–415.

Chemin, M.E. 1937. Le developpement des spores chez les Rhodophycées. *Rev. Gen. Bot. 49*: 205–535.

Cornish, M. L. and D.J. Garbary. 2010. Antioxidants from macroalgae: potential applications in human health and nutrition. *Algae 25*: 155–171.

Darehshouri, A., M. Affenzeller and U. Lutz-Meindl. 2008. Cell death upon H_2O_2 induction in the unicellular green alga *Micrasterias*. *Pl. Biol. 10*: 732–745.

Delivopoulos, S.G. 2002. Ultrastructure of trichoblasts in the red alga *Osmundea spectabilis* var. *spectabilis* (Rhodomelaceae, Ceramiales). *Eur. J. Phycol. 37*: 329–338.

Dixon, P.S. 1973. *The biology of red algae*. Edinburgh, Oliver & Boyd. pp. 285.

Dolan, L. and K. Roberts. 1995. Secondary thickening in roots of *Arabidopsis thaliana*: anatomy and cell surface changes. *New Phytol. 131*: 121–128.

Duckett, J.G., J.S. Buchanan, M.C. Peel and M.C. Martin. 1974. An ultrastructural study of pit connections and percurrent proliferations in the red alga *Nemalion helminthoides* (Vell. in With.) Batt. *New Phytol. 73*: 497–507.

Dumais, J., K. Serikawa and D.F. Mandoli. 2000. *Acetabularia*: a unicellular model for understanding subcellular localization and morphogenesis during development. *J. Plant Growth Regul. 19*: 253–264.

Eckersley, L.K. and D.J. Garbary 2007. Developmental and environmental sources of variation on annual growth increments of *Ascophylllum nodosum* (Phaeophyceae). *Algae 22*: 107–116.

Enstone, D.E., Peterson, C.A. and F. Ma. 2003. Root epidermis and exodermis: structure, function and responses to the environment. *J. Plant Growth Regul. 21*: 335–351.

Evert, R.F. 2006. *Esau's plant anatomy*, 3rd ed. John Wiley & Sons, Hoboken, NJ, pp. 601.

Feldmann-Mazoyer, G. 1940. Recherches sur les Céramiacées de la Méditerrannée. Alger, pp. 510 [Reprint Otto Koeltz 1977, Koenigstein, Germany].

Filion-Myklebust, C. and T.A. Norton. 1981. Epidermal shedding in the brown seaweed *Ascophyllum nodosum* (L.) Le Jolis and its ecological significance. *Mar. Biol. Lett. 2*: 45–51.

Franklin, D.J., C.P.D. Brussaard and J.A. Berges. 2006. What is the role and nature of programmed cell death in phytoplankton ecology? *Eur. J. Phycol. 41*: 1–14.

Fritsch, F.E. 1935. *The structure and reproduction of the algae. Vol. 1*. Cambridge University Press, Cambridge. pp. 791.

Fritsch, F.E. 1945. *The structure and reproduction of the algae. Vol. 1I*. Cambridge University Press, Cambridge. pp. 939.

Gabrielson, P.W. and D.J. Garbary. 1986. Systematics of red algae (Rhodophyta). *CRC Crit. Rev. Plant Sci. 3*: 325–366.

Garbary, D.J., C.J. Bird and K.Y. Kim. 2005a. *Sporocladopsis jackii*, sp. nov. (Chroolepidaceae, Chorophyta): a new species from eastern Canada and Maine symbiotic with the mud snail, *Ilyanassa obsoleta* (Gastropoda). *Rhodora 107*: 52–68.

Garbary, D.J. and B. Clarke. 2001. Apoptosis in trichoblast development in *Polysiphonia harveyi* (Rhodophyta). *Phycologia 40*: 324–329.

Garbary, D.J., R.J. Deckert and C.B. Hubbard. 2005b. *Ascophyllum* and its symbionts. VII. Three-way interactions among *Ascophyllum nodosum* (Phaeophyceae), *Mycophycias ascophylli* (Ascomycetes) and *Vertebrata lanosa* (Ceramiales, Rhodophyta). *Algae 20*: 353–361.

Garbary, D.J. and H.W. Johansen. 1982. Scanning electron microscopy of *Corallina* and *Haliptilon* (Corallinaceae, Rhodophyta): surface structures and their taxonomic implications. *J. Phycol. 18*: 211–219.

Garbary, D.J., G. Lawson, K. Clement and M.E. Galway. 2009. Cell division in the absence of mitosis: the unusual case of the fucoid *Ascophyllum nodosum. Algae 24*: 239–248.

Garbary, D. and C. Tam. 1989. *Blidingia minima* var. *stolonifera* var. nov. (Ulvales, Chlorophyta) from British Columbia: systematics, life history and morphogenesis. *Nordic J. Bot. 9*: 321–328.

Gibor, A. 1973. Observations on the sterile whorls of *Acetabularia. Protoplasma 78*: 195–202.

Gordeeva, A.V., Y.A. Labas and R.A. Zvyagilskaya. 2004. Apoptosis in unicellular organisms: mechanisms and evolution. *Biochemistry (Moscow) 69*: 1055–1066.

Giuliani, C, G. Consonni, G. Gavazz, M. Colombo and S. Dolfini. 2002. Programmed cell death during embryogenesis in maize. *Ann. Bot. 90*: 287–292.

Graham, L.E. and L.W. Wilcox. 2000. *Algae*. Prentice Hall, Upper Saddle River, NJ, USA. pp. 640.

Greenberg J.T. 1996. Programmed cell death: a way of life for plants. *Proc. Natl. Acad. Sci. USA 93*: 12094–12097.

Guiry, M.D. and G. M. Guiry. 2011. AlgaeBase. World-wide electronic publication, National University of Ireland, Galway. http://www.algaebase.org.

Guiry, M.D., W. R. Kee and D.J. Garbary. 1987. Morphology, temperature and photoperiodic responses of *Audouinella botryocarpa* (Harvey) Woelkerling (Acrochaeticaeae, Rhodophyta) from Ireland. *Giorn. Bot. Ital. 121*: 229–246.

Gunawardena, A.H.L.A.N. 2008. Programmed cell death and tissue remodelling in plants. *J. Exp. Bot. 59*: 445–451.

Gunawardena, A.H.L.A.N. and N.G. Dengler. 2006. Alternative modes of leaf dissection in monocotyledons. *Bot. J. Lin. Soc. 150*: 25–44.

Gunawardena, A., J.S. Greenwood and N.G. Dengler. 2004. Programmed cell death remodels lace plant leaf shape during development. *Plant Cell 16*: 60–73.

Gunawardena, A., J.S. Greenwood and N.G. Dengler. 2007. Cell wall degradation and modification during programmed cell death in lace plant, *Aponogeton madagascariensis* (Aponogetonaceae). *Am. J. Bot. 94*: 1116–1128.

Gunawardena, A.H.L.A.N., D.M. Pearce, M.B. Jackson, C.R. Hawes and D.E. Evans. 2001. Characterisation of programmed cell death during aerenchyma formation induced by hypoxia and in roots of maize (*Zea mays* L.). *Planta 212*: 205–214.

Gunawardena, A.H.L.A.N., K. Sault, P. Donnelly, J.S. Greenwood and N.G. Dengler. 2005. Programmed cell death and leaf morphogenesis in *Monstera oblique. Planta* 221: 607–618.

Hamamoto, L., Hawes, M.C. and T.L. Rost. 2006. The production and release of living root cap border cells is a function of root apical meristem type in dicotyledonous angiosperm plants. *Ann. Bot. 97*: 917–923.

Hao, L., P.H. Goodwin and T. Hsiang. 2007. Expression of a metacaspase gene of *Nicotiana benthamiana* after inoculation with *Colletotrichum destructivum* or *Pseudomonas syringae* pv. tomato, and the effect of silencing the gene on the host response. *Plant Cell Rep. 26*: 1879–1888.

Heath, M. 2000. Hypersensitive response-related cell death. *Plant Mol. Biol. 44*: 321–334.

Huang, H.L., S.L. Wu, H.F. Liao, C.M. Jiang, R.L. Huang, Y.Y. Chen, Y.C. Yang and Y.J. Chen. 2005. Induction of apoptosis by three marine algae through generation of reactive oxygen species in human leukemic cell lines. *J. Agricul. Food Chem. 53*: 1776–1781.

Hubbard, C.B., D.J. Garbary, K.Y. Kim and D.M. Chiasson. 2004. Host specificity and growth of kelp gametophytes symbiotic with filamentous red algae (Ceramiales, Rhodophyta). *Helgol. Mar. Res. 58*: 18–25.

Hurd, C. L., R.S. Galvin, T.A. Norton and M.J. Dring. 1993. Production of hyaline hairs by intertidal species of *Fucus* (Fucales) and their role in phosphate uptake. *J. Phycol. 29*: 160–165.

Humphrey, J.E. 1887. On the anatomy and development of *Agarum turneri* Post. & Rupr. *Proc. Am. Acad. Sci. Boston 22*: 195–204.

Hymes, B.J. and K.M. Cole. 1983. The cytology of *Audouinella hermannii* (Rhodophyta, Florideophyceae). I. Vegetative and hair cells. *Can. J. Bot. 61*: 3366–3376.

Johansen, H.W. 1981. Coralline algae, a first synthesis. CRC Press, Boca Raton, FL. pp. 239.

Judson, B.L. and C.M. Pueschel. 2002. Ultrastructure of trichocyte (hair cell) complexes in *Jania adhaerens* (Corallinales, Rhodophyta). *Phycologia 41*: 68–78.

Keats, D.W., M.A. Knight and C.M. Pueschel. 1997. Antifouling effects of epithallial shedding in three crustose coralline algae (Rhodophyta, Corallinales) on a coral reef. *J. Exp. Mar. Biol. Ecol. 213*: 281–293.

Kornmann, P. and P.-H. Sahling. 1978. Die *Blidingia*-Arten von Helgoland (Ulvales, Chlorophyta). *Helgol. Wiss. Meeresunters. 31*: 391–413.

Khurana, S.M.P., Pandey, S.K., Sarkar, D. and A. Chanemougasoundharam. 2005. Apoptosis in plant disease response: A close encounter of the pathogen kind. *Curr. Sci. 88*: 740–752.

Kroemer, G., L. Galluzzi, P. Vandenabeele, J. Abrtams, E.S. Alnemri, E.H. Baehrecke, M.V. Blagosklonny, W.S. El-Deiry, P. Goldstein, D.R. Green, M. Hengartner, R.A. Knight, S. Kumar, S.A. Lipton, W. Malomi, G. Nuñez, M.E. Peter, J. Tschopp, J. Yuan, M. Placentini, B. Zhivotovsky and G. Melino. 2009. Classification of cell death: recommendations of the Nomenclature Committee on Cell Deaths 2009. *Cell Death Diff. 16*: 3–11.

Kwon, H.J., S.Y. Bae, K.H. Kim, C.H. Han, S.H. Cho, S.W. Nam, Y.H. Choi and B.W. Kim. 2007. Induction of apoptosis in HeLa cells by ethanolic extract of *Corallina pilulifera*. *Food Chem. 104*: 196–201.

Kwon, M.J. and T.J. Nam. 2006. Porphyran induces apoptosis related signal pathway in AGS gastric cancer cell lines. *Life Sci. 79*: 1956–1962.

Kwon, M.J. and T.J. Nam. 2007. A polysaccharide of the marine algae *Capsosiphon fulvescens* induces apoptosis in AGS gastric cancer cells via IGF-IR-mediated P13K/Akt pathway. *Cell Biol. Intn. 31*: 768–775.

Lee, J.H., S.E. Park, M.A. Hossain, M.Y. Kim, M.N. Kim, H.Y. Chung, J.S. Choi, Y.H. Yoo and N.D. Kim. 2007. 2,3,6-tribromo-4,5-dihydroxybezyl methyl ether induces growth inhibition and apoptosis in MCF-7 human breast cancer cells. *Arch. Pharm. Res. 30*: 1132–1137.

Lee, R.E. 2008. *Phycology,* 4th ed. Cambridge, Cambridge University Press. pp. 547.

Lim, P.O., H.J. Kim and H.G. Nam. 2007. Leaf senescence. *Ann. Rev. Plant Biol. 58*: 115–136.

Lord, C.E.N. and A.H.L.A.N. Gunawardena. 2010. Isolation of leaf protoplasts from the submerged aquatic monocot *Aponogeton madagascariensis*. *Am. J. Plant Sci. Biotechnol. 4 (special issue 2)*: 6–11.

Lord, C.E.N. and A.H.L.A.N. Gunawardena. 2011. Environmentally induced programmed cell death in leaf protoplasts of *Aponogeton madagascariensis. Planta 233*: 407–421.

Mandoli, D.F. 1998. Elaboration of body plan and phase change during development of *Acetabularia*: How is the complex architecture of a giant unicell built? *Ann. Rev. Plant Physiol. Plant Mol. Biol. 49*: 173–198.

McCully, M.E. 1999. Roots in soil: unearthing the complexities of roots and their rhizospheres. *Annu. Rev. Plant Physiol. Plant Mol. Biol. 50*: 695–718.

McLachlan, J. 1974. Effects of temperature and light on growth and development of embryos of *Fucus edentatus* and *F. distichus ssp. distichus*. *Can. J. Bot. 52*: 943–951.

McLachlan, J. 1977. Effects of nutrients on growth and development of embryos of *Fucus edentatus* Pyl. (Phaeophyceae, Fucales). *Phycologia 16*: 329–338.

McLachlan, J. and R.G.S. Bidwell. 1983. Effects of colored light on the growth and metabolism of *Fucus* embryos and apices in culture. *Can. J. Bot. 61*: 1993–2003.

McLachlan, J., L.C.-M. Chen and T. Edelstein. 1971. The culture of *Fucus* under laboratory conditions. *Can. J. Bot. 49*: 1463–1469.

McLachlan, J., J. Quinn and C. MacDougall. 1989. The structure of the plant of *Chondrus crispus* Stackhouse (Irish moss). *J. Appl. Phycol. 1*: 311–317.

Morgan, P.W. and M.C. Drew. 2004. Plant cell death and cell differentiation. *In*: (L.D. Noodén, ed.) *Plant cell death processes.* Elsevier, Amsterdam. pp. 19–36.

Moss, B. 1969. Apical meristems and growth control in *Himanthalia elongata* (S. F. Gray). *New Phytol. 68*: 387–397.

Moss, B. 1970. Meristems and growth control in *Ascophyllum nodosum* (L.) Le Jol. *New Phytol. 69*: 253–260.

Moss, B.L. 1982. The control of epiphytes by *Halidrys siliquosa* (L.) Lyngb. (Phaeophyta, Cystoseiraceae). *Phycologia 21*: 185–191.

Ngo, D.A., P.A. Garland, and D.E. Mandoli. 2005. Development and organization of the central vacuole of *Acetabularia acetabulum*. *New Phytol. 165*: 731–746.

Noodén, L.D. 2004. Introduction. *In*: (Noodén, L.D., ed) *Plant cell death processes*. Elsevier, Amsterdam. pp. 1–18.

Norris, R.E. and J.N. Norris. 1973. *Kallymenia pertusa* (Rhodophyceae, Cryptonemiales) from the Gulf of California. *Phycologia 12*: 71–74.

Oates, B.R. and K.M. Cole. 1994. Comparative studies on hair cells of two agarophyte red algae, *Gelidium vagum* (Gelidiales, Rhodophyta) and *Gracilaria pacifica* (Gracilariales, Rhodophyta). *Phycologia 33*: 420–433.

Palavan-Unsal, N, E.D. Buyuktuncer and M. Tufekci. 2005. Programmed cell death in plants. *J. Cell Mol. Biol. 4*: 9–23.

Papini, A, G. Tani, P.D. Falco and L. Brighigna. 2010. The ultrastructure of the development of *Tillandsia* (Bromeliaceae) trichome. *Flora 205*: 94–100.

Pennell, R.I. and C. Lamb. 1997. Programmed cell death in plants. *The Plant Cell 9*: 1157–1168.

Pontier, D., O. del Pozo and E. Lam. 2004. Cell death in plant disease: mechanisms and molecular markers. *In*: (Noodén, L.D., ed) *Plant cell death processes*. Elsevier, Amsterdam. pp. 37–50.

Pueschel, C.M. 1988. Cell sloughing and chloroplast inclusions in *Hildenbrandia rubra* (Rhodophyta, Hildenbrandiales). *Brit. Phycol. J. 23*: 17–23.

Pueschel, C.M. 1990. Cell structure. *In*: (K.M. Cole and R.G. Sheath, eds) *Biology of the red algae*. Cambridge University Press, Cambridge, UK. pp. 7–41.

Pueschel, C.M., B.L. Judson, J.E. Esken and E.L. Beiter. 2002. A developmental explanation for the *Corallina*- and *Jania*-types of surfaces in articulated coralline red algae (Corallinales, Rhodophyta). *Phycologia 41*: 79–86.

Pueschel, C.M., T.J. Miller and B.B. McCausland. 1996. Development of epithallial cells in *Corallina officinalis* and *Lithophyllum impressum* (Corallinales, Rhodophyta). *Phycologia* 35: 161–169.

Puiseus-Dao, S. 1970. Acetabularia *and cell biology*. Logos Press, London. pp. 162.

Reape, T. and P.F. McCabe. 2008. Apoptotic-like programmed cell death in plants. *New Phytol. 180*: 13–26.

Reape, T.J. and McCabe, P.F. 2010. Apoptosis-like regulation of programmed cell deaths in plants. *Apoptosis 15*: 249–256.

Reape, T.J., E.M. Molony and P.F. McCabe. 2008. Programmed cell death in plants: distinguishing between different modes. *J. Exp. Bot. 59*: 435–444.

Rosenvinge, L.K. 1911. Remarks on the hyaline unicellular hairs of the Florideae. Biologiske Arbejder tilegnede Eug. Warming. Copenhagen. pp. 203–216.

Ross, C., L. Santiago-Vazquez and V. Paul. 2006. Toxin release in response to oxidative stress and programmed cell death in the cyanobacterium *Microcystis aeruginosa. Aquatic Toxicol. 78*: 66–73.

Russell, G. and C.J. Veltkamp. 1984. Epiphyte survival on skin-shedding macrophytes. *Mar. Ecol. Prog. Ser. 18*: 149–153.

Sauvageau, M.C. 1918. Recherches sur les laminaires des côtes de France. *Mémoires de l'Academie des Sciences de Institute de France 56*: 1–240.

Schoenwaelder, M.E.A. 2008. The biology of phenolic containing vesicles. *Algae 23*: 163–175.

Shishkova, S., and Dubrovsky J.G. 2005. Developmental programmed cell death in primary roots of Sonoran desert Cactaceae. *Am. J. Bot. 92*: 1590–1594.

Solms-Laubach, H. 1895. Monograph of the Acetabulariae. *Trans. Linn. Soc. Lond. Bot., Ser. II, 5*: 1–39.

Steen, H. 2003. Apical hair formation and growth of *Fucus evanescens* and *F. serratus* (Phaeophyceae) germlings under various nutrient and temperature regimes. *Phycologia 42*: 26–30.

Svedelius, N. 1908. Über den Bau and die Entwicklung der Florideengattung *Martensia*. Kungl. Svenska Vetenskap. Handl. 43 (7): 1–101.

Tarakhovskaya, E.R., Y.I. Maslov and M.F. Shishova. 2007. Phytohormones in algae. *Rus. J. Plant Physiol. 54*: 163–170.

Taylor, J.E., and C.A. Whitelaw. 2001. Signals in abscission. *New Phytol. 151*: 323–339.

Toth, R. 1976. The release, settlement and germination of zoospores in *Chorda tomentosa* (Phaeophyceae, Laminariales). *J. Phycol. 12*: 222–233.

Tsuzuki, T., K. Tanaka, S. Kuwahara and T. Miyazawa. 2005. Synthesis of the conjugated trienes 5E, 7E, 9E, 14Z, 17Z-eicosapentaenoic acid and 5Z, 7E, 9E, 14Z, 17Z-eicosapentaenic acid, and their induction of apoptosis in DLD-1 colorectal adenocarcinoma cells. *Lipids 40*: 147–154.

Veldhuis, M.J.W. and C.P.D. Brussaard. 2006. Harmful algae and cell death. *In:* (E. Granéli and J.T. Turner, eds) *Ecology of harmful algae*. Ecological Studies 189, Springer-Verlag, Berlin. pp. 153–162.

Wang, G.-G., X.Y. Liu, X.-H. Li, W. Lin, X.J. Yan and D.-L. Duan. 2004. Programmed cell death in *Laminaria japonica* (Phaeophyta) tissues infected with alginic acid decomposing bacterium. *Prog. Natural Sci. 14*: 1064–1068.

Wang, H, J. Li, R.M. Bostock and D.G. Gilchrist. 1996. Apoptosis: a functional paradigm for programmed cell death induced by host-selective phytotoxin and invoked during development. *Plant Cell 8*: 375–391.

Wang, Y., Liu, R., Chen, L., Wang, Y., Liang, Y., Wu, X., Li, B., Wu, J., Liang, Y., Wang, X., Zhang, C., Wang, Q., Hong, X., and H. Dong. 2009. *Nicotiana tabacum* TTG1 contributes to ParA1-induced signalling and cell death in leaf trichomes. *J. Cell Sci. 122*: 2673–2685.

Wegeberg, S. and C.M. Pueschel. 2002. Epithallial and initial cell fine structure in species of *Lithothamnion* and *Phymatolithon* (Corallinales, Rhodophyta). *Phycologia 41*: 228–244.

Weinberger, F. 2007. Pathogen induced defense and innate immunity in macroalgae. *Biol. Bull. 213*: 290–302.

Whitton, B.A. 1988. Hairs in eukaryotic algae. *In*: (F.E. Round, ed.) *Algae and the aquatic environment*. BioPress, Bristol. pp. 446–460.

Williams, B., and M. Dickman. 2008. Plant programmed cell death: can't live with it; can't live without it. *Mol. Plant Path. 9*: 531–544.

Wright, H., W.G. Van Doorn and A.H.L.A.N. Gunawardena. 2009. In vivo study of developmentally programmed cell death using the Lace Plant (*Aponogeton madagascariensis*; Aponogetonaceae) leaf model system. *Am. J. Bot. 96*: 865–876.

Xu, H., R.J Deckert and D.J. Garbary. 2008. *Ascophyllum* and its symbionts. X. Ultrastructure of the interaction between *A. nodosum* (Phaeophyceae) and *Mycophycias ascophylli* (Ascomycetes). *Botany 86*: 185–193.

Zhu, T. and T.L. Rost. 2000. Directional cell-to-cell communication in the *Arabidopsis* root apical meristem III. Plasmodesmata turnover and apoptosis in meristem and root cap cells during four weeks after germination. *Protoplasma 213*: 99–107.

Zuppini, A., C. Andreoli and B. Baldan. 2007. Heat stress: an inducer of programmed cell death in *Chlorella saccharophila*. *Plant Cell Physiol. 48*: 1000–1009.

2 Endosymbiosis, gene transfer and algal cell evolution

Shinichiro Maruyama and John M. Archibald

The evolution of plastids

It is well established that plastids (chloroplasts) evolved from prokaryotic endosymbionts related to modern-day cyanobacteria. The endosymbiont hypothesis proposes that these prokaryotes were first captured by a phagotrophic eukaryote and retained inside it instead of being digested as food. Over time, the host-endosymbiont relationship matured, driven by the transfer of genetic material from the endosymbiont to the host. The endosymbionts eventually became completely dependent on their hosts and evolved into vertically inherited photosynthetic organelles: 'primary plastids' (Gray 1992; McFadden 2001). We now know that some of the eukaryotes harboring primary plastids were themselves engulfed by other phagotrophic eukaryotes via a process called 'secondary endosymbiosis', giving rise to a variety of highly distinctive algal lineages (Table 2.1). It is generally believed that the primary endosymbiotic origin of plastids occurred only once in the history of eukaryotes and secondary endosymbiosis took place on at least three occasions (Reyes-Prieto et al. 2007; Gould et al. 2008; Archibald 2009a). There is, however, by no means unanimous agreement on these points amongst workers in the field. Despite a rapidly increasing number of complete algal genome sequences available for comparison, how the plastids of modern-day algae are related to one another remains one of the most controversial aspects of eukaryotic evolution.

The endosymbiont hypothesis for the origin of plastids provides a robust framework for understanding the evolution of the algal cell, explaining 'how' eukaryotes acquired the ability to carry out oxygenic photosynthesis. Many researchers, however, also want to know 'what' kinds of cells were actually involved in this process. This question is difficult to address because of the diverse nature of eukaryotic phototrophs and the antiquity of the endosymbiotic events that gave rise to their plastids. It is thus anything but straightforward to decisively and convincingly reconstruct the early evolution of photosynthetic eukaryotes. In the simplest case, algal cells have three genome-bearing organelles, the nucleus, plastid and mitochondrion. The evolution of the algal cell is thus a composite of the histories of these three distinct lineages. Figure 2.1 illustrates different scenarios for how primary plastid-bearing eukaryotes could have arisen and evolved; that is, the multiple ways in which the phylogenies of the plastid (endosymbiont) and the algal nucleus (host) can be superimposed upon one another. If secondary endosymbiosis is to be considered, we need to reconstruct an even more complicated picture with another layer of phylogenetic signals from the nucleus of the secondary endosymbiont. Genomic data has provided the means with which to solve this puzzle, but at the same time, has led to the realization that even the 'simplest' models for the origin and evolution of plastids may be far too simplistic.

Table 2.1 Cyanobacterium-derived organelles.

1st rank classification	2nd rank classification	Organism	Secondary plastids
Plastid (syn. Chloroplast *sensu lato*)	Chloroplast *sensu stricto*	green algae and land plants	euglenophytes, chlorarachniophytes, the dinoflagellate *Lepidodinium*
	Rhodoplast	red algae	cryptophytes, haptophytes, stramenopiles, dinoflagellates, chromerids, apicomplexans[2]
	Cyanelle (Muroplast)[1]	glaucophytes	

[1] See text for discussion on the terminology.
[2] The red versus green origin of 'apicoplasts' in apicomplexans is still contentious (Cai et al. 2003; Funes et al. 2004; Lau et al. 2009; Obornik et al. 2009; Janouskovec et al. 2010).

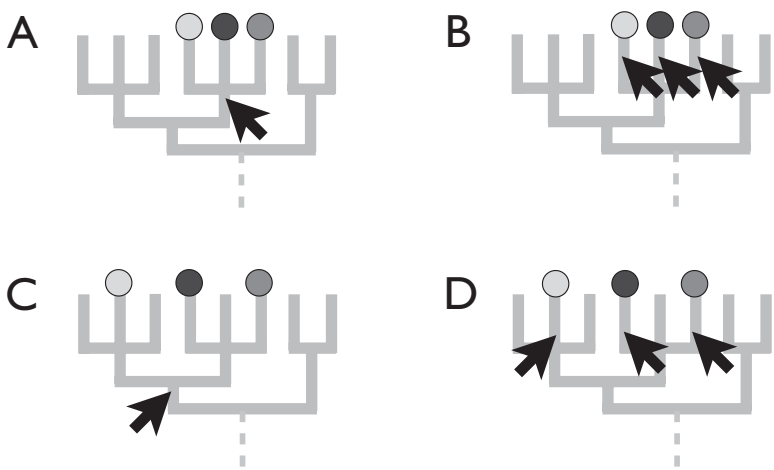

	A	B	C	D
plastid origin	single	multiple	single	multiple
host lineages	single clade	single clade	multi-clades	multi-clades
plastid bearers	monophyletic	?	'paraphyletic'	polyphyletic

Figure 2.1 Competing scenarios for the origin(s) of primary plastids. Four possible schemes for the origins of primary plastids are shown. (A) A pervasive view assumes that the primary plastid was acquired by a derived eukaryote via a single event of primary endosymbiosis (arrow). (B) Multiple primary endosymbioses restricted to within a single lineage of eukaryotes are assumed to have occurred in this scenario. (C) Following a single primary endosymbiosis, primary plastids were retained in some lineages but lost in others. (D) Primary endosymbionts were acquired in separate lineages and evolved into plastids on multiple occasions. Some lineages have lost plastids secondarily.

Endosymbiotic gene transfer (EGT), the transfer of genetic material from endosymbiont to host, has had a profound impact on the genetic make up of algal nuclear genomes. Modern-day plastid genomes are extremely limited in their coding capacity; the vast majority of the plastid proteome in photosynthetic eukaryotes is encoded by nuclear genes whose products are co- or post-translationally targeted to the organelle. In practice, however, it can be difficult to distinguish between nuclear genes derived from an organelle, a transient endosymbiont or an ingested prey organism. As we shall see, distinguishing between these different possibilities is both difficult and extremely important. In this chapter, we discuss algal cell evolution from the perspective of phylogenetics and comparative genomics. With the wealth of genomic data now available to us significant advances have been made. However, there is still much debate as to how, and in what situations, we can infer that endosymbioses have actually occurred in the past.

The primary endosymbiotic origin of plastids

Plastid genome content

Many lines of phylogenetic, biochemical and morphological evidence strongly support the idea that extant cyanobacteria and plastids share a common ancestor (McFadden 2001; Archibald 2009b). Nevertheless, there are huge gaps between the two. Perhaps most significant is the fact that most plastid genomes are 10–20% of the size of the smallest cyanobacterial genomes sequenced to date, such as the 1.66 megabase (Mb) genome of *Prochlorococcus* sp. strain MED4 (Rocap et al. 2003), and the 1.44 Mb genome of the uncultured unicellular marine cyanobacterium UCYN-A (Tripp et al. 2010). The discrepancy in the size and gene content between cyanobacterial and plastid genomes suggests that a drastic reduction of the plastid genome size occurred in the ancestors of primary plastid-bearing eukaryotes.

The loss of genes from plastid genomes is anything but random. In 1999, Race et al. noted that of the thousands of genes encoded in extant cyanobacterial genomes, only 46 protein-encoding genes are commonly retained in all the plastid genomes sequenced at that time, most of which encode photosynthesis machinery or ribosomal proteins (Race et al. 1999). The genomes of non-photosynthetic plastids are typically even further reduced, but still retain tRNA, ribosomal protein and other 'house-keeping' genes (Krause 2008). Notably, some non-photosynthetic plastids still retain genes related to photosynthesis, though not necessarily those involved in light harvesting. For example, an *rbcL* gene encoding the large subunit of RuBisCO (ribulose-1,5-bisphosphate carboxylase/oxygenase), which catalyzes the first step of carbon fixation, is found in the plastid genome of the euglenophyte *Euglena longa* (formally named *Astasia longa*: Gockel and Hachtel 2000) and the RuBisCO gene cluster *rbsLS-cbbX* persists in the cryptomonad *Cryptomonas paramecium* (Donaher et al. 2009). Although RuBisCO has been shown to be involved in lipid biosynthesis in developmentally non-photosynthetic plastids in land plant seeds (Schwender et al. 2004), its function in the secondarily non-photosynthetic plastids of unicellular algae remains unclear (Krause 2008).

Which cyanobacterial lineage is most closely related to the plastid progenitor?

While genome reduction and EGT provide insight into the process of endosymbiosis, they also greatly impede our effort to elucidate the origin of plastids. Much genetic information useful for the reconstruction of organelle phylogeny has undoubtedly been transferred from the plastid to the nucleus, but it can be difficult to determine with certainty which nuclear genes truly came from the cyanobacterial progenitor of the plastid. Researchers often rely on nuclear genes with 'strong' cyanobacterial signatures in their phylogenetic trees. We cannot be too cautious in our attempts to avoid inferring plastid phylogeny using genes that are not in fact derived from the organelle.

Studies published to date have not answered the question of which lineage of extant cyanobacteria is most similar to the ancestor of plastids. Phylogenetic analyses using a traditional gene marker, the 16S ribosomal RNA (rRNA) gene, place plastid sequences "near the root of the cyanobacterial line of descent" (Turner et al. 1999) or "most closely related to N_2-fixing unicellular cyanobacteria" (Falcón et al. 2010). Phylogenomic analyses using multiple protein sequences favor a basal branching of plastids rather than an affiliation with a specific cyanobacterial lineage (Rodríguez-Ezpeleta et al. 2005; Sato 2006; Criscuolo and Gribaldo 2011). Interestingly, recent phylogenetic analyses and gene content surveys based on gene presence and absence (Deusch et al. 2008) suggest that the plastid progenitor might have been an organism similar to heterocyst-forming nitrogen-fixing filamentous cyanobacteria (e.g., *Anabaena*, *Nostoc*). A weakness of these analyses is the limited number of taxa available for whole-genome comparison. On balance, each of these lines of evidence is still inconclusive.

What can be done to obtain a more meaningful picture of the relationship between plastids and cyanobacteria? The number of plastid genomes sequenced to date is still quite limited, in most cases covering only representative species from a variety of algal lineages (Krause 2008; Kim and Archibald 2009). Increased sampling within the major algal clades would thus presumably be beneficial. Inclusion of as-yet-unidentified taxa branching basally in the cyanobacterial tree would also be an important step forward. Yet regardless of these sampling issues, analysis of the data now in hand have led to the realization that plastid genomes are of mixed ancestry. This greatly complicates efforts to infer the origin of plastids in modern-day plants and algae.

How heterogeneous was the ancestral plastid genome?

A non-cyanobacterial RuBisCO operon in red algae

A major challenge in inferring the evolution of plastids is that their genomes are not simply miniaturized cyanobacterial genomes. One of the first examples of plastid genome heterogeneity was the discovery that red algal and red algal-derived plastids have different types of RuBisCO large (*rbcL*) and small (*rbcS*) subunit genes that are more similar to those found in proteobacteria than those of cyanobacteria, green plant and glaucophyte plastids (Morden et al. 1992; Delwiche and Palmer 1996). These analyses are complicated by the fact that *rbcS* genes are much shorter than *rbcL*, and are present in the nuclear genomes of green plants and glaucophytes, in contrast to the *rbcLS* operon in red algal plastid genomes. What we refer to here as 'proteobacteria' includes several

different proteobacterial lineages, and it is not clear which of these the red algal *rbcLS* genes are most closely related to (Marin et al. 2007). Hereafter we refer to the red algal *rbcLS* genes as 'non-cyanobacterial' type genes to avoid confusion.

The *rbcL* gene is one of the most extensively used phylogenetic markers, one that has been sequenced from many lineages, and its incongruence with the evolutionary history of other plastid genes, such as 16S and 23S rRNA, highlight the heterogeneous nature of plastid genomes. Although many intermediates are possible, two extreme scenarios have been considered to account for the observed *rbcL* phylogeny: one is lateral gene transfer (LGT) from a proteobacterial lineage to the plastid genome of red algae, and the other is ancestral gene duplication prior to the divergence of primary plastid-bearing eukaryotes and subsequent gene losses (Delwiche and Palmer 1996).

The debate is far from settled. There are currently no known green algae, plants or glaucophytes in possession of the non-cyanobacterial *rbcL* gene, and no eukaryotes have been shown to harbor both cyanobacterial and non-cyanobacterial *rbcLS* genes. Maier et al. addressed this issue by focusing on another gene family called *cbbX*, which is known to form an operon structure with *rbcLS* in many, but not all, red algal and red algal-derived plastids and some prokaryotes (Maier et al. 2000). These authors found that, in the cryptophyte alga *Guillardia theta,* the *cbbX* genes are encoded in the genomes of both the red alga-derived plastid and the 'nucleomorph', i.e., the highly reduced nucleus of the secondary endosymbiont, and that these two *cbbX* genes in *G. theta* are orthologous to genes from prokaryotes possessing the non-cyanobacterial RuBisCO (Maier et al. 2000). This finding was recently corroborated by Fujita et al. who showed that the red algal-type nuclear (including the cryptophyte nucleomorph) and plastid *cbbX* genes are orthologous to each other (Fujita et al. 2008a), and that both types of *cbbX*s likely function as transcription regulators of the RuBisCO operon in the unicellular red alga *Cyanidioschyzon merolae* (Fujita et al. 2008b). Furthermore, on the strength of circumstantial evidence of an *Oryza sativa* cDNA clone possibly encoding a 'homolog' of *cbbX*, Maier et al. proposed that the ancestor of plastids possessed both the cyanobacterial and non-cyanobacterial *rbcL-S-cbbX* operons for a period of time, and that the ancestors of each of three lineages (green plants, red algae and glaucophytes) differentially lost one of the two operons (Maier et al. 2000). At face value, this hypothesis is most consistent with the 'duplication and differential loss' scenario for the evolution of the *rbcLS* operon. However, the phylogenetic origin of the *O. sativa cbbX* homolog has not been determined and it remains to be elucidated whether the origin of non-cyanobacterial *rbcL-S-cbbX* operons can in fact be traced back to the common ancestor of primary plastids.

'Chimeric' origins of the menaquinone/phylloquinone biosynthesis gene cluster

Gross et al. conducted phylogenetic analyses on the plastid and nuclear *men* gene clusters and provided interesting insight into plastid genome evolution (Gross et al. 2008). The *men* cluster is widely conserved in both prokaryotes and eukaryotes and encodes a series of enzymes that catalyze the biosynthesis of vitamin K such as menaquinone and phylloquinone. These authors showed that among eukaryotes this gene cluster is found only in phototrophs and that, while most *men* genes are in the plastid genomes in an acidothermophilic red algal group called Cyanidiales, green plants and diatoms possess nuclear genes including the *menF-D-C-H* fusion gene called *PHYLLO*. Moreover,

many of these nuclear *men* cluster genes encoding putatively plastid-localized proteins, as well as the Cyanidiales plastid genes, are most closely related to the sequences from non-cyanobacterial prokaryotes. Significant discrepancies in patterns of phylogenetic affiliations between red algal and green plant genes were also found. For instance, members of the Cyanidiales possess a gammaproteobacterial type plastid-encoded MenA, as well as a Chlorobi/gammaproteobacterial type plastid-encoded MenE and a nuclear-encoded MenG. Meanwhile, among the nuclear genes in green plants, MenA and MenG are cyanobacterial-type, and MenE is of deltaproteobacterial origin. Gross et al. (2008) maintained that the complicated patterns seen in their phylogenetic trees are evidence for evolutionary 'chimerism' in the genome of the ancestor of plastids. They also suggested that the ancestor might have been actively incorporating extracellular DNA mediated by viruses such as cyanophages.

In phylogenetic trees of the Men proteins, less consistent were the interrelationships between prokaryotic clades used as the outgroup in the analysis (Gross et al. 2008). Apparent LGT events between bacterial lineages were also inferred for some trees (e.g., the MenH tree). While it is often possible to reasonably infer that an LGT event has happened, it is often much more difficult to infer its directionality and timing. The menaquinone/phylloquinone gene cluster is more complicated than that of *rbcL* because the origins of both the plastid and nuclear genes of a single gene family must be taken into consideration. Even if we take the Men protein tree topologies at face value, there are still several ways to interpret the results and in many cases it is not easy to say which interpretation is the most likely. Although the MenA and MenG sequences in green plants are sister to the cyanobacterial counterparts, green plant MenA sequences branch within the most distal subclade of the cyanobacterial clade, in contrast to the early divergence of green plant MenG sequences from cyanobacterial clades (Gross et al. 2008). Is this due to phylogenetic artifacts and problems associated with missing data? Or does it suggest that one (or both) of these genes were acquired from free-living or symbiotic cyanobacteria independently of endosymbiosis, rather than from the actual cyanobacterial progenitor of the plastid?

Consider the possibility that the ancestral cyanobacterial genome possessed *men* cluster genes that were closely related to the genes in the extant Chlorobi/Gammaproteobacteria. After primary endosymbiosis, while the ancestral *men* genes were retained by the plastid progenitor, modern-day cyanobacterial lineages acquired another *men* gene cluster via LGT from a source organism distantly related to cyanobacteria themselves. This would result in the separation of plastid and extant cyanobacterial lineages in phylogenetic trees inferred from present-day sequences (see Figure 2.2B in comparison to 2.2A). Moreover, if the ancestor of green plants acquired the genes from extant cyanobacteria via LGT, the position of the green plants in the tree would change from being the sister clade of Cyanidiales to that of cyanobacteria. In this case, the *men* genes in green plants and extant cyanobacteria would not be orthologous to one another. The question thus becomes which of these scenarios are more likely, two instances of LGT or a 'chimeric ancestor' hypothesis, perhaps with viruses providing both types of gene sets to the ancestral host? There is no clear answer.

The *men* gene cluster analyses of Gross et al. (2008) underscore the fact that it is critical to interpret the data with the background assumptions clearly in mind. Genomic studies have revealed unexpectedly complex histories of cyanobacterial and plastid genes, and researchers have not yet reached a consensus on which cyanobacteria are

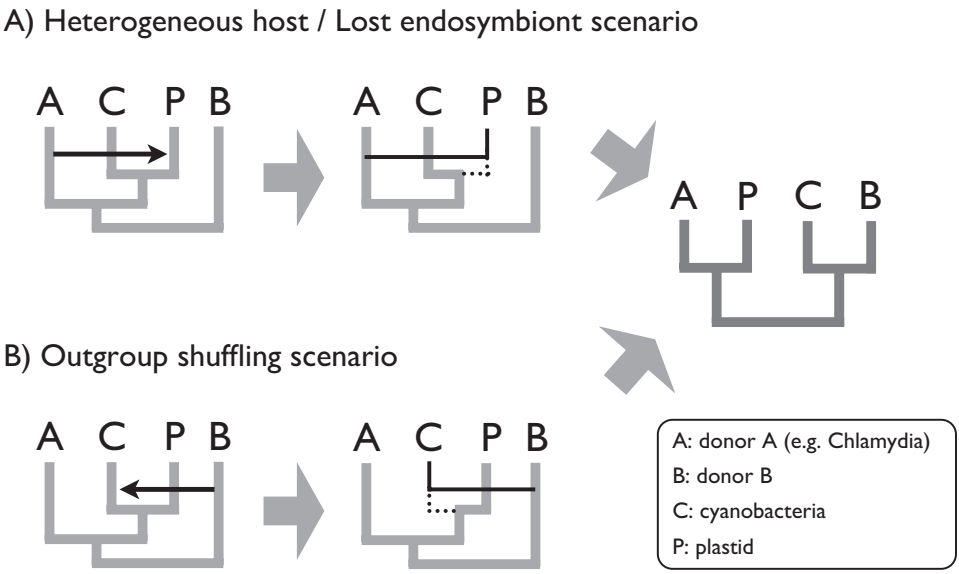

Figure 2.2 Interpreting the origins of non-cyanobacterial genes in plants and algae. The diagram shows two possible scenarios to explain the sisterhood of non-cyanobacterial and plastid-derived genes in phylogenetic analyses. (A) A prokaryotic lineage 'A' established an interactive relationship with a plastid-bearing eukaryote, which is not found today, and donates genes to this eukaryote but not to cyanobacteria. (B) A prokaryotic lineage 'B' donates genes to an ancestral cyanobacterial lineage after the divergence/evolution of plastids. Both schemes are consistent with the known distribution of non-cyanobacterial genes in primary plastid-bearing eukaryotes.

most closely related to plastids, or the extent to which chimerism in the ancestral plastid genome should be invoked to explain the evolution of modern-day organelles. In order to trace the evolutionary path of the *men* gene cluster, we need to unravel the entangled phylogenetic patterns of both plastid and nuclear genes as well as consider the possibility of LGTs among the 'outgroup' prokaryotic genomes. The case of the plastid *rbcL* genes is somewhat simpler, but the same confounding factors still must be considered. In the next section, we review the current debate on the origin of primary plastids, and the difficulties in superimposing primary plastid phylogenies onto the evolutionary history of the nuclear genome.

Archaeplastida: monophyletic, paraphyletic or polyphyletic?

Taxonomic treatment of primary plastid-bearing eukaryotes

Compared to the ancestor of the plastid itself, we have a much less clear picture of what the ancestral host of the primordial plastid must have been like. Land plants and algae were historically classified as separate taxa until a taxonomic scheme unifying them in a single kingdom called Viridiplantae was proposed (Cavalier-Smith 1981). Cavalier-Smith also classified red algae and glaucophytes as belonging to

the Kingdom Biliphyta (phycobilisome-containing algae). Uniting members of the Viridiplantae and Biliphyta, Cavalier-Smith erected the kingdom Plantae as a simpler system only "suitable for very elementary teaching" (Cavalier-Smith 1981). Molecular phylogenies later provided some support for the union of the Plantae (e.g., Moreira et al. 2000). Modern taxonomy often holds that green plants, glaucophytes and red algae represent a monophyletic group and that primary plastids evolved via a single primary endosymbiosis in their common ancestor. Adl et al. coined the term 'Archaeplastida' for the group including these three lineages, noting that its 'plastid' can be "secondarily lost or reduced in some" members (Adl et al. 2005). Thus, in their system, Archaeplastida is not necessarily restricted to phototrophic eukaryotes. As we shall see, phylogenomic studies using multi-gene datasets differ in their support – or lack of support – for Archaeplastida monophyly depending on the dataset used in the analysis (Rodríguez-Ezpeleta et al. 2005; Burki et al. 2008; Hampl et al. 2009; Parfrey et al. 2010).

Primary plastid-bearing eukaryotes share many common cellular and genomic features, but each of the three lineages also possess their own distinctive suite of characteristics. For example, green plants use the photosynthetic pigment chlorophyll *b* as an antenna pigment, in contrast to the phycobilins found in cyanobacteria, glaucophytes and red algae (Kim and Archibald 2009). Red algae possess the above-mentioned non-cyanobacterial RuBisCO enzyme, and glaucophyte plastids are unique in their retention of a peptidoglycan wall, as found in extant cyanobacteria but not in other algae (Löffelhardt and Bohnert 2004). How these distinctive characters should be interpreted in light of plastid evolution is a topic of ongoing debate.

How many times did primary plastids arise?

Various hypotheses for the origin of primary plastids are summarized in Figure 2.1. Four basic hypotheses are presented in the context of a hypothetical eukaryotic tree with primary plastid-bearing eukaryotes occupying different positions. As we shall see, the position of the root on these trees is important for interpreting the distribution of plastids. Figure 2.1A depicts the most popular and currently prevailing scenario, i.e., that all primary plastids originated only once from the single primary endosymbiosis, in the common ancestor of a monophyletic clade of primary plastid-bearing eukaryotes. In this case, the phylogenies of plastids and host nuclei should be congruent with one another. Scenario B (Figure 2.1B) shows the same relationship between the three primary plastid-bearing lineages but invokes separate acquisitions of plastids. Under this view, any plastid-associated characteristic shared by the three lineages is assumed to be due to convergence or non-vertical inheritance. In Figure 2.1C, three primary plastid-bearing lineages reside in separate clades, but the plastids originated from a common ancestor. Scenario C thus holds that multiple plastid loss events occurred independently in plastid-lacking lineages, the host components of which share the same origin with those of the non-monophyletic ('paraphyletic') primary plastid-bearing eukaryotes. Finally, in Figure 2.1D, three lineages of primary plastids were acquired independently in separate eukaryotic lineages, resulting in the polyphyletic distribution of the primary plastid-bearing eukaryotes. Scenario D does not necessarily entail consistency between plastid and host nuclear gene phylogenies.

It has been argued that a single origin of plastids is more parsimonious than the independent evolution of two or three similar organelles from very similar (or essentially identical) sources (McFadden 2001; Palmer 2003). In addition to similarities in plastid gene content and genome structure, the nuclear genomes of primary plastid-bearing eukaryotes also encode several plastid-associated post-endosymbiotic 'inventions', such as non-cyanobacterial Calvin cycle enzymes and specific components of the plastid protein import machinery that lack obvious homologs in present-day cyanobacteria (Palmer 2003; Howe et al. 2008). In the context of a 'multiple origins' hypothesis, such features must be explained by convergent evolution, which is less parsimonious. However, even the most ardent proponents of Scenario A would acknowledge that, no matter how many plastid-associated similarities we find between the three primary plastid-bearing lineages, it is very difficult to say with absolute confidence that these similarities are not the result of convergence in the context of Scenario B (see Palmer 2003; Stiller et al. 2003; Stiller 2007 and references therein for discussion). Indeed, if primary endosymbioses were 'common' during the early stages of plastid evolution, Scenario B is certainly plausible. One might argue that it is unlikely because, if primary endosymbiosis was and is frequent, primary plastids should be found in numerous distantly related eukaryotic lineages, as depicted in Scenario D. Others might prefer a broad distribution of plastids but maintain a single origin, necessitating frequent loss of plastids, as in Scenario C.

It is problematic to invoke multiple primary plastid origins from similar cyanobacterial groups (Raven 1970) because the 'distinctness' of such groups is neither verifiable nor falsifiable from the currently available data (McFadden 2001; Larkum et al. 2007; Howe et al. 2008). As mentioned above, although the three lineages of primary plastids share a large number of common features with one another, they also possess lineage-specific characteristics at the genomic (e.g., non-cyanobacterial *rbcLS* in red algae) and biochemical level (e.g., chlorophyll *b* in green plants and phycobilins in red and glaucophyte algae) (Kim and Archibald 2009). To what extent can these lineage-specific features be taken as evidence for independent plastid acquisitions? Howe et al. have emphasized the importance of "finding a prokaryotic lineage that broke up the monophyletic plastid group" in plastid-related gene phylogenies to "refute the monophyletic hypothesis" (Howe et al. 2008). Nonetheless, even if such a prokaryote were to be found, plastid-associated characters (both genomic and biochemical) would not reliably distinguish between scenarios B and D.

The above discussion highlights the fact that inferring the origin of plastids is highly dependent on the phylogeny of the plastid and host lineages, which are distinct but inseparable, as well as the frequency of plastid gain and loss. Primary endosymbiosis is often considered to be an extremely rare evolutionary event because it is so 'difficult' to establish translocation systems for metabolites and nuclear-encoded plastid-targeted proteins (Cavalier-Smith 1982; McFadden and van Dooren 2004). Complete loss of primary plastids is also assumed to be 'rare' because these organelles are the site of important biochemical processes such as fatty acid biosynthesis (Cavalier-Smith 1999); examples of primary plastid loss have not been uncovered to date. Nonetheless, this 'rare gain/loss' argument and the 'single origin' hypothesis pose a risk of circular reasoning, and should be considered separately.

Rooting the tree of eukaryotes is also critical to understanding plastid evolution. For the sake of consistency, each of the four schemes in Figure 2.1 has the root in

the same position. However, in Figure 2.1A, for example, if the root turned out to be wrong and was in fact within primary plastid-bearing eukaryotes, the monophyletic clade would be separated into multiple basally-branching clades. To our knowledge, no data have thus far excluded the possibility that primary plastid-bearing eukaryotes are the most basal eukaryotes. One popular rooting of the eukaryotic tree is between unikonts (animals, fungi, choanoflagellates and amoebozoans) and bikonts (all other eukaryotes), but this is still controversial (Stechmann and Cavalier-Smith 2002, 2003; Richards and Cavalier-Smith 2005; Roger and Simpson 2009; Cavalier-Smith 2010).

The 'cyanelle' of glaucophytes retains ancestral features but is not an ancient plastid

In terms of cellular level heterogeneity, the plastid of glaucophytes is significant in that it possesses a layer of peptidoglycan between its outer and inner envelopes (Löffelhardt and Bohnert 2004). This distinctive feature, together with the carboxisome-like pyrenoid structure recognized in some glaucophyte species, has been interpreted as evidence that the glaucophyte plastid is an evolutionary 'coelacanth', retaining ancestral characters found in cyanobacteria but not in the other two primary plastid-bearing lineages (Fathinejad et al. 2008). This situation is reminiscent of the mitochondrial genome of the excavate protist *Reclinomonas americana*. The *R. americana* mitochondrial genome is unusually gene-rich and retains several genes encoding prokaryotic RNA polymerase subunits, which have been lost in all other mitochondrial genomes examined to date (Lang et al. 1997). This ancestral (genomic) character indicates that the *R. americana* genome is 'conservative' in its gene repertoire, but does not necessarily mean that this organism truly belongs to an early branching eukaryotic lineage.

In the case of glaucophytes, even though the plastid peptidoglycan wall is very likely of cyanobacterial origin, in and of itself this morphological character tells us little about when and how glaucophytes diverged from other primary plastid-bearing eukaryotes. In fact, sequencing of the plastid genome of the glaucophyte *Cyanophora paradoxa* revealed that its size and gene composition are not 'primitive' at all but similar to those of red and green algae (Ohta et al. 2003). Moreover, genes encoding enzymes functioning in peptidoglycan wall synthesis have been shown to be essential to the maintenance of plastids in the moss *Physcomitrella patens* (Machida et al. 2006). This suggests that the peptidoglycan wall might not be a plesiomorphic character retained only in glaucophytes but one that is also conserved in some plants (Takano and Takechi 2010). Seen in this light, use of the terms cyanelle or muroplast in reference to the glaucophyte plastid is somewhat misleading (Table 2.1).

Some phylogenetic analyses of plastid- and nuclear-encoded proteins suggest that glaucophytes are the earliest diverging among the three primary plastid-bearing eukaryotic lineages (e.g., Rodríguez-Ezpeleta et al. 2005; Reyes-Prieto and Bhattacharya 2007b). However, a recent comparative analysis observed an early branching of green algae and land plants in phylogenies of plastid genes and plastid-derived nuclear genes (Deschamps and Moreira 2009). In addition, Deschamps and Moreira provided evidence for 'signal conflict' between the plastid-derived nuclear genes and resident host nuclear

genes, the latter of which favor the early branching of glaucophytes (Deschamps and Moreira 2009). It has also been shown that the 'model' glaucophyte *C. paradoxa* possesses a nuclear-encoded cyanobacterial-like class II fructose bisphosphate aldolase (FBA), in contrast to green and red algae, which possess a class I plastid-targeted enzyme which was thought to have been originally acquired through duplication of the cytosolic enzyme (Rogers and Keeling 2004). Under the scenario of an early branching glaucophyte lineage, one possible explanation for the distribution of FBA is duplication of class I enzymes after the divergence of glaucophytes followed by selective loss of class II enzymes in green plants and red algae. However, a more complicated explanation is needed if green algae, not glaucophytes, diverged first (Deschamps and Moreira 2009). Although most of the above-mentioned phylogenetic studies assume the monophyly of primary plastid-bearing eukaryotes as depicted in Figure 2.1A, the apparent conflicting signals (e.g., Deschamps and Moreira 2009) might be more consistent with one of the alternate schemes shown in Figure 2.1. More data from glaucophytes are needed for evaluating various hypotheses for the branching pattern of primary plastid-bearing eukaryotes.

Do rare gene replacements support the single origin of primary plastid-bearing eukaryotes?

An alternative approach to investigating the 'how-many-origins?' question for plastids is to consider the distribution of rare genomic characters (Rokas and Holland 2000). Examination of metabolic pathways in plants and algae has shown that while many nuclear genes encoding plastid-localized enzymes are of cyanobacterial origin, others are not (Martin et al. 2002; Suzuki and Miyagishima 2010). Such mosaicism is the result of the complexities of EGT. Algal nuclear genomes have incorporated many plastid-derived genes that encode plastid-targeted proteins, but in some cases non-cyanobacterial genes have been co-opted for this purpose. For example, Martin and Schnarrenberger (1997) showed that Calvin cycle enzymes in the flowering plant *Arabidopsis* are a mosaic of proteins of both cyanobacterial and non-cyanobacterial origin (Martin and Schnarrenberger 1997). Significantly, a similar pattern was also seen in the red alga *Cyanidioschyzon* (Matsuzaki et al. 2004) and in glaucophytes (Reyes-Prieto and Bhattacharya 2007a). If primary plastids evolved multiple times, a similar pattern of mosaicism would not be expected. Thus the overall similarity of the evolutionary origins of Calvin cycle genes in primary plastid-bearing eukaryotes would seem to favor a single origin of primary plastids. Under such a scenario, the most likely explanation for the complex gene ancestries discussed above for *rbcLS* and *FBA* is LGT and/or gene duplication events followed by differential losses, rather than independent acquisitions of similar but distinct endosymbionts (Reyes-Prieto and Bhattacharya 2007a).

Phylogenetic analyses of haem biosynthesis enzymes also illustrate a shared mosaic pattern in primary plastid-bearing eukaryotes, whereby some genes are of non-cyanobacterial origin while most are cyanobacterial (Obornik and Green 2005). In this case, separation of proteobacterial-like ferrochelatase sequences in red algae from cyanobacterial-like counterparts in green plants and diatoms was interpreted as a result of LGT. Finally, the heterogeneous composition of the multi-protein translocons of the inner and

outer envelope membranes of plastids (McFadden and van Dooren 2004), the 'phased-in' distribution of single-, double- and triple-helix proteins of the light-harvesting complex antenna protein superfamily (Durnford et al. 1999; Engelken et al. 2010) and the mosaic origins of the plastid solute transporters (Tyra et al. 2007) are all important innovations that must have occurred early in the evolution of the plastid. Accordingly, they have been interpreted as evidence supporting the common ancestry of primary plastids.

What about alternative scenarios? Is it possible that primary plastids evolved three times independently (Figure 2.1B and 2.1D) but that the process of EGT and replacement was constrained such that similar patterns of gene mosaicism arose multiple times independently? As noted by Palmer in 2003, 'the overall weight of evidence continues' 'to strongly favor a monophyletic origin of primary plastids' but 'this issue should not be considered settled' (Palmer 2003). New data could conceivably change our view on the 'weight of evidence' by providing insight into what 'constraints' could lead to similar patterns of gene mosaicism. Cryptic LGT (or EGT) between separate lineages could also explain shared patterns of mosaicism. Little is known about the fine details of plastid-to-nucleus gene transfer and the factors determining which genes are lost and replaced by host–derived versions. In the following section, we review recent studies on the extent to which genes derived from non-cyanobacterial prokaryotes have contributed to the nuclear genomes of primary plastid-bearing eukaryotes, and discuss what these data can tell us about the early evolution of algal genomes and cells.

Impact of EGT on the nuclear genomes of primary plastid-bearing eukaryotes

Plastid-to-nucleus gene transfer and its implications

Analyses of whole genome and transcriptome sequence data from 'model' organisms belonging to each of three primary plastid-bearing lineages (the land plant *Arabidopsis*, the green alga *Chlamydomonas*, the red alga *Cyanidioschyzon* and the glaucophyte *Cyanophora*) suggest that the contribution of cyanobacterial endosymbionts to the nuclear genome varies from organism to organism but is consistently significant (Martin et al. 2002; Sato et al. 2005; Reyes-Prieto et al. 2006; Moustafa and Bhattacharya 2008). Furthermore, these analyses suggest that many cyanobacterial-derived genes might encode proteins that function in the cytosol rather than in plastids (Martin et al. 2002). This was an unexpected result, contrary to what would be expected under the so-called 'product specificity corollary' (Weeden 1981), whereby organelle-derived genes encode proteins that are targeted to the organelle post-translationally. This scenario implicitly postulates that most nuclear-encoded, organelle-targeted proteins are derived from endosymbionts and were retained in the nuclear genome because they were important for plastid function. It is difficult to compare the analyses of plastid-to-nucleus EGT in *Arabidopsis* (Martin et al. 2002), *Chlamydomonas* (Moustafa and Bhattacharya 2008), *Cyanidioschyzon* (Matsuzaki et al. 2004) and *Cyanophora* (Reyes-Prieto et al. 2006) due to differences in data quality and analytical method. Nevertheless, these studies clearly indicate that the impact of EGT on the host nuclear genome is complex, well beyond a simple subtraction of the plastid proteome from the core proteins of extant cyanobacteria (Lane and Archibald 2008).

Chlamydia: A 'lost endosymbiont' predating or concomitant with the cyanobacterial endosymbiosis?

The discovery of a number of plant/algal-like genes in the genome of the human bacterial pathogen *Chlamydia* led to another turn in the debate on the origin of primary plastids (Stephens et al. 1998; Brinkman et al. 2002). Huang and Gogarten examined the phylogeny of these 'plant-like' chlamydial genes and proposed a hypothesis whereby the ancestor of primary plastid-bearing eukaryotes once possessed a chlamydial endosymbiont prior to the acquisition of the cyanobacterial ancestor of plastids (Huang and Gogarten 2007). A total of 55 putative *Chlamydia*-derived genes were subsequently identified in plant/algal nuclear genomes by Moustafa et al. (2008). These authors emphasized the probable mixotrophic nature of the ancestor of primary plastid-bearing eukaryotes, and postulated the concomitant existence of chlamydial and cyanobacterial endosymbionts in the ancestral host (Moustafa et al. 2008). Becker et al. independently found 39 chlamydial genes in the genomes of primary plastid-bearing eukaryotes and interpreted them as supporting the 'lost endosymbiont' hypothesis (Becker et al. 2008).

Beyond the fact that different investigations have produced different estimates of the number of chlamydial genes identified (Huang and Gogarten 2007; Becker et al. 2008; Moustafa et al. 2008), these studies underscore the challenges associated with data interpretation. To what extent can we reliably infer the existence of past endosymbiotic events from genome sequences when no organelle or endosymbiont remains? Since chlamydial genes have thus far not been found in plastid genomes, interpretation is more complicated. To what extent is it possible to know whether a nuclear chlamydial-like gene was acquired before or after the cyanobacterial endosymbiosis, mediated via EGT or transferred via LGT directly from free-living bacteria to the host nucleus?

Heterogeneous origins of nuclear-encoded organelle-targeted proteins

The discovery of chlamydial-like genes in the nuclear genomes of primary plastid-bearing eukaryotes is reminiscent of previous studies on the origins of mitochondrion-localized proteins. It is well established that mitochondria are derived from an alphaproteobacterial-like endosymbiont (Gray 1992; Esser et al. 2004). The mitochondrial genome of modern-day aerobic eukaryotes possesses <10% of the 1,000+ genes it must once have possessed. However, phylogenomic studies revealed that many of the nuclear-encoded, mitochondrion-targeted proteins appear not to be closely related to the hypothesized endosymbiont (Gabaldón and Huynen 2007; Szklarczyk and Huynen 2010). Many of the genes present in the bacterial progenitor of the mitochondrion are argued to have been lost and replaced by genes that already existed in the nuclear genome or had been acquired by LGT (Szklarczyk and Huynen 2010).

A similar pattern appears to exist in plastids. Suzuki and Miyagishima (2010) employed a phylogenomics approach similar to that used in the chlamydial gene mining studies cited above together with consideration of proteomic data of land plant plastids (Suzuki and Miyagishima 2010). These authors found that ~20% of the plastid proteome common to green algae/plants and red algae is in fact most closely related to non-cyanobacterial prokaryotes (including Chlamydia and various proteobacteria), and hypothesized that plastid function has been complemented by 'metagenomic' material

derived from a variety of bacteria other than the ancestral plastid and nucleus. In a sense, this study integrates the previous chlamydial 'lost endosymbiont' argument into a larger framework of host genome heterogeneity towards the goal of evaluating environmental and endosymbiotic bacterial contributions to eukaryotic genomes.

Here again, however, we are faced with the difficulty of inferring the past using the genomes of extant organisms. If a canonical plastid-targeted protein is found to be of non-cyanobacterial affinity, most researchers prefer an explanation whereby its gene replaced an original endosymbiont-derived homolog. A similar trend can be seen in the debate on the origin of mitochondria. In these cases, the recipient (i.e., the host) is seen as flexible and plastic, while the bacterial donor taxa are seen as 'fixed'. This is a reasonable assumption in that an organism capable of accommodating endosymbionts and their genes (i.e., the eukaryotic host) is also likely to be taking up foreign genes from other organisms. However, it is useful to consider whether we would reach the same conclusion if we consider the possibility that bacterial genomes have been continuously shuffled by LGT over time.

Extant cyanobacteria and the plastid ancestor

In the simplest of terms, if all the genes encoding plastid-localized proteins are derived from the cyanobacterial progenitor of the plastid, then the existence of non-cyanobacterial nuclear genes for plastid-targeted proteins (Huang and Gogarten 2007; Becker et al. 2008; Moustafa et al. 2008; Suzuki and Miyagishima 2010) would indicate that the common ancestor of extant cyanobacteria was significantly influenced by LGT and gene loss after the divergence of the ancestor of plastids. Figure 2.2 shows a schematic representation of two interpretations of LGT in the context of an unrooted gene/protein tree. The 'heterogeneous origins' scenario is simpler in that the phylogenetic pattern is taken at face value and includes fewer assumptions on the unidentified gene exchanges within the outgroup taxa (Figure 2.2A). But this is true only when we assume that it is better to consider that the relationships among the outgroup lineages as being stable (i.e., retained since the birth of the plastid). In light of ample evidence for rampant LGT between prokaryotes throughout evolution (Doolittle 1999; Zhaxybayeva et al. 2006; Dagan and Martin 2009), this is probably unrealistic. One could argue that this 'heterogeneous origins' hypothesis is an artifact of underestimating the flow of LGT among the outgroup lineages, and that 'lineage A' can be positioned next to the plastid genes due to LGT from another non-cyanobacterial 'lineage B' to modern-day cyanobacteria (Figure 2.2B). Here it is critical to evaluate the extent to which cyanobacteria have been influenced by LGT before and after the evolution of plastids. The observation that plastid genes are more homogeneous in origin than nuclear genes seems to favor an interpretation that cyanobacteria (and the plastid progenitor) were less significantly impacted than eukaryotic nuclear genomes (Suzuki and Miyagishima 2010). Nonetheless, most of the plastid genes encode proteins for photosynthesis and translation machinery, suggesting that functional constraints might have acted as a 'barrier' of LGT between modern-day cyanobacteria and other donor lineages (Jain et al. 1999; Race et al. 1999).

Overall, we know little about which aspects of past evolutionary events we can, and cannot, accurately reconstruct from genomic data. This unsettled question awaits future

exploration of the mechanisms of gene exchange (e.g., LGT) from different perspectives. Gene phylogenies are one thing, but genome phylogenies are another. It is widely accepted from the viewpoints of morphology, biochemistry and genomic analyses that the mitochondrion originated from an alphaproteobacterial-like endosymbiont and plastids from cyanobacterial-like prokaryotes. Molecular phylogenetics has provided enormous amounts of data and a more quantitative way of inferring the history of genes of interest. 'Phylogenomic' studies attempt to combine the gene data as much as possible to reconstruct the history of the genome, assuming that the genome of an organism is by and large homogeneous in origin. When a genome is small in size and relatively homogeneous, like plastid genomes, most researchers are comfortable with a simple explanation that entails a general trend with only minor exceptions. With time, however, an increasing number of 'exceptions' have arisen, and the same question again emerges: how do we interpret the evolution of algal cells from mutually conflicting data? Organelle genomes are still a puzzle, but nuclear genomes represent an even greater challenge. As data accumulate year by year, we need to be more flexible in interpreting them.

Plastid loss

The phagotrophic ancestry of algae

Figure 2.1 illustrates the importance of considering the evolution of plastids and host nuclear lineages separately in our efforts to infer the evolutionary history of phototrophic eukaryotes. As mentioned above, it was originally believed that the morphological features of primary plastid-bearing eukaryotes were not convincing enough to unite them as a single taxonomic group (Cavalier-Smith 1981). Although analyses of single nuclear genes were inconclusive (Douglas 1998), concatenated nuclear gene trees have lent some support to the monophyletic positioning of primary plastid-bearing eukaryotes (Moreira et al. 2000), leading to a proposal of the taxonomic group Archaeplastida (Adl et al. 2005). As genomic information has accumulated, resolving the eukaryotic tree of life by large-scale phylogenomic analysis using more than 100 genes has been actively pursued. However, as is the case with single gene trees, some concatenated gene trees support the monophyly of primary plastid-bearing eukaryotes (Rodríguez-Ezpeleta et al. 2005; Burki et al. 2008) while others do not (Hampl et al. 2009; Parfrey et al. 2010). In addition, it has been shown that trees constructed using only the most slowly evolving genes result in a non-monophyletic topology of primary plastid-bearing eukaryotes (Nozaki et al. 2009).

These results clearly show that different methods and data reveal different kinds of evolutionary signals in the nuclear genomes of algae and plants (Deschamps and Moreira 2009), suggesting that taxon sampling and analytical methods need to be taken seriously. Regardless, it is worth considering what the non-monophyly of primary plastid-bearing eukaryotes would actually mean. Would it indicate that primary plastids were lost in some lineages? This would be true if we assume a single origin of primary plastids (Figure 2.1C), but not necessarily if multiple origins are invoked (Figure 2.1D). Plastid loss and the loss of photosynthetic ability should also clearly be distinguished (Keeling 2010). While several primary plastid-bearing eukaryotes have secondarily become non-photosynthetic, no instances of complete plastid loss within red, green and glaucophyte algae are known to date (Chen et al. 2009). This observation speaks to the

general importance of plastids for their hosts beyond photosynthesis, but it is difficult to evaluate how (and how often) plastids could conceivably have been lost without a more detailed understanding of plastid functions and the full extent of their integration with eukaryotic cellular metabolism (Kořený and Oborník 2011).

It is generally believed that the ancestors of early eukaryotic phototrophs retained a prey cyanobacterial prokaryote as an endosymbiont instead of digesting it, ultimately giving rise to the primary plastid (Reyes-Prieto et al. 2007). It seems likely that this ancestor would have continued on with its phagotrophic lifestyle for a period of time after the establishment of the plastid progenitor, ingesting diverse organisms in addition to cyanobacteria. Some of these mixotrophic ancestors might have lost their cyanobacteria/plastids; it might have been more energetically 'expensive' to maintain photosynthetic endosymbionts than to hunt prey organisms, the environment might have been sufficiently nutrient-rich such that these ancestors could live on their own without endosymbionts, or it might have simply been accidental. The life cycle of the peculiar katablepharid protist *Hatena*, in which after cell division one daughter cell maintains a green algal endosymbiont while the other loses it and needs to engulf another endosymbiont, has been suggested to serve as an analogy to this situation (Okamoto and Inouye 2005). If the daughter cells of *Hatena* were to evolve into two independent lineages, one photosynthetic and one aplastidic, it would be difficult to tell that both were derived from a photosynthetic ancestor.

Is the eukaryotic tree of life really a tree?

It is possible that organisms currently classified as non-photosynthetic protists will turn out to be plastid-lacking lineages that evolved from a primary plastid-bearing eukaryote. However, this is currently very difficult to confirm or refute. Such a plastid-lacking lineage would, by definition, be phenotypically similar to a protist that has never experienced primary endosymbiosis, and the only available data with which to distinguish between these two possibilities is genomic data. As we have seen, analyses of such sequences often fail to provide decisive answers. It is now clear that eukaryotic genomes have been significantly influenced by LGT from prokaryotes and other eukaryotes (Keeling and Palmer 2008), many of which appear to be completely independent of plastid evolution (Friesen et al. 2006; Simpson et al. 2008). Tree topologies inferred using multi-gene datasets from the whole of eukaryotes are often difficult to interpret and accumulating data suggest that LGT might be too rampant to cleanly resolve the puzzle of mosaicism (Lane and Archibald 2008). Whether or not 'plastid-lacking algae' are ultimately shown to exist depends on which scheme in Figure 2.1 is most likely (Maruyama et al. 2009).

Given the evidence for extensive nuclear genome mosaicism, is a tree a suitable representation of the evolutionary history of eukaryotes? If so, what is the rationale for it? While the concept of a tree is useful in taxonomy, it clearly has its limits when it comes to representing the evolutionary processes driving the evolution of algae and their organelles (Lane and Archibald 2008). Debate continues on the existence of a prokaryotic tree of life. Some prefer a pattern of tree-like evolution represented by 'core' genes (Ciccarelli et al. 2006; Shi and Falkowski 2008) while others favor a web-like representation of life, a complex reticulation driven by rampant LGT (Doolittle 1999; Dagan and

Martin 2009; Haggerty et al. 2009). In the case of eukaryotes, we should keep questioning what a 'tree' should look like and how it should be represented.

Acknowledgements

Comparative genomics research in the Archibald laboratory is supported by the Canadian Institutes of Health Research (CIHR), the Natural Sciences and Engineering Research Council of Canada, and Dalhousie University's Centre for Comparative Genomics and Evolutionary Bioinformatics. S.M. is supported by JSPS Postdoctoral Fellowships for Research Abroad from the Japan Society for the Promotion of Science and J.M.A. is a Scholar of the Canadian Institute for Advanced Research, Program in Integrated Microbial Biodiversity. J.M.A. is also the recipient of a CIHR New Investigator Award.

References

Adl, S.M., A.G.B. Simpson, M.A. Farmer, R.A. Andersen, O.R. Anderson, J.R. Barta*, et al.* 2005. The new higher level classification of eukaryotes with emphasis on the taxonomy of protists. *J. Eukaryot. Microbiol. 52*: 399–451.

Archibald, J.M. 2009a. The origin and spread of eukaryotic photosynthesis: evolving views in light of genomics. *Bot. Mar. 52*: 95–103.

Archibald, J.M. 2009b. The puzzle of plastid evolution. *Curr. Biol. 19*: R81–88.

Becker, B., K. Hoef-Emden, and M. Melkonian. 2008. Chlamydial genes shed light on the evolution of photoautotrophic eukaryotes. *BMC Evol. Biol. 8*: 203.

Brinkman, F.S.L., J.L. Blanchard, A. Cherkasov, Y. Av-Gay, R.C. Brunham, R.C. Fernandez*, et al.* 2002. Evidence that plant-like genes in *Chlamydia* species reflect an ancestral relationship between Chlamydiaceae, cyanobacteria, and the chloroplast. *Genome Res. 12*: 1159–1167.

Burki, F., K. Shalchian-Tabrizi, and J. Pawlowski. 2008. Phylogenomics reveals a new 'megagroup' including most photosynthetic eukaryotes. *Biol. Lett. 4*: 366–369.

Cai, X., A.L. Fuller, L.R. McDougald, and G. Zhu. 2003. Apicoplast genome of the coccidian *Eimeria tenella. Gene 321*: 39–46.

Cavalier-Smith, T. 1981. Eukaryote kingdoms: seven or nine? *Biosystems 14*: 461–481.

Cavalier-Smith, T. 1982. The origins of plastids. *Biol. J. Linn. Soc. 17*: 289–306.

Cavalier-Smith, T. 1999. Principles of protein and lipid targeting in secondary symbiogenesis: euglenoid, dinoflagellate, and sporozoan plastid origins and the eukaryote family tree. *J. Eukaryot. Microbiol. 46*: 347–366.

Cavalier-Smith, T. 2010. Kingdoms Protozoa and Chromista and the eozoan root of the eukaryotic tree. *Biol. Lett. 6*: 342–345.

Chen, Y., T. Asano, M.T. Fujiwara, S. Yoshida, Y. Machida, and Y. Yoshioka. 2009. Plant cells without detectable plastids are generated in the crumpled leaf mutant of *Arabidopsis thaliana. Plant Cell Physiol. 50*: 956–969.

Ciccarelli, F.D., T. Doerks, C. von Mering, C.J. Creevey, B. Snel, and P. Bork. 2006. Toward automatic reconstruction of a highly resolved tree of life. *Science 311*: 1283–1287.

Criscuolo, A., and S. Gribaldo. 2011. Large-scale phylogenomic analyses indicate a deep origin of primary plastids within Cyanobacteria. *Mol. Biol. Evol. 28*: 3019–3032.

Dagan, T., and W. Martin. 2009. Getting a better picture of microbial evolution en route to a network of genomes. *Philos. Trans. R. Soc. Lond., B, Biol. Sci. 364*: 2187–2196.

Delwiche, C.F., and J.D. Palmer. 1996. Rampant horizontal transfer and duplication of rubisco genes in eubacteria and plastids. *Mol. Biol. Evol. 13*: 873–882.

Deschamps, P., and D. Moreira. 2009. Signal conflicts in the phylogeny of the primary photosynthetic eukaryotes. *Mol. Biol. Evol. 26*: 2745–2753.

Deusch, O., G. Landan, M. Roettger, N. Gruenheit, K.V. Kowallik, J.F. Allen*, et al.* 2008. Genes of cyanobacterial origin in plant nuclear genomes point to a heterocyst-forming plastid ancestor. *Mol. Biol. Evol. 25*: 748–761.

Donaher, N., G. Tanifuji, N.T. Onodera, S.A. Malfatti, P.S.G. Chain, Y. Hara*, et al.* 2009. The complete plastid genome sequence of the secondarily nonphotosynthetic alga *Cryptomonas paramecium*: reduction, compaction, and accelerated evolutionary rate. *Genome Biol. Evol. 2009*: 439–448.

Doolittle, W.F. 1999. Phylogenetic classification and the universal tree. *Science 284*: 2124–2129.

Douglas, S.E. 1998. Plastid evolution: origins, diversity, trends. *Curr. Opin. Genet. Dev. 8*: 655–661.

Durnford, D.G., J.A. Deane, S. Tan, G.I. McFadden, E. Gantt, and B.R. Green. 1999. A phylogenetic assessment of the eukaryotic light-harvesting antenna proteins, with implications for plastid evolution. *J. Mol. Evol. 48*: 59–68.

Engelken, J., H. Brinkmann, and I. Adamska. 2010. Taxonomic distribution and origins of the extended LHC (light-harvesting complex) antenna protein superfamily. *BMC Evol. Biol. 10*: 233.

Esser, C., N. Ahmadinejad, C. Wiegand, C. Rotte, F. Sebastiani, G. Gelius-Dietrich*, et al.* 2004. A genome phylogeny for mitochondria among alpha-proteobacteria and a predominantly eubacterial ancestry of yeast nuclear genes. *Mol. Biol. Evol. 21*: 1643–1660.

Falcón, L.I., S. Magallón, and A. Castillo. 2010. Dating the cyanobacterial ancestor of the chloroplast. *ISME J. 4*: 777–783.

Fathinejad, S., J.M. Steiner, S. Reipert, M. Marchetti, G. Allmaier, S.C. Burey*, et al.* 2008. A carboxysomal carbon-concentrating mechanism in the cyanelles of the 'coelacanth' of the algal world, *Cyanophora paradoxa*? *Physiol. Plant. 133*: 27–32.

Friesen, T.L., E.H. Stukenbrock, Z. Liu, S. Meinhardt, H. Ling, J.D. Faris*, et al.* 2006. Emergence of a new disease as a result of interspecific virulence gene transfer. *Nat. Genet. 38*: 953–956.

Fujita, K., S. Ehira, K. Tanaka, K. Asai, and N. Ohta. 2008a. Molecular phylogeny and evolution of the plastid and nuclear encoded *cbbX* genes in the unicellular red alga *Cyanidioschyzon merolae. Genes. Genet. Syst. 83*: 127–133.

Fujita, K., K. Tanaka, Y. Sadaie, and N. Ohta. 2008b. Functional analysis of the plastid and nuclear encoded CbbX proteins of *Cyanidioschyzon merolae. Genes. Genet. Syst. 83*: 135–142.

Funes, S., A. Reyes-Prieto, X. Pérez-Martínez, and D. González-Halphen. 2004. On the evolutionary origins of apicoplasts: revisiting the rhodophyte vs. chlorophyte controversy. *Microbes Infect. 6*, 305–311.

Gabaldón, T., and M.A. Huynen. 2007. From endosymbiont to host-controlled organelle: the hijacking of mitochondrial protein synthesis and metabolism. *PLoS Comput. Biol. 3*: e219.

Gockel, G., and W. Hachtel. 2000. Complete gene map of the plastid genome of the nonphotosynthetic euglenoid flagellate *Astasia longa. Protist 151*: 347–351.

Gould, S.B., R.F. Waller, and G.I. McFadden. 2008. Plastid evolution. *Annu. Rev. Plant Biol. 59*: 491–517.

Gray, M.W. 1992. The endosymbiont hypothesis revisited. *Int. Rev. Cytol. 141*: 233–357.

Gross, J., J. Meurer, and D. Bhattacharya. 2008. Evidence of a chimeric genome in the cyanobacterial ancestor of plastids. *BMC Evol. Biol. 8*: 117.

Haggerty, L.S., F.J. Martin, D.A. Fitzpatrick, and J.O. McInerney. 2009. Gene and genome trees conflict at many levels. *Philos. Trans. R. Soc. Lond., B, Biol. Sci. 364*: 2209–2219.

Hampl, V., L. Hug, J.W. Leigh, J.B. Dacks, B.F. Lang, A.G.B. Simpson*, et al.* 2009. Phylogenomic analyses support the monophyly of Excavata and resolve relationships among eukaryotic "supergroups". *Proc. Natl. Acad. Sci. USA 106*: 3859–3864.

Howe, C.J., A.C. Barbrook, R.E.R. Nisbet, P.J. Lockhart, and A.W.D. Larkum. 2008. The origin of plastids. *Philos. Trans. R. Soc. Lond., B, Biol. Sci. 363*: 2675–2685.

Huang, J., and J.P. Gogarten. 2007. Did an ancient chlamydial endosymbiosis facilitate the establishment of primary plastids? *Genome Biol. 8*: R99.

Jain, R., M.C. Rivera, and J.A. Lake. 1999. Horizontal gene transfer among genomes: the complexity hypothesis. *Proc. Natl. Acad. Sci. USA 96*: 3801–3806.

Janouskovec, J., A. Horák, M. Obornik, J. Lukes, and P.J. Keeling. 2010. A common red algal origin of the apicomplexan, dinoflagellate, and heterokont plastids. *Proc. Natl. Acad. Sci. USA 107*: 10949–10954.

Keeling, P.J. 2010. The endosymbiotic origin, diversification and fate of plastids. *Philos. Trans. R. Soc. Lond., B, Biol. Sci. 365*: 729–748.

Keeling, P.J., and J.D. Palmer. 2008. Horizontal gene transfer in eukaryotic evolution. *Nat. Rev. Genet. 9*: 605–618.

Kim, E., and J.M. Archibald. 2009. Diversity and evolution of plastids and their genomes. *In*: (A.S. Sandelius and H. Aronsson, eds) *The Chloroplast*. Springer, Berlin/Heidelberg. pp. 1–39.

Kořený, L., and M. Oborník. 2011. Sequence evidence for the presence of two tetrapyrrole pathways in *Euglena gracilis. Genome Biol. Evol. 3*: 359–364.

Krause, K. 2008. From chloroplasts to "cryptic" plastids: evolution of plastid genomes in parasitic plants. *Curr. Genet. 54*: 111–121.

Lane, C.E., and J.M. Archibald. 2008. The eukaryotic tree of life: endosymbiosis takes its TOL. *Trends Ecol. Evol. 23*: 268–275.

Lang, B.F., G. Burger, C.J. O'Kelly, R. Cedergren, G.B. Golding, C. Lemieux*, et al.* 1997. An ancestral mitochondrial DNA resembling a eubacterial genome in miniature. *Nature 387*: 493–497.

Larkum, A.W.D., P.J. Lockhart, and C.J. Howe. 2007. Shopping for plastids. *Trends Plant. Sci. 12*: 189–195.

Lau, A.O.T., T.F. McElwain, K.A. Brayton, D.P. Knowles, and E.H. Roalson. 2009. *Babesia bovis*: a comprehensive phylogenetic analysis of plastid-encoded genes supports green algal origin of apicoplasts. *Exp. Parasitol. 123*: 236–243.

Löffelhardt, W., and H. Bohnert. 2004. The cyanelle (muroplast) of *Cyanophora paradoxa*: A paradigm for endosymbiotic organelle evolution. *In*: (J. Seckbach ed) *Symbiosis.* Springer, Netherlands. pp. 111–130.

Machida, M., K. Takechi, H. Sato, S.J. Chung, H. Kuroiwa, S. Takio*, et al.* 2006. Genes for the peptidoglycan synthesis pathway are essential for chloroplast division in moss. *Proc. Natl. Acad. Sci. USA 103*: 6753–6758.

Maier, U.G., M. Fraunholz, S. Zauner, S. Penny, and S. Douglas. 2000. A nucleomorph-encoded CbbX and the phylogeny of RuBisCo regulators. *Mol. Biol. Evol. 17*: 576–583.

Marin, B., E.C.M. Nowack, G. Glöckner, and M. Melkonian. 2007. The ancestor of the *Paulinella* chromatophore obtained a carboxysomal operon by horizontal gene transfer from a *Nitrococcus*-like gamma-proteobacterium. *BMC Evol. Biol. 7*: 85.

Martin, W., T. Rujan, E. Richly, A. Hansen, S. Cornelsen, T. Lins*, et al.* 2002. Evolutionary analysis of *Arabidopsis*, cyanobacterial, and chloroplast genomes reveals plastid phylogeny and thousands of cyanobacterial genes in the nucleus. *Proc. Natl. Acad. Sci. USA 99*: 12246–12251.

Martin, W., and C. Schnarrenberger. 1997. The evolution of the Calvin cycle from prokaryotic to eukaryotic chromosomes: a case study of functional redundancy in ancient pathways through endosymbiosis. *Curr. Genet. 32*: 1–18.

Maruyama, S., M. Matsuzaki, K. Misawa, and H. Nozaki. 2009. Cyanobacterial contribution to the genomes of the plastid-lacking protists. *BMC Evol. Biol. 9*: 197.

Matsuzaki, M., O. Misumi, T. Shin-I, S. Maruyama, M. Takahara, S.-Y. Miyagishima*, et al.* 2004. Genome sequence of the ultrasmall unicellular red alga *Cyanidioschyzon merolae* 10D. *Nature 428*: 653–657.

McFadden, G.I. 2001. Primary and secondary endosymbiosis and the origin of plastids. *J. Phycol. 37*: 951–959.

McFadden, G.I., and G.G. van Dooren. 2004. Evolution: red algal genome affirms a common origin of all plastids. *Curr. Biol. 14*: R514–516.

Morden, C., C.F. Delwiche, M. Kuhsel, and J.D. Palmer. 1992. Gene phylogenies and the endosymbiotic origin of plastids. *Biosystems 28*: 75–90.

Moreira, D., H. Le Guyader, and H. Philippe. 2000. The origin of red algae and the evolution of chloroplasts. *Nature 405*: 69–72.

Moustafa, A., and D. Bhattacharya. 2008. PhyloSort: a user-friendly phylogenetic sorting tool and its application to estimating the cyanobacterial contribution to the nuclear genome of *Chlamydomonas. BMC Evol. Biol. 8*: 6.

Moustafa, A., A. Reyes-Prieto, and D. Bhattacharya. 2008. Chlamydiae has contributed at least 55 genes to Plantae with predominantly plastid functions. *PLoS ONE 3*: e2205.

Nozaki, H., S. Maruyama, M. Matsuzaki, T. Nakada, S. Kato, and K. Misawa. 2009. Phylogenetic positions of Glaucophyta, green plants (Archaeplastida) and Haptophyta (Chromalveolata) as deduced from slowly evolving nuclear genes. *Mol. Phylogenet. Evol. 53*: 872–880.

Obornik, M., and B.R. Green. 2005. Mosaic origin of the heme biosynthesis pathway in photosynthetic eukaryotes. *Mol. Biol. Evol. 22*: 2343–2353.

Obornik, M., J. Janouskovec, T. Chrudimský, and J. Lukes. 2009. Evolution of the apicoplast and its hosts: from heterotrophy to autotrophy and back again. *Int. J. Parasitol. 39*: 1–12.

Ohta, N., M. Matsuzaki, O. Misumi, S.-Y. Miyagishima, H. Nozaki, K. Tanaka*, et al.* 2003. Complete sequence and analysis of the plastid genome of the unicellular red alga *Cyanidioschyzon merolae. DNA Res. 10*: 67–77.

Okamoto, N., and I. Inouye. 2005. A secondary symbiosis in progress? *Science 310*: 287.

Palmer, J.D. 2003. The symbiotic birth and spread of plastids: How many times and whodunit? *J. Phycol. 39*: 4–12.

Parfrey, L.W., J. Grant, Y.I. Tekle, E. Lasek-Nesselquist, H.G. Morrison, M.L. Sogin*, et al.* 2010. Broadly sampled multigene analyses yield a well-resolved eukaryotic tree of life. *Syst. Biol. 59*: 518–533.

Race, H.L., R.G. Herrmann, and W. Martin. 1999. Why have organelles retained genomes? *Trends Genet. 15*: 364–370.

Raven, P.H. 1970. A multiple origin for plastids and mitochondria. *Science 169*: 641–646.

Reyes-Prieto, A., A.P.M. Weber, and D. Bhattacharya. 2007. The origin and establishment of the plastid in algae and plants. *Annu. Rev. Genet. 41*: 147–168.

Reyes-Prieto, A., and D. Bhattacharya. 2007a. Phylogeny of Calvin cycle enzymes supports Plantae monophyly. *Mol. Phylogenet. Evol. 45*: 384–391.

Reyes-Prieto, A., and D. Bhattacharya. 2007b. Phylogeny of nuclear-encoded plastid-targeted proteins supports an early divergence of glaucophytes within Plantae. *Mol. Biol. Evol. 24*: 2358–2361.

Reyes-Prieto, A., J.D. Hackett, M.B. Soares, M.F. Bonaldo, and D. Bhattacharya. 2006. Cyanobacterial contribution to algal nuclear genomes is primarily limited to plastid functions. *Curr. Biol. 16*: 2320–2325.

Richards, T.A., and T. Cavalier-Smith. 2005. Myosin domain evolution and the primary divergence of eukaryotes. *Nature 436*: 1113–1118.

Rocap, G., F.W. Larimer, J. Lamerdin, S. Malfatti, P. Chain, N.A. Ahlgren*, et al.* 2003. Genome divergence in two *Prochlorococcus* ecotypes reflects oceanic niche differentiation. *Nature 424*: 1042–1047.

Rodríguez-Ezpeleta, N., H. Brinkmann, S.C. Burey, B. Roure, G. Burger, W. Löffelhardt*, et al.* 2005. Monophyly of primary photosynthetic eukaryotes: green plants, red algae, and glaucophytes. *Curr. Biol. 15*: 1325–1330.

Roger, A., and A.G.B. Simpson. 2009. Evolution: revisiting the root of the eukaryote tree. *Curr. Biol. 19*: R165-R167.

Rogers, M.B., and P.J. Keeling. 2004. Lateral transfer and recompartmentalization of Calvin cycle enzymes of plants and algae. *J. Mol. Evol. 58*: 367–375.

Rokas, A., and P. Holland. 2000. Rare genomic changes as a tool for phylogenetics. *Trends Ecol. Evol. (Amst.) 15*: 454–459.

Sato, N. 2006. Origin and evolution of plastids: Genomic view on the unification and diversity of plastids. *In*: (R.R. Wise and J.K. Hoober, eds) *The Structure and Function of Plastids.* Springer, Dordrecht. pp. 75–102.

Sato, N., M. Ishikawa, M. Fujiwara, and K. Sonoike. 2005. Mass identification of chloroplast proteins of endosymbiont origin by phylogenetic profiling based on organism-optimized homologous protein groups. *Genome inform. 16*: 56–68.

Schwender, J., F. Goffman, J.B. Ohlrogge, and Y. Shachar-Hill. 2004. Rubisco without the Calvin cycle improves the carbon efficiency of developing green seeds. *Nature 432*: 779–782.

Shi, T., and P.G. Falkowski. 2008. Genome evolution in cyanobacteria: the stable core and the variable shell. *Proc. Natl. Acad. Sci. USA 105*: 2510–2515.

Simpson, A.G.B., T.A. Perley, and E. Lara. 2008. Lateral transfer of the gene for a widely used marker, alpha-tubulin, indicated by a multi-protein study of the phylogenetic position of *Andalucia* (Excavata). *Mol. Phylogenet. Evol. 47*: 366–377.

Stechmann, A., and T. Cavalier-Smith. 2002. Rooting the eukaryote tree by using a derived gene fusion. *Science 297*: 89–91.

Stechmann, A., and T. Cavalier-Smith. 2003. The root of the eukaryote tree pinpointed. *Curr. Biol. 13*: R665–666.

Stephens, R.S., S. Kalman, C. Lammel, J. Fan, R. Marathe, L. Aravind*, et al.* 1998. Genome sequence of an obligate intracellular pathogen of humans: *Chlamydia trachomatis. Science 282*: 754–759.

Stiller, J.W. 2007. Plastid endosymbiosis, genome evolution and the origin of green plants. *Trends Plant. Sci. 12*: 391–396.

Stiller, J.W., D. Reel, and J. Johnson. 2003. A single origin of plastids revisited: convergent evolution in organellar genome content. *J. Phycol. 39*: 95–105.

Suzuki, K., and S.-Y. Miyagishima. 2010. Eukaryotic and eubacterial contributions to the establishment of plastid proteome estimated by large-scale phylogenetic analyses. *Mol. Biol. Evol. 27*: 581–590.

Szklarczyk, R., and M.A. Huynen. 2010. Mosaic origin of the mitochondrial proteome. *Proteomics 10*: 4012–4024.

Takano, H., and K. Takechi. 2010. Plastid peptidoglycan. *Biochim. Biophys. Acta 1800*: 144–151.

Tripp, H.J., S.R. Bench, K.A. Turk, R.A. Foster, B.A. Desany, F. Niazi*, et al.* 2010. Metabolic streamlining in an open-ocean nitrogen-fixing cyanobacterium. *Nature 464*: 90–94.

Turner, S., K.M. Pryer, V.P. Miao, and J.D. Palmer. 1999. Investigating deep phylogenetic relationships among cyanobacteria and plastids by small subunit rRNA sequence analysis. *J. Eukaryot. Microbiol. 46*: 327–338.

Tyra, H.M., M. Linka, A.P.M. Weber, and D. Bhattacharya. 2007. Host origin of plastid solute transporters in the first photosynthetic eukaryotes. *Genome Biol. 8*: R212.

Weeden, N.F. 1981. Genetic and biochemical implications of the endosymbiotic origin of the chloroplast. *J. Mol. Evol. 17*: 133–139.

Zhaxybayeva, O., J.P. Gogarten, R.L. Charlebois, W.F. Doolittle, and R.T. Papke. 2006. Phylogenetic analyses of cyanobacterial genomes: quantification of horizontal gene transfer events. *Genome Res. 16*: 1099–1108.

3 *Phaeodactylum tricornutum* polymorphism: an overview

Veronique Martin-Jézéquel and Benoit Tesson

Introduction

Diatoms belong to the heterokontophytes, and are one of the major lineages of photosynthetic eukaryotes, evolved from a secondary endosymbiosis between a photoautotrophic eukaryote close to a red alga and a heterotrophic eukaryote host (Medlin et al. 1997; Kooistra 2007; Kooistra et al. 2007). They are divided in centric, the most ancient group according to silicified fossil records from around 120 Myr before present (Raven and Waite 2004), and pennate, a younger group which evolved from the polar centric diatoms in the Late Cretaceous (Medlin et al. 2000; Sims et al. 2006; Kooistra et al. 2007). Modern diatoms are diploid organisms in the vegetative state, which possess a more or less intricate cell wall made of amorphous silica, the frustule, with a specific organization depending on the class. Their classification was first principally based on morphological observations (Round et al. 1990), but recently revisited by the use of molecular phylogeny. They are separated in two classes, centrics and pennates. Centric diatoms show either radial or polar symmetry while pennate diatoms (raphid and araphid) are characterized by a general bilateral symmetry, even though some show tripolar symmetry (Pickett-Heaps et al. 1990; Round et al. 1990; Medlin and Kaczmarska 2004; Kooistra 2007; Kooistra et al. 2007). Raphid diatoms possess a raphe which consists of two slits located on the midrib of the valve. This raphe is recognized to participate in motility through active excretion of organic material (see details in Pickett-Heaps et al. 1990; Round et al. 1990).

Phaeodactylum tricornutum belongs to the raphid clade (Medlin et al. 1996; Kooistra et al. 2003, 2008) but is an atypical species because of its pleiomorphy (Mann 1999), and is now the only representative of the suborder Phaeodactylineae, family Phaeodactylaceae and genus *Phaeodactylum* (Lewin 1958; Lewin et al. 1958). Recent molecular phylogenetic analysis confirmed *Phaeodactylum* in the Naviculales order (Round et al. 1990; Medlin and Kaczmarska 2004; Sims et al. 2006).

Evolutionary and ecological considerations

Valve morphological traits used to be the criteria for diatom phylogeny until the recent development of molecular tools. The phylogenetic position of *Phaeodactylum* was difficult to determine before the recognition of its pleiomorphy, characterized by three morphotypes: oval (Figure 3.1A-C), triradiate (Figure 3.1D) and fusiform (Figure 3.1E). The fusiform shape was first isolated by Allen and Nelson (1910) and described as *Nitzschia closterium* f. *minutissima.* The triradiate form had previously been described by Bohlin (1897) and named *Phaeodactylum tricornutum.* Wilson (1946) first described the polymorphic nature of *Phaeodactylum* (under the name of *Nitzschia closterium*

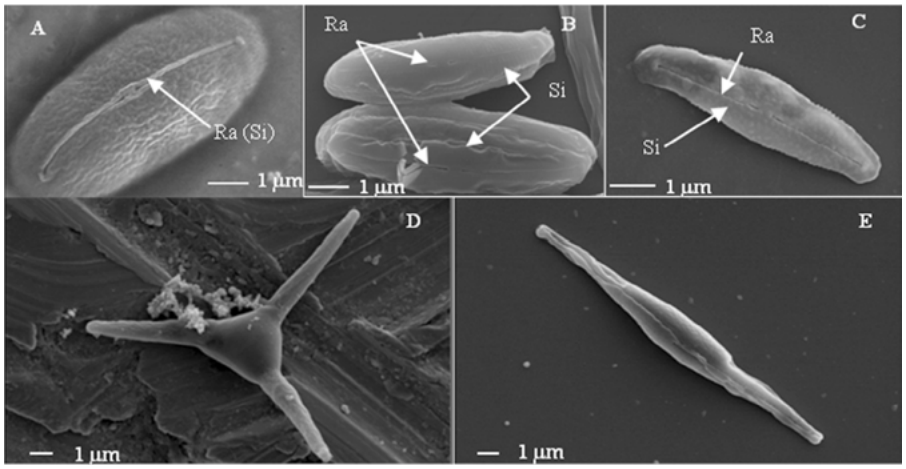

Figure 3.1 *Phaeodactylum tricornutum*: scanning electron micrographs of morphotypes. (A–C) oval cells with different degrees of silicification: (A) only the raphe is silicified; (C) the entired valve is silicified; (B) intermediate state between (A) and (C); (D) triradiate cell (Atlantic strain); (E) fusiform cell (Blackpool strain Pt1 8.6). Ra = raphe, Si = siliceous structures.

f. *minutissima*) and revealed the existence of three morphotypes of the same species. The absence of a silicified structure in the cell wall of *P. tricornutum* led to the conclusion that this algae could not be classified as a diatom (Hendey 1954). It was after the observation of a silicified raphe in the oval form that Lewin (1958) assigned *Phaeodactylum* to the class of Bacillariophyceae, and its place in the pennate lineage was confirmed by molecular phylogeny (Medlin et al. 2000; Medlin and Kaczmarska 2004).

Chloroplastic and nuclear genomes of *Phaeodactylum* have recently been sequenced (Oudot-Le Secq et al. 2007; Bowler et al. 2008), and despite the unique pleiomorphy of this species, this genome is actually considered to be representative of the pennate diatoms (Bacillariophyceae). The *Phaeodactylum* genome is slightly smaller than the genome of the centric diatom *Thalassiosira pseudonana* (Armbrust et al. 2004). It shares only 57% of its genes with this species, a difference explained by the very rapid evolutionary rate of the two genomes and their richness in long terminal repeat (LTR) retrotransposons (Bowler et al. 2008; Vardi et al. 2009).

Ecology

Phaeodactylum tricornutum is a brackish water species with a worlwide distribution. Since the last century, it has been isolated from different geographic areas, mostly from coastal waters, its main habitat, (Hendey 1964). It has also been observed in an alkaline salt lake (Rushforth et al. 1988; Johansen 1991). The three morphotypes have been globally reported (Table 3.1). The oval form is preferentially benthic, while the fusiform and triradiate types are planktonic (Round et al. 1990; De Martino et al. 2007). In comparison with the majority of microalgae whose ability to grow at high pH is limited (Hansen 2002; Hinga 2002), *Phaeodactylum* can grow at high pH with an upper limit of

Table 3.1 *Phaeodactylum tricornutum* strains, genotypes and location of sampling; different conditions for production and growth of the oval morphotype with sufficient nutrients, optimal light and temperature (a); transformation from one morphotype to another morphotype (b) and reverse transformation when observed.

Name – Genotype[(c)]	Location of sampling[(c)]	Oval growth conditions[(d,e)]	Transformation[(b)]	Reverse	References
Pt1-A	Blackpool, UK	solid	fusiform→oval		Abdullahi et al. (2006)
		liquid/solid	fusiform→oval		Stanley & Callow (2007)
		solid	fusiform→oval	yes	Tesson et al. (2009a)[(f)]
Pt2-A	English Channel (Plymouth), UK	liquid/solid	fusiform→oval	yes	Wilson (1946)[(f)]
			triradiate→oval	yes	
			triradiate→fusiform	yes	
			triradiate→fusiform		Bartual et al. (2008)[(f)]
			fusiform→oval	yes	Erga et al. (2010)
		solid	fusiform→oval	yes	Gutenbrunner et al. (1994)[(f)]
		liquid/solid	fusiform→oval		Stanley & Callow (2007)
Pt3-A	English Channel (Plymouth), UK	solid	fusiform→oval	yes	Barker (1935)
		solid	fusiform→oval		De Martino et al. (2007)
		liquid/solid	fusiform→oval		Stanley & Callow (2007)
Pt5-C	Gulf of Maine, USA	liquid/solid	fusiform→oval		Stanley & Callow (2007)
Pt6-D	Nantucket Bay (Woods Hole), USA	liquid or solid	fusiform→oval triradiate→oval	yes	Lewin et al. (1958)[(f)]
		liquid	fusiform→oval		Reimann & Volcani (1968)
		liquid or solid	fusiform→oval		Borowitzka & Volcani (1978)
		liquid	fusiform→oval		Marsot & Houle (1989)
		liquid	fusiform→oval		Johansen (1991)
		liquid/solid	fusiform→oval		Stanley & Callow (2007)
Pt8-D	Vancouver, Canada	liquid	fusiform→oval triradiate→fusiform		De Martino et al. (2007)[(f)]
		liquid/solid	fusiform→oval		Stanley & Callow (2007)

Table continued on next page.

Table 3.1 (Continued)

Name – Genotype[(c)]	Location of sampling[(c)]	Oval growth conditions[(d,e)]	Transformation[(b)]	Reverse	References
Pt9-A	Guam, Micronesia	liquid: 15–19°C	fusiform→oval	yes	De Martino et al. (2007)
			fusiform→oval		Stanley & Callow (2007)
Atlantic[(g)]	Atlantic coasts France	solid	triradiate→oval triradiate→fusiform	yes	Tesson et al. (2009a)[(f)]
Chinese strains[(g)]	Qingdao, Shangai, Zhejiang, Xiamen	liquid: 4–8°C	fusiform→oval triradiate→oval triradiate→fusiform	yes yes	Lu et al. (2001)

a – Data not shown for production of oval cells in starved media or stationary growth phase.
b – Fusiform and triradiate morphotypes were produced in liquid media (see text), or on solid media (Lewin et al. 1958, Borowitzka et al. 1977). Conditions of growth for oval morphotype are in column c in Tab. 3.1.
c – From Table 1 in De Martino et al. (2007).
d – Liquid/solid: oval cells were attached to the sides or on the bottom of the medium-containing culture vessel.
e – Liquid or solid: the morphotypes were produced either in liquid media or on solid media.
f – Studies that have described or illustrated the morphological changes during transformation.
g – Unknown genotype.

10.3 (Goldman et al. 1982; Olsen et al. 2006,) and in a wide salinity range (5–65 psu) (Abdullahi et al. 2006).

The ability of *Phaeodactylum* to grow at alkaline pH is perhaps due to its characteristic for carbon assimilation, as the alkalinization of waters induces an increase of bicarbonate species in dissolved inorganic carbon (DIC). This may indicate the specialization of its enzymatic systems depending on ecological niches. The transport of the inorganic carbon species (CO_2 and HCO_3^-) seems to be different in *Phaeodactylum* compared to centric species (Rotatore et al. 1995). *Phaeodactylum* possesses several DIC transport systems, including a K^+-dependent HCO_3^- transporter induced at alkaline pH (Chen et al. 2006), and multiple carbonic anhydrase (CA) isoenzymes that allow great flexibility for carbon assimilation (Burns and Beardall 1987; Szabo and Colman 2007). Indeed, the *in silico* analysis of the genomes of *Phaeodactylum* and *T. pseudonana* revealed differences in DIC assimilation systems (Kroth et al. 2008). Three genes that encode putative systems of bicarbonate uptake were found in *Phaeodactylum*, showing homology with a sodium/bicarbonate transporter, a sodium-dependent anion exchanger and a chloride-bicarbonate exchanger, whereas the genome of *T. pseudonana* only possesses one sodium-bicarbonate transporter (Kroth et al. 2008). Differences were also found in carbonic anhydrases and seven CAs were predicted for *Phaeodactylum*, which possess signal peptides. Two CAs of *Phaeodactylum* are of the B-type, while the others belong to

the alpha family as those of *Thalassiosira,* which also possess several CAs, but only one which has a signal peptide (Satoh et al. 2001; Kroth et al. 2008). In addition to its photosynthetic activity, *Phaeodactylum* is also known to have heterotrophic capacities and is able to grow on a broad range of organic sources, such as sugars, alcohols, amino acids, urea, etc. (Lewin and Lewin 1960; Antia et al. 1991 and ref therein; Fabregas et al. 1997; Ceron Garcia et al. 2005). This flexibility in nutrient sources gives *Phaeaodactylum* a competitive advantage over other diatoms.

Moreover, in contrast to other species, *Phaeodactylum* is the only diatom which does not require silicon to grow, even if its three morphotypes assimilate silicon (Lewin et al. 1958; Borowitzka and Volcani 1978; Nelson et al. 1984; Riedel and Nelson 1985; Del Amo and Brzezinski 1999). Silicon assimilation in *Phaeodactylum* differs from other diatoms, with Si uptake kinetics characterized by large Ks values (Martin-Jézéquel et al. 2000). Del Amo and Brzezinski (1999) have shown unusual biphasic uptake kinetics for the oval morphotype, depending on the external pH and Si concentration. These authors interpreted this phenomenon by the possible presence of two different transport systems in *Phaeodactylum* i.e. assimilation of $SiO(OH)_3$ in addition to undissociated silicic acid $Si(OH)_4$. It is however equally possible that *Phaeodactylum* does not differ from other diatoms with regards to silicon uptake characteristics. The tolerance to a wide pH range observed for *Phaeodactylum* could explain these results, as silicon could be adsorbed on cell walls instead of true silicon assimilation. In fact, this process was described in an alkalinization experiment with the fusiform and triradiate morphotypes by Tesson et al. (2008a) and opens the question of the possible misinterpretation of former data on Si uptake by *Phaeodactylum*. Nevertheless, silicified structures are not essential for *Phaeodactylum,* which can divide without the addition of silica, as reported by Brzezinski et al. (1990).

Genotypes

The global distribution of *Phaeodactylum* would suggest that a correlation with genotype could be expected, however, genotypes of *Phaeodactylum* do not align with the different world populations. Molecular tools recently used by De Martino et al. (2007) identified four genotypes A, B, C and D, from ten strains (Pt1 to Pt10) isolated from European, American, Chinese and Micronesian waters (see Table 3.1). Noticeably, no particular genotype could be attributed to the different morphotypes, suggesting that morphological changes rely on environmental condition and not on genotype.

Life and Morphology

General characteristics of cells

Cell walls

Despite the difference in the morphology, the three morphotypes, oval, fusiform and triradiate have similar cellular ultrastructure except for their cell wall and vacuolar organization (Borowitzka and Volcani 1978). All three morphotypes possess silicified structures that are localized on the epitheca, in the area corresponding to the girdle band

region, but contrary to other diatoms, the cell wall is essentially composed of organic compounds (Borowitzka and Volcani 1978; Francius et al. 2008; Tesson et al. 2008a, 2009b). The oval form is the only one that can synthesise a silicified valve with pores and that displays the same morphology as raphid pennate diatoms with central raphes (Lewin 1958; Lewin et al. 1958; Borowitzka and Volcani 1978; Tesson et al. 2009a).

Diatom cell walls are typically composed of three layers: an outer organic layer, an intermediate silicified layer and an inner organic layer, the diatotepum, deposited on the outer surface of the plasma membrane after the silica valves have been formed (Volcani 1981; Round et al. 1990; Hoagland et al. 1993). Cell walls of *Phaeodactylum* also possess a three-layered structure (Figure 3.2). These layers were described in the fusiform morphotype with a thickness of 7, 5 and 3 nm from the outside to the inside, by Reimann and Volcani (1968), Borowitzka et al. (1977) and Borowitzka and Volcani (1978), and were observed in triradiate cells by Borowitzka et al. (1977) and Borowitzka and Volcani (1978). The inner part was depicted as fibrillar material within an amorphous matrix, and the middle layer was found less opaque in TEM micrographs than the other two (Borowitzka and Volcani 1978). The outer layer was described in detail as a corrugated structure with ridges by Reimann and Volcani (1968) and Borowitzka and Volcani (1978) (Figure 3.2C). The corrugated appearance of the outer layer could be due to the presence of unstained material, as it was only observed in transmission electron micrographs (Reimann and Volcani 1968; Borowitzka and Volcani 1978), and is invisible in atomic force microscopy (Francius et al. 2008). The unstained material may arise from amorphous weakly polymerized silicon (Johansen 1991) inserted between stained protrusions of the wall.

Unlike the silicified frustule of other diatoms (Martin-Jézéquel and Lopez 2003), cell walls of the three *Phaeodactylum* morphotypes have been known from early studies to be essentially organic (Hendey 1954; Bourrelly and Dragesco 1955; Lewin 1958; Lewin et al. 1958) and some organic constituents of the *Phaeodactylum* cell walls are similar to those of other diatoms. Different macromolecules are sequentially deposited during wall formation in diatoms, such as the diatotepum composed of polyanionic polysaccharides added at the end of this process (Kates and Volcani 1968; Volcani 1981; Round et al. 1990; Kröger et al. 1996; McConville et al. 1999; Chiovitti et al. 2005). It was suggested that the diatotepum that hugs the plasma membrane, helps to maintain the integrity of the frustule (Von Stosch 1981). In *Navicula pelliculosa* the diatoteptic layer was described as sulfated glucuromannans set in fine fibrils formed during the later stages of the cell maturation (Volcani 1981). Similarly, sulfated glucuromannans were discovered in *Phaeodactylum* by Ford and Percival (1965) and described as fibrils located in the proximal portion of the wall, probably forming a network that maintains cell geometry (Volcani 1981). These structural features have been confirmed in recent work of Tesson et al. (2009b) who used X-ray photoelectron spectroscopy to explore the chemical composition of the *Phaeodactylum* cell wall surface (equivalent analyzed depth <10nm). These authors determined polysaccharides as the major constituent in cell walls of all *Phaeodactylum* morphotypes. Sulphate groups were detected and attributed to monoester sulfated glucuromannan. Tesson and collaborators (2009b) also characterized protonated nitrogen attributed to phosphoproteins and probably corresponding to silaffins. A high concentration of peptides (20% to 50%) was found at the surface of fusiform and triradiate cells, but oval cells only contained 12 to 19% peptides, probably a consequence of the capsular material that surrounds the oval morphotype. In

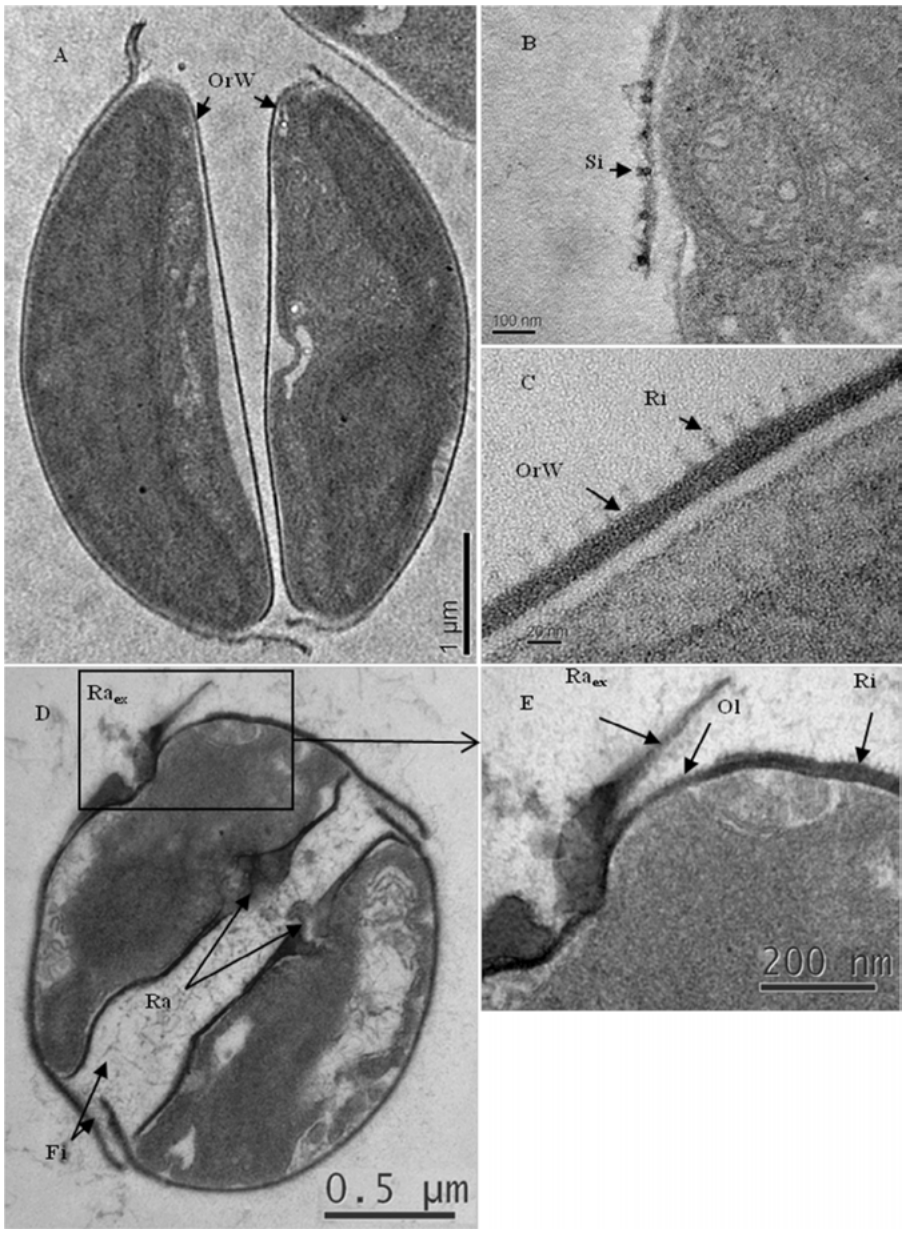

Figure 3.2 *Phaeodactylum tricornutum*: transmission electron micrographs (Blackpool strain Pt1 8.6). Fusiform morphotype (A) final division stage; (B) high resolution micrograph of the girdle band region; (C) high resolution micrograph of the cell wall; (D–E) oval morphotype: (D) oval cell in division forming new raphes; (E) higher magnification of (D) showing the absence of ridge structures beneath the silicified structure and the extrusion of the raphe from the epitheca. Ew = expelled, Fi = fibrillar material, Ol = organic layer, OrW = organic wall, Ra = raphe, Ri = ridges of the corrugated layer, Si = silica bands.

addition, a high concentration of lipids (carboxylic esters) with values between 6.8 and 46.0% was measured at the surface of the cell walls of *Phaeodactylum* (Tesson et al. 2009b). A similar result has also been obtained at the surface of the silica matrix of the centric diatom *T. pseudonana*, where lipids (triacylglycerol) have been recently detected by NMR spectroscopy (Tesson et al. 2008b). These values on lipid content are much higher than those given by Kates and Volcani (1968), who measured 0.78 to 5.2% (pennates) and 12.7% (centric) lipids over total organic matter in marine diatom cell walls and around 3.5% in the fusiform and oval morphotypes of *Phaeodactylum*. From the work of Kates and Volcani (1968), the lipidic composition of the cell walls of *Phaeodactylum* is close to that of other diatoms, with oleic –, palmitoleic – and palmitic acid being dominant. However *Phaeodactylum* cell walls are characterized by a high proportion of bound relative to free lipids, in comparison with the low content of bound lipids in other diatoms walls. Phosphorus attributed to phospholipids was also found in the X-ray study of *Phaeodactylum* by Tesson et al. (2009b), a result that confirms the description of Kates and Volcani (1968) who measured a phosphorus content (chiefly phosphatidyl glycerol) in diatoms walls. The phosphorous content was similar in cell walls of *Cyclotella cryptica* and the fusiform type of *Phaeodactylum*, 4% and 7%, respectively, but much higher in the oval form of *Phaeodactylum* (28%).

Surprisingly, in addition to the organic compounds found in all diatom walls, ESTs suggest that *Phaeodactylum* produces extracellular components from the mammalian lineage, such as laminin (glycoproteins found in basement membrane), elastin (protein found in connective tissue), and other extracellular proteins such as tenascin and fibronectin (extracellular matrix glycoproteins), mucin (glycosylated proteins producing gels in epithelial tissues), and also elicitin (small proteins secreted by *Phytophtora* species) (Scala et al. 2002; Sapriel et al. 2009). The functions and regulations of these compounds have not yet been explored.

As stated before, one of the characteristics of *Phaeodactylum* is its light silicification, and this was confirmed by the determination of its silicon content (Tesson et al. 2009b). Two types of silicon were detected, a condensed silica (SiO_2) and a weakly polymerized silica (polysilicic acid or silicate esters), the amounts of each varies with morphotype. In comparison, *T. pseudonana* has a higher concentration of silicon mainly composed of condensed silica. It appeared that SiO_2 present at the surface of *T. pseudonana* is replaced by polysaccharides at the surface of *Phaeodactylum*.

Silicification processes have been extensively described in biochemical and molecular studies on diatoms, notably using recent genome analysis and expression profiles of genes involved in frustule formation. The first step of silicon assimilation involves an active transport, which is provided by silicic acid transporters (SITs), a new class of transporters described in several diatoms species (Thamatrakoln and Hildebrand 2005, 2007; Hildebrand 2008). Silicic acid transporters have been found in similar numbers in the genomes of *Phaeodactylum* and *Thalassiosira pseudonana* (Bowler et al. 2008). The SIT gene family of the four different PtSITs of *Phaeodactylum* has been studied by Sapriel et al. (2009). These genes are made of an uninterrupted open reading frame, named PtSIT1, PtSIT2–1, PtSIT2–2 ans PtSIT3, located on 3 different chromosomes. Like other silicic acid transporters, a GXQ motif is characteristic and it is assumed that it is a potential silicic acid binding site. A CMLD motif is also preserved and it has been proposed to be involved in Si capture via Zn^{2+} ion binding (Sherbakova et al.

2005; Thamatrakoln et al. 2006). In the phylogenetic tree of SITs amino acid sequences, silicic acid transporters of *Phaeodactylum* fit well in a clade containing all pennate SITs sequences and very few SITs of centric species (two *Porosira* species, and SIT3 of *T. pseudonana*), with the other clade corresponding to centric diatoms only (27 species) (Sapriel et al. 2009). Analyzing the spatial distribution of SITs in oval and fusiform morphotypes and in dividing cells, Sapriel et al. (2009) observed GFP fluorescence mainly at the plasma membrane and in intracellular vesicles. These authors also analyzed the expression of the PtSITs genes of oval (strain Pt0) and fusiform (strain Pt1) morphotypes in Si-free medium and showed that PtSIT2 was upregulated for both morphotypes, whereas PtSIT1 was upregulated only in fusiform cells. In contrast, PtSIT3 was not significantly expressed under silica starvation. In addition, they showed that under the Fcp promoter, the amount of SIT protein increases in Si-free medium. Their work suggests that the expression of the PtSIT2 gene could be both transcriptionally and post-transcriptionally regulated in oval and fusiform morphotypes.

Frustule morphogenesis is a complex mechanism in diatoms. Different classes of organic components present inside the walls have been recognized to be involved in the silica polymerization: Long Chain Polyamines (LCPA) and specific proteins (silaffins, silacidins and cingulins) are constituent of the cell wall, such as the frustulins, a new family of calcium-binding proteins located at the surface of the wall (see Kröger 2007; Hildebrand 2008; Kröger and Poulsen 2008; Wenzl et al. 2008; Scheffel et al. 2011). The *Phaeodactylum* genome contains one gene encoding for a silaffin-like protein, close to silaffin-1 from *Cylindrotheca fusiformis* (rich in Ser, Gly and Lys residues) (see refs in Kröger and Poulsen 2008) and another gene encoding a putative glycosylated matrix protein having PT-repeats and described in *Thalassiosira pseudonana* silaffins (Sumper and Brunner 2008). These genes have been shown to be upregulated with high silicic acid (Sapriel et al. 2009). *Phaeodactylum* lacks homologues of silacidins (Bowler et al. 2008) and possesses frustulins that contain only the TRD (tryptophan-rich domain) but lack ACR (acidic cysteine-rich residues) domains (Kröger and Poulsen 2008). One alpha-frustulin encoding gene, already described in *Cylindrotheca fusiformis* and in the genome of *Thalassiosira pseudonana* (Scala et al. 2002), was shown to be highly expressed in ESTs of *Phaeodactylum* under different conditions of growth, as was epsilon-frustulin (Maheswari et al. 2010). In contrast, another gene encoding epsilon-frustulin was shown to be lightly expressed under the same conditions (Maheswari et al. 2010). Genes involved in the polyamine biosynthesis pathway have also been characterized (Sapriel et al. 2009). A gene of bacterial origin encoding agmatinase is present in *Phaeodactylum* but was not found in the genome of *T. pseudonana*. Agmatinase catalyzes the conversion of agmatine to putrescine or carbamoyle putrescine, and is involved in polyamine biosynthesis (Allen et al. 2006).

Storage products

As for the other diatoms, the storage product chrysolaminarin, a 1,3-β-D-glucan, is localized to the vacuole of *Phaeodactylum* (Ford and Percival 1965; Chiovitti et al. 2004). Hot water extracts of *Phaeodactylum* contain large amounts of 3-linked glucosyl residues (Abdullahi et al. 2006), confirming chrysolaminarin as a storage component of *Phaeodactylum*. Recent genome annotation showed that *Phaeodactylum* possesses several

enzymes involved in chrysolaminarin digestion, four putative exo-1,3-β-glucanases as opposed to only one in *T. pseudonana*, and three putative endo-1,3-β-glucanases which diverge from those of the centric species (Kroth et al. 2008).

Phaeodactylum osmoregulates using different compounds: mainly proline, DMSP, glycine betaine, free amino acids, glycerol and K^+ (Dickson and Kirst 1987; Boyd and Gradmann 2002). Some low–molecular-weight (LMW) components are also present in *Phaeodactylum*, characterized by a linkage of constituent monosaccharides different from those of the other diatoms (Chiovitti et al. 2004). These authors suggest that *Phaeodactylum* contains florodoside and/or isofloridoside, which are glycerol galactoside components generally present in red algae, as well as trehalose, a disaccharide found in algae (Craigie 1974). These features have been confirmed in the genome of *Phaeodactylum*. A sequence encoding a glycerol uptake facilitator protein was found in *Phaeodactylum*, also present in the green alga C*hlamydomonas reinhardtii* and the red alga *Cyanidioschyzon merolae* but absent in the genome of the centric diatom *T. pseudonana* (Montsant et al. 2005).

Vegetative division and sexual reproduction

In comparison to other diatoms, *Phaeodactylum* seems to have an unusual life cycle. *Phaeodactylum* apparently lacks an auxosporulation cycle, and sexual reproduction has never been observed in this species (Chepurnov et al. 2004).

Phaeodactylum follows the general vegetative processes found in other diatoms, in which cell division allows each daughter cell to inherit one maternal valve as the epitheca, and to synthesize one new valve as the hypotheca (Round et al. 1990; Martin-Jézéquel et al. 2000; Bowler et al. 2010). These processes involve a temporal and spatial rearrangement of the nuclear and cytoplasmic material. Studies on the mechanisms of mitotic division have shown that diatoms have a Microtubule Organizing Center (MTOC) with two components involved during interphase and mitosis, the MTOC and the PC (polar complex), respectively. They function in nuclear division, spindle development and the chromosome segregation during diatom division (see details in Pickett-Heaps et al. 1990; Pickett-Heaps 1991). In *Phaeodactylum* only microtubules near the nucleus during nuclear division have been described (Borowitzska et al. 1977). Using the complete genome sequences of *Phaeodactylum*, De Martino et al. (2009) identified molecular components of the MTOC which function during division of *Phaeodactylum*, which is in agreement with the description of diatom morphogenesis from previous works. They also have identified homologues of animal mitotic checkpoint and spindle-associated regulatory proteins. Like other diatoms, *Phaeodactylum* shows division characteristics of both animal and plants, with an actin ring that is involved in cytokinesis at the cleavage furrow and surrounds the growing edges of the SDV during cell wall deposition (De Martino et al. 2009). However, even if *Phaeodactylum* cells divide vegetatively, the size-reduction/restitution cycle which prevails in other diatoms was not observed until today (Chepurnov et al. 2004).

Oval morphotype

Cellular morphology

The oval form is the only one of the three morphotypes that possesses a silica valve characteristic of diatoms (Lewin et al. 1958), but oval cells with purely organic valves have

also been observed in some strains (Lewin et al. 1958; Borowitzka and Volcani 1978). The degree of silicification of the walls is variable, ranging from only a raphe to a silicified valve with a raphe (Figure 3.1A–C). The two types of silicon found in diatoms, the condensed silica (SiO_2) and the weakly polymerized silica, have been detected in oval cell walls, but polysaccharides replace part of the silica the latter being characteristic on the surface of *T. pseudonana* (Tesson et al. 2009b). In contrast to the centric species, where the majority of silicon is in the form of condensed silica (17% molecular weight) and 6.9% as weakly polymerized silica, SiO_2 contributes only 1.1%, and polysilicic acid 0.86% to wall structure of the oval form of *Phaeodactylum* (Tesson et al. 2009b).

Oval cell ultrastructure was described by Borowitzka and Volcani (1978). The valve is composed of an organic internal part outside the cell's plasmalemma and a silicified portion forming the raphe, which is localized in the center and attached to the organic layer of the valve. The raphe is more commonly found in the hypotheca (Figure 3.2D), The organic layer situated beneath the silicified raphe is thinner than the peripheral portion and probably corresponds to the inner part of the fusiform and triradiate cell walls. Details of the wall also show that the organic part extended beneath the raphe does not possess the corrugated features of the outer layer (Figure 3.2E). Commonly, oval cells do not maintain two raphes, as described by Borowitzka and Volcani (1978; Woods Hole and Long Island strains) and shown here for the Blackpool strain (Figure 3.2D). Cells maintain the newly formed raphe synthesized in the hypotheca, while the other raphe is lost from the epitheca by an unknown mechanism. As suggested for other diatoms by McConville et al. (1999), the organic parts of the wall support the siliceous structure and allow the expulsion of the silicified part.

The raphe in the oval cells resembles a rib with a denser central nodule (Desclée et al. 2007), and its structure and pattern of formation closely resemble that of other pennate diatoms (Round et al 1990). As for other diatoms (see Pickett-Heaps et al. 1990; Pickett-Heaps 1991; Hildebrand 2003, 2008), the process of silicification and organization of the valve structure involves the cytoskeleton, SDV membrane (the silicalemma) and organic molecules taking part in nanoscale control of the three-dimensional structure of the wall. In *Phaeodactylum,* silica deposition is spatially regulated during the raphe formation, a control already described in pennate diatoms where the raphe fiber (a structure observed at the inner side of the raphe), has been suggested to control Si deposition through a close association with microtubules (MTs) that extend from the MTOC (Edgar and Pickett-Heaps 1984; Pickett-Heaps et al. 1990). In pennate diatoms, such as *Navicula*, the development was shown to be centrifugal, with formation of raphe ribs first and these then initiate the transapical ribs and pores (Reimann et al. 1966; Chiappino and Volcani 1977). A similar process has been described in *Phaeodactylum* by Vartanian et al. (2009), who studied developmental stages of valve formation of the oval form, and demonstrated that raphe formation is initiated in a clearly defined order, allowing the raphe to control further deposition of silicon. First the primary raphe ribs are being elongated from the central nodule ressembling a π. During this first sequence, one side of the primary ribs developed more rapidly than the other. In the second stage, the elongation of the secondary ribs starts, then the primary ribs U-turn and fuse with the secondary ribs producing the Voigt discontinuity. The latter stage corresponds to the elongation of the transapical costae by a lateral deposition of silica from the sternum to form cross-costae. The process seems to be determined before the completion of the raphe, and spatially directed. Additional silica is deposited

after this growth between the already created first transapical costae, suggesting a new phase separation process, to form complex cross-setae and fractal-like structures.

As for other diatoms, silica deposition in *Phaeodactylum* takes place in an acidic compartment (Vrieling et al. 1999; Martin-Jézéquel and Lopez 2003). Vartanian et al. (2009) have shown this using a vacuolar-ATPase inhibitor, disrupting the activity of proton transporters leading to alkalinisation of intracellular compartments, which resulted in a decrease of the average valve size and change in valve morphology (thinner and bent valve, aberrant morphology). Raphe symmetry as well as valve geometry were affected by the inhibitor.

Motility and excretion of organic material

Diatoms are known to secrete exopolymeric substances (EPS), involved in motility, or in stabilization, colony formation and adhesion. Both centric and pennate diatoms are able to secrete EPS and possess pores in their cell walls. In addition, raphid pennate diatoms secrete specific polymeric substances through their raphe, favoring cell adhesion and gliding, by association with an intracellular actin-myosin system (Hoagland et al. 1993; Wetherbee et al. 1998; Underwood and Paterson 2003; Chiovitti et al. 2006; Molino and Wetherbee 2008). The chemical nature of this exopolymeric mucilage is probably clycoproteinic, as reported by Chiovitti et al. (2003). The adhesion to the substratum is mediated by extracellular polymeric strands, and cell movement occurs via an actin/myosin motor located adjacent to the raphe and connected to the strands probably via transmembrane proteins, the entire system has been called the adhesion complex (AC) (Wetherbee et al. 1998; Poulsen et al. 1999) or adhesion motility complex (AMC) (Molino and Wetherbee 2008). The raphe in contact with the substrate is called 'the driving raphe' and the raphe of the opposite valve the 'non-driving raphe'. Several genera of diatoms, such as *Achnanthes* or *Cocconeis* possess only one raphe, the second is a pseudoraphe.

Like all raphid pennate diatoms, and in contrast to the other morphotypes, oval cells of *Phaeodactylum* are capable of gliding (Iwasa et al. 1971; Iwasa and Shimizu 1972). Dugdale et al. (2006) using AFM (Atomic Force Microscopy), have characterized adhesive nanofibers at the surface of the oval morphotype and they suggested that these nanofibers could be made through the assembly of modular proteins. Characteristics of adhesion were also measured in culture by Stanley and Callow (2007). They have shown that only oval cells adhere to substrate, with some variations in adhesive properties between the different strains of *Phaeodactylum*.

EPS are excreted by all three *Phaeodactylum* morphotypes, but significant differences have been shown between the oval and fusiform types in the proportion of monosaccharides and anionic composition, the chain terminal saccharides and the degree of sulphation (Abdullahi et al. 2006). Compared to the fusiform type, oval cells possess more xylose in their colloidal (media-soluble) fraction of EPS, and different proportions of glucose, mannose, galactose, arabinose and fucose in all extractables fractions (hot water, bicarbonate or alkali conditions). When grown on solid media, oval type produces highly branched polymers with a relative increase of terminal residues, a pattern also found for the fusiform cells under increased stress conditions (i.e. P limitation or salinity stress). A very large increase of sulfate concentration characterized the oval cells EPS, whereas rhamnose and uronic acid concentrations were relatively unchanged in response to growth on solid media.

Fusiform and triradiate morphotypes

Cellular morphology

Silicified portions of the fusiform and triradiate morphotypes differ from those of oval forms. The surface composition of the fusiform and triradiate morphotypes is very similar, mainly composed of polysaccharides, proteins and a small amount of lipids (Tesson et al. 2009b). As for the oval cells, both types of silicon, condensed silica and weakly polymerized silica, have been detected in their walls. But contrary to oval cells, fusiform and triradiate cells have a higher silicon concentration in the form of silicates compared to condensed silica. Surface composition expressed in weight percent of SiO_2 are in the range of 1.16 to 4.8 for weakly polymerized silica and 0.53 to 1.26 for condensed silica (Tesson et al. 2009b).

In the fusiform and triradiate morphotypes, condensed silica is present only in silica-rich bands approximately 30 nm in diameter (Neuville et al. 1971; Borowitzska and Volcani 1978). These silica bands replace girdles bands found in other diatoms, and are located on the epitheca at the junction of the two valves, and sometimes on the hypotheca of old cells (Borowitzka and Volcani 1978) (Figure 3.2B). They are probably added during cell growth and vary in number (Reimann and Volcani 1968; Neuville et al. 1971; Borowitzka and Volcani 1978). Cellular location of the weakly polymerized silicon is not known, however Johansen (1991) suggests that it could be diffused and embedded in organic material.

Excretion of organic material

In their study on the adhesive properties of *Phaeodactylum*, Stanley and Callow (2007) demonstrated that the fusiform morphotype did not adhere significantly to surfaces in contrast to the oval cells. Interestingly, this could be due to difference in the amount and the composition of EPS that is secreted through pores of the frustule and the raphe and have been recently characterized using AFM (Chiovitti et al. 2006).

Under standard culture conditions, soluble substances secreted by fusiform cells are similar to those found in other diatoms (Bellinger et al. 2005; Abdullahi et al. 2006 and refs. therein). The polysaccharides are very complex and highly branched, containing the dominant sugars mannose, glucose, galactose, xylose and rhamnose and only low levels of uronic acid (Abdullahi et al. 2006). Hot water extractable polymers are enriched in uronic acid, proteins or amino acids and probably aromatic compounds and contain a small amount of sulfated polysaccharides (Serriti et al. 1994; Abdullahi et al. 2006; Tesson et al. 2008a). As detected in other diatoms, dissolution of the mucilage coating releases mainly rhamnose, as well as mannose, xylose, galactose and fucose (see Abdullahi et al. 2006).

Exopolymer excretion increases during the stationary phase of growth and in response to phosphate limitation or salinity stress (Smith and Underwood 2000; Abduhalli et al. 2006). Excretion of acidic polysaccharides (EPS) which exhibits sticky properties similar to those of TEP was correlated with alkalinization of the culture medium, and leads to the formation of cell aggregates (Tesson et al. 2008a). These gel-like structures can induce the formation of crystalline magnesium hydroxide (Brucite) starting in the girdle bands area and eventually covering the cells (Tesson et al. 2008a). This material contains

a large amount of uronic acid, sulfated, deoxy- and O-methylated sugars that increase in reactivity and sticky properties (Holloway and Cohen 1997; Abdullahi et al. 2006). These physico-chemical properties lead to ionic cross-linking and enhance sorption of solute and particle substances (Reynolds 1963; Passow 2002). In addition, these extracellular substances autofluorescence in blue under UV light (Tesson et al. 2008a), a property probably due to phenolic compounds like amino acids (tyrosine, tryptophan) and products of riboflavin degradation (Seritti et al. 1994, 1996). This fluorescent property was already observed in extracellular polymers of *Fucus* embryos and in stalks of *Achnanthes longipes* that autofluoresce blue possibly due to the presence of polyphenolic compounds forming a network with the extracellular polysaccharides of the stalk (Wutsman et al. 1997).

Interestingly, observation of Tesson et al. (2008a) suggests that excretion of EPS occurs in the girdle band region of the fusiform and triradiate morphotypes. Very few works have localized excretion in the girdle band region, active excretion of organic compounds generally occurs via silicified specific regions of the frustule, the strutted processes (fultoportulae) in the centric order Thalassiosirales, the labiate process (rimoportulae) present in many orders, the raphe in pennate diatoms, and small pores located in specific valve regions named ocelli or pseudocelli (Round et al. 1990). These structures are generally extended internally into the silica valve and have complex connection with plasmalemma and cellular organelles to allow secretion of specific organic matter involved in adhesion, motility and control of sinking, and of other compounds involved in chemical signaling such as pheromones (Round et al. 1990; Schmid et al. 1996). Because girdle band region is the only silicified part of fusiform and triradiate cells, one can postulate that these two morphotypes have kept this structure to maintain this secretory pathway. It is noteworthy that secretion in the girdle band region was also observed in the biofouling centric diatom *Toxarium undulatum* by Dugdale et al. (2005) during initial adhesion.

Mechanical characteristics of the three morphotypes

Differences between the three morphotypes have been described by mapping of the cell surface using AFM (Francius et al. 2008). The fine external structure of the three morphotypes was observed as well as polymer footprints in the vicinity of oval cells, showing that characteristics of oval cells are similar to other diatoms and provide higher mechanical resistance than valves of the other two morphotypes.

High resolution images of the fusiform and triradiate cells revealed a non-structured and smooth surface, whereas oval cells showed a rough surface with streaks in the scanning direction which were probably due to excreted polymers. Differences in mechanical properties have been found depending on the cellular location. AFM nano-indentation measurements determined the elasticity of the three forms, and variations were observed across different parts of the cells. Fusiform and triradiate cells gave an average Young's modulus of 81 kPa and 102 kPa respectively, which is much smaller than what was found in other diatoms. In these two morphotypes, the values measured in the core region were larger than those in the arms, a difference probably due to the internal organisation of the cell where organites are located in the cell center, and the arms are mostly occupied by a vacuole (Tesson et al. 2009a). Girdle band stiffness appears more heterogeneous than those of valves with an average Young's modulus of 32 kPa, a character

probably attributable to the particular location of the girdle bands at the edge of the valve (Tesson et al. 2009a). In contrast to the other forms, oval cells were stiffer and characterized by a high Young's modulus of 501 kPa, in the range found in uncleaned silicified diatoms. As for the fusiform morphotype, the girdle band region of oval cells was softer than the valve, with Young's modulus values 79 and 316 kPa respectively, reflecting their lower degree of silicification.

Polymorphism and transformation

Phaeodactylum tricornutum is a brackish water species (Hendey 1964) and its ability to form different morphotypes may be an adaptation to the changing environment found in coastal waters. The three morphotypes may represent distinct ecophenotypes, each one specifically adapted for growth under particular conditions (De Martino et al. 2007). The large peripheral vacuoles also make fusiform and triradiate morphotypes more buoyant than oval cells (Wilson 1946; Lewin et al. 1958), perhaps better suited to a planktonic lifestyle.

Numerous researchers have tried to understand the polymorphism of this species and the conditions leading to the appearance of each form. Volcani (1981) noted that the most stable morphotype is the fusiform one, which is indeed the form generally observed in cultures and the form usually isolated from natural waters (De Martino et al. 2007). The triradiate morphotype has also been found in field samples (Bohlin 1897; Wilson 1946; Johansen, 1991; De Martino et al. 2007) and has been observed in laboratory cultures (Wilson 1946; Borowitzka and Volcani 1978; De Martino et al. 2007; Bartual et al. 2008) while the oval morphotype has been observed only in culture collections (Barker 1935; Wilson 1946; Lewin et al. 1958; Iwasa et al. 1971; Borowitzka and Volcani 1978; Marsot and Houle 1989; Johansen 1991; Gutenbrunner et al. 1994; De Martino et al. 2007; Gauthier et al. 2006; Erga et al. 2010).

Despite these observations, the physico-chemical conditions that promote growth and maintenance of each morphotype are still poorly understood. Moreover, few publications document the steps of endogenous transformation from one morphotype to another (Wilson 1946; Lewin et al. 1958; Gutenbrunner et al. 1994; De Martino et al. 2007; Bartual et al. 2008, Tesson et al. 2009a). The most complete descriptions of morphology and ultrastructure of *Phaeodactylum* cells, or of conditions leading to morphological changes are the works of Wilson (1946), Borowitzka et al. (1977), Borowitzka and Volcani (1978) and Tesson et al. (2009a).

Cellular plasticity

All three morphotypes have been shown to be variable in their morphology depending on growth conditions. However, these conditions do not always trigger transformation into another morphotype.

The shape of the oval cells is either thin and elongated or round, and laboratory-based observations suggest that the expression of cellular morphology is correlated with growth conditions rather than genotype. It is noteworthy that round-shape cells are produced under stress conditions. The long thin shape is the most often found in laboratory cultures,

probably corresponding to the normal shape of this morphotype. It was described in strains of genotype A and D (Wilson 1946; Reimann and Volcani 1968; Johansen 1991; De Martino et al. 2007) and observed in the Atlantic strain of an unknown genotype (Tesson et al. 2009a). On the other hand, the formation of the round shape appears to be correlated with unfavourable growth conditions; cells of this form tend to aggregate surrounded by mucilage and adhere to the culture flask walls (Wilson 1946; Johansen 1991; De Martino et al. 2007).

The fusiform and triradiate morphotypes also have different shapes, depending of growth conditions. Divergence in morphology may have occurred over the duration on laboratory cultures, as cellular dimensions of the fusiform morphotype of strain Pt6 in the works of Lewin et al. (1958) and Johansen (1991) differed from those described by De Martino et al. (2007). On the other hand, the shape and size of Plymouth strain Pt2 described by Wilson (1946) and Lewin (1958) were confirmed by the work of De Martino et al. (2007) and Bartual et al. (2008). Morphological variability among strains does not seem to depend on genotype, as demonstrated for the fusiform morphotype of the ten strains belonging to four genotypes grown under the same good culture conditions (see Table 2 in De Martino et al. 2007).

Plasticity of the cell morphology is not always related to transformation of the morphotype. Numerous studies have investigated the sensitivity of *Phaeodactylum* to physico-chemical parameters, and demonstrated that stress could affect cell morphometry or cause shape deformities and alterations, as already known for other diatoms (Martin-Jézéquel and Lopez 2003; Falasco et al. 2009). For example, hight copper concentrations induced shorter and swollen fusiform cells with increased volume (Levy et al. 2008). In addition, cells form chains joined together in the central region of the valve a phenomenon previously observed by Borowitzska et al. (1977). Increased cell volume was interpreted as a consequence of inhibition of cell division, induced by a lower ration of reduced to oxidized glutathione and inhibition of mitotic spindle formation (Levy et al. 2008). Inhibition of cell division could also be evoked by UV stress leading to DNA damage and a decoupling between cell growth and cell division (Behrenfeld et al. 1992; Holzinger and Lütz 2006). Similarly, although *Phaeodactylum* is highly tolerant to Fe limitation, the fusiform morphotype was shown to react to Fe stress by decreasing in cell diameter and cell volume (Allen et al. 2008). This is common in many microalgae in response to decreased efficiency of the photosystems and changes in ROS regulation (Geider et al. 1993; Allen et al. 2008 and refs therein). High pH values also have been shown to induce larger cell volume and surface area in the triradiate and fusiform morphotypes, for both saturating and subsaturating light conditions (Bartual et al. 2008). This was accompanied by a decrease in growth rate when cells were maintained at low light, but without changes in growth under saturating light conditions. Irregular forms have also been found when salinity is low (Wilson 1946).

Cellular pleiomorphy

Observations on morphotype occurrence in *Phaeodactylum* vary among strains and culture conditions (Table 3.1). Work by Darley (1968) suggests that the fusiform, triradiate and oval forms do not represent an alternation of haploid and diploid generations. Moreover, nothing in the occurrence of the different morphotypes suggests that the oval morphotype could be a life stage different from the fusiform or triradiate morphotype,

such as a resting spore. Environmental or growth conditions that lead to transformation of one morphotype to another vary, and transformation has been related to different culture conditions rather than being viewed as an intrinsic characteristic of the different strains (De Martino et al. 2007). Morphotype analysis of ten accessions of *Phaeodactylum* resulted in a limited correlation between morphology and geographical localization (De Martino et al. 2007), and the expression of morphotype appears to be independent of genotype. However, morphological stability might be dependent on genotype because clones of some strains have a greater tendency for pleiomorphy than clones of others (Borowitzka and Volcani 1978).

Strains often have a preferential morphotype when maintained in laboratory cultures. Under normal culturing conditions (i.e. liquid enriched media), the fusiform morphotype is common, while the oval or triradiate forms rarely dominate (De Martino et al. 2007; Stanley and Callow 2007). The fusiform morphotypes of strains Pt6 and Pt7 were also observed on agar plate (Lewin et al. 1958; Borowitzka et al. 1977). The triradiate form was the predominant form in liquid media for one strain (Pt8) among the ten accessions in the study of De Martino et al. (2007), for the strain of unknown genotype isolated from Atlantic waters (Figures 3.1D and 3.5A), for six clones isolated in China (from Zhejiang and Xiamen) by Lu et al. (2001), and in some cultures of the Plymouth (Pt2: Wilson 1946; Bartual et al. 2008) and Long Island strains (Pt7: Borowitzka et al. 1977; Borowitzka and Volcani 1978). The triradiate morphotype of strain Pt6 was also produced on agar plates in a study by Lewin et al. (1958). However, stability of the triradiate morphotype is lower than for other morphotypes; as a consequence the triradiate morphotype often becomes fusiform or oval during successive subculturings (Wilson 1946; De Martino et al. 2007). The maintenance of oval forms requires specific growth conditions (Table 3.1); it is the only form that survives under low-light conditions and an extended period of nutrient limitation (De Martino et al. 2007; Erga et al. 2010). This form was also observed to survive in a sol-gel of silicon, with a far longer survival capacity than another pennate diatom, *Cylindrotheca fusiformis* (Gauthier et al. 2006).

Transformation to oval cells can be induced in all strains independently of genotype, by keeping triradiate and fusiform morphotypes in nutrient-deplete media (De Martino et al. 2007), a feature observed in studies on: the Pt2 strain (Plymouth strain: Wilson 1946; Gutenbrunner et al. 1994; Erga et al. 2010) and the clone Pt1 8.6 (Blackpool strain) with genotype A; the Woods Hole strain with genotype D (Lewin et al. 1958); the Atlantic triradiate strain of unknown genotype. Oval cells can also be produced under good culture conditions (i.e. enriched media and sufficient light) (Table 3.1) on solid media, with a reverse transformation upon transfer to liquid media. This phenomenon was shown for strains with genotype A (Plymouth and Blackpool strains), genotype D (Woods Hole and Long Island strains) and the Atlantic strain (Table 3.1). The oval morphotype has also been obtained in liquid culture in numerous studies, with cells generally adhering to the culture flask in either static or shaken liquid batch culture (genotype A: strains Pt1, Pt2, Pt3; genotype D: strains Pt6, Pt7, Pt8; genotype C: strain Pt5; Table 3.1). It seems, however, that the induction of the oval morphotype in enriched medium may be dependent on genotype. Oval morphotypes of genotype A are better maintained for growth on agar plate than in liquid culture, as observed for Pt1 (Abdullahi et al. 2006), the clone MUR 138 (Pt2) (Gutenbrunner et al. 1994) and Pt3 (De Martino et al. 2007). Comparatively, strains of genotype D (Pt6 and Pt7, Table 3.1) transform more often into oval morphotypes

in liquid media than strains with other genotype, and some oval clones of these two strains have been better maintained in liquid media than on agar plate (Borowitzka et al.1977; Borowitzka and Volcani 1978).

Impact of abiotic parameters

DIC, salinity, nutrients and trace elements

Changes in the relative abundance of the fusiform and triradiate morphotypes were reported by Bartual et al. (2008) in relation to variations of the inorganic carbon. Strain CCAP 1052/1A of AWI (strain Pt2) maintained at about 50% of the fusiform and triradiate forms was studied across different pH and levels of carbon dioxide. A slight decrease of the triradiate morphotype at pH 7.9 and an increase at pH 8.9 and 9.5 were observed compared to natural seawater pH of 8.2. Compared to natural DIC concentrations, lower or higher concentrations induced higher triradiate abundance.

Salinity was shown to affect only the morphology of some clones of the Plymouth strain Pt2. A subclonal culture of Pt2 (named Pt3) was grown in freshwater media and comprised predominantly of oval cells (De Martino et al. 2007; Maheswari et al. 2010). However, the salinity effect is not consistent and Wilson (1946) reported that in another clone of the Plymouth strain Pt2, low salinity led to formation of cells with swollen tips on the arms of fusiform and triradiate cells, but no oval forms. Similarly, Erga et al. (2010) demonstrated that fusiform cells of the Pt2 strain, maintained in different salinity layers, did not react by changing morphotype, but were likely to adapt their buoyancy to control ascend/descend displacements in the artificial water column, irrespective of being inoculated in the surface or the bottom layers. Fusiform cells tended to form aggregates and stay in the bottom layer when nutrients were growth limiting (Erga et al. 2010). Moreover, cells did not regulate their buoyancy by changing cellular size under salinity stress (Dickson and Kirst 1970; Erga et al. 2010). Furthermore, salinity variations did not influence transformation behaviour of the fusiform and triradiate morphotypes of Woods Hole and Long Island strains (Borowitzka and Volcani 1978), the fusiform morphotype of the clone MUR 138 (Pt2) (Gutenbrunner et al. 1994), nor the Blackpool strain Pt1 (Abdullahi et al. 2006).

Neither agitation, nor variation in silicate concentration induce morphotype transformation in fusiform and triradiate morphotypes of Woods Hole and Long Island strains (Borowitzka and Volcani 1978). However, Garcia Camacho et al. (2001) observed a reduction in cell volume in fusiform cells through decrease of both length and width when submitted to hydrodynamic stress in aerated media. Phosphate limitation did not affect the fusiform morphotype of the Blackpool strain (Abdullahi et al. 2006). Low calcium concentration has been reported to induce transformation from oval to fusiform morphotypes (Cooksey and Cooksey 1974), but this was not confirmed by Borowitzka and Volcani (1978). It has also been suggested that transformation may be induced by excreted substances like phytohormones (Iwasa et al. 1971; Borowitzka and Volcani 1978).

Light and temperature

Little information is available on the effects of other physico-chemical conditions on the transformation of *Phaeodactyluum* cells. Low temperature (4–8°C) induces the production

of oval cells in fusiform and triradiate cultures of the Chinese strains (Lu et al. 2001). Low temperature (19°C instead of 25–28°C) also induced morphotype transformation from fusiform to oval cells in Pt9 isolated from Micronesian waters; the reverse transformation occured upon transfer to temperature of its natural environment (i.e 25–28°C) (De Martino et al. 2007). In both studies low temperature is sub-optimal for growth of the strains. It can therefore be concluded that the production of oval morphotype in these studies is the result of unfavorable growth conditions.

Influence of light on *Phaeodactylum* transformation is poorly documented. Borowitzka and Volcani (1978) noted that light intensity did not affect the fusiform and triradiate morphotypes of the Woods Hole and Long Island strains. On the other hand, Bartual et al. (2008) detected that the relative abundance of the triradiate form was higher under subsaturating than saturating light for strain Pt2, however, the difference was significant only for pH and DIC values higher than the normal levels, suggesting that morphological change was induced by interactions of carbon stress and light conditions.

Transformation mechanisms

Only Wilson (1946), using the Plymouth strain, describes in detail external morphological changes of the three morphotypes. The complete process of transformation is not easy to follow, and other authors have observed only parts of the steps leading to morphological changes of the different forms.

Transformation into oval morphotype

Mechanisms producing oval cells from fusiform and triradiate morphotypes observed in the Plymouth strain Pt2 (Wilson 1946), the Blackpool strain (Pt1) and the triradiate type of the Atlantic strain do not differ. Inflated fusiform or triradiate parent cells produce the primary oval cell within the centrally enlarged region. This is followed by the first division to form a pair of oval daughter cells (Figures 3.3–3.5; fusiform morphotype MUR 138 (Pt2), Gutenbrunner et al. 1994; fusiform morphotype Pt6, Lewin et al. 1958; fusiform morphotype Pt8, De Martino et al. 2007). After this step, oval cells are not necessarily released from the parent fusiform or triradiate cells and numerous oval cells may arise by successive divisions inside the parent cells, as observed in the Blackpool strain Pt1-A (Figure 3.3E, F, I), the triradiate Atlantic strain (Figure 3.6B), the Plymouth strain Pt2 (Wilson 1946), and the Vancouver strain Pt8 (De Martino et al. 2007). The release of oval cells from the parent-cell occurs in both fusiform and triradiate cells as described for normal cell division by Borowitzka and Volcani (1978) by parental cell rupture along the girdle band region (Figures 3.3I, 3.4D–F and 3.6). During the transition from the fusiform or triradiate morphotype to the oval morphotype, the primary oval cell and the daughter oval cells are oriented in the parent cell parallel to the arms of the fusiform morphotype and longitudinally along the two most widely spaced arms of the triradiate morphotype (Figures 3.3–3.5).

In the fusiform or triradiate cells, the arms contain mostly vacuoles (Borowitzka and Volcani 1978). To form the oval cell from fusiform or triradiate morphotypes, the protoplasm of the parent cell retracts from the apices of the cell walls and becomes located

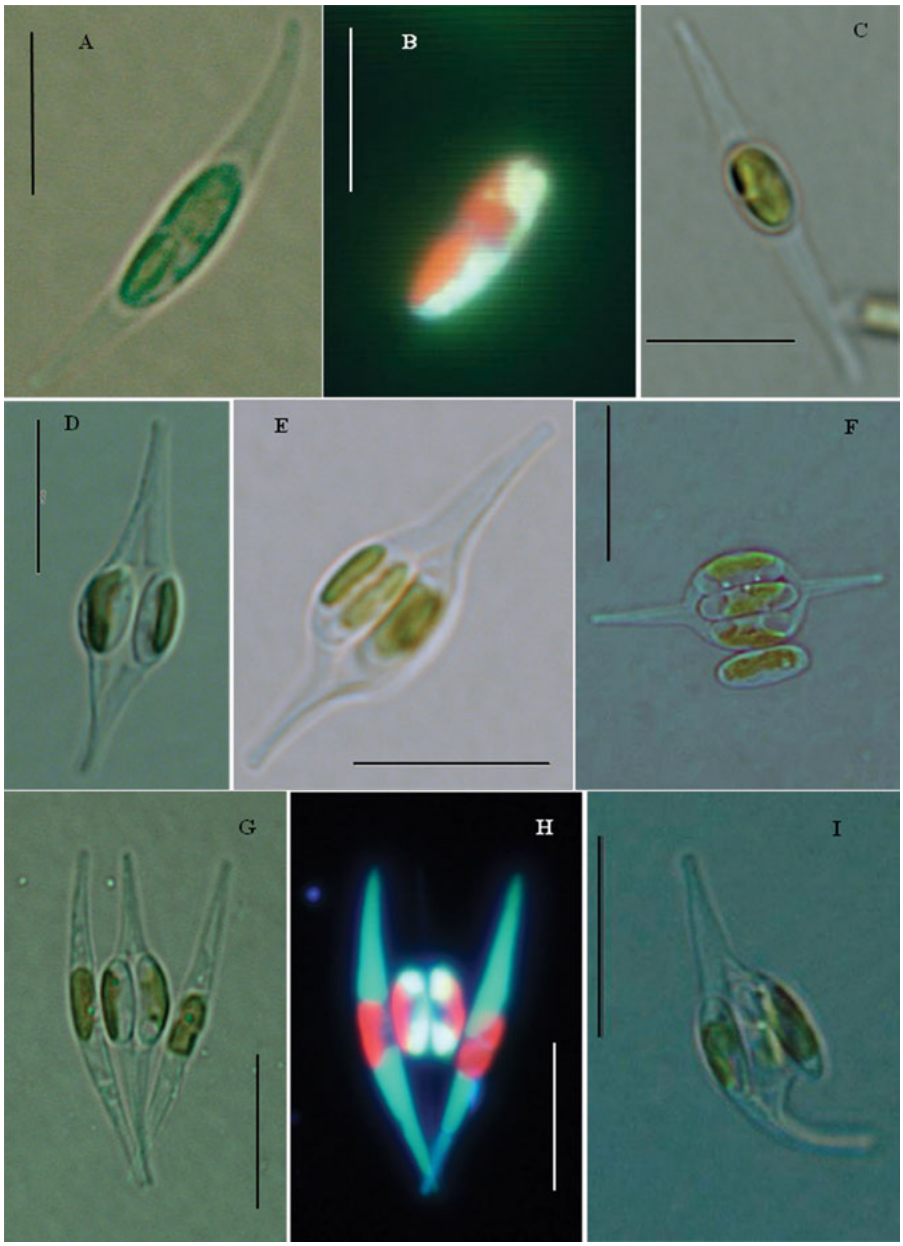

Figure 3.3 *Phaeodactylum tricornutum*: light micrographs of the different stages of transformation from fusiform to oval morphotype (Blackpool strain Pt1 8.6). (A–C) Retraction of the protoplasm and formation of the primary oval cell inside the fusiform cell; (D–H) division of the oval cell and daughter-oval cells inside the fusiform cell; (I) breakage of the cell wall of the fusiform cell; (B) and (H) epifluorescence images of PDMPO (lysosensor™ yellow/blue DND-160; Molecular Probes) stained cells. Scale bars = 10 μm.

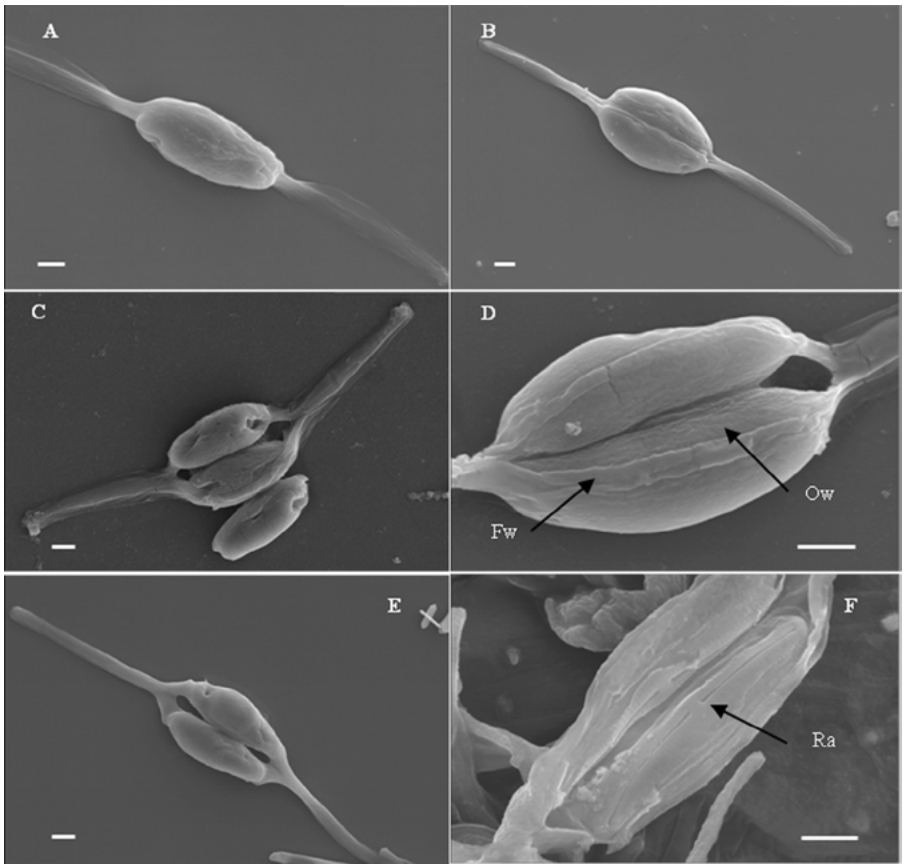

Figure 3.4 *Phaeodactylum tricornutum*: scanning electron micrographs of different stages of transformation from fusiform to oval morphotype (Blackpool strain Pt1 8.6). (A) Primary oval cell formed inside a fusiform cell; (B) primary oval cell in division; (C–F) daughter oval cells inside a fusiform cell. Fw = fusiform cell wall, Ow = oval cell wall, Ra = raphe. Scale bars = 1 μm.

in the cell centre (Figures 3.3A–C, 3.4A and 3.5B). The involvement of the vacuole in the differentiation to the oval morphology has been demonstrated by the expression of cytosolic eYFP (cytosolic Yellow Fluorescent Protein) in genetically transformed cells of the Vancouver strain Pt8 (De Martino et al. 2007), and in cells of the Blackpool strain by fluorescent labelling (Tesson et al. 2009a). The formation of the primary oval cell leads to the disappearance of fluorescence from the arms of the parent cell and fluorescence becomes localized in the oval cell, indicating the contraction of the protoplast and the loss of internal structure within the parental cells (Figure 3.3B–H).

During the differentiation of the oval cells, arms of the fusiform or triradiate parent-cells are filled by a fibrillar substance (stained in TEM micrographs) (Figures 3.6A, B and 3.7A, B). This fibrillar structure surrounds oval cells and may therefore constitute a form of mold for the oval cell shape. These observations suggest that the fibrillar material participates in retraction of the protoplast and in the stabilization of the newly formed oval cell in the center of the parent cell. Selective secretion of mucilage, probably polysaccharides

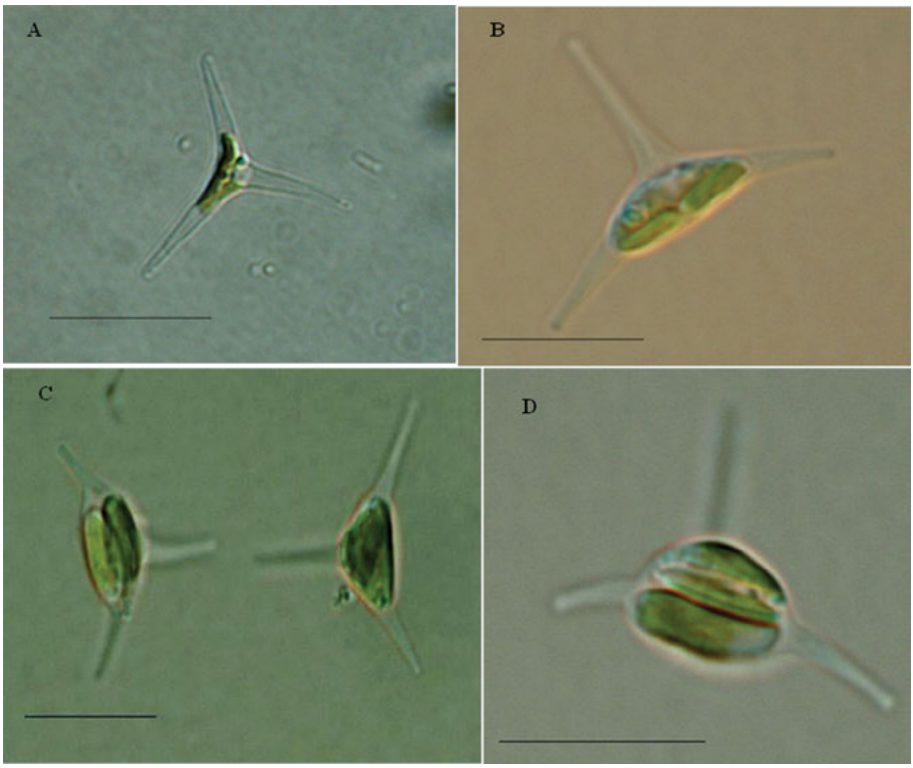

Figure 3.5 *Phaeodactylum tricornutum*: light micrographs of different stages in the transformation from triradiate to oval morphotype (Atlantic strain). (A) Triradiate cell; (B) retraction of the protoplasm of the triradiate cell; (C) and (D) division of the oval cell inside the triradiate cell. Scale bars = 10 μm.

potentially derived from Golgi vesicles, was sometimes observed during cell division in diatoms. Similar material was observed in the space between daughter protoplasts in *Thalassiosira eccentrica* (Schmid 1984) and in several pennate diatoms (Pickett-Heaps et al. 1990). Interestingly, thin fibrillar material has also been observed in the intercellular space between the two new cells and in the girdle band region during cytokinesis and wall formation in *Phaeodactylum* (Borowitzka and Volcani 1978) (Figure 3.2D). The origin of this fibrillar material is unclear; there are two possible explanations, viz. (1) it may be excreted during the formation of oval cells, a process resembling EPS secretion and released into the subfrustular zone before excretion (Hoagland et al. 1993) or (2) it may originate from the inner part of the cell wall of the parent cell, due to the disorganization of the internal layer, as this layer is composed of polysaccharide-based fibrillar material (Borowitzka and Volcani 1978). Oval cells confined within the parent cell do not remain attached to each other or to the fibrillar material, which is disrupted when daughter cells are released from the parent cell (Figure 3.6).

Wilson (1946) proposed that the primary oval cell arises by unequal division of the parent cell, but this hypothesis was rejected by Lewin et al. (1958), and it is currently

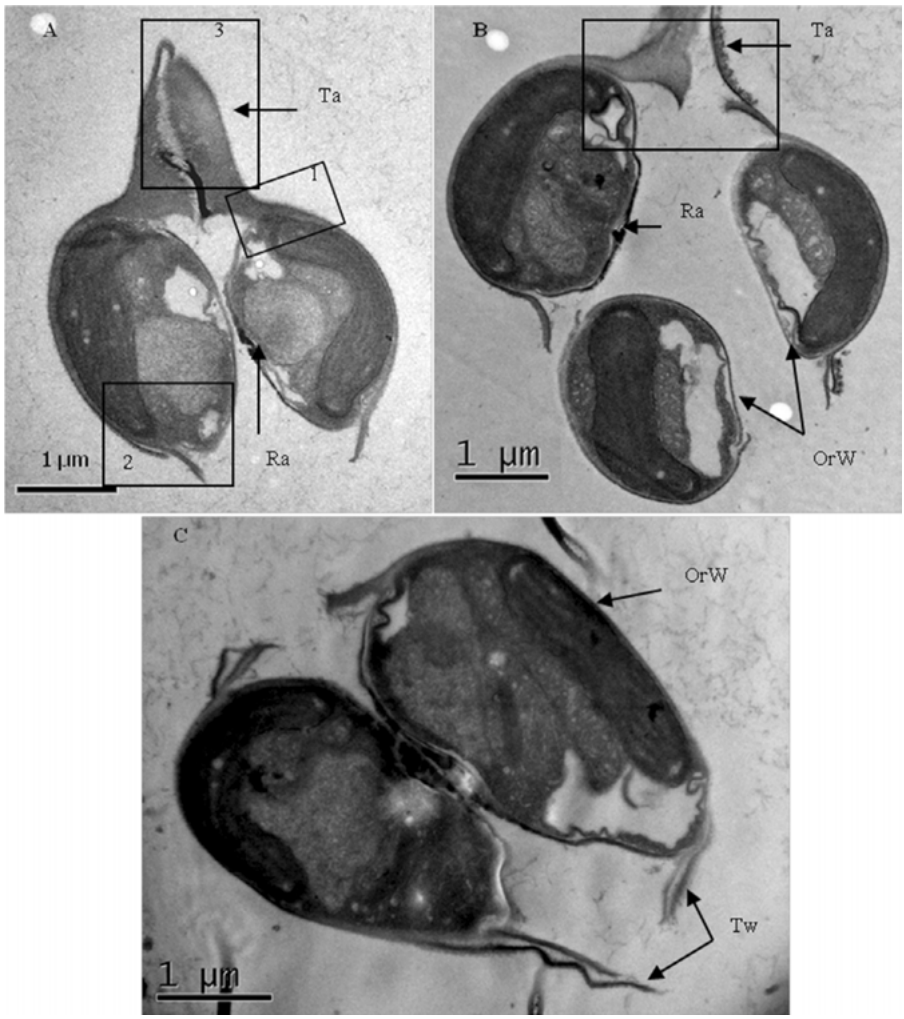

Figure 3.6 *Phaeodactylum tricornutum*: transmission electron micrographs of the transformation from triradiate to oval morphotype (Atlantic strain). (A) Two newly formed daughter oval cells inside a triradiate cell; (B) release of three oval cells (the fourth oval cell was probably not observed because it was in another section); (C) two daughter oval cells with residual triradiate wall. Panels represent zones of higher magnification shown in Figure 3.7. OrW = organic wall, Ra = raphe, Ta = triradiate arm, Tw = triradiate cell wall.

thought that the formation of the primary oval cell originates from two acytokinetic mitoses (Gutenbrunner et al. 1994), a process that leads to the formation of only one cell (Figure 3.8). During acytokinetic mitosis, additionally formed nuclei degenerate quickly (Chepurnov et al. 2002; Mills and Kaczmarska 2006), which explains why the oval cell has only one nucleus at the end of the process (Figure 3.6). Involvement of acytokinetic mitosis during oval cell differentiation is supported by the observation that the wall of

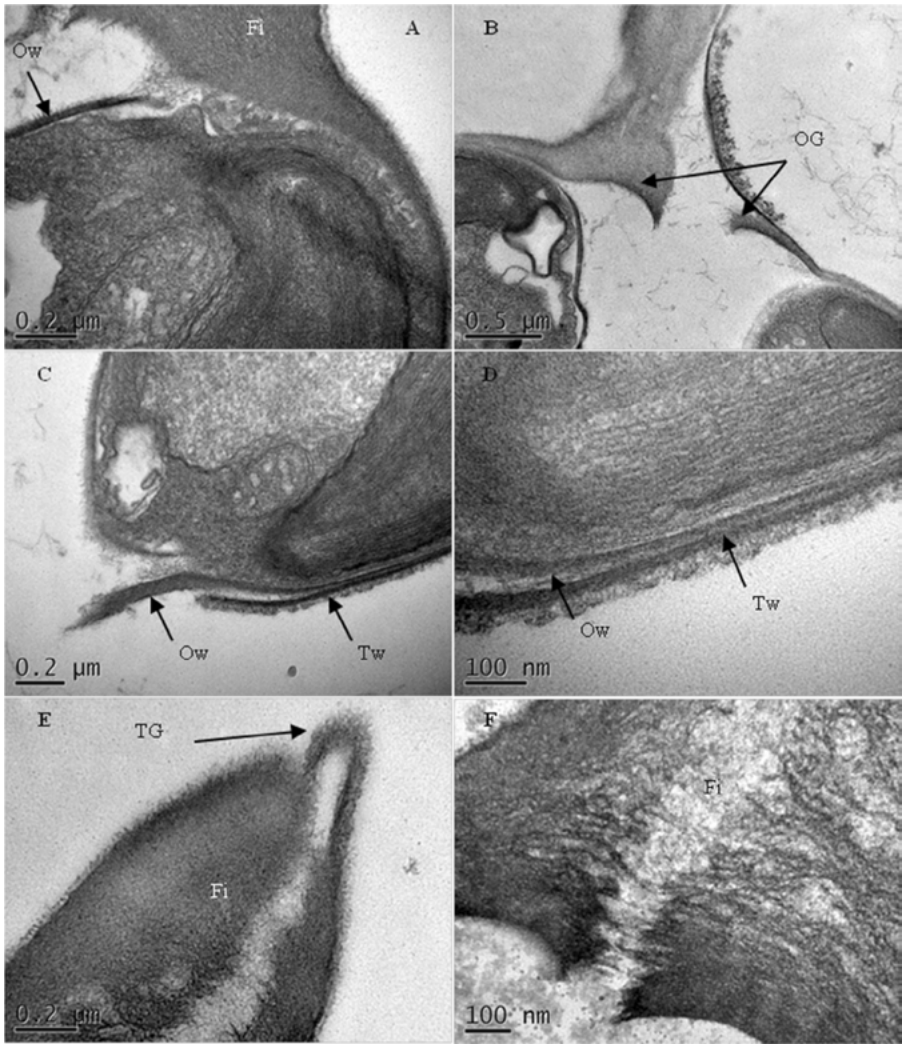

Figure 3.7 *Phaeodactylum tricornutum*: high-resolution electron micrographs of panels in Figure 3.6. (A–D) Details of junctions between newly formed oval and parent triradiate cell walls: (A) and (B) correspond, respectively, to panels in zones A1 and B in Figure 3.6; (C) and (D) correspond to zone A2 in Figure 3.6; (E) and (F) details of triradiate arm and fibrillar material corresponding to zone A3 in Figure 3.6. Fi = fibrillar substance, OG = oval girdle band region, Ow = oval cell wall, TG = triradiate girdle band region, Tw = triradiate cell wall.

the primary cell is entirely composed of organic material (Figure 3.6). Silicification only takes place after the first division, an optional raphe being formed in the new hypotheca of the two daughter oval cells (Figure 3.6). The division of the primary oval cell inside the transformed parent cell then follows the process of a normal division, and the ultrastructure of the oval cells formed inside the parent cell is similar to that described

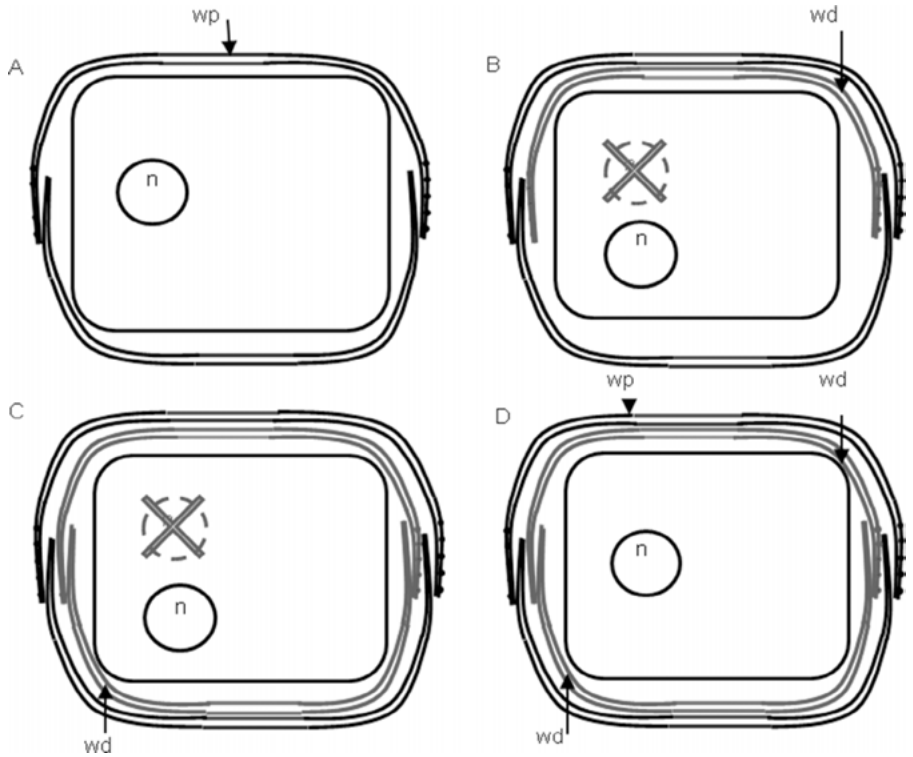

Figure 3.8 *Phaeodactylum tricornutum*: schematic representation of acytokinetic mitoses involved in the formation of oval cells. (A) Parent cell; (B) first acytokinetic mitosis, one nucleus degenerates and one new valve is formed; (C) second acytokinetic mitosis, one nucleus degenerates and the second new valve is formed; (D) new oval cell within parent cell. n: nucleus, wd: oval cell wall; wp: parental cell wall.

for free oval cells (Figure 3.6) (see Borowitzka and Volcani 1978). However, after the division of the primary oval cell, daughter oval cells may be attached to the remaining part of the parent wall (Figure 3.6C). Partially fused cell walls leading to chain formation whereby cells remain attached in the centres of the newly formed valves have been previously described by Borowitzka et al. (1977) during normal division of fusiform and triradiate morphotypes in the Long Island strain Pt7. As possible mechanisms, the authors (op. cit.) suggested that either the pressure within the chain leads to contact between the two forming valves, or the absence of fibrillar material prevents the fusion of the cell wall during organic deposition. Similar mechanisms may be involved in the transformation from fusiform and triradiate cells to the oval morphotype. Oval cells develop and divide inside parent cells where pressure may be responsible for cell wall fusion in zones where fibrillar material is absent, i.e. in the middle of the epitheca of the two daughter oval cells. This explains the observation in the Blackpool and Atlantic strains (Figures 3.3F, I and 3.6B, C) and in some other works (Wilson 1946; De Martino et al. 2007) that some oval cells adhered to the wall of the parent cell before being completely released in the medium.

The genetic mechanisms leading to induction of transformation are not known, but structural changes of the parent cell are accompanied by changes in biochemical composition. During oval cell formation from fusiform morphotypes, Gutenbrunner et al. (1994) observed that normal fusiform cells could be distinguished from transforming fusiform cells by toluidine blue staining; transforming fusiform cells stained to the same extent as oval cells, whereas normal fusiform cells stained only slightly, a characteristic also observed by Abdullahi et al. (2006). According to the authors, the metachromatic shift in transformed fusiform and oval cells may indicate an increase in cell surface-associated acidic groups. The authors (op. cit.) reported that most of the antibodies generated against surface components of oval cells do not cross react with the wall of fusiform morphotypes. The different ability for labelling cell surface component observed between the two morphotypes in these two studies could be due to differences in exopolymeric substances and proteoglycans (Hoagland et al. 1993; Abdullahi et al. 2006), or to modular proteins found only on the surface of oval cells (Dugdale et al. 2006). Biochemical changes are supported by different protein patterns of cytoplasmic extracts from oval and fusiform morphotypes and by the restoration of the fusiform protein pattern when oval cells transform to the fusiform morphology (Gutenbrunner et al. 1994).

Transformation into fusiform and triradiate morphotypes

Reverse transformation of the oval morphotype into fusiform or triradiate morphotypes has been described in several studies (Table 3.1) and is mainly associated with transfer from solid or nutrient-deprived liquid media to fresh liquid media. Reverse transformation yields fusiform morphotypes if oval cells originate from fusiform cells (as observed in the Plymouth strain and the Blackpool strain: see Table 3.1). The outcome of reverse transformation is more variable when oval cells developed from the triradiate morphotype, produce either fusiform or triradiate cells (Plymouth strain: Wilson 1946; Woods Hole strain: Lewin et al. 1958; Atlantic strain: see Table 3.1). Reverse transformation of the oval form requires enlargement of oval cells and steady growth of arms, two for the fusiform and three for triradiate morphotypes, leading to a progressive and regular transformation of shape. Progressive elongation of arms was described by Wilson (1946) for the Pt2 strain and is shown for the Atlantic strain in Figure 3.9A–C.

Transformation of triradiate cells to fusiform cells occurs in liquid media and leads to asymmetrical shape. The production of fusiform cells from triradiate cells was described for the Plymouth strain by Wilson (1946), who also noted a high percentage of "short-arm" cells in the triradiate population leading to the fusiform cells. Transformation stages are characterized by the cell having one arm considerably shorter than the other two, or having one long and two short arms, which has also been shown by Bartual et al. (2008) for the same strain (Pt2) and De Martino et al. (2007) for the Vancouver (Pt8) strain. Boomerang-shaped cells as a result of the above transformation process were also observed for the Woods Hole, Long Island (Borowitzka and Volcani 1978) and Atlantic strains (Figure 3.9D–E). Transformation of fusiform cells to triradiate forms was observed only by Wilson (1946), but with a slower increase in population change than for the inverse transformation.

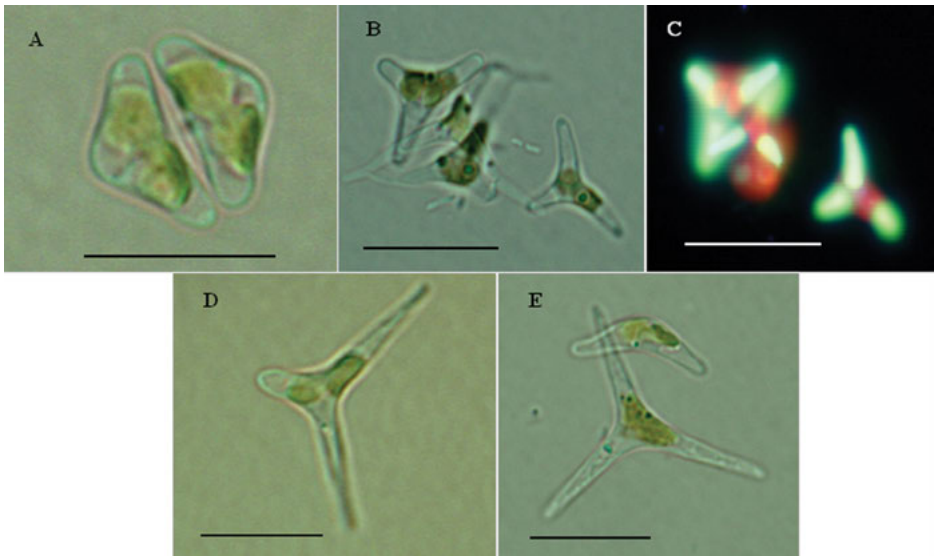

Figure 3.9 *Phaeodactylum tricornutum*: light micrographs of Atlantic strain intermediate forms: (A–C) between oval and triradiate cell; (D–E) between triradiate and fusiform cell (boomerang-shaped cell); (C) epifluorescence micrograph of PDMPO (lysosensor™ yellow/blue DND-160; Molecular Probes) stained cells. Scale bars= 10 µm.

Discussion

Pleiomorphy of *Phaeodactylum* cannot be counted as a common characteristic of raphid diatoms. Some centric diatoms of the genera *Triceratium, Lithodesmium, Ditylum, Biddulphia* or *Biddulphiopsis* also exhibit triradiate morphology, but tripolarity is not the regular valve pattern in pennate species because of their bilateral development. However, tripolar forms have been observed in some genera of raphid diatoms, such as *Achnanthes* and *Denticula*. In these cases, tripolar replace bipolar forms in changing environmental conditions, after regeneration from resting stages, and should be considered as a morphological defect (Schmid 1997). Pleiomorphy is in contrast a well known behaviour of araphid pennates that encompass most morphologically different forms (Kooistra et al. 2008). Tripolarity is a feature common in various genera belonging to the class Fragilariophyceae, *Fragilaria, Tabellaria, Pseudostaurosiropsis* (see Schmid 1997; Morales 2005). Change from planktonic or benthic lifestyles result in variability of morphological traits of valves or colony formation. As a matter of fact, most araphid species that show a planktonic lifestyle possess lightly silicified frustules in comparison to benthic species, and all of them form colonies, while benthic species are solitary or form small colonies. In contrast, despite a similar reduction in silicification, *Phaeodactylum* changes the morphology of the planktonic fusiform and triradiate morphotypes without regular colony formation, even if chains of fusiform or triradiate cells have been observed in some cultures (Borowitzka et al. 1977; Bowler et al. 2010). The question could be why *Phaeodactylum* developed such an adaptation in which a benthic oval form is transformed into two different planktonic forms that seem to exploit the same ecological niche?

Based on this review, it is noteworthy that many adverse growth conditions (i.e. high metal concentration, high light, high temperature, UV exposure, salinity stress) that induce morphological changes in many diatoms and lead to teratological forms, resting spores or sexual reproduction (see Schmid 1979; Martin-Jézéquel and Lopez 2003; Falasco et al. 2009), did not induce change of morphotypes in *Phaeodactylum* in cultures. In fact, few growth conditions can be related to transformation. Transformation of the fusiform to the triradiate morphotype was obtained under alkaline pH or sub-saturating light levels. With the exception of the very common induction of morphological changes by nutrient limitation and the tropisme of oval cells for solid support, transformation of the fusiform – or triradiate – to oval morphotypes was observed at sub-optimal temperature (cold-temperature stress), low calcium concentration and in a few cases under salinity stress. This suggests that transformation to oval forms is instigated by external factors governing cell density and flotation (see Margalef 1978; Boyd and Gradmann 2002) while reverse transformation between the fusiform and triradiate forms are mainly induced by growth conditions linked to carbon availability.

Change in gross morphology in response to changes in environmental conditions may correspond to specific signals or regulations, probably giving an ecological advantage to the arising morphotype. For some time, authors have observed that fusiform and triradiate cells are more buoyant than the oval ones (Lewin et al. 1958). To sustain pelagic lifestyles, these two forms are adapted to flotation by the expansion of the cell surface and the increase of the surface/volume (S/V) ratio which is known to decrease sinking rates (Smayda 1970; Margalef 1978; Raven and Waite 2004). Changes of cell shape and extension of vacuolation are also significant in terms of acquisition of limiting resources, nutrition and energetic balances. In particular, increasing the surface area per unit volume of cytoplasm favours the acquisition of nutrients (Margalef 1978) as well as gaseous chemicals and photon absorption (Raven 1997), a pattern that would explain the extent of tripolarity in *Phaeodactylum* under sub-saturating light and alkaline conditions of growth.

In addition, the fusiform or triradiate forms helps to increase cell suspension in comparison to the oval forms, since spherical forms have higher sinking rates (Smayda 1970). Moreover, even if the two morphotypes do not induce positive buoyancy by enlarging surface area (Boyd and Gradmann 2002), they allow a better control over buoyancy when reducing silification and increasing the size of vacuolar compartments (Margalef 1978; Boyd and Gradmann 2002; Raven and Waite 2004). Increasing buoyancy can be achieved by decreasing the density of the vacuolar content, by changing organic solutes and by excluding heavy ions such as Mg^{2+} and Ca^{2+} in favour of lighter ones like Na^{+} (Raven 1997; Boyd and Gradmann 2002). In the case of *Phaeodactylum*, this behaviour could be facilitated in the fusiform and triradiate morphotypes having large vacuoles. Matter of fact, calcium concentrations are higher in *Phaeodactylum* compared to other marine diatoms and was shown to increase during stationary growth phases, coinciding with loss of buoyancy for staying in suspension (Hayward 1970). Cellular plasticity can also be an advantage for adaptation in a changing environment. Even if an organic wall is energetically more expensive than a silicified one, it is also more versatile (Raven 1983), permitting planktonic cells of *Phaedactylum* to react rapidly by changing cell shape and regulating the protoplast density via the change of vacuolar size and composition (Raven 1997; Raven and Waite 2004). Changing shape and filling arms with large vacuoles

would be made possible by flexible girdle bands, as it was shown in *Centronella reicheltii* Voigt by Schmid (1997). From another perspective, oval forms are likely the result of environmental stress. In this case, acquisition of silicified walls would act as 'ballast' enabling sinking (Raven and Waite 2004). Transformation to oval forms under adverse conditions also prevents cell dispersion and limits metabolic costs, with a lower energetic requirement for maintenance of silicified frustules than polysaccharidic walls (Raven 1983). Reduction of vacuole size increases the cytoplasm ratio in oval forms reducing energetic costs and resulting in an increase in dessication tolerance (Raven 1997).

During the process of transformation of the morphotypes, complex cellular modifications are required. Pleiomorphy favours *Phaeodactylum* morphotypes with mostly organic cell walls, which provide plasticity, and large vacuoles enabling control over the retraction of the protoplasm. Morphological changes of *Phaeodactylum* probably use similar mechanisms as those involved in diatom division, where the cytoskeleton, tension of the cytoplasmic cortex and plasma membranes and cell turgor influence the final frustule shape (Pickett-Heaps et al. 1990; Pickett-Heaps 1991; Schmid 1994). Mechanisms of transformation from fusiform or triradiate to oval forms and *vice versa* are however very different. The former involve retraction of the protoplast followed by mitosis which allows cells to synthesize a wall adapted to its new shape (molded inside the new oval protoplast). The dense fibrillar material observed inside the transforming cell is likely to form a compression-resistant mechanical component which could stabilize the oval protoplast before formation of the new cell wall. In contrast, transformation to fusiform or triradiate forms requires *de novo* synthesis of cell wall component to form the arms, probably following a similar mechanism employed during plant cell growth, where microtubules control the polarity of growth and actin microfilaments are involved in the targeting of vesicles filled with cell wall material at the site of expansion (Mathur and Hülskamp 2002).

Conclusion

Phaeodactylum is a peculiar species, as 44% of POF (proteins with obscure functions) were found in its putative proteome, which is considerabely higher than the 18 to 38% of POFs found in other eukaryotic proteomes (Gollery et al. 2006). However, advances in understanding *Phaeodactylum* physiology were recently achieved by comparing differential genes expression and correlating these with various growth conditions (Montsant et al. 2005; Maheswari et al. 2005, 2009, 2010 and refs therein). Recent studies used *in silico* analysis and molecular tools to explore metabolic and regulatory pathways to understand the functions of genes. This includes explorations of carbon pathways (Kroth et al. 2008); pigments (Coesel et al. 2008); N and Fe metabolisms (Allen et al. 2006, 2008); stress adaptation (Vardi et al. 2008); silicification processes (Sapriel et al. 2009; Vartanian et al. 2009) and regulation of cell cycles (Huysman et al. 2010).

However, despite these recent advances and past morphological and biochemical examinations, our knowledge of the induction of pleiomorphy of *Phaeodactylum* is still limited. Pleiomorphy and mechanisms of transformation are probably the result of differential gene expression involved in morphogenesis. As stated by Schmid (1997) (in a study on tripolarity in other diatoms) and as shown by work of De Martino et al. (2007), the morphological patterns observed in *Phaeodactylum* are unlikely to be due to mutation, but are probably the manifestation of morphogenetic mechanisms

epigenetically controlled and sensitive to external factors. Biochemical processes during transformation (accompanied by the excretion of external compounds) of the parent cell may require specific gene expression and posttranslational modifications (Gutenbrunner et al. 1994). The mechanisms involved in oval cell formation differ from those required for fusiform and triradiate transformations, and therefore involve differential control of gene expression because only oval cells possess silicified cell walls with raphes. The alpha-3-frustulin gene is likely involved in the regulation of cell wall formation in oval forms as it is highly expressed in the oval cells. In contrast, the epsilon-frustulin gene was not differently expressed in 16 ESTs libraries from oval and fusiform morphotypes analyzed by Maheswari et al. (2010). Differential gene expression may also control the synthesis of modular proteins involved in cell motility and adhesion, and the synthesis of the raphe, which is known to be involved in extracellular matrix formation and motility.

Genomic studies on *Phaeodactylum* under different ecological conditions, such as the work of Mahesawari et al. (2010), provide some clues for the comprehension of its pleiomorphy. They showed that each morphotype expressed different genes, for example oval cells (clone Pt3) over-expressed genes of lipid metabolism whereas triradiate morphotype (clone Pt8) library showed over expression of genes encoding active transport processes. These results provide evidence that change of morphotype enables development of distinct strategies under changing growth conditions. Future work should focus on decoding genes involved in cellular regulation of pleiomorphy. Tools are in place to allow such investigations; clone Pt1 8.6 (De Martino et al. 2007) has been sequenced (http://genome.jgi psf.org/Phatr2/Phatr2.home.html; Maheswari et al. 2005). It has already been successfully transformed (Apt et al. 1996; Falciatore et al. 1999; Zaslavskaia et al. 2000; Siaut et al. 2007) and gene silencing is possible using RNA interference (De Riso et al. 2009). Functional genomics would thus allow further exploration of the mechanisms of pleiomorphism in this peculiar diatom.

Acknowledgements

We are grateful to C. Gaillard (INRA) for its assistance in electron microscopy. We thank P. Gaudin for the preparation of the cultures, and Innovalg (Bouin, France) for providing triradiate cells natural samples. We thank M. Jézéquel and C. Bannister for the correction of the manuscript. We are grateful to anonymous reviewers and Prof. K. Heimann for critical reading of the earlier version of this manuscript. Research of V. Martin-Jézéquel is supported by the Centre National de la Recherche Scientifique (CNRS) and University of Nantes. B. Tesson was funded by the Region Pays de Loire, the University of Nantes and the EC Sixth Framework Programme 'Diatomics' (LSHG-CT-2004-512035).

References

Abdullahi, A.S., G.J.C. Underwood and M.R. Gretz.2006. Extracellular matrix assembly in diatoms (Bacillariophyceae). V. Environmental effects on polysaccharide synthesis in the model diatom, *Phaeodactylum tricornutum. J. Phycol. 42*: 363–378.

Allen, A.E., A.Vardi and C. Bowler. 2006. An ecological and evolutionary context for integrated nitrogen metabolism and related signaling pathways in marine diatoms. *Curr. Opin. Plant Biol. 9*: 264–273.

Allen, A.E., J. LaRoche, U. Maheswari, M. Lommer, N. Schauer, P.J. Lopez, G. Finazzi, A.R. Fernie and C. Bowler. 2008. Whole-cell response of the pennate diatom *Phaeodactylum tricornutum* to iron starvation. *Proc. Natl. Acad. Sci.USA. 105*: 10438–10443.

Allen, E.J. and E.W. Nelson. 1910. On the artificial culture of marine plankton organisms. *J. Mar. Biol. Assoc, UK. 8*: 421–474.

Armbrust, E.V., J.A. Berges, C. Bowler, B.R. Green, D. Martinez, et al. 2004. The genome of the diatom *Thalassiosira pseudonana*: ecology, evolution, and metabolism. *Science 306*: 79–86.

Antia, N.J., P.J. Harrison and L. Oliveira.1991. The role of dissolved organic nitrogen in phytoplankton nutrition, cell biology and ecology. *Phycologia* 30: 1–89.

Apt, K.E., P.G. Kroth-Pancic, A.R. Grossman.1996. Stable nuclear transformation of the diatom *Phaeodactylum tricornutum. Mol. Gen. Genet. 252*: 572–579.

Barker, H.A. 1935. Photosynthesis in diatoms. *Arch. Mikrobiol. 6*: 141.

Bolhin, K. 1897. Zur morphologie und biologie einzelliger algen. *Öfvers. Kongl. Vetens. -Akad. Förh. 9*: 507–529.

Bartual, A., J.A. Galvez and F. Ojeda. 2008. Phenotypic response of the diatom *Phaeodactylum tricornutum* Bohlin to experimental changes in the inorganic carbon system. *Bot. Mar. 51*: 350–359.

Behrenfeld, M.J., J.T. Hardy and H. Lee.1992. Chronic effects of ultraviolet-B radiations on growth and cell volume of *Phaeodactylum tricornutum* (Bacillariophyceae). *J. Phycol. 58*: 757–760.

Bellinger, B.J., A.S. Abdullahi, M.R. Gretz and G.J.C. Underwood. 2005. Biofilm polymers: relationship between carbohydrate biopolymers from estuarine mudflats and unialgal cultures of benthic diatoms. *Aquat. Microb. Ecol. 38*: 169–80.

Borowitzka, M.A., M.L. Chiappino and B.E. Volcani. 1977. Ultrastructure of chain forming diatom *Phaeodactylum tricornutum. J. Phycol. 13*: 162–170.

Borowitzka, M.A. and B.E. Volcani. 1978. The polymorphic diatom *Phaeodactylum tricornutum*: ultrastructure of its morphotypes. *J. Phycol. 14*: 10–21.

Bourrelly, P., J. Dragesco. 1955. Contribution à la connaissance d'une algue rarissime *'Phaeodactylum tricornutum'* Bohlin. *Bull. Micr. Appl. 2*: 5–41.

Bowler, C., A.E. Allen, J.H. Badger, J. Grimwood, K. Jabbari et al. 2008. The *Phaeodactylum* genome reveals the evolutionary history of diatom genomes. *Nature 456(7219)*: 239–244.

Bowler, C., A. De Martino and A. Falciatore. 2010. Diatom cell division in an environmental context. *Curr. Opin. Plant Biol. 13*: 623–630.

Boyd, C.M. and D. Gradmann. 2002. Impact of osmolytes on buoyancy of marine phytoplankton. *Mar. Biol. 141*: 605–618.

Brzezinski, M., R.J. Olson and S.W. Chisholm. 1990. Silicon availability and cell-cycle progression in marine diatoms. *Mar. Ecol. Prog. Ser. 67*: 83–96.

Burns, B.D. and J. Beardall. 1987. Utilization of inorganic carbon by marine microalgae. *J. Exp. Mar. Biol. Ecol. 107*: 75–86.

Ceron Garcia, M.C., A. Sánchez Mirón, J.M. Fernández Sevilla, E. Molina Grima and F. Garcıa Camacho. 2005. Mixotrophic growth of the microalga *Phaeodactylum tricornutum*. Influence of different nitrogen and organic carbon sources on productivity and biomass composition. *Process Biochem. 40*: 297–305.

Chen, X., C.E. Qiu and J.Z. Shao. 2006. Evidence for K^+-dependent HCO_3^- utilization in the marine diatom *Phaeodactylum tricornutum. Plant Physiol*. 141: 731–736.

Chepurnov, V.A., D.G. Mann, W. Vyverman, K. Sabbe and D.B. Danielidis. 2002. Sexual reproduction, mating system, and protoplast dynamics of *Seminavis* (Bacillariophyceae). *J. Phycol. 38*: 1004–1019.

Chepurnov, V.A., D.G. Mann, K. Sabbe and W. Vyverman W. 2004. Experimental studies on sexual reproduction in diatoms. *Int. Rev. Cytol. 237*: 91–154.

Chiappino, M.L. and B.E. Volcani. 1977. Studies on the biochemistry and fine structure of silica shell formation in diatoms. VIII. Sequential cell wall development in the pennate *Navicula pelliculosa. Protoplasma 93*: 205–221.

Chiovitti, A., M.J. Higgins, R.E. Harper, R. Wetherbee and A. Bacic. 2003. The complex polysaccharides of the raphid diatom *Pinnularia viridis* (Bacillariophyceae). *J. Phycol. 39*: 543–554.

Chiovitti, A., P. Molino, S.A. Crawford, R. Teng, T. Spurck and R. Wetherbee. 2004. The glucans extracted with warm water from diatoms are mainly derived from intracellular chrysolaminaran and not extracellular polysaccharides. *Eur. J. Phycol*. 39: 117–128.

Chiovitti, A., R.E. Harper, A. Willis, A. Bacic, P. Mulvaney and R. Wetherbee. 2005. Variation in the substituted 3-linked mannans closely associated with the silicified wall of diatoms. *J. Phycol. 41*: 1154–1161.

Chiovitti, A., T.M. Dugdale and R. Wetherbee. 2006. Diatom adhesives: molecular and mechanical properties. *In*: (A.M. Smith and J.A. Callow, eds.) *Biological Adhesives*. Springer-Verlag, Berlin/Heidelberg, pp. 79–103.

Coesel, S., M. Obornık, J. Varela, A. Falciatore and C. Bowler. 2008. Evolutionary Origins and Functions of the Carotenoid Biosynthetic Pathway in Marine Diatoms. *PLoS One* 3, Issue 8, e2896.

Cooksey, K.E. and B. Cooksey. 1974. Calcium deficiency can induce the transition from oval to fusiform cells in cultures of *Phaeodactylum tricornutum* Bolhin. *J. Phycol. 10*: 89–90.

Craigie, J.S. 1974. Storage products. *In*: (W.D.P. Stewart, ed) *Algal physiology and biochemistry*. Blackwell Scientific Publication, Oxford, pp. 207–235.

Darley, W.M. 1968. Deoxyribonucleic acid content of the three cell types of *Phaeodactylum tricornutum* Bolhin. *J. Phycol. 4*: 219–220.

De Martino, A., A. Meichenin, J. Shi, K. Pan and C. Bowler. 2007. Genetic and phenotypic characterization of *Phaeodactylum tricornutum* (Bacillariophyceae) accession. *J. Phycol. 43*: 992–1009.

De Martino, A., A. Amato and C. Bowler. 2009. Mitosis in diatoms: rediscovering an old model for cell division. *BioEssays 31*: 874–884.

De Riso, V., R. Raniello, F. Maumus, A. Rogato, C. Bowler and A. Falciatore. 2009. Gene silencing in the marine diatom *Phaeodactylum tricornutum. Nucleic Acids Res. 37*, no. 14 e96.

Del Amo,Y. and M.A. Brzezinski. 1999. The chemical form of dissolved Si taken up by marine diatoms. *J. Phycol*. *35*: 1162–1170.

Desclés, J., M. Vartanian, A. El Harrak, M. Quinet, N. Bremond, G. Sapriel, J. Bibette and P.J. Lopez. 2008. New tools for labeling silica in living diatoms. *New Phytol. 177*: 822–829.

Dickinson, H.G. and P.R. Bell. 1970. The development of the sacci during pollen formation in *Pinus banksiana. Grana 10*: 101–108.

Dickson, D.M.J. and G.O. Kirst. 1987. Osmotic adjustment in marine eukariotic algae: the role of inorganic ions, quaternary ammonium, tertiry sulphonium and carbogydrate solutes. I. Diatoms and a Rhodophyte. *New Phytol. 106*: 645–655.

Dugdale, T.M., R. Dagastine, A. Chiovitti, P. Mulvaney and R. Wetherbee. 2005. Single adhesive nanofibers from a live diatom have the signature fingerprint of modular proteins. *Biophys. J. 89*: 4252–4260.

Dugdale, T.M., A. Willis and R. Wetherbee. 2006. Adhesive modular proteins occur in the extracellular mucilage of the motile, pennate diatom *Phaeodactylum tricornutum. Biophys. J. 90*: L58–L60.

Edgar, L.A. and J.D. Pickett-Heaps. 1984. Valve morphogenesis in the pennate diatom *Navicula cuspidata. J. Phycol. 20*: 47–61.

Erga, S.R., G.C. Lie, L.H. Aarø, K. Aursland, C. Daae Olseng, O. Frette and B. Hamre. 2010. Fine scale vertical displacement of *Phaeodactylum tricornutum* (Bacillariophyceae) in stratified waters: Influence of halocline and day length on buoyancy control. *J. Exp. Mar. Biol. Ecol. 384*: 7–17.

Fabregas, J., E.D. Morales, T. Lamela and O. Cabezas. 1997. Mixotrophic productivity of the marine diatom *Phaeodactylum tricornutum* cultured with soluble fractions of rye, wheat and potatoe. *World J. Microbiol. Biotechnol.113*: 349–351.

Falasco, E., F. Bona, G. Badino, L. Hoffmann and L. Ector. 2009. Diatom teratological forms and environmental alterations; a review. *Hydrobiologia 623*: 1–35.

Falciatore, A., R. Casotti, C. Leblanc, C. Abrescia and C. Bowler. 1999. Transformation of nonselectable reporter genes in marine diatoms. *Mar. Biotechnol. 1*: 239–251.

Falciatore, A., M.R. d'Alcala, P. Croot and C. Bowler. 2000. Perception of environmental signals by a marine diatom. *Science 288*: 2363–2366.

Ford, C.W. and E. Percival. 1965. The carbohydrates of *Phaeodactylum tricornutum*. Part II. A sulfated glucuromannan. *J. Chem. Soc. 1298*: 7042–7046.

Francius, G., B. Tesson, E. Dague, V. Martin-Jézéquel and Y.F. Dufrêne. 2008. Nanostructure and nanomechanics of live *Phaeodactylum tricornutum* morphotypes. *Environ. Microbiol. 10*: 1344–1356.

Garcia Camacho, F., E. Molina Grima, A. Sanchez Miron, V. Gonzales Pascual and Y. Chisti. 2001. Carboxymethyl cellulose protects algal cell against hydrodynamic stress. *Enzym. Microb. Technol. 29*: 602–610.

Gauthier, C., J. Livage, T. Coradin and P.J. Lopez. 2006. Sol–gel encapsulation extends diatom viability and reveals their silica dissolution capability. *Chem. Comm.*: 4611–4613. DOI: 10.1039/b609121k

Geider, R.J., J. La Roche, R.M. Greene and M. Olaizola. 1993. Response of the photosynthetic apparatus of *Phaeodactylum tricornutum* (Bacillariophyceae) to nitrate, phosphate or iron starvation. *J. Phycol*. *29*: 755–766.

Goldman, J.C., C.B. Riley and M.R. Dennett. 1982. The effect of pH in intensive microalgal cultures. II. Species competition. *J. Exp. Mar. Biol. Ecol*. *57*: 15–24.

Gollery, M., J. Harper, J. Cushman, T. Mittler, T. Girke, J.K. Zu, J. Bailey-Serres and R. Mittler. 2006. What makes species unique? The contribution of proteins with obscur features. *Genome Biol. 7*: R57.

Gutenbrunner, S.A., J. Thalhamer and A.M.M. Schmid. 1994. Proteinaceous and immunochemical distinctions between the oval and fusiform morphotypes of *Phaeodactylum tricornutum* (Bacillariophyceae). *J. Phycol. 30*: 129–136.

Hansen, P.J. 2002. Effect of high pH on the growth and survival of marine phytoplankton: implications for species succession. *Aquat. Microb. Ecol. 28*: 279–288.

Hayward, J. 1970. Studies on the growth of *Phaeodactylum tricornutum*. VI. The relationship to sodium, potassium, calcium and magnesium. *J. Mar. Biol. Assoc. UK 50*: 293–299.

Hendey, N.I. 1954. Note on the Plymouth *Nitzschia* culture. *J. Mar. Biol. Assoc, UK. 33*: 335.

Hendey, N.I. 1964. An Introductory Account of the Smaller Algae of British Coastal Waters. *Fishery Investigations Series IV*. Part V Bacillariophyceae (Diatoms). Her Majesty's Stationery Office, F. Midler and Sons (eds), London, pp. 317.

Hildebrand, M. 2003. Biological processing of nanostructured silica in diatoms. *Progress Organic Coating 47*: 256–266.

Hildebrand, M. 2008. Diatoms, Biomineralization Processes, and Genomics. 2008. *Chem. Rev. 108*: 4855–4874.

Hinga, K.R. 2002. Effects of pH on coastal marine phytoplancton. *Mar. Ecol. Prog. Ser. 238*: 281–300.

Hoagland, K.D., J.R. Rosowski, M.R. Gretz and S.C. Roemer. 1993. Diatom extracellular polymeric substances: function, fine structure, chemistry, and physiology. *J. Phycol. 29*: 537–566.

Holloway, C.F. and J.P. Cowen. 1997. Development of a scanning confocal laser microscopic technique to examine the structure and composition of marine snow. *Limnol. Oceanogr. 42(6)*: 1340–1352.

Holzinger, A. and C. Lütz. 2006. Algae and UV irradiation: Effects on ultrastructure and related metabolic functions. *Micron 37*: 190–207.

Huysman, M.J.J., C. Martens, K. Vandepoele, J. Gillard, E. Rayko E., M. Heijde, C. Bowler, D. Inze, Y. Van de Peer, L. De Veylder and W. Vyverman. 2010. Genome-wide analysis of the diatom cell cycle unveils a novel type of cyclins involved in environmental signalling. *Genome Biol. 11*: R17

Iwasa, K., S. Murakami, A. Shimizu and K. Imahori. 1971. Mechanisms of dimorphism and motility of the diatom *Phaeodactylum tricornutum* Bohlin. *Proc. Int. Seaweed Symp. 7*: 319–322.

Iwasa, K. and A. Shimizu. 1972. Motility of the diatom *Phaeodactylum tricornutum. Exp. Cell Res. 74*: 552–558.

Johansen, J.R. 1991. Morphological variability and cell wall composition of *Phaeodactylum tricornutum* (Bacillariophyceae). *Great Basin Nat. 51*: 310–315.

Kates, M. and B.E. Volcani. 1968. Studies on the biochemistry and fine structure of silica shell formation in diatoms. Lipid components of the cell walls. *Zeitschr. Pflanzenphysiol. 60*: 19–29.

Kooistra, W.C.H.F. 2007. The Evolution of the Diatoms. Chap. 6. *In*: (E. Baüerlein, ed.) *Handbook of Biomineralization*, Vol. 1.Wiley, Weinheim, pp. 95–112.

Kooistra, W.H.C.F., M. DeStefano, D.G. Mann and L.K. Medlin. 2003. The phylogeny of the diatoms. *In*: (W.E.G. Müller, ed.) *Prog. Mol. Subcell. Biol*. 33. Springer-Verlag, Berlin, pp 63–97.

Kooistra, W.H.C.F., R. Gersonde, L.K. Medlin and D.G. Mann. 2007. The origin and evolution of the diatoms: their adaptation to a planktonic existence. Chap. 11. *In*: (P.G. Falkowski and A.H. Knoll, eds.) *Evolution of primary producers in the sea.*, Academic Press, pp. 207–249.

Kooistra, W.H.C.F., G. Forlani and M. De Stefano. 2008. Adaptations of araphid pennate diatoms to a planktonic existence. *Mar. Ecol. 30(1)*: 1–15.

Kröger, N. 2007. Prescribing diatom morphology: toward genetic engineering of biological nanomaterials. *Curr. Opin. Chem. Biol. 11*: 662–669.

Kröger, N., C. Bergsdorf and M. Sumper. 1996. Frustulins: Domain conservation in a protein family associated with diatom cell walls. *Eur. J. Biochem. 239*: 259–264.

Kröger, N. and N. Poulsen. 2008. Diatoms-From Cell Wall Biogenesis to Nanotechnology. *Annu. Rev. Genet. 42*: 83–107.

Kroth, P.G., A. Chiovitti, A. Gruber, V. Martin-Jézéquel, T. Mockt, M. Schnitzler-Parker, M. Stanley, A. Kaplan, L. Caron, T. Weber, U. Maheswhari, A.V. Armbrust and C. Bowler. 2008. A model for carbohydrates metabolism in the diatom *Phaeodactylum tricornutum* deduced from whole genome analysis and comparative genomic analyses with *Thalassiosira pseudonana* and other photoautotrophs. *PLoS One. 3(1)*: e1426. doi:10.1371/journal.pone.0001426.

Levy, J.L., B.M. Angel, J.L. Stauber, W.L. Poon, S.L. Simpson, S.H.Cheng and D.F. Jolley. 2008. Uptake and internalisation of copper by three marine microalgae: Comparison of copper-sensitive and copper-tolerant species. *Aquat. Toxicol. 89*: 82–93.

Lewin, J.C. 1958. The taxonomic position of *Phaeodactylum tricornutum. J. Gen. Microbiol. 18*: 427–432.

Lewin, J.C., R.A. Lewin and D.E. Philpott. 1958. Observations on *Phaeodactylum tricornutum. J. Gen. Microbiol. 18*: 418–426.

Lewin, JC. and R.A. Lewin.1960. Auxotrophy and heterotrophy in marine littoral diatoms. *Can. J. Microbiol. 6*: 127–31.

Lu, K., X. Lin and Y. Qian. 2001. Studies on the morphotype and morphological variation of *Phaeodactylum tricornutum. J. Ocean University Qingdao. 31*: 61–68.

Maheswari, U., A. Montsant, J. Goll, S. Krishnasamy, K.R. Rajyashri, V.M. Patel and C. Bowler. 2005. The diatom EST database. *Nucleic Acids Res. 33*: D344–347.

Maheswari, U., T. Mock, E.V. Armbrust and C. Bowler. 2009. Update of the Diatom EST Database: a new tool for digital transcriptomics. *Nucleic Acids Res. 37*: D1001–1005.

Maheswari, U., K. Jabbari, J.L. Petit, B.M. Porcel, A.E. Allen, J.P. Cadoret, A. De Martino, M. Heijde, R. Kaas, J. La Roche, P.J. Lopez, V. Martin-Jézéquel, A. Meichenin, T. Mock, M. Schnitzler-Parker, A. Vardi, E.V. Armbrust, J. Weissenbach, M. Katinka and C. Bowler. 2010.

Digital expression profiling of novel diatom transcripts provides insight into their biological functions. *Genome Biol. 11*: R85

Mann, D.G. 1999. The species concept in diatoms. *Phycologia 38*: 437–495.

Margalef, R. 1978. Life-forms of phytoplankton as survival alternatives in an unstable environment. *Oceanologica Acta 1(4)*: 493–509.

Marsot, P. and L. Houle. 1989. Excrétion cellulaire et morphogénèse de *Phaeodactylum tricornutum* (Bacillariophyceae). *Bot. Mar. 32*: 355–367.

Martin-Jézéquel V., M. Hildebrand and M.A. Brzezinski. 2000. Silicon metabolism in diatoms: Implications for growth. *J. Phycol. 36*: 821–840.

Martin-Jézéquel, V. and P.J. Lopez. 2003. Silicon – a central metabolite for diatom growth and morphogenesis. *In*: (W.E.G. Muller, ed.) *Silicon biomineralization: biology, biochemistry, biotechnology. Progress in Molecular and Subcellular Biology*. Springer-Verlag Berlin Heildelberg, pp. 99–124.

Mathur, J. and M. Hülskamp. 2002. Microtubules and microfilaments in cell morphogenesis in higher plants. *Curr. Biol. 12*: 669–676.

McConville, M.J., R. Wetherbee and A. Bacic. 1999. Subcellular location and composition of the wall and secreted extracellular sulphated polysaccharides/proteoglycans of the diatom *Stauroneis amphioxys* Gregory. *Protoplasma. 206*: 188–200.

Medlin, L.K., W. Kooistra, R. Gersonde and U. Wellbrock. 1996. Evolution of the diatoms (Bacillariophyta). 2. Nuclear-encoded small-subunit rRNA sequence comparisons confirm a paraphyletic origin for the centric diatoms. *Mol. Biol. Evol. 13*: 67–75.

Medlin, L.K., W.H.C.F. Kooistra, D. Potter, G.W. Saunders and R.A. Andersen. 1997. Phylogenetic relationships of the "golden algae" (hepatophytes, heterokont chrysophytes) and their plastids. *Plant Syst. Evol. Suppl. 11*: 187–210.

Medlin, L.K., W.H.C.F. Kooistra and A.-M.M. Schmid. 2000. A review of the evolution of the diatoms – a total approach using molecules, morphology and geology. *In*: (A. Witkowski and J. Siemimska, eds.) *The origin and early evolution of the diatoms: Fossil, molecular and biogeographical approaches*. Cracow, Poland, Szafer Institute of Botany, Polish Academy of Science, pp. 13–35.

Medlin, L.K. and I. Kaczmarska. 2004. Evolution of the diatoms: V. Morphological and cytological support for the major clades and a taxonomic revision. *Phycologia 43*: 245–270.

Mills, K.E. and I. Kaczmarska. 2006. Autogamic reproductive behavior and sex cell structure in *Thalassiosira angulata* (Bacillariophyta). *Bot. Mar. 49*: 417–430.

Molino, P.J. and R. Wetherbee. 2008. The biology of biofouling diatoms and their role in the development of microbial slimes. *Biofouling 24(5)*: 365–379.

Montsant, A., K. Jabbari, U. Maheswari and C. Bowler. 2005. Comparative genomics of the diatom *Phaeodactylum tricornutum. Plant Physiol. 137*: 500–513.

Morales, E.A. 2005. Observations of the morphology of some known and new fragilarioid diatoms (Bacillariophyceae) from rivers in the USA. *Phycol. Res. 53:* 113–133

Nelson, D.M., G.F. Riedel, R. Millan-Munez and J.R. Lara-Lara. 1984. Silicon uptake by algae with no known silicon requirement. I. True cellular uptake and pH induced precipitation by *Phaeodactylum tricornutum* (Bacillariophyceae) and *Platymonas* sp. (Prasinophyceae). *J. Phycol. 20*: 141–147.

Neuville, D., P. Daste and L. Genevès. 1971. Sur une souche axénique de *Phaeodactylum tricornutum* (Bolhin) isolée à partir d'une claire ostréicole de l'île d'Oléron. *C. R. Acad. Sci. Paris. 273*: 1221–1223.

Olsen, L.M., M. Öztürk, E. Sakshaug and G. Johnsen. 2006. Photosynthesis induced phosphate precipitation in seawater: ecological implications for phytoplankton. *Mar. Ecol. Prog. Ser. 319*: 103–110.

Oudot-Le Secq, M.P., J. Grimwood, H. Shapiro, E.V. Armbrust, C. Bowler and B.R. Green. 2007. Chloroplast genomes of the diatoms *Phaeodactylum tricornutum* and *Thalassiosira pseudonana*:

comparison with other plastid genomes of the red lineage. *Mol. Genet. Genomics 277*: 427–439. DOI 10.1007/s00438–006–0199–4

Passow, U. 2002. Transparent exopolymer particles (TEP) in aquatic environments. *Progr. Oceanogr. 55*: 287–333.

Pickett-Heaps, J. 1991. Cell Division in Diatoms. *Int. Rev. Cytol. 128*: 63–108.

Pickett-Heaps, J., A-M.M. Schmid and L.A. Edgar.1990. The cell biology of the diatom valve formation. *In*: (F.E. Round and D.J.K. Capman, eds.) *Progr. Phycol. Res*. Bristol, UK: Biopress Ltd, pp.1–168.

Poulsen, N.C., I. Spector, T.F. Spurck, T.F. Schultz and R. Wetherbee.1999. Diatom gliding is the result of an actin-myosin motility system. *Cell Motil. Cytoskelet 44*: 23–33.

Raven, J.A. 1983. The transport and function of silicon in plants. *Biol. Rev. 58*: 179–207.

Raven, J.A. 1997. The vacuole: a cost-benefit analysis. *Adv. Bot. Res. 35*: 59–86.

Raven, J.A. and A.M. Waite. 2004. The evolution of silicification in diatoms: inescapable sinking and sinking as escape? *New Phytol. 162*: 45–61.

Reimann, B.E.F., J.C. Lewin and B.E. Volcani. 1966. Studies of the biochemistry and fine structure of silica shell formation in diatoms. II. The structure of the cell wall of *Navicula pelliculosa* (Bréb.) Hilse. *J. Phycol. 2*: 74–84.

Reimann, B.E. and B.E. Volcani. 1968. Studies on the biochemistry and fine structure of silica shell formation in diatoms. III. The structure of the cell wall of *Phaeodactylum tricornutum* Bohlin. *J. Ultrastruct. Res. 21*: 182–193.

Reynolds, E.S., 1963. The use of lead citrate at high pH as an electronopaque stain in electron microscopy. *J. Cell Biol. 17*: 208–212.

Riedel, G.F. and D.M. Nelson. 1985. Silicon uptake by algae with no known Si requirement. II. Strong pH dependence of uptake kinetic parameters in *Phaeodactylum tricornutum* (Bacillariophyceae). *J. Phycol. 21*: 168–171.

Rotatore, C., B. Colman, M. Kuzma. 1995. The active uptake of carbon dioxide by the marine diatoms *Phaeodactylum tricornutm* and *Cyclotella* sp. *Plant Cell Environ. 18:* 913–918.

Round, F.E., R.M. Crawford and D.G. Mann. 1990. *The diatoms: Biology and morphology of the genera.* Cambridge University Press, Cambridge, 747 p.

Rushforth, S.R., J.R. Johansen and D.L. Sorensen. 1988. Occurence of *Phaeodactylum tricornutum* in the great salt lake, Utah, USA. *Great Basin Naturalist 48*: 324–326.

Sapriel, G., M. Quinet, M. Heijde, L. Jourdren, V. Tanty, G. Luo, S. Le Crom and P.J. Lopez. 2009. Genome-wide transcriptome analyses of silicon metabolism in *Phaeodactylum tricornutum* reveal the multilevel regulation of silicic acid transporters. *PLoS One 4(10)*: e7458. doi:10.1371/journal.pone.0007458.

Satoh, D., Y. Hiraoka, B. Colman and Y. Matsuda. 2001. Physiological and Molecular Biological Characterization of Intracellular Carbonic Anhydrase from the Marine Diatom *Phaeodactylum tricornutum. Plant Physiol. 126*: 1459–1470.

Scala, S., N. Carels, A. Falciatore, M.L. Chiusano and C. Bowler. 2002. Genome properties of the diatom *Phaeodactylum tricornutum. Plant Physiol. 129*: 996–1002.

Scheffel, A., N. Poulsen, S. Shian and N. Kröger. 2011. Nanopatterned protein microrings from a diatom that direct silica morphogenesis. *Proc. Natl.Acad. Sci. USA 108*: 3175–3180.

Schmid, A.-M.M. 1979. Influences of environmental factors on the development of the valve of diatoms. *Protoplasma 99*: 99–115.

Schmid, A.-M.M. 1984. Tricornate spines in *Thalassiosira eccentrica* as a result of valve modeling. *In*: (D.G. Mann, ed.) *Proc. 7th Int. Symp. On Living and Fossil Diatom*s. O. Koeltz, Koenigstein, pp 71–95.

Schmid, A.-M.M. 1994. Aspects of morphogenesis and function of diatom cell walls with implications for taxonomy. *Protoplasma 181*: 43–60.

Schmid, A.-M.M. 1996. Pattern of morphogenesis in cell walls of diatoms and pollen grains: a comparison. *Protoplasma 193*: 144–173.

Schmid, A.-M.M. 1997. Intraclonal variation of the tripolar pennate diatom '*Centronella reichelti'* in culture: strategies of reversion to the bipolar *Fragilaria*-form. *Nova Hedwigia. 65*: 27–45.

Seritti, A., E. Morelli, L. Nannicini and R. Del Vecchio. 1994. Production of hydrophobic fluorescent organic matter by the marine diatom *Phaeodactylum tricornutum. Chemosphere 28(1)*: 117–129.

Seritti, A., L. Nannicini and R. Del Vecchio. 1996. Use of synchronous scan excitation spectra to detect fluorescent metal organic ligands producted by the marine diatom *Phaeodactylum tricornutum. Environ. Technol. 17*: 25–33.

Sherbakova, T.A., Y. Masyukova, T. Safonova, D. Petrova, A. Vereshagin, T. Minaeva, R. Adelshin, T. Triboy, I. Stonok, N. Aizdaitcher et al. 2005. Conserved motif CMLD in silicic acid transport proteins of diatoms. *Mol. Biol. (Mosk) 39*: 269–280.

Siaut, M., M. Heijde, M. Mangogna, A. Montsant, S. Coesel, A. Allen, A. Manfredonia, A. Falciatore and C. Bowler. 2007. Molecular toolbox for studying diatom biology in *Phaeodactylum tricornutum. Gene 406*: 23–35.

Sims, P.A., D.G. Mann and L.K. Medlin. 2006. Evolution of the diatoms: insight from fossil, biological and molecular data. *Phycologia 45*: 361–402.

Smayda, T.J. 1970. The suspension and sinking of phytoplankton in the sea. *Oceanogr. Mar. Biol. Ann. Rev. 8*: 353–414.

Smith, D.J. and G.J.C. Underwood. 2000. The production of extracellular carbohydrates by estuarine benthic diatoms: the effects of growth phase and light and dark treatment. *J Phycol. 36*: 321–333.

Stanley, M.S. and J.A. Callow. 2007. Whole cell adhesion strength of morphotypes and isolates of *Phaeodactylum tricornutum* (Bacillariophyceae). *Eur. J. Phycol. 42*: 191–197.

Stosch, H.A. Von. 1981. Structural and histochemical observations on the organic layers of the diatom cell wall. *In*: (R. Ross, ed.) *Proceedings of the 6th Symposium on Recent and Fossil Diatoms*. Koenigstein, O. Koeltz, pp 231–252.

Sumper, M. and E. Brunner. 2008. Silica biomineralization in diatoms: the model organism *Thalassiosira pseudonana. Chem. Biochem. 9:* 1187–1194.

Szabo, E. and B. Colman. 2007. Isolation and characterization of carbonic anhydrases from the marine diatom *Phaeodactylum tricornutum. Physiologia Plantarum 129*: 484–492.

Tesson, B., C. Gaillard and V. Martin-Jézéquel. 2008a. Brucite formation mediated by the diatom *Phaeodactylum tricornutum. Mar. Chem. 109*: 60–76.

Tesson, B., S. Masse, G. Laurent, J. Maquet, J. Livage, V. Martin-Jezezquel and T. Coradin. 2008b. Contribution of multi-nuclei solid state NMR to the characterization of *Thalassiosira pseudonana* diatom cell wall. *Anal. Bioanal. Chem. 390*: 1889–1898.

Tesson, B., C. Gaillard and V. Martin-Jézéquel. 2009a. Mini Review. Insights into the polymorphism of the diatom *Phaeodactylum tricornutum* Bohlin. *Bot. Mar. 52*: 104–116.

Tesson, B., M.J. Genet, V. Fernandez, S. Degand, P.G. Rouhext and V. Martin-Jezequel V. 2009b. Surface chemical composition of diatoms. *ChemBioChem 10*: 2011–2024.

Thamatrakoln, K. and M. Hildebrand. 2005. Approaches for functionnal characterization of diatom silicic acid transporters. *J. Nanoscience Nanotechno. 5*: 1–9.

Thamatrakoln, K., A.J. Alverson and M. Hildebrand. 2006. Comparative sequence analysis of diatom silicon transporters: Toward a mechanistic model of silicon transport. *J. Phycol. 42:* 822–834.

Thamatrakoln, K. and M. Hildebrand. 2007. Analysis of *Thalassiosira pseudonana* silicon transporters indicates distinct regulatory levels and transport activity through the cell cycle. *Eukariot. Cells 6*: 271–279.

Underwood, J.C. and D.M. Paterson. 2003. The importance of extracellular carbohydrate production by marine epipelic diatoms. *In*: (J.A. Callow, ed.). *Adv. Bot. Res. Vol. 40*, Oxford: Elsevier Academic Press. pp.184–240.

Vardi, A., K.D. Bidle, C. Kwityn, D.J. Hirsh, S.M. Thompson, J.A. Callow, P. Falkowski and C. Bowler. 2008. A Diatom Gene Regulating Nitric-Oxide Signaling and Susceptibility to Diatom-Derived Aldehydes. *Curr. Biol. 18*: 895–899.

Vardi, A., K. Thamatrakoln, K.D. Bidle and P.G. Falkowski. 2009. Diatom genomes come of age. *Genome Biol. 9*: 245

Vartanian, M., J. Desclés, M. Quinet, S. Douady and P.J. Lopez. 2009. Plasticity and robustness of pattern formation in the model diatom *Phaeodactylum tricornutum. New Phytol. 182*: 429–442.

Volcani, B.E. 1981. Cell wall formation in diatoms: morphogenesis and biochemistry. *In*: (T.L. Simpson and B.E. Volcani, eds.) *Silicon and siliceous structure in biological systems.* Springer-Verlag, New York, pp. 157–200.

Vrieling, E.G., W.W.C. Gieskes and T.P.M. Beelen. 1999. Silicon deposition in diatoms: Control by the pH inside the silicon deposition vesicle. *J. Phycol. 35*: 548–559.

Wenzl, S., R. Hett, P. Richthammer and M. Sumper. 2008. Silacidins: highly acific phosphopeptides from diatom shells assist in silica precipitation in vitro. *Angewandte Chemie 47*: 1729–1732.

Wetherbee, R., J.L. Lind and J. Burke. 1998. The first kiss: establishment and control of initial adhesion by raphid diatoms. *J. Phycol. 34*: 9–15.

Wilson, D.P. 1946. The triradiate and other forms of *Nitzschia closterium* (Ehrenberg) Wm. Smith forma *minutissima* of Allen and Nelson. *J. Mar. Biol. Assoc*, UK. *26*: 235–270.

Wustman, B.A., M.R. Gretz and K.D. Hoagland. 1997. Extracellular matrix assembly in diatoms (Bacillariophyceae). II A model of adhesives based on chemical characterization and localization of polysaccharides from the marine diatom *Achnanthes longipes* and other diatoms. *Plant Physiol. 113*: 1059–1069.

Zaslavskaia, L.A., J.C. Lippmeier, P.G. Kroth, A.R. Grossman and K.E. Apt 2000. Transformation of the diatom *Phaeodactylum tricornutum* (Bacillariophyceae) with a variety of selectable marker and reporter genes. *J. Phycol 36*: 379–386.

4 Cytological and cytochemical aspects in selected carrageenophytes (Gigartinales, Rhodophyta)

Leonel Pereira

Introduction

Red algae (Rhodophyta) are a widespread group of uni- to multicellular aquatic photoautotrophic plants. They exhibit a broad range of morphologies, simple anatomy and display a wide array of life cycles. About 98% of the species are marine, 2% freshwater and a few rare terrestrial/sub-aerial representatives (Gurgel and Lopez 2007).

Red algae are true plants in the phylogenetic sense since they share, with the green lineage (green algae and higher plants), a single common ancestor (Adl et al. 2005). However, the phylum Rhodophyta is easily distinguished from other groups of eukaryotic algae due to a number of features listed below (Woelkerling 1990; Grossman et al. 1993; Gurgel and Lopez 2007):

(i) Total absence of centrioles and any flagellate phase.
(ii) Presence of chlorophylls *a* and *d*, and accessory pigments (light-harvest) called phycobilins (phycoerythrin and phycocyanin).
(iii) Plastids with unstacked thylakoids, and no external endoplasmic reticulum.
(iv) Absence of parenchyma and presence of pit-connections between cells (i.e. incomplete cytokinesis).
(v) Floridean starch as storage product.

Traditionally, red algae can be morphologically separated in three major groups: (1) a unicellular group with reproduction by binary cell division only, (2) a multicellular group where a carpogonial branch is absent or incipient (Bangiophyceae *sensu lato*) and (3) a multicellular group with well developed carpogonial branches (Florideophyceae).

Gigartinales

This family presents, like other Florideophyceae, development of a specialized female filament called carpogonial branch. The female gamete (carpogonium) is easily recognizable by the presence of the trichogyne, an elongated extension responsible for receiving the male gametes (spermatium). Germination *in situ* of the zygote and consequent formation of a group of spores (carpospores) or a parasite generation of female gametophyte, which produce carpospores (carposporophyte) inside the cystocarp.

The cystocarp is composed of the carposporophyte plus all protective sterile haploid tissue of the female gametophyte encircling and interacting with it (pericarp). Carpospores develop into a second free-living phase called tetrasporophyte, which can be

morphologically similar (isomorphic alternation of generations) or different (heteromorphic alternation of phases) from the gametophytes. Tetrasporophyte plants produce tetrasporangia by meiosis, which release tetraspores. This pattern of meiotic cell division in the tetrasporangium is stable in red algae and can be one of three types: cruciate, tetrahedral and zonate. When released, each tetraspore will give rise to either a male or a female haploid gametophyte (Gurgel and Lopez 2007).

In general Gigartinales present triphasic isomorphic or heteromorphic, diplo-haplotic (haploid gametophyte, diploid carposporophyte and diploid tetrasporophyte) or diphasic diplo-haplotic lifecycles (Maggs 1990; Brown et al. 2004; Thornber 2006).

A large number of genera of high economic interest (carrageenophytes), are members of this order and most of them are phylogenetically related (Freshwater et al. 1994; Fredericq et al. 1996).

Algal cell walls are composed of cellulose fibrils (rarely xylan fibrils) and a matrix of hydrocolloids. Cell wall hydrocolloid matrixes in red algae are formed by sulphated polysaccharides classified in two main groups: agar and carrageenan.

Red algal hydrocolloids (phycocolloids) are polysaccharides with gel-forming capabilities. They can be classified in two classes, each bearing a basic sugar skeleton consisting of 1,3-linked ß-D-galactopyranose plus either 1,4-linked 3,6-anhydro-α-L-galactopyranose (i.e. agars) or 1,4-linked 3,6-anhydro-α-D-galactopyranose units (i.e. carrageenans). However, several other sugar residues are present making all natural phycocolloid products (whether agars or carrageenans) a complex mixture of neutral and charged polysaccharides. Phycocolloid gel quality is measured by its rheological properties such as gel strength, density, gelling and melting points. These properties are in turn influenced by the overall chemical composition of the gels, i.e. the ratio among different polysaccharides and modified sugar residues found in it. Some groups of red algae exhibit higher concentrations of one particular class and thus are known as either agarophytes (agar-producers, e.g. Gracilariales, Gelidiales and Ceramiales) or carrageenophytes (carrageenan-producers, e.g. most families currently in the Gigartinales such as Caulacanthaceae, Cystocloniaceae, Dumontiaceae, Furcellariaceae, Gigartinaceae, Hypneaceae, Kallymeniaceae, Polyideaceae, Rhizophyllidaceae, Solieriaceae, Sphaerococcaceae, Tichocarpaceae, to name a few) (Pereira et al. 2003; Gurgel and Lopez 2007).

Cytological and spectroscopic analysis techniques

Vibrational spectroscopy

Samples of ground, dried algal material were analyzed by FTIR-ATR and FT-Raman for determination of natural phycocolloids composition, according to the method described by Pereira (2006) and Pereira et al. (2009). The FTIR spectra of ground dried seaweed, native and alkali-modified carrageenan, were recorded on an IFS 55 spectrometer, using a Golden Gate single reflection diamond ATR system, with no need for sample preparation. All spectra reported in this paper are the average of two counts, with 128 scans each and a resolution of 2 cm^{-1}. The room temperature FT-Raman spectra were recorded on a RFS-100 Bruker FT-spectrometer using a Nd:YAG laser with excitation wavelength of 1064 nm. Each spectrum was the average of two repeated measurements, with 150 scans at a resolution of 2 cm^{-1}.

NMR spectroscopy

^{1}H-NMR spectra were taken on a Bruker AMX600 spectrometer operating at 500.13 MHz at 65°C. Typically 64 scans were taken with an interpulse delay of 5 s (T_1 values for the resonance of the anomeric protons of κ- and ι-carrageenan are shorter than 1.5 s). Sample preparation for the ^{1}H-NMR experiments involved dissolving the carrageenan sample (5 mg mL^{-1}) at 80°C in D_2O containing 1 mM TSP (3-(trimethylsilyl) propionic-*2,2,3,3-d*$_4$ acid sodium salt) and 20 mM Na_2HPO_4, followed by sonication three times for 1 h each in a sonicator bath (Branson 2510). Chemical shifts (δ) are referred to internal TSP standard (δ = −0.017 ppm) relative to the IUPAC recommended standard DSS for ^{1}H according to van de Velde et al. (2004). Assignments of the ^{1}H-NMR spectra were based on the chemical shift data summarized by van de Velde et al. (2002, 2004) and Pereira and van de Velde (2011).

Cytological localization of polymers

Two methods were applied for the localization of the cellulose (β-glucan): a – observation of fresh sections in fluorescence microscopy (ultraviolet light, 345–365 nm, Nikon Diaphot microscope equipped with UV 2A filter), after staining with Calcofluor-white (fluorescent brightener 28 of Sigma) at 0.04% (Gretz et al. 1997); b – observation of identical sections in polarization microscope (Nikon Optiphot), with cross polarization filters (birefringence studies) looking for crystalline or para-crystalline structures (Gretz et al. 1997).

For the identification and localization of sulphated polysaccharides (carrageenans), two techniques were also used: a – staining of the sections with toluidine blue (0.05% in 0.1 M acetate buffer, pH 4.4) using light microscopy, for the detection of acid polysaccharides metachromasia (Gretz et al. 1997); b – energy dispersive X-ray analysis (EDX), to detect the variation of sulphur concentration (Russ 1974; McCandless et al. 1999), conducted on a Hitachi H900 electron microscope, associated with an X-ray spectrometer and respective detector.

Other cytochemical stains used were: e.g. Thiéry test, for the identification and localization of floridean starch in electron microscopy; Periodic acid Schiff (PAS), for the detection of polysaccharides (floridean starch); and Black Sudan B, for the detection of lipids using light microscopy (MacManus 1948; Thiéry 1967; Bronner 1975).

Morphological, anatomical and cytological aspects

Ahnfeltiopsis devoniensis and *Gymnogongrus crenulatus* (Phyllophoraceae)

G. crenulatus thallus (see Figure 4.1A–B) consists of cartilaginous flattened dark red fronds a rising from a short cylindrical stipe, attached to substrate by a small disc (holdfast) with 10 mm in diameter. Fronds repeatedly dichotomous with rounded apices sometimes bleached (Ardré 1977; Gayral and Cosson 1986; Cabioch et al. 1995).

This alga has a diphasic lifecycle without carposporophyte. The monoecious gametophytes of *G. crenulatus* form a post-fertilization structure (see Figure 4.1C–D) variously termed a tetrasporoblast (Schotter 1968; Ardré 1977) or carpotetrasporophyte (Dixon and Irvine 1977). These develop from auxiliary cells and form wart-like excrescences from the gametophyte that bear tetrasporangial nemathecia. Meiosis apparently occurs during tetrasporogenesis (McCandless and Vollmer 1984).

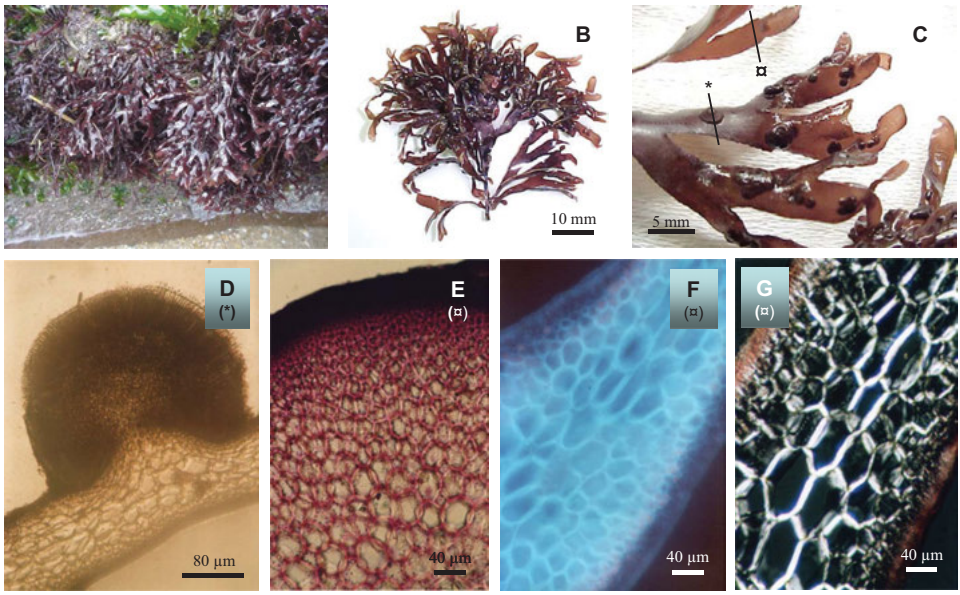

Figure 4.1 *Gymnogongrus crenulatus*: tetrasporoblastic thalli (A–D); branches with tetrasporoblasts (C); tetrasporoblast cross section according to the orientation shown in Figure C (D); thalli cross section according the orientation shown in Figure C (E–G), stained with toluidine blue (E), calcofluor-white (F) and observed with polarizing microscopy (G).

A. devoniensis is difficult to distinguish from *G. crenulatus*, however this species has generally smaller dimensions, with a maximum length of 10 cm (see Figure 4.2A–B). It forms a medium-sized flattened frond with regular dichotomous branching. The branches have parallel sides and the reproductive structures (cystocarps) are internal (Cabioch et al. 1995).

A. devoniensis (formerly *Gymnogongrus devoniensis*) was separated from the *Gymnogongrus* genus because it has a heteromorphic triphasic lifecycle, in which carpospores give rise to an encrusting tetrasporophyte (Maggs et al. 1992; Cabioch et al. 1995).

In Portugal, *A. devoniensis* grew abundantly on damp shaded rocks and in rock-pools at and below water of neap tides, on moderately wave-sheltered shores. Plants were brownish-red, and many were bleached to a pale colour. Small tufts of fronds were attached by holdfasts about 3 mm wide. According to Maggs et al. (1992), approximately 50% of the thalli were male. Males were softer than the succulent female plants, and small, pale, slightly raised spermatangial sori were visible a few millimetres from the apices.

Chondracanthus teedei and *C. teedei* var. *lusitanicus* (Gigartinaceae)

Chondracanthus teedei (Roth) Kützing (formerly *Gigartina teedei*) present flattened main axes, regularly pinnately branched (Guiry; Zinoun et al. 1993). The fronds, cartilaginous-membranous, have a purplish-violet colour that darkens by desiccation, becoming greenish-yellow through decay (see Figure 4.3A–I) (Rodrigues 1957; Gayral 1982). This

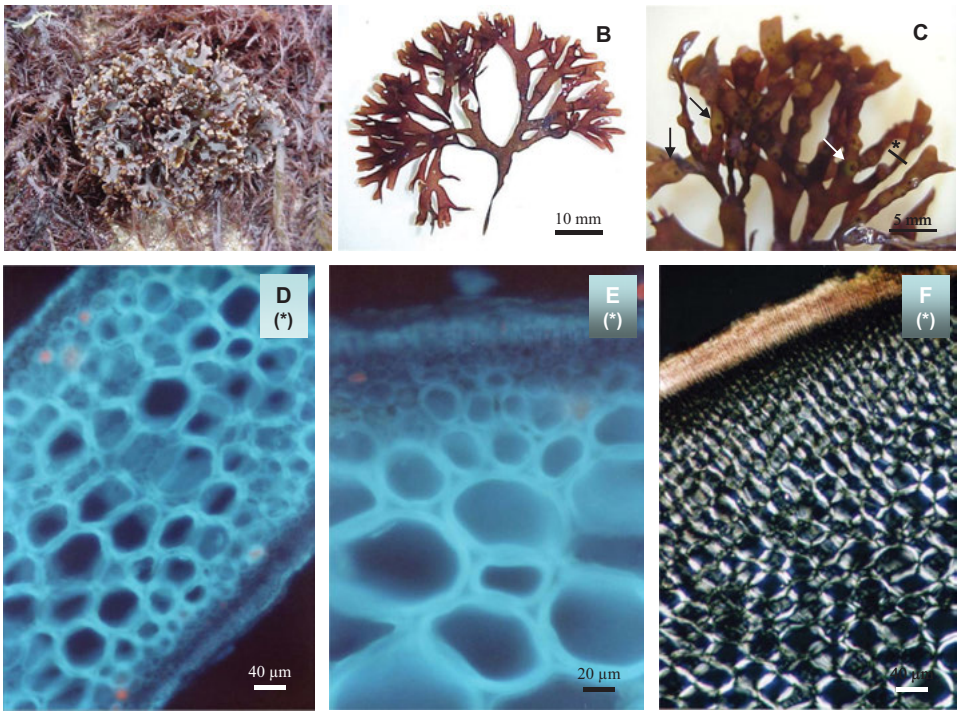

Figure 4.2 *Ahnfeltiopsis devoniensis*: fructified female gametophyte (A–C); branches with cystocarps – arrows (C); thalli cross section according to orientation shown in Figure C (D–F); light microscopical cytochemical aspects showing a cross section after calcofluor-white staining (D–E) and polarized microscopy (F).

species is abundant throughout the year in the lower horizon of the intertidal zone and is often confused with *Gelidium* sp. (Zinoun et al. 1993).

However, the specimens collected in Buarcos bay (Portugal) have very obvious differences compared to specimens taken from Brittany (France), Barcelona (Spain) and the Mediterranean Sea. Thus, the principal axes of the fronds and their ramifications are wider (reaching 1 cm in the older portions) and, therefore, the plants look more robust, often reaching 20 cm in length; it's branches are more dense and lush and the pinnules not only develop on the margins of the branches, but also on their surfaces; the cystocarps are spherical and sessile, being present in large numbers on the pinnules, margins of the branches and thalli surface (see Figure 4.3J–M and Figure 4.7A–C) (Rodrigues 1958; Pereira 2004). Due to these characteristics, the specimens collected in central and northern Portugal belong to the taxon *Chondracanthus teedei* var. *lusitanicus* (Rodrigues 1958; Bárbara and Cremades 1996). This alga has an isomorphic triphasic life cycle (Guiry 1984; Braga 1985, 1990) and appears on the rocks and intertidal pools, generally in shallow water (Gayral 1982).

Tetrasporophytes (Figure 4.4) exhibit tetrasporangial sori with the appearance of dark red spots, prominent in the thallus, on the main axis and lateral branches (Figure 4.4C–D). Sori, with cruciately divided tetrasporangia (Figure 4.4E–G), are released by rupturing

Figure 4.3 *Chondracanthus teedei*: non-fructified thalli collected in Roscoff, France (A–C); tetrasporic thallus (D, F), non-fructified (E, G) and female gametophyte (H–I), collected in Baleal, Portugal; non-fructified thallus of *C. teedei* var. *lusitanicus* collected in Buarcos (J, L), detailed view (M).

of the cortex and old sori, after tetraspore liberation, are filled with medullary filaments (Gury 1994; Pereira 2004).

Examination of thallus transverse sections shows a multiaxial structure (Figure 4.4G–L), with two types of filaments: with unlimited or limited growth. Filaments of unlimited

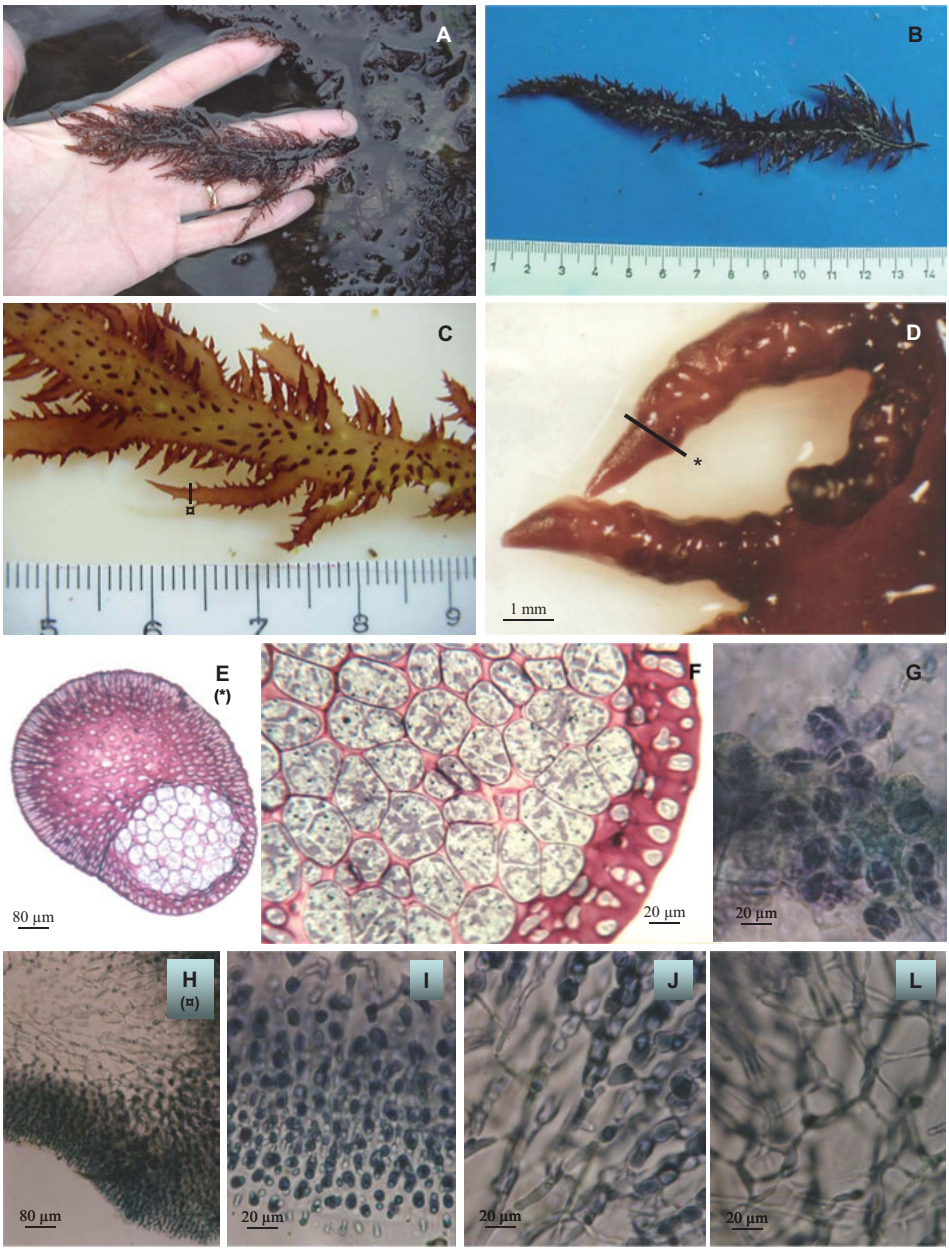

Figure 4.4 *Chondracanthus teedei* var. *lusitanicus*: fructified tetrasporophyte, with tetrasporangial sori, collected in Buarcos bay, Portugal (A–D); detail of branches with tetrasporangial sori (C); branch cross section at the level of tetrasporangial sori, according to the orientation shown in Figure D (E); detail of tetrasporangia and tetraspores (F–G); thalli cross section according to the orientation shown in Figure C (H); details of cortex (I), transition zone (J) and medulla (L). Staining with Toluidine blue (E–F) and lactophenol blue (G–L).

growth, present in the medullary zone (Figure 4.4H, L), show hyaline elongated cells, with apparent star shapes (Figure 4.4L). The limited growth filaments form the cortical zone (Figure 4.4H, I), whose hyaline irregular cells shape, located on the inside, become elliptical and rounded towards the edges. The cortical zone (at the thallus middle region) shows 8 to 9 (± 2) cell layers. It is possible to define a transition zone between the cortical and medullary zone (Figure 4.4J).

In Figure 4.4E and F (semi-thin sections at the level of tetrasporangial sorus) the areas most intensely stained by toluidine blue were located in the intercellular spaces, especially in the cortical zone.

The ultrastructure of tetrasporogenesis (Figure 4.5) in *C. teedei* var. *lusitanicus* can be summarized as follows: the nucleus with a well developed nucleolus, contains

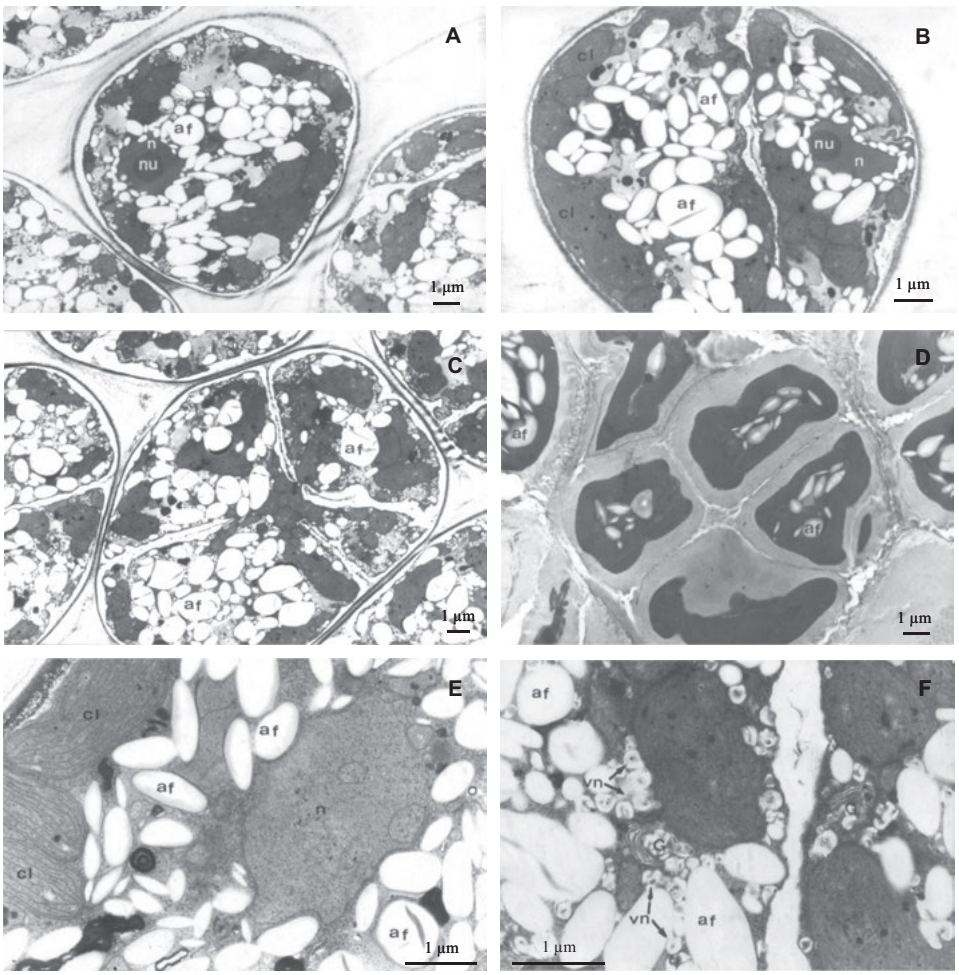

Figure 4.5 *Chondracanthus teedei* var. *lusitanicus* (ultrastructure of tetrasporogenisis): successive tetraspore stages of division (A–D); partial views of tetrasporangial maturation stages showing ultrastructural details of the nucleus and chloroplasts (E), Golgi and cored vesicles (F). **af** – floridean starch, **cl** – chloroplast, **G** – Golgi, **n** – nucleus, **nu** – nucleolus, **vn** – cored vesicles.

little condensed chromatin (Figure 4.5A–B); chloroplasts, in addition to their typical non-association with internal and peripheral thylakoids, show several areas of DNA and electron-dense inclusions (Figure 4.5B, E); in addition to floridean starch grains, which represent the most abundant cellular component, a large part of the remaining cytoplasm is occupied by very active dictyosomes producing numerous vesicles with a dense core (cored vesicles) (Figure 4.5F). This system and starch grains react positively the Thiéry test (Figure 4.6A–C). As in tetrasporogenesis in *Chondria tenuissima* (Tsekos et al. 1985), the ultrastructure of *C. teedei* var. *lusitanicus* during tetrasporogenesis shows straight, large dictyosomes which produce cored vesicles, an abundance of starch grains and form fully developed chloroplasts. The cored vesicles contain Thiéry-positive material and contribute to the formation of vacuoles (Figure 4.6C) with fibrous content (fibrillar vacuoles) which are dominant in tetraspores before liberation.

Female gametophytes (Figure 4.7) present prominent spherical cystocarps (Figure 4.7C), producing carpospores (Figure 4.7D–F). The thallus transverse section shows a multiaxial structure (Figure 4.7G–H), similar to that of tetrasporophyte one. In general, carposporangial ultrastructure (female gametophyte) is not significantly different from that observed during tetrasporogenesis (tetrasporophyte), before cell division (Figure 4.8) and similar to that described in *C. teedei* by Tsekos (1984).

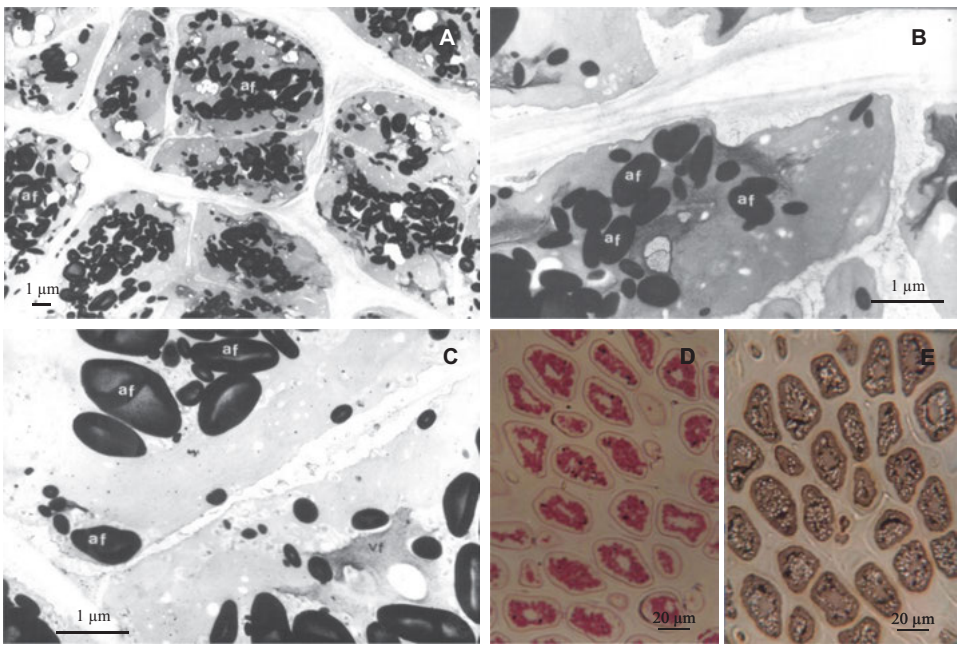

Figure 4.6 *Chondracanthus teedei* var. *lusitanicus*: light- (D–E) and electron microscopical aspects (A–C) of the tetrasporophyte; Thiéry test (A–C); PAS (D) and Black Sudan B staining (E). Note the positive reaction to Thiéry test not only with the floridean starch, but also with the fibrillar vacuoles and portions of the cell wall. **af** – floridean starch grains, **vf** – fibrillar vacuoles.

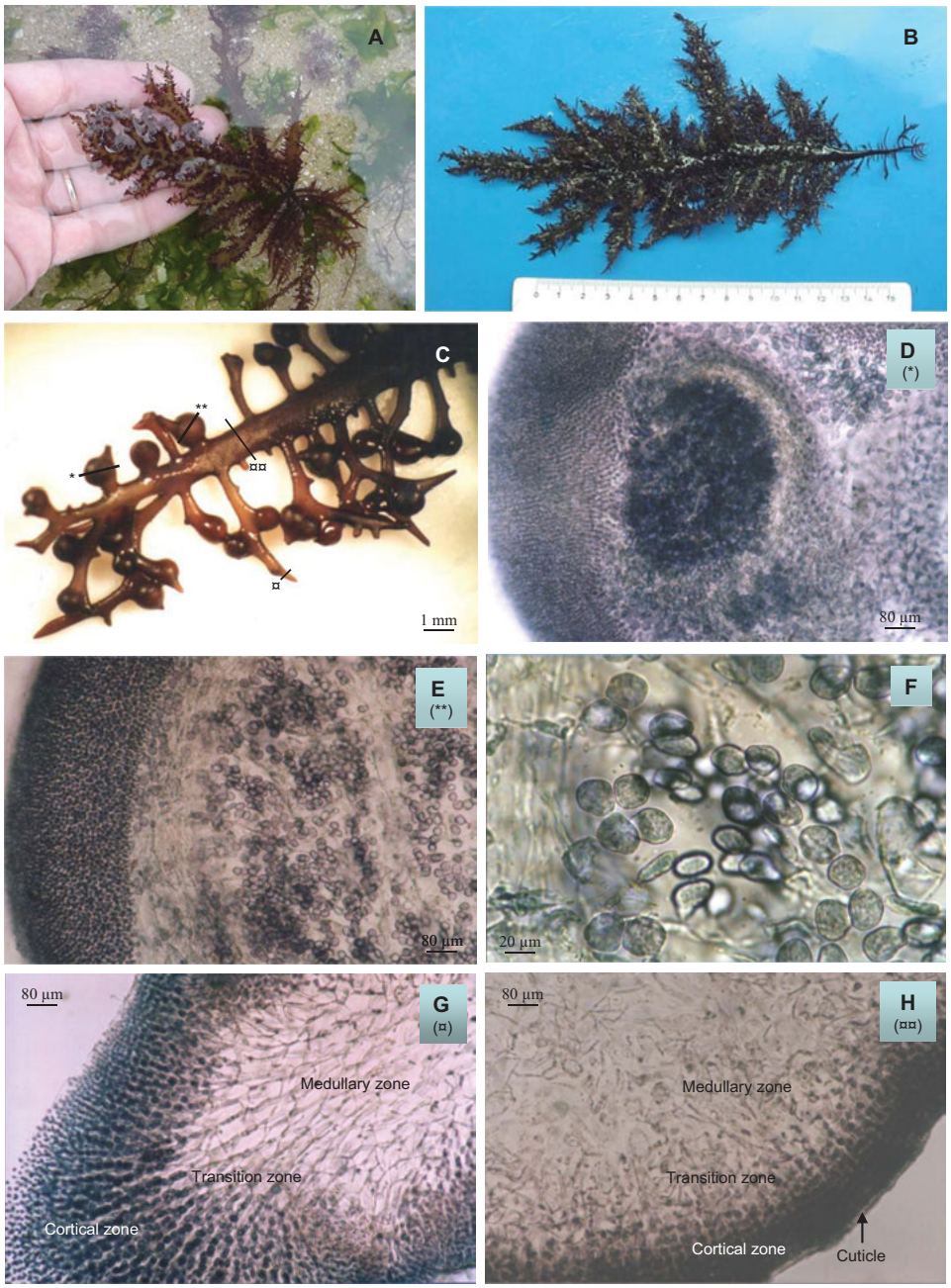

Figure 4.7 *Chondracanthus teedei* var. *lusitanicus*: fructified female gametophyte, with cystocarps, collected in Buarcos, Portugal (A–B); detail of a branch with cystocarps (C); cystocarp cross section according to the orientation shown in Figure C (D–E); carpospores within cystocarps (F); thallus cross section according to the orientation indicated in Figure C (G, H); staining with lactophenol blue (D, H).

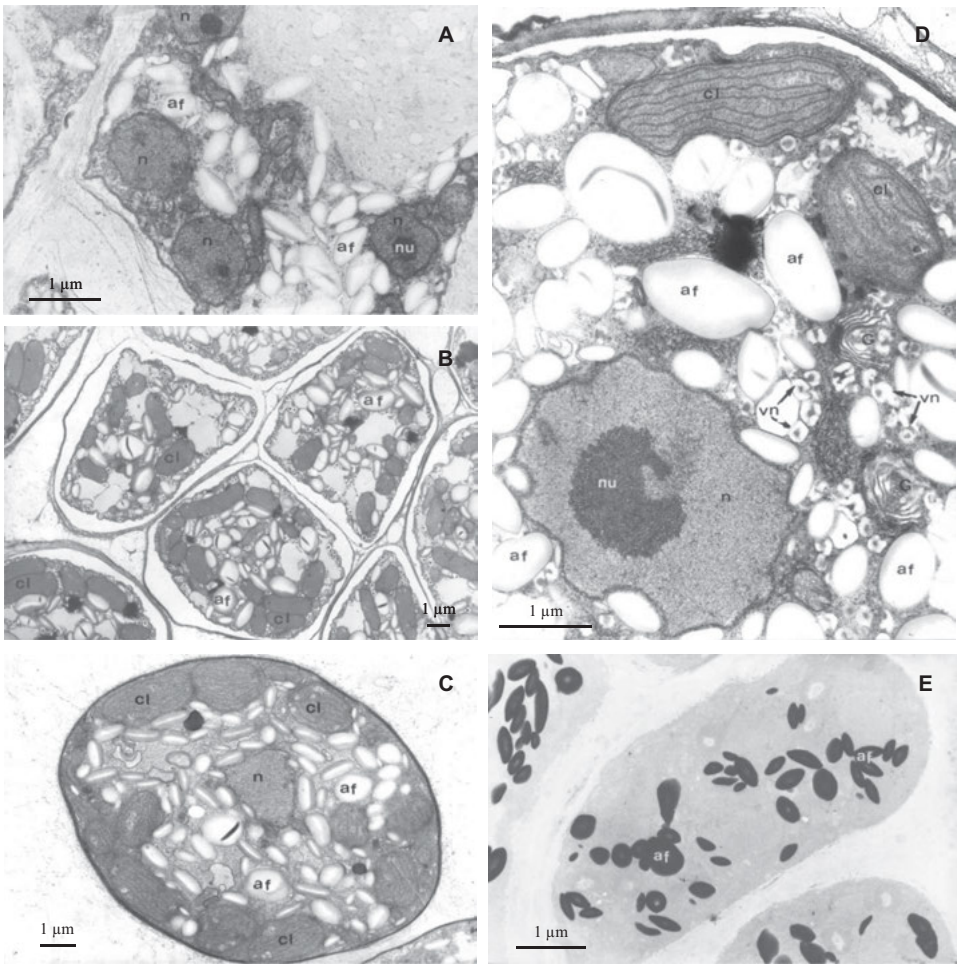

Figure 4.8 *Chondracanthus teedei* var. *lusitanicus*: ultrastructure of the female gametophyte showing partially a multinucleate cell (A) and some aspects of the differentiation of carpospores (B–C); ultrastructural details of the carposporangium, in particular with respect to the nucleus, chloroplasts, Golgi and cored vesicles (E); note the abundance of floridean starch grains giving a positive reaction with the Thiéry test (E). **af** – floridean starch grains, **cl** – chloroplast, **G** – Golgi, **n** – nucleus, **nu** – nucleolus, **vn** – cored vesicles.

Gigartina pistillata (Gigartinaceae)

G. pistillata is the type species of the genus *Gigartina* (Kim 1976; Hommersand et al. 1993). The thallus consists of a group of erect fronds, up to 20 cm tall, dark-red or reddish-brown, cartilaginous, elastic, dichotomously branched (see Figure 4.9A–D and Figure 4.10A–D), attached to the substrate with a small disk (10 mm in diameter). Branching is repeatedly dichotomous (up to 4 times), a few secondary lateral branches sometimes appear in old plants and after damage; branches usually in one plane, but with

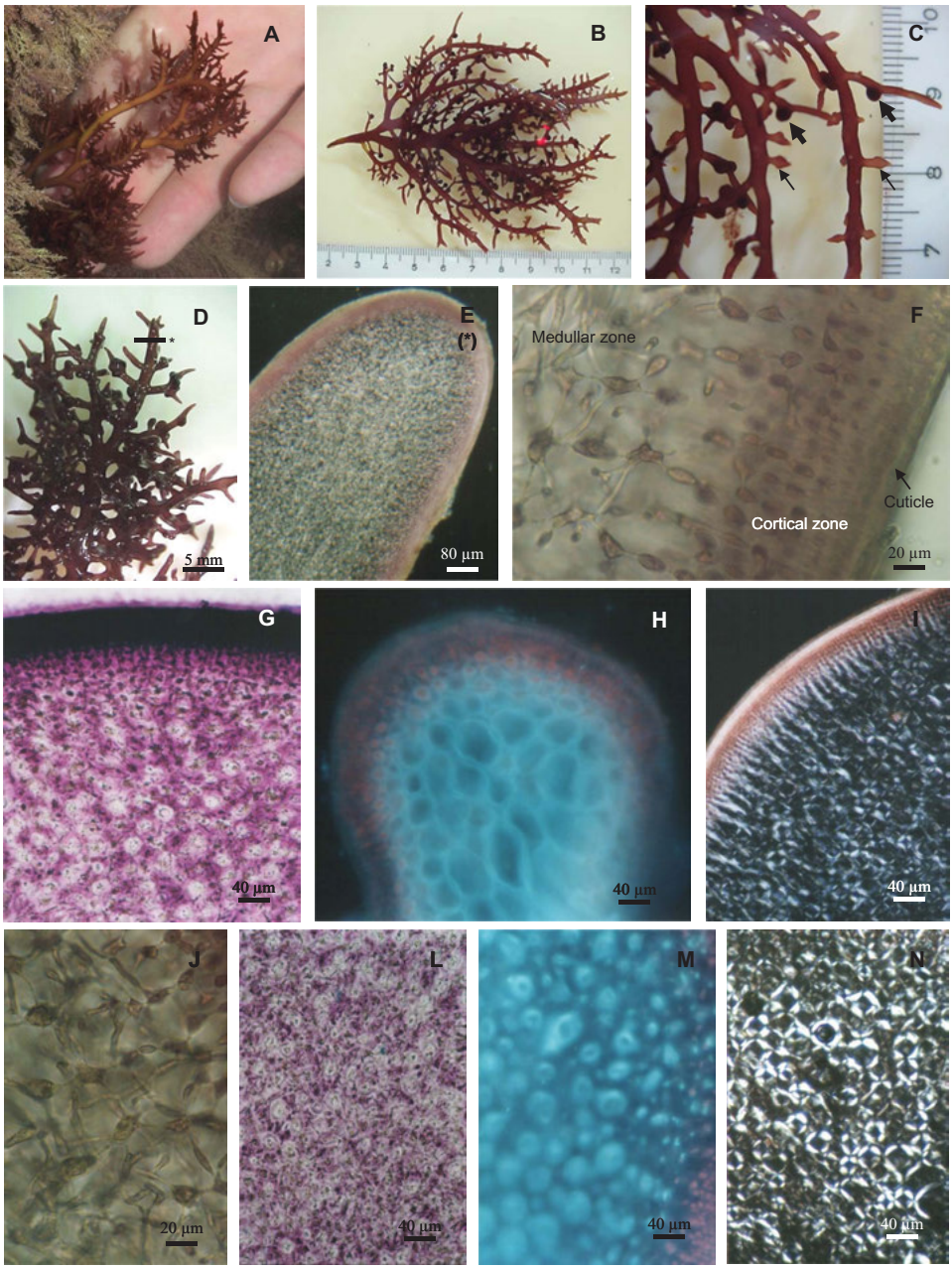

Figure 4.9 *Gigatina pistillata*: fructified female gametophyte (A, N); branches with cystocarps (C–D); thalli cross section according to the orientation shown in Figure C (E–F); Light microscopical cytochemical aspects after staining with toluidine blue (G) and calcofluor-white (H), and observation with a polarizing microscope (I); cytochemical aspects of the medullar zone (J) after staining with toluidine blue (L) and calcofluor-white (M) and observation with a polarizing microscope (N).

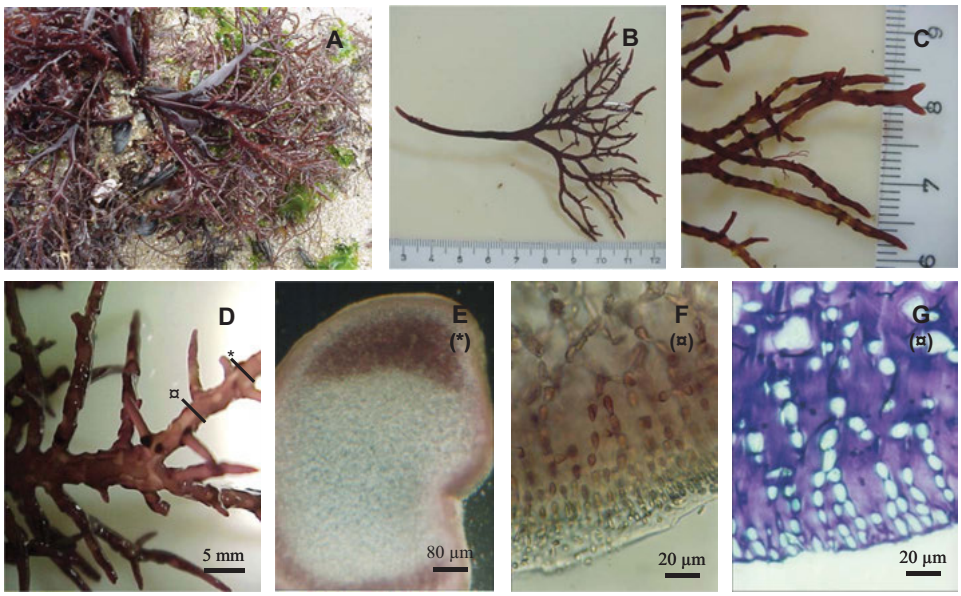

Figure 4.10 *Gigartina pistillata*: fructified tetrasporophyte (A–G); branch with tetrasporangial sori (C–D); branch cross section at the level of the tetrasporangial sori according to the orientation shown in Figure D (E); thalli cross section according to the orientation shown in Figure D (F–G). Staining with toluidine blue (G).

twisted axes. The female gametophytes exhibit a dichotomous branching more profuse than tetrasporophytes (Dixon and Irvine 1995; Pereira 2004).

G. pistillata has an isomorphic triphasic lifecycle (Hommersand et al. 1992); however, heterosporous thalli (with cystocarps and tetrasporangia in the same thallus) were identified in populations of South Africa (Isaac and Simons 1954) and Portugal (Pereira et al. 2002).

The thallus of this alga exhibits a multiaxial structure, where it is possible to recognize a central area with large stellate elements (Figure 4.9F) and a cortical zone of dense small cells, heavily pigmented, forming branched chains (Figure 4.9F and Figure 4.10F).

The female gametophyte has cystocarps which initially do not protrude from the thallus surface (Figure 4.9C – narrow arrows) becoming evident in the final stage of their development (Figure 4.9C – large arrows). These cystocarps are usually sessile (Figure 4.9B–D), but when present in a terminal position, appear to be pedunculated.

The tetrasporophytes present sori, with cruciately divided tetrasporangia, embedded in the surface of the thallus (Figure 4.10D, E) in marginal areas, mainly located in branching zones. Sporangia (tetraspores) in each tetrasporangial sorus are evidently released as a unit at maturity, leaving an exposed surface which is repaired by means of proliferation of subcortical cells (Hommersand et al. 1992; Pereira 2004).

In both phases (gametophytes and tetrasporophytes), the medullary region of the frond is composed of star-shaped cells, very similar to those of the inner cortical cells (Figure 4.9F), the demarcation between medulla and cortex is not clear.

Ultrastrucural features during carposporogenesis (Figure 4.11A), in addition to typical features of the Rhodophyta (chloroplasts with peripheral thylakoid and non-associated internal thylakoids, extraplastidial floridean starch grains, etc.), show well developed Golgi apparati which are very active with an abundance of dictyosomes and cored vesicles. As already mentioned, this would appear to play a key role in the genesis of fibrillar vacuoles and subsequent cell wall edification (Figure 4.11) (Pereira 2004).

Apart from its cruciately divided tetrasporangia (Figure 4.11B – arrows), the ultrastructural characteristics of the tetraspore mother-cells (Figure 4.11B) appear to be identical to those observed during carposporogenesis. During the final stage of tetraspore differentiation, the number and size of floridean starch grains are substantially reduced, indicating that this reserve polysaccharide is probably used in the synthesis of the structural components of the cell wall (Zinuon 1993). The walls of these cells result from the contribution of dictyosome-derived vesicles and also from mucilage sacs originating from cytoplasmic concentric membranes (Delivopoulos and Diannelidis 1990a, b) or from the endoplasmic reticulum (Delivopoulos and Tsekos 1986; Tsekos and Schnepf 1991; Tsekos 1996).

Overall, the reproductive cells (carpospores and tetraspores), while they are still contained in their reproductive structures (cystocarps and tetrasporagial sori, respectively), are embedded in a confluent mucilage (see Figures 4.12 and 4.13) and have characteristics that, in general, are consistent with previous descriptions (see Tsekos 1981, 1983; Tsekos and Schnepf 1983; Delivopoulos and Tsekos 1986; Delivopoulos and Diannelidis 1990a, b).

Spectroscopic analysis

In relation to the phycocolloid nature, spectroscopic analysis showed that the selected carrageenophytes (see Table 4.1) have a similar variation as seen in other species of the Gigartinales family (Chopin et al. 1999; Pereira 2004). The gametophyte and non-fructified stages of *C. teedei* var. *lusitanicus, G. pistillata, A. devoniensis* and *G. crenulatus* produce carrageenans of the kappa family (hybrid kappa/iota/mu/nu-carrageenan). The tetrasporophytes produce carrageenans of the lambda family (hybrid xi/theta or xi/lambda-carrageenan). The alkaline-extracted carrageenan from female gametophytes showed lower sulphate content and a decrease in galactose to the benefit of 3,6-anhydrogalactose. This corresponds to the conversion of the 4-linked galactose-6-sulfate in native samples to anhydro-galactose in the alkaline modified samples. Thus the biological precursor's mu- and nu-carrageenan were converted into kappa and iota carrageenan, respectively (Pereira and Mesquita 2004).

Cytochemical aspects

Transverse sections of *G. pistillata* (Figure 4.9G, L and Figure 4.10G) and *G. crenulatus* (Figure 4.1E) show a strong reaction with toluidine blue in the cortical zone, and weaker staining of the inner areas (medullary zone). Also noteworthy, in *G. pistillata*, the intercellular material between the tetrasporangia (Figure 4.12A–B) had a stronger reaction with toluidine blue than did the intercellular material present between carpospores (Figure 4.13A–B).

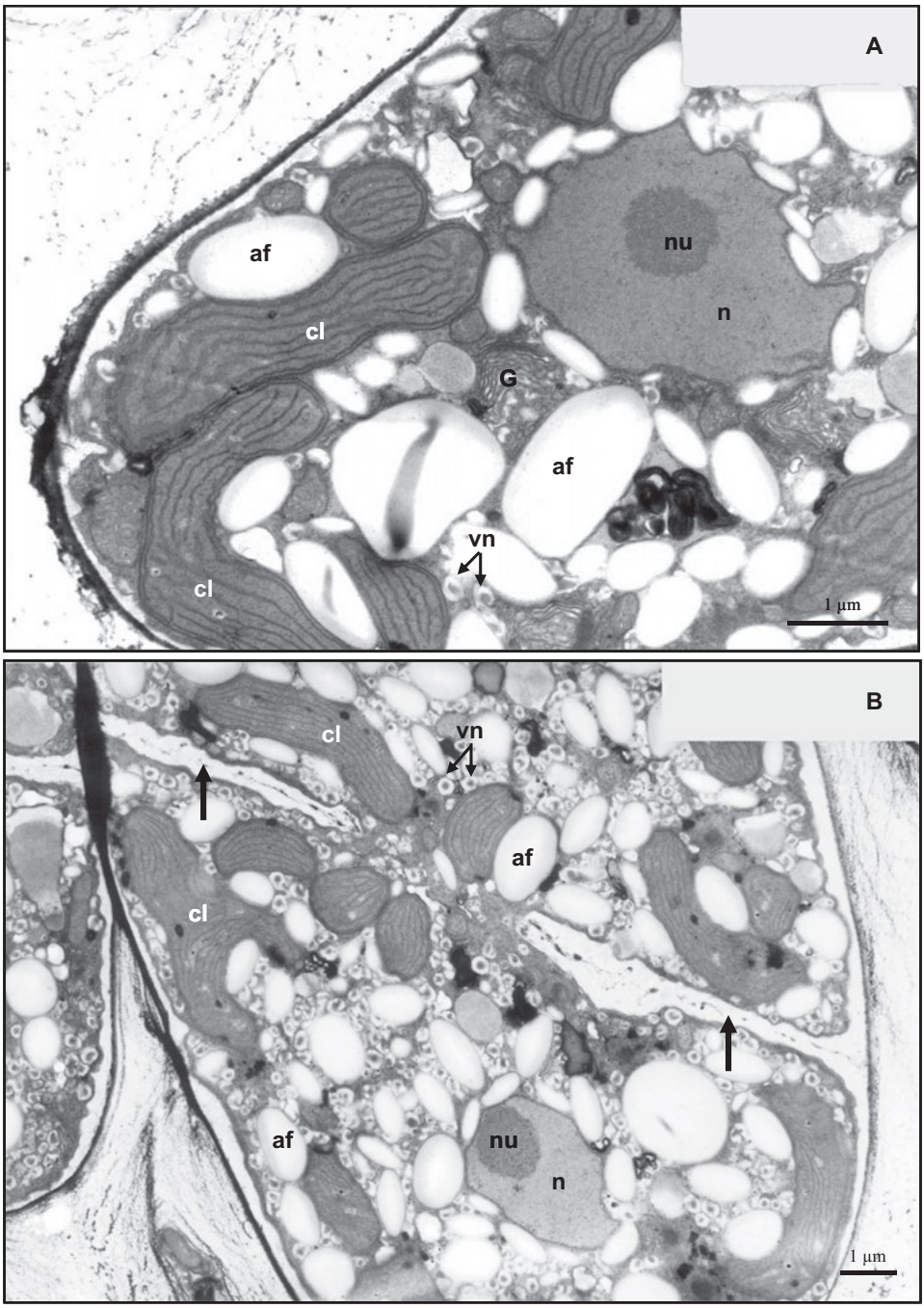

Figure 4.11 *Gigatina pistillata*: A – ultrastructure of developing carpospores (carposporogenesis); B – ultrastructure of developing tetraspores (tetrasporogenesis). **af** – floridean starch, **cl** – chloroplasts, **G** – Golgi, **n** – nucleus, **nu** – nucleulus, **vn** – cored vesicles.

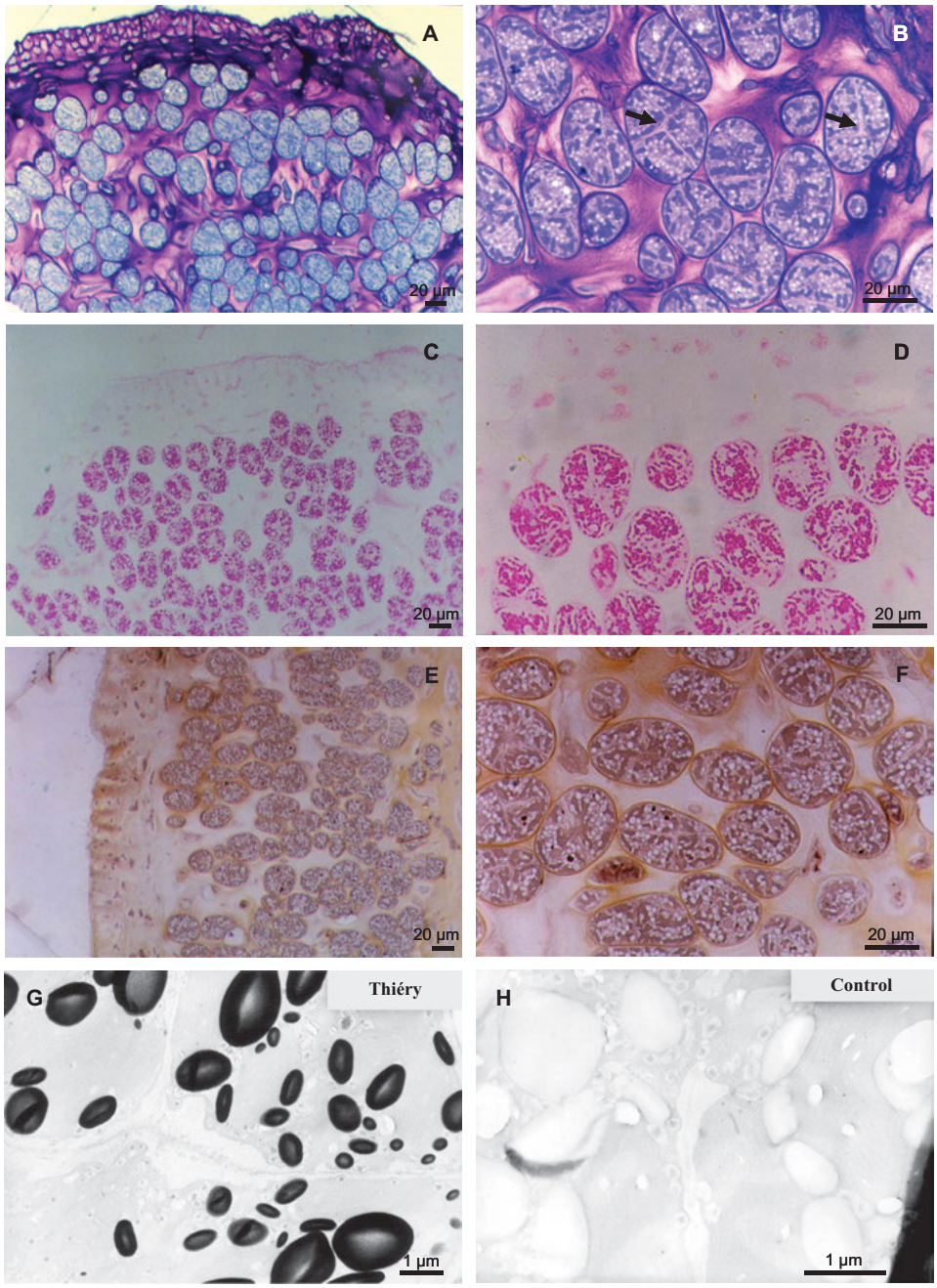

Figure 4.12 *Gigartina pistillata*: tetrasporogenesis (A–H); light- (A, F) and electron microscopical (G–H) cytochemical aspects; toluidine blue staining (A–B), PAS reaction (C–D), Black Sudan B staining (E–F) and Thiéry test (G).

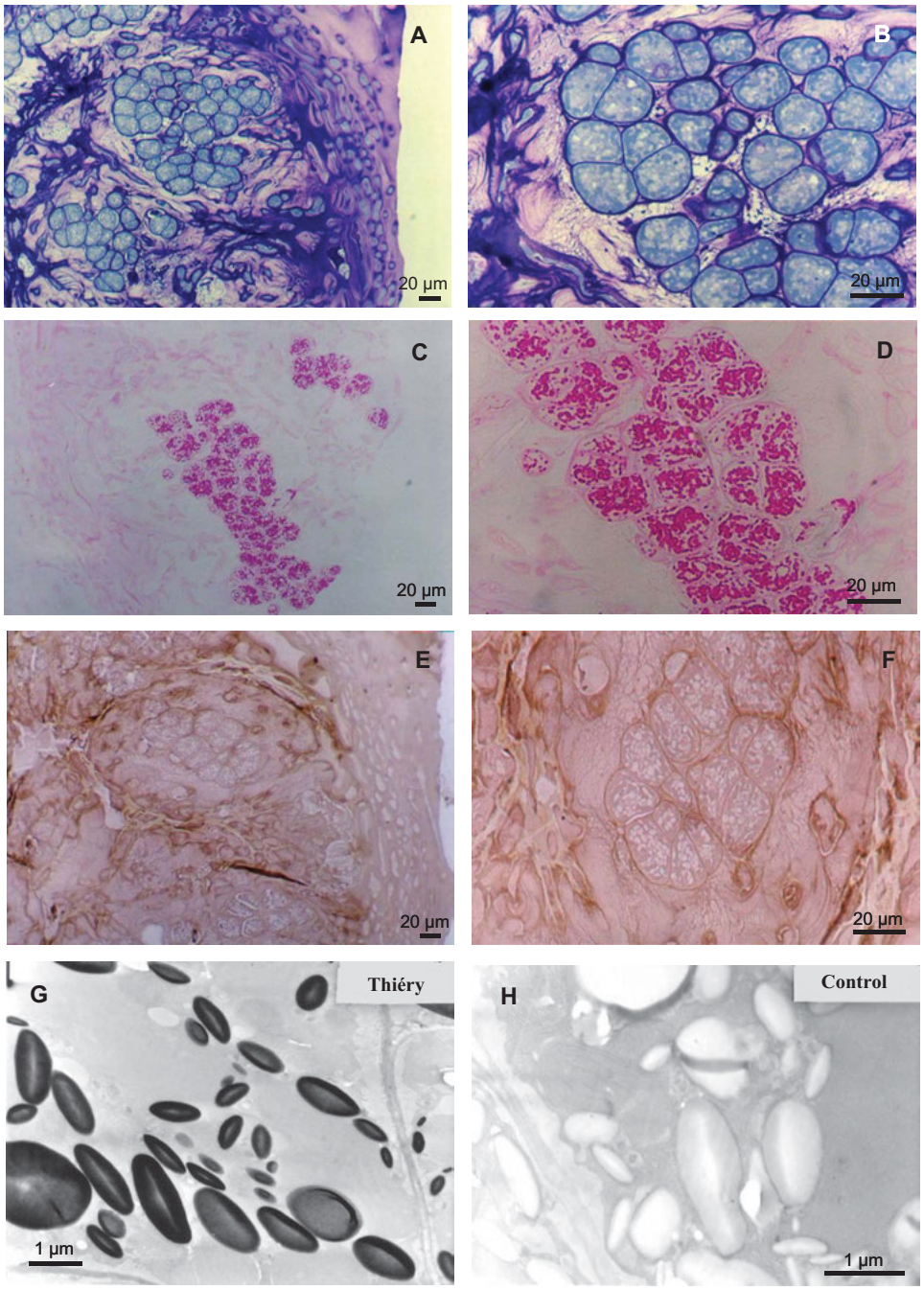

Figure 4.13 *Gigartina pistillata*: carposporogenesis (A–H); light- (A, F) and electron microscopical (G–H) cytochemical aspects; toluidine blue staining (A–B), PAS reaction (C–D), Black Sudan B staining (E–F) and Thiéry test (G).

Table 4.1 Carrageenan composition determined by vibrational spectroscopy (FTIR-ATR and FT-Raman) and [1]H-NMR (adapted from Pereira and Mesquita 2007; Pereira and van de Velde 2011).

Species	Lifecycle phase	Date of harvest	Carrageenan		
			Yield[1]	Alkali extracted[2] (%mol)	Native[3]
Gigartina pistillata	Female gametophyte	Mar. 2002	49.8 %	48.7 κ, 44.5 ι	κ – ι (μ/ν)
Chondracanthus teedei var. *lusitanicus*	Non-fructified	Jun. 2001	35.0 %	55.8 κ, 44.2 ι	κ – ι (μ/ν)
C. teedei var. *lusitanicus*	Female gametophyte	Jun. 2001	43.6 %	58.1 κ, 41.9 ι	κ – ι (μ/ν)
Ahnfeltiopsis devoniensis	Gametophyte	Jul. 2001	13.6 %	16.7 κ, 81.1 ι, 2.2 ν	ι – κ (ν)
A. devoniensis	Non-fructified	Aug. 2001	11.5 %	19.8 κ, 80.2 ι	ι – κ (ν)
Gymnogongrus crenulatus	Tetrasporoblastic	Apr. 2002	9.7 %	64.1 κ, 30.8 ι	κ – ι (μ)
A. devoniensis	Gametophyte	Dec. 2001	11.5 %	22.3–34.7 κ, 65.3–77.7 ι	ι – κ (ν)
G. crenulatus	Tetrasporoblastic	Nov. 2001	11.0 %	60.0 κ, 28.9 ι	κ – ι (μ)
G. pistillata	Tetrasporophyte	Apr. 2002	55.6 %	ξ, λ	ξ – λ
C. teedei var. *lusitanicus*	Tetrasporophyte	Jun. 2001	36.6 %	67.0 ξ, 37.0 θ	ξ – θ

[1]expressed in percentage of dry weight; [2]composition determined by [1]H-NMR; [3]composition determined by FTIR-ATR and FT-Raman analysis of ground seaweed samples; the carrageenans are identified according to the Greek lettering system (Chopin et al. 1999); the letters between parenthesis () correspond to the biological precursors of the carrageenans, present in native samples.

The cytoplasmic reserve inclusions (floridean starch grains) show a positive PAS reaction (see Figures 4.6D and 4.12, 4.13C, D); these inclusions also react positively with the Thiéry test (Figures 4.6A–B, 4.8E, 4.12G and 4.13G). It is noted that the cytoplasmic reserve inclusions (floridean starch grains), which react positively to PAS and the Thiéry test, do not stain with toluidine blue or with Sudan black B (Figures 4.12E–F and 4.13E–F).

Cellular localization and characterization of cellulose and carrageenan polymers

As red algae inhabit aquatic environments quite different to those typical of land plants, it is not perhaps unexpected to discover that the composition and organization of their

intercellular matrix are distinct from those commonly found in the latter (Gretz et al. 1997). The extracellular matrix of red algae is composed of cellulose microfibril networks associated with amorphous polymers containing sulphated galactans, mucilage and cellulose. In contrast to the relatively rigid walls in other algae, the majority of red algae are flexible with a soft consistency due to the presence of large amounts of amorphous material and less fibrillar components (cellulose) (Gretz and Vollmer 1989; Gretz et al. 1997; Graham and Wilcox 2000).

Inner zones of *G. pistillata* react with Calcofluor-white more intensely than peripheral areas (Figure 4.9H, M), due to the presence of β-glucan in the walls of the medullary cells. Note also the very strong reaction in medullary cells of *G. crenulatus* (Figure 4.1F), and in particular of *A. devoniensis* (Figure 4.2D–E). These areas come birefringent when observed with a polarizing optical microscope, confirming the presence of a structure with crystalline organization (Figures 4.1G and 4.2F).

The intercellular matrix of carrageenophytes is mainly composed of hydrophilic sulphated oligogalactans, with D-galactose and anhydro-D-galactose, in contrast to the less sulphated agars, where anhydro-L-galactose is predominant (Knutsen et al. 1994; Pereira and Mesquita 2007). The function and physiological significance of the matrix are related to the mechanical adaptation, hydration and osmotic regulation of carrageenophytes in their marine habitat (Kloareg and Quatrano 1988; Carpita and Gibeaut 1993; Whitney et al. 1999).

The distribution of sulphated polysaccharides in the thalli of *C. teedei* var. *lusitanicus* (Figure 4.4E–F), *G. pistillata* (Figure 4.9G, L), and *Gymnogongrus crenulatus* (Figure 4.1E) shows a gradient similar to that observed in several other carrageenophytes, particularly in *C. crispus* (Gordon and Mccandless 1973; Gordon-Mills and Mccandless 1975; Gordon-Mills et al. 1978) and agarophytes such as *Pterocladiella capillacea* (Rascio et al. 1991); there is a higher concentration of sulphated polysaccharides in the outer part of the thalli, especially in the cortical zone (see Figures 4.1E and 4.9G) compared to the innermost part (medullary zone).

EDX microanalysis

The data obtained by EDX analysis of tissues from *G. pistillata* (female gametophyte), in the form of % (atomic percentage) of sulphur, are interpreted as corresponding to the presence of carrageenan (McCandless et al. 1977). Within cortical cells (cytoplasm, plastids and floridean starch grains) sulphur levels are below detection, but significant quantities are present in cell walls and in the intercellular matrix. The amounts of sulphur detected shows a concentration gradient with the inner part of the cell wall containing far less compared to the intercellular matrix (see Figure 4.14): inner cell wall (3.98%); outside the cell wall (7.19%); transition zone between the wall and the matrix (10.39%); intercellular matrix (11.43%).

The results of the analysis by EDX show that the highest concentrations of sulphur and, therefore, carrageenan are located in the cell walls and intercellular matrix and a

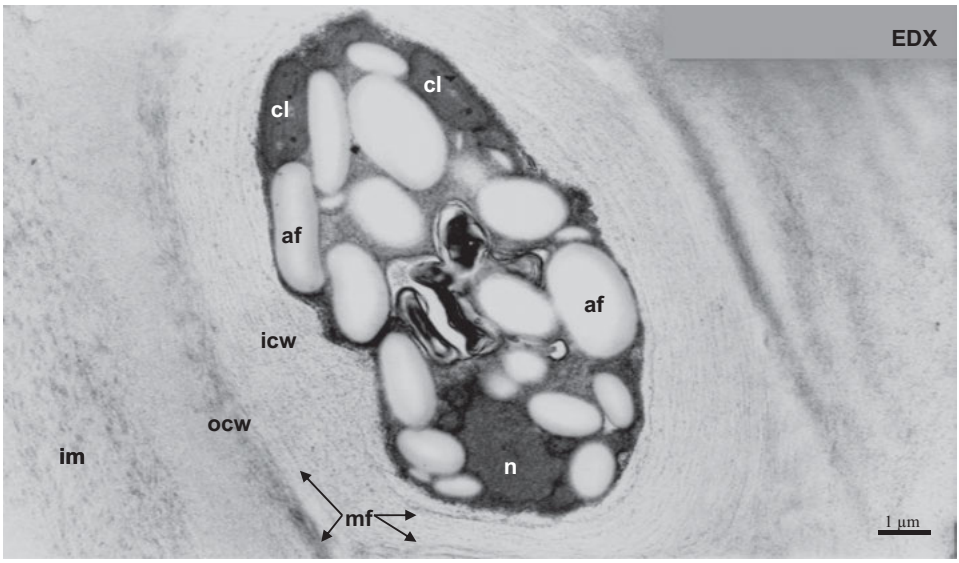

Figure 4.14 *Gigartina pistillata*: cortical cell and their cell wall ultrastructure – localization of sulphated polysaccharides (carrageenan) (EDX analysis for sulphur); the microfibrills (**mf**) are arranged concentrically in a less dense way on the inside zone (**icw**) and denser in the outer zone (**ocw**); the intercellular matrix (**im**) has a granular appearance. **af** – floridean starch grains, **cl** – chloroplasts, **n** – nucleus.

gradient of increasing carrageenan innermost region of the cell wall towards the intercellular matrix, as observed in *C. crispus* (McCandless et al. 1977).

Conclusions

The combination of FTIR and Raman spectroscopy allows identification of the natural composition of phycocolloids present in seaweeds (Pereira 2004; Pereira 2006). Since the vibrational spectrometers (FTIR and FT-Raman) are now standard equipment in many laboratories, the techniques used (Pereira et al. 2003; Pereira and Mesquita 2004; Pereira et al. 2009) are useful for studying carrageenophyte populations, substituting traditional tests of iridescence and resorcinol (Braun et al. 2004). These techniques are also useful for the development and implementation of strategies for sustainable seaweed harvest, the evaluation of the natural seaweed composition and for control of the quality of the different batches of algal material harvested and/or cultivated (Pereira et al. 2003; Pereira et al. 2009).

However, ^{1}H-NMR spectroscopy is necessary for the quantitative analysis of the different repeating units of the hybrid carrageenans, extracted from the studied algae (Pereira 2004). ^{1}H-NMR allows for the identification and quantification of the different carrageenan types based on the intensity and the chemical shift of the resonances of the anomeric protons (van de Velde et al. 2002; Pereira and van de Velde 2011).

Cytological localization of intercellular matrix polymers *in situ* provides valuable information complementary to chemical and physical characterization of extracted

components. Thus, based on this cytochemical study, the following conclusions might be drawn: in the carrageenophytes studied here (*C. teedei* var. *lusitanicus, G. pistillata, G. crenulatus* and *A. devoniensis*), the two main components of the cell walls and intercellular matrix are cellulose and carrageenans (polymers of sulphated galactans). At the thallus level, concentrations of theese sulphated polysaccharides decrease from the cortex to the medulla, while the cellulose gradient is inversed. At the cellular level, cellulose is the main fibrillar component of the cell walls. This has also been observed in carrageenophytes with a high commercial value (*Chondrus crispus* and *Kappaphycus alvarezzi*). Moreover, the cristallinity of cellulose changes with the cell size (Gordon and McCandless 1973; Gretz et al. 1997).

The EDX analysis for sulphur showed (like in *C. crispus*) an increasing gradient of carrageenans from the innermost region of the cell wall to the intercellular matrix (Gretz et al. 1997). This is in agreement with the direct analyses of carrageenan concentrations.

References

Adl, S.M., A.G.B. Simpson, M.A. Farmer, et al. 2005. The new higher level classification of eukaryotes with emphasis on the taxonomy of protists. *J. Eukaryot. Microbiol. 52*: 399–451.

Barbara, I. and J. Cremades. 1996. Seaweeds of the Ria de A Coruna (NW Iberian Peninsula, Spain). *Bot. Mar. 39*: 371–388.

Bixler, H.J. 1995. Recent developments in manufacturing and marketing carrageenan. *Hydrobiologia 327*: 35–57.

Bronner, R. 1975. Simultaneous demonstration of lipids and starch in plant-tissues. *Stain Tech. 50*: 1–4.

Brown, M.T., A. Neish and D. Harwood. 2004. Comparison of three techniques for identifying isomorphic phases of *Chondrus crispus* (Gigartinaceae). *J. Appl. Phycol. 16(6)*: 447–450.

Carpita, N.C. and D.M. Gibeaut. 1993. Structural models of primary cell walls in flowering plants: consistency of molecular structure with physical properties of the walls during growth. *Plant J*. 3: 1–30.

Chopin, T., B.F. Kerin and R. Mazerolle. 1999. Phycocolloid chemistry as taxonomic indicator of phylogeny in the Gigartinales, Rhodophyceae: A review and current developments using Fourier transform infrared diffuse reflectance spectroscopy. *Phycological Research 47*: 167–188.

Craigie, J.S. 1990. Cell walls. *In*: (K.M. Cole and R.G. Sheath, eds). *Biology of the Red Algae*. Cambridge University Press, Cambridge. pp. 221–257.

Delivopoulos, S.G. and I. Tsekos. 1986. Ultrastructure of carposporogenesis in the Red Alga *Gracilaria verrucosa* (Gigartinales, Gracilariaceae). *Bot. Mar. 29*: 27–35.

Delivopoulos, S.G. and Diannelidis, B.E. 1990a. Ultrastructure of Carposporophyte Development in the Red Alga *Caulacanthus ustulatus* (Gigartinales, Caulacanthaceae). *Mar. Biol. 106*: 145–52.

Delivopoulos, S.G. and B.E Diannelidis. 1990b. Ultrastructure of carposporogenesis in the Red Alga *Caulacanthus ustulatus* (Gigartinales, Caulacanthaceae). *Ann. Botany 66*: 387–95.

Dixon, P.S., L.M. Irvine. 1995. *Seaweeds of the British Isles, Volume I Rodophyta, Part 1 – Introduction, Nemaliales, Gigartinales*. The Natural History Museum, HMSO, London. pp. 167–251.

Fredericq, S., M.H. Hommersand and D.W. Freshwater.1996. The molecular systematics of some agar- and carrageenan-containing marine red algae based on *rbc*L sequence analysis. *Hydrobiologia 327*: 125–135.

Freshwater, D.W., S. Fredericq, B.S. Butler and M. Hommersand. 1994. A gene phylogeny of the red algae (Rhodophyta) based on plastid rbcL. *Proc. Natl. Acad. Sci. USA 92*: 7281–7285.

Gayral, P. 1982. *Les algues de côtes Françaises (Manche & Atlantique)*. Éditions Doin, Paris. pp. 21–29.

Gordon-Mills, E.M. and E.L. Mccandless. 1975. Carrageenans in the cell walls of *Chondus crispus* Stack. (Rhodophycaea, Gigartinales). I. Localization with fluorescent antibody. *Phycologia 14*: 275–281.

Gordon-Mills, E.M., J. Tas and E.L. Mccandless. 1978. Carrageenans in cell-walls of *Chondrus crispus* Stack (Rhodophyceae Gigartinales). 3. Metachromasia and topooptical reaction. *Phycologia 17(1)*: 95–104.

Graham, L.E. and L.W. Wilcox. 2000. *Red algae (chap. 16), Algae*. Prentice-Hall Inc., Upper Saddle River, NJ. pp. 343–396.

Gretz, M.R. and C. Vollmer. 1989. Cell walls of red algae. *In*: (C. Schuerch and A. Sarko, eds) *Cellulose and wood-chemistry and technology*. Wiley, New York. pp. 623–637.

Gretz, M.R., J.C. Mollet and R. Falshaw. 1997. Analysis of red algal extracellular matrix polysaccharides – cellulose and carrageenan. *In*: (R.R. Townsend and A.T. Hotchkiss, eds) *Techniques in Glycobiology*. Marcel Dekker, Inc., New York. pp. 613–628.

Grossman, A.R., M.R. Schaefer, G.C. Chiang and J.L. Collier. 1993. The phycobilisome, a light-harvesting complex responsive to environmental-conditions. *Microbiol. Rev. 57*: 725–749.

Gurgel, C.F.D. and J. Lopez-Bautista. 2007. *Red Algae*. Encyclopedia of Life Sciences. John Wiley & Sons, Ltd., Chichester, UK, doi:10.1002/9780470015902.a0000335

Hoffmann, R.A., M.J. Gidley, D. Cooke and W.J. Frith. 1995. Effect of isolation procedures on molecular composition and physical properties of *Eucheuma cottonii* carrageenan. *Food Hydrocolloids 9*: 281–289.

Hommersand, M., S. Fredericq and J. Cabioch. 1992. Developmental morphology of *Gigartina pistillata* (Gigartinaceae, Rhodophyta). *Phycologia 31(3–4)*: 300–325.

Isaac, W.E. and S.M. Simons. 1954. Some observations on *Gigartina pistillata* (Gmel.) Stackh. from Port Alfred with a record of plants bearing both tetraspores and carpospores. *J. S. Afr. Bot. 20(1)*: 117–125.

Kloareg, B. and Quatrano, R. S. 1988. Structure of the cell-walls of marine-algae and ecophysiological functions of the matrix polysaccharides. *Oceanogr. Mar. Biol. 26*: 259–315.

Knutsen, S. H., D.E. Myslabodski, B. Larsen and A.I. Usov. 1994. A modified system of nomenclature for red algal galactans. *Bot. Mar. 37*: 163–9.

Lechat, H., M. Amat, J. Mazoyer, A. Buleon and M. Lahaye. 2000. Structure and distribution of glucomannan and sulfated glucan in the cell walls of the red alga *Kappaphycus alvarezii* (Gigartinales, Rhodophyta). *J. Phycol. 36(5)*: 891–902.

Lechat, H., M. Amat, J. Mazoyer, T. Gallant, A. Buleon and M. Lahaye. 1997. Cell wall composition of the carrageenophyte *Kappaphycus alvarezzi* (Gigartinales Rhodophyta) partitioned by wet sieving. *J. Appl. Phycol. 9*: 565–572.

McCandless, E.L., W.T. Okada, J.N.A. Lott, C.M. Vollmer and E.M. Gordon-Mills. 1999. Structural studies of *Chondrus crispus*: the effect of extraction of carrageenan. *Can. J. Bot. 55*: 2053–2064.

MacManus, J.F.A. 1948. Histological and histochemical uses of periodic acid. *Stain Technol. 23*: 99–108.

Pereira L, A.M. Amado, A.T. Critchley, F. van de Velde and P.J.A. Ribeiro-Claro. 2009. Identification of selected seaweed polysaccharides (phycocolloids) by vibrational spectroscopy (FTIR-ATR and FT-Raman). *Food Hydrocolloids*, *23*: 1903–1909

Pereira, L. 2006. Identification of phycocolloids by vibrational spectroscopy. *In*: (A.T. Critchley, M. Onho and D.B. Largo, eds) *World Seaweed Resources – An Authoritative Reference System*, ETI Information Services Ltd.

Pereira, L. and F. van de Velde. 2011. Portuguese carrageenophytes: Carrageenan composition and geographic distribution of eight species (Gigartinales, Rhodophyta). *Carbohydr. Polym. 84*: 614–623.

Pereira, L. and J.F. Mesquita, 2004. Population studies and carrageenan properties of *Chondracanthus teedei* var. *lusitanicus* (Gigartinaceae, Rhodophyta). *J. Appl. Phycol. 16*: 369–383.

Pereira, L., 2004. *Estudos em macroalgas carragenófitas (Gigartinales, Rhodophyceae) da costa portuguesa – aspectos ecológicos, bioquímicos e Citológicos*. PhD Thesis, University of Coimbra, Coimbra. pp. 293.

Pereira, L., A. Sousa, H. Coelho, A.M. Amado and P.J.A. Ribeiro-Claro. 2003. Use of FTIR, FT-Raman and ^{13}C-NMR spectroscopy for identification of some seaweed phycocolloids. *Biomol. Eng. 20(4–6)*: 223–228.

Pereira, L., J.F. Mesquita and J.D.S. Dias. 2002. Optical and electron microscope study of heterosporic thalli (carpospores/tetraspores) in *Gigartina pistillata* (Gmel.) Stackh. (Rhodophyta), *Proceedings of ICEM 15, Vol. 2 – Biology and Medicine*, South Africa, Durban. pp. 747–748.

Pereira, L. and J.F. Mesquita. 2007. Cytochemical studies on portuguese carrageenophytes (Gigartinales, Rhodophyta). *In* (C.A. Long and P. Anninos, eds) *Bio'07: Proceedings of the 3rd WSEAS International Conference on Cellular and Molecular Biology, Biophysics and Bioengineering*. World Scientific and Engineering Acad. and Soc., Athens. pp. 66–71.

Rascio, N., P. Mariani, F.D. Vecchia and R. Trevisan. 1991. The vegetative thallus of *Pterocladia capillacea* (Gelidiales, Rhodophyta). 1. An ultrastructural and cytochemical study. *Bot. Mar. 34(3)*: 177–185.

Rodrigues, J.E.M. 1957. Contribuição para o conhecimento das algas marinhas da baía de Buarcos. *Publicações do XXIII Congresso Luso-Espanhol, Separata do Tomo V*: 1–15.

Rodrigues, J.E.M. 1958. A new variety of *Gigartina teedii* (Roth) Lamouroux. *Bol. Soc. Brot. 32(2)*: 91–94.

Russ, J.C. 1974. X-ray microanalysis in the biological sciences. *J. Submicr. Cytol.* 6: 55–79.

Schotter, G. 1968. Recherches sur les Phyllophoracées. *Bulletin de l'Institut Océanographique de Monaco 67(1383)*: 1–99.

Thornber, C.S. 2006. Functional properties of the isomorphic biphasic algal life cycle. *Integr. Comp. Biol. 46(5)*: 605–614.

Thiéry, J.P. 1967. Mise en évidance des polysaccharide sur coupes fines en microscopie électronique. *J. Microsc. 6*: 987–1018.

Tsekos, I. 1983. The ultrastructure of carposporogenesis in *Gigartina teedii* (Roth) Lamour (Gigartinales, Rhodophyceae) – Gonimoblast cells and carpospores. *Flora 174*:191–211.

Tsekos, I. 1996. The supramolecular organization of red algal cell membranes and their participation in the biosynthesis and segregation of extracellular polysaccharides: a review. *Protoplasma 193(1–4)*: 10–32.

Tsekos, I., E. Schnepf and A. Makrantonakis.1985. The ultrastructure of tetrasporogenesis in the marine red alga *Chondria tenuissima* (Good. et Woodw.) (Ceramiales, Rhodomelaceae). *Annals of Botany 55*: 607–619.

Tsekos, I. and E. Schnepf. 1991. Acid-phosphatase-activity during spore differentiation of the Red Algae *Gigartina teedii* and *Chondria tenuissima. Plant Syst. Evol. 176*: 35–51.

van de Velde, F., H.A. Peppelman, H.S. Rollema and R.H. Tromp. 2001. On the structure of kappa/iota-hybrid carrageenans. *Carbohydr. Res. 331(3)*: 271–283.

van de Velde, F., L. Pereira and H.S. Rollema. 2004. The NMR chemical shift data of carrageenans revised. *Carbohydr. Res. 339(13)*: 2309–2313.

van de Velde, F., S.H. Knutsen, A.I. Usov, H.S. Rollema and A.S. Cerezo. 2004. ^{1}H and ^{13}C high resolution NMR spectroscopy of carrageenans: application, research and industry. *Trends Food Sci. Tech. 13*: 73–92.

Vreeland, V and B. Kloareg. 2000. Cell wall biology in red algae: divide and conquer. *J. Phycol. 36(5)*: 793–797.

Whitney, S. E. C., M.G.E. Gothard, J.T. Mitchell and M.J. Gidley. 1999. Roles of cellulose and xyloglucan in determining the mechanical properties of primary plant cell walls. *Plant Physiol. 121*: 657–63.

Woelkerling, W.J. 1990. An introduction. *In*: (K.M. Cole and R.G. Sheath, eds) *Biology of the red algae*. Cambridge University Press, Cambridge. pp. 1–6.

5 Evolution of vacuolar targeting in algae

Burkhard Becker and Kerstin Hoef-Emden

Introduction

Vacuoles are single membrane-bound compartments within the cytoplasm of a cell that are required for various cellular functions (see Becker 2007 for a recent review on plant and green algal vacuoles). The vacuole is essential for cell viability in angiosperms (Rojo et al. 2001). In angiosperms, the large central vacuole provides structural support, serves as storage and waste disposal compartment, and is required for cell protection and cell growth (Marty 1999). In algae, vacuoles differ considerably in size. Whereas in unicells vacuoles tend to be small (about 1 μm), coenocytic and multicellular algae may contain a single large vacuole in their cells, similar to the large central vacuole seen in embryophytes. It is generally assumed that vacuoles in algae perform similar functions as in embryophytes (Becker 2007; Domozych 1991).

Vacuoles are part of the endomembrane system of a cell, i.e. the vacuole is linked with other compartments of the endomembrane system by vesicular transport (Surpin and Raikhel 2004). Most vacuolar proteins are synthesized by ribosomes bound to the rough endoplasmic reticulum and cotranslationally translocated into the ER (Vitale and Raikhel 1999). Coated vesicles transport vacuolar proteins from the ER through the Golgi apparatus to the vacuole (Vitale and Raikhel 1999). In angiosperms there is also evidence for direct trafficking of vacuolar proteins from the ER to vacuoles bypassing the Golgi apparatus (Vitale and Galili 2001). The situation in angiosperms is further complicated by the presence of two types of vacuoles in the same plant cell (Park et al. 2004), which apparently serve different functions: an acidic hydrolytic lysosome-like vacuole generally termed lytic vacuole (LV) and a less acidic vacuole with the capacity to accumulate reserve material termed protein storage vacuole (PSV). However, whether all angiosperm cells contain these two different types of vacuoles is controversial (summarized by Frigerio et al. 2008).

Soluble proteins destined for the vacuole contain vacuolar sorting signals (VSS). VSS bind to vacuolar sorting receptors (VSR) in the trans-Golgi network (TGN) and are then transported in clathrin-coated vesicles to the prevacuolar compartment. Upon arrival at the prevacuolar compartment, the complex of cargo protein and VSR dissociates and the VSRs are retrieved to the Golgi complex (Da Silva et al. 2005). Three different unrelated VSRs have been described in eukaryotes. In mammalian cells, sorting of lysosomal proteins is mainly mediated by the mannose-6-phosphate receptor (Ghosh et al. 2003). In addition, a few lysosomal hydrolases are targeted to the lysosome by sortilin (Ni et al. 2006; Canuel et al. 2008), which shares extensive homology with the yeast vps10p receptor in the luminal cargo binding domain (Petersen et al. 1997). The vps10p VSR of yeast represents the second type of eukaryotic VSR (Marcusson et al. 1994). In addition an unrelated third type has been described in angiosperms (Cao et al. 2000).

Protein trafficking to vacuoles in angiosperms has been investigated in some detail over the last years (summarized recently by Becker 2007). Three different types of VSSs have been identified in angiosperms (Neuhaus and Rogers 1998) and assigned to specific transport routes (Vitale and Raikhel 1999): The first type has a sequence-specific VSS located at the N- or C-terminus (e.g N-terminal NPIR [Asn-Pro-Ile-Arg]). A second type of VSS is located at the C-terminus, has a variable length and often contains hydrophobic amino acids. In addition to these two VSS, some proteins appear to require large stretches of different parts of the polypeptide for successful targeting to the vacuole.

The first VSR identified in plants was a pea trans-membrane protein named BP-80 (Kirsch et al. 1994; Paris et al. 1997). In *Arabidopsis thaliana*, VSRs of the BP-80 type form a small protein family with seven members (now known as AtVSR 1–7; Masclaux et al. 2005; Paris and Neuhaus 2002; Shimada et al. 2003). This protein family has been suggested to be restricted to plants (Humair et al. 2001; Paris et al. 1997). All known angiosperm members of this protein family have the following characteristics (Cao et al. 2000; Mahon and Bateman 2000; Masclaux et al. 2005; Paris et al. 1997): A large N-terminal luminal domain of about 400 aa containing at its N-terminus a protease-associated domain (PA-domain). The C-terminal part of the luminal domain contains several epidermal growth factor (EGF) signature sequences, a single trans-membrane region and a short cytoplasmic tail containing a YXXØ tyrosine-motif (with X being any amino acid and Ø a bulky hydrophobic amino acid). The PA-domain and the EGF repeats have been implicated in ligand binding (Cao et al. 2000; Mahon and Bateman 2000) and the tyrosine-motif is apparently involved in sorting the receptor ligand complex into clathrin-coated vesicles formed at the TGN (Happel et al. 2004).

Recently, a second type of vacuolar sorting receptor has been identified. This protein belongs to a unique receptor-like protein family containing a ReMembR-H2 domain and has been named RMR (Park et al. 2005; Wang et al. 2011). RMR is apparently restricted to members of the Tracheophyta (Becker 2007) and most likely this protein is involved in transport to the storage vacuole in plants (Park et al. 2005, 2007; Wang et al. 2011).

Masclaux et al. (2005) suggested that the three phylogenetic clades observed for the seven VSRs from *A. thaliana* reflect different functions of the VSRs and have tentatively assigned the three groups of VSRs to the lytic, the storage vacuole and a putative endocytotic pathway. However, more recent findings regarding the intracellular localization (Miao et al. 2006) and function of VSRs (Zouhar et al. 2010) suggest that, although some functional specialization within VSRs exists (Zouhar et al. 2010), many VSRs perform redundant functions (Zouhar 2010). Regardless of these new results, the role of the different VSRs and RMR isoforms and their *in vivo* cargo are clearly not completely understood (Zouhar et al. 2010; Wang et al. 2011) and require further work.

Nothing is known about protein trafficking to the vacuoles in eukaryotic algae. In a recent study, we searched completed algal genomes for AtVSR homologues to examine the evolution of vacuolar sorting in algae (Becker and Hoef-Emden 2009). We demonstrated that all viridiplants investigated contain at least one plant-type VSR. In contrast, red algae and probably also glaucophytes lack a homologue of AtVSRs. In addition, several members of the chromalveolates obtained a putative VSR from a green alga by either horizontal or endocytotic gene transfer. We now revisit this topic and include additional species in our analyses: *Ectocarpus siliculosus, Albugo laibachii, Emiliania huxleyi, Fragilariopsis cylindrus, Phytophthora infestans, Picea sitchensis, Selaginella moellendorffii* and *Coccomyxa* sp. C169 genomes, *Klebsormidium subtile* and *Coloechaete scutata* ESTs.

In addition, we noticed that in a few cases the protein sequences have been slightly modified in new genome releases (different μ-Adaptin motifs for *Tetrahymena thermophila, Phaeodactylum tricornutum* VSR2, *Chlorella* sp. NC64A and *Micromonas pusilla*), which were subsequently used in our analyses. The final version of the *Phytophthora sojae* genome includes now a VSR protein of similar length as in other chromealveolates.

Identification of putative vacuolar sorting receptors in protists

To investigate vacuolar targeting in algae, we have screened public databases for the presence of the plant-type and the vps10p type VSR in protists using the BLASTP (tBLASTN for ESTs) program and a conservative cut-off for the expectancy value of e-20. Table 5.1 shows the distribution of these two genes among eukaryotes. As is evident from Table 5.1, plant-type VSRs are restricted to viridiplants, stramenopiles and ciliates, whereas putative vps10p homologues were detected in ophistokonts, alveolates and chlorophytes. As some eukaryotic groups apparently lack both types of VSRs, these groups might utilize additional unrelated VSRs for protein targeting to the vacuole. In the following we will concentrate on the plant-type VSR and its structure and evolution in algae.

Table 5.1 Distribution of vps10p and plant-type vacuolar sorting receptors among eukaryotes. Phyla are grouped into the currently discussed 5 eukaryotic supergroups.

	vps10p	**plant-type VSR**
Plantae		
Glaucophytes	–	–
Rhodophytes	–	–
Chlorophytes	+	+
Streptophytes	–	+
Chromalveolata		
Stramenopiles		
Pelagophytes	–	+
Oomycetes	–	+
Bacillariophytes	–	+
Phaeophytes	–	+
Haptophytes	–	–
Alveolates		
Ciliates	+	+
Apicomplexa	+	–
Dinoflagellates	+	(+)
Ophistokonts		
Amoebozoa	+	–
Animals	+	–
Fungi	+	–
Excavata	(+)	–
Rhizaria	–	–

(+) short ESTs only, similarity might be restricted to single domain; – No similar protein detected (BLASTP or tBLASTN analysis using an e-value cut-off of e-20 and the protein [EST] database at NCBI).

At least one protein with significant similarity to *Arabidopsis thaliana* VSRs was detected in green algae, ciliates, diatoms, brown algae, pelagophytes and oomycetes, but not in haptophytes, rhodophytes or glaucophytes (Table 5.1, see Table 5.2 for the accession number of putative protist VSRs). Several protists with BLASTP hits to plant VSRs contained more than one putative homologue to AtVSRs. Two putative VSRs have been found in the genomes of both strains of *Micromonas* sp., *Chlorella* sp., *Coccomyxa* sp., *Albugo laibachii*, and of *Thalassiosira pseudonana*, respectively (Table 5.2 and Table 5.3). BLASTP searches against the genome of *Phaeodactylum tricornutum* and *Fragilariopsis cylindrus* yielded in both cases three putative VSRs (Table 5.2 and Table 5.3). A fourth protein sequence from *Phaeodactylum tricornutum* showing similarity to plant VSRs is highly modified and could not be used in the phylogenetic analyses. Similarly, the sequence retrieved for *Aureococcus anophageferrrens* is highly derived and contains an additional scramblase domain. An additional sequence included in the new release of the *Tetrahymena thermophila* genome shows also similarity to viridiplant VSR, however the similarity is restricted to the N-terminal part of plant VSR and might therefore not represent a real VSR homologue. Both sequences were not used for further analyses. The genome of *Paramecium tetraurelia* contained even nine putative VSRs (not shown). For simplicity and to indicate the presence of a small protein family in *P. tetraurelia*, only sequences for the best three BLASTP hits (Table 5.2 and Table 5.3) were retrieved for *Paramecium tetraurelia* and used for phylogenetic analyses and protein structure predictions.

Table 5.2 VSR-homologues in protists, bryophytes and pteridophytes.

***Arabidopsis thaliana* VSR query**	**VSR 1 – VSR 7**
Albugo laibachii	gi|325181646| gi|325186519|
Aphanomyces euteiches	ESTs
Aureococcus anophageferrens	gi|323446517|
Ceratopteris richardii	ESTs
Chlamydomonas reinhardtii	gi|159486314|
Chlorella sp. NC64A	jgi|ChlNC64A_1|144184| jgi|ChlNC64A_1|144100|
Closterium peracerosum	ESTs
Coccomyxa sp. C169	jgi|Coc_C169_1|49231| jgi|Coc_C169_1|26335|
Coleochaete scutata	ESTs
Ectocarpus siliculosus	gi|299473335|
Fragilariopis cylindrus	jgi|Fracy1|171314| jgi|Fracy1|269990| jgi|Fracy1|244424|
Klebsormidium subtile	ESTs
Marchantia polymorpha	ESTs
Micromonas pusilla	jgi|MicpuC2|43569| jgi|MicpuC2|56945|

Table continued on next page.

Table 5.2 (Continued)

***Arabidopsis thaliana* VSR query**	**VSR 1 – VSR 7**
Micromonas sp. RCC299	jgi|MicpuN2|58183| jgi|MicpuN2|66647|
Oryza sativa	gi|115469398| gi|115481614| gi|115487010
Ostreococcus lucimarinus	gi|145349231
Ostreococcus tauri	gi|116059033|
Paramecium tetraurelia[1]	gi|146184097| gi|145501005| gi|145504074|
Phaeodactylum tricornutum	jgi|Phatr2|38456| jgi|Phatr2|32074| jgi|Phatr2|32073| jgi|Phatr2|36020|
Physcomitrella patens	ref|XP_001759820.1| ref|XP_001777810.1| ref|XP_001776090.1| ref|XP_001765481.1| ref|XP_001751750.1| ref|XP_001785165.1| ref|XP_001759928.1| gb|AAG60258.1|
Phytophthora infestans	gi|301122137| gi|262099557|
Phytophthora ramorum	jgi|Phyra1_1|83434
Phytophthora sojae	jgi|Physo3|506174|
Picea sitchensis	gi|148909214| gi|148909165|
Prototheca wickerhamii	ESTs
Selaginella moellendorffii	gi|302770398| gi|302788188| gi|302768689| gi|302821453|
Tetrahymena thermophila	gi|146184097| gi|118348244|
Thalassiosira pseudonana	jgi|Thaps3|42545| jgi|Thaps3|25062|
Volvox carteri	jgi|Volca1|119519|
Rhodophyta (NCBI ESTs, and *Galdieria sulphuraria* and *Cyanidioschyzon merolae* genomes)	No protein similar to AtVSRs found
Glaucocystophyceae (NCBI ESTs)	Haptophyta (*Emiliania huxleyi*)

[1]The *Paramecium* genome contains a large number of hypothetical proteins, which show similarity to plant VSRs, for simplicity and to indicate the presence of a protein family, only three members are used in the phylogenetic analyses.

Table 5.3 In-silico characterization of putative viridiplant and chromalveolate VSRs.

Organism	Protein length (aa)	SP prediction[1]	TMD prediction[2]	µ-adaptin binding motif[3]	Asx-hydroxyl[4]	EGF1 signature[4]	EGF2-signature[4]	EGF-Ca-signature[4]	PA-domain[5]
Chromalveolates									
Ciliophora									
Paramecium tetraurelia 1	452	16	392–414	YIKF	–	–	–	–	24–149
Paramecium tetraurelia 2	456	16	396–418	YIQF	–	–	–	–	8–145
Paramecium tetraurelia 3	477	12	420–442	YYAM	–	–	–	–	18–161
Tetrahymena thermophila 1	481	17	422–444	YFAL	–	–	–	–	9–165
Phaeophytes									
Ectocarpus siliculosus	535	26	458–480	YMPL	–	–	–	–	53–197
Diatoms									
Fragilariopis cylindrus 2	414	?	345–367	YMPL	–	–	–	–	1–89
Fragilariopis cylindrus 3	534	26	485–507	?*	–	–	–	–	98–172
Phaeodactylum tricornutum 1	538	21	457–479	YMPL	–	–	–	–	58–185
Phaeodactylum tricornutum 3	557	18	484–506	YMPL	–	–	–	–	51–196
Phaeodactylum tricornutum 4	504	21	459–481	YLQL	–	–	–	–	44–163
Thalassiosira pseudonana 1	513	18	444–466	YMPL	–	–	–	–	49–192
Thalassiosira pseudonana 2	535	?	472–494	YMPI	–	–	–	–	75–219
Oomycetes									
Albugo laibachii 1	530	16	447–469	YMPL	–	–	–	–	52–182

Table continued on next page.

Table 5.3 (Continued)

Organism	Protein length (aa)	SP prediction[1]	TMD prediction[2]	μ-adaptin binding motif[3]	Asx-hydroxyl[4]	EGF1 signature[4]	EGF2-signature[4]	EGF-Ca-signature[4]	PA-domain[5]
Albugo laibachii 2	551	28	465–487	YMPM	–	–	–	–	63–199
Phytophthora sojae	550	24	456–480	YMPL	–	–	–	–	62–191
Phytophthora ramorum	1396	?	1305–1327	YMPL	–	–	–	–	910–1035
Phytophthora infestans	546	21	455–477	YMPL	–	–	–	–	59–188
Viridiplants									
Chlorophyta									
Chlorella spec. NC64A 1	632	18	564–586	YLPL	–	–	–	–	49–184
Chlorella spec. NC64A 2	672	30?	13–35 565–587	YMHL	2	–	–	1	61–199
Chlamydomonas reinhardtii	700	22	561–583	YMPL	1	–	–	–	49–200
Coccomyxa sp. C169 1	699	37	21–40 618–640	YMPL	1	–	1	1	64–188
Coccomyxa sp. C169 2	710	23	7–26 639–661	YMPL	1	1	–	1	54–138
Micromonas pusilla 1	814	?	39–61 707–729	YMPL	–	–	1	–	86–241
Micromonas pusilla 2	789	?	641–663	YLPL	1	–	3	–	92–117
Micromonas sp. N 1	718	?	17–36 643–665	YMPL	–	–	1	–	69–198
Micromonas sp. N 2	569	?	523–545	YMPL	–	–	1	–	26–154

Table continued on next page.

Table 5.3 (Continued)

Organism	Protein length (aa)	SP prediction[1]	TMD prediction[2]	μ-adaptin binding motif[3]	Asx-hydroxyl[4]	EGF1 signature[4]	EGF2-signature[4]	EGF-Ca-signature[4]	PA-domain[5]
Ostreococcus tauri	730	?	21–40 647–669	YMPL	1	–	1	1	67–194
Ostreococcus lucimarinus	595	?	550–572	YMPL	1	–	1	1	28–156
Volvox carterii	735	?	584–606	YMPL	1	–	–	1	5–149
Streptophyta									
A. thaliana VSR 1	623	19	564–586	YMPL	1	–	1	1	46–173
A. thaliana VSR3	628	24	569–591	YMPL	1	–	1	1	51–178
A. thaliana VSR7	625	26	7–29? 564–586	YMPL	1	1	1	1	53–176
Physcomitrella patens 1	616	13	558–580	YMPL	1	1	–	1	40–165

[1]Target P and/or Phobius, the number indicates the length of the signal peptide. ? no clear signal peptide. In two cases (*O. lucimarinus* and *Micromonas* spc. N 1) the protein sequence did not start with a methionine, indicating that protein sequences did not contain the N-terminus. [2]Target P and/or Phobius. The position of the trans-membrane helix is indicated. ? = 60–80% probability. [3]Sequence of the YXXØ-motif. Amino acids different from the conserved YMPL-sequence motif are unterlined. [4]The number of signature sequences detected with Prosite scan (Expasy server) is given. [5]The position of the PA-domain as predicted by the CD server (conserved domain search, NCBI) is given. *No clear YXXØ motif.

Evolution of vacuolar sorting receptors in algae

For phylogenetic analyses we added a few translated ESTs representing mainly streptophyte groups currently not represented by a complete genome. We excluded the ESTs from pelagophytes and dinoflagellates from further analyses, as they were rather short and we cannot not exclude the possibility, that the similarity of these ESTs is restricted to a single domain of the plant-type VSR. Therefore, these proteins might not function as a VSR. Figure 5.1 shows an unrooted maximum likelihood tree inferred from plant and putative protist VSRs. The tree is clearly split into three highly supported monophyletic clades, Viridiplantae (Chlorophyta and Streptophyta), Ciliophora (*Paramecium tetraurelia* and *Tetrahymena thermophila*) and Stramenopiles (oomycetes, brown algae and diatoms). The streptophyte lineage was separated with high support from all other groups, whereas the chromalveolate VSRs (Stramenopiles and Ciliophora) emerged from within the Chlorophyta, thus may have evolved from chlorophyte VSRs (Figure 5.1).

VSR gene families have been found in ciliates, in diatoms, in some chlorophyte algae (*Chlorella* sp., *Coccomyxa* sp. and both *Micromonas* strains), and in land plants (Figure 5.1). The gene duplications in ciliates, stramenopiles and viridiplants apparently occurred independently, since the VSR tree corresponded in this respect largely to the taxon tree (Figure 5.1). This was not generally true, however, for gene duplications within the three large clades (see below).

In the spermatophytes, a split into two paralogous clades, representing the three known VSR families (angiosperm VSRs 1: subfamily 1 [AtVSR 1 and 2], subfamily 2 [AtVSR 3 and 4]; angiosperm VSRs 2: subfamily 3 [AtVSR 5–7]), could be found, indicating that a gene duplication took place at least in the common ancestor to spermatophytes (*Picea sitchensis, Oryza sativa, Arabidopsis thaliana*). The VSR proteins of the moss *Physcomitrella patens* form a separate clade basal to the spermatophyte clade, whereas the four sequences of the spike moss *Selaginella moellendorffii,* three isoforms of the fern *Ceratopteris richardii* and the two sequences of the liverwort *Marchantia polymorpha* group each independently within the two different angiosperm/gymnosperm clades. The VSRs of streptophyte algae form a separate clade basal to land plants. However, within the streptophytes the VSR tree does not match the accepted organismal phylogeny and this branching pattern was not supported (Figure 5.1).

A gene duplication took also place in the common ancestor of the chlorophytes (Figure 5.1). The sequences *Micromonas pusilla* 1*, Micromonas* sp., *Coccomyxa* sp. 2 and *Chlorella* sp. 2 seemed to be orthologous to the proteins of *Volvox carteri* and *Chlamydomonas reinhardtii,* although with low support, whereas in the paralogous branch (*Coccomyxa* sp. 1, *Chlorella* sp. 1, *Micromonas pusilla* 2 and *Micromonas* sp. 2) a sequence of the colorless *Prototheca wickerhamii* was found (Figure 5.1).

A VSR gene family evolved also in the common ancestor to the diatoms resulting in several paralogous proteins found in *Phaeodactylum tricornutum, Fragilariopsis cylindrus* and *Thalassiosira pseudonana* (Figure 5.1), however, the exact relationships between the different diatoms could not be resolved. Interestingly, the brown alga *Ectocarpus siliculosus* does encode only a single VSR, suggesting that the different diatom isoforms represent a recent expansion of the diatom VSR protein family.

Several VSR sequences derived from ESTs were considerably shorter than most of the other sequences in the alignment (e.g. *Ceratopteris richardii* 1 and 2: 224 and 194

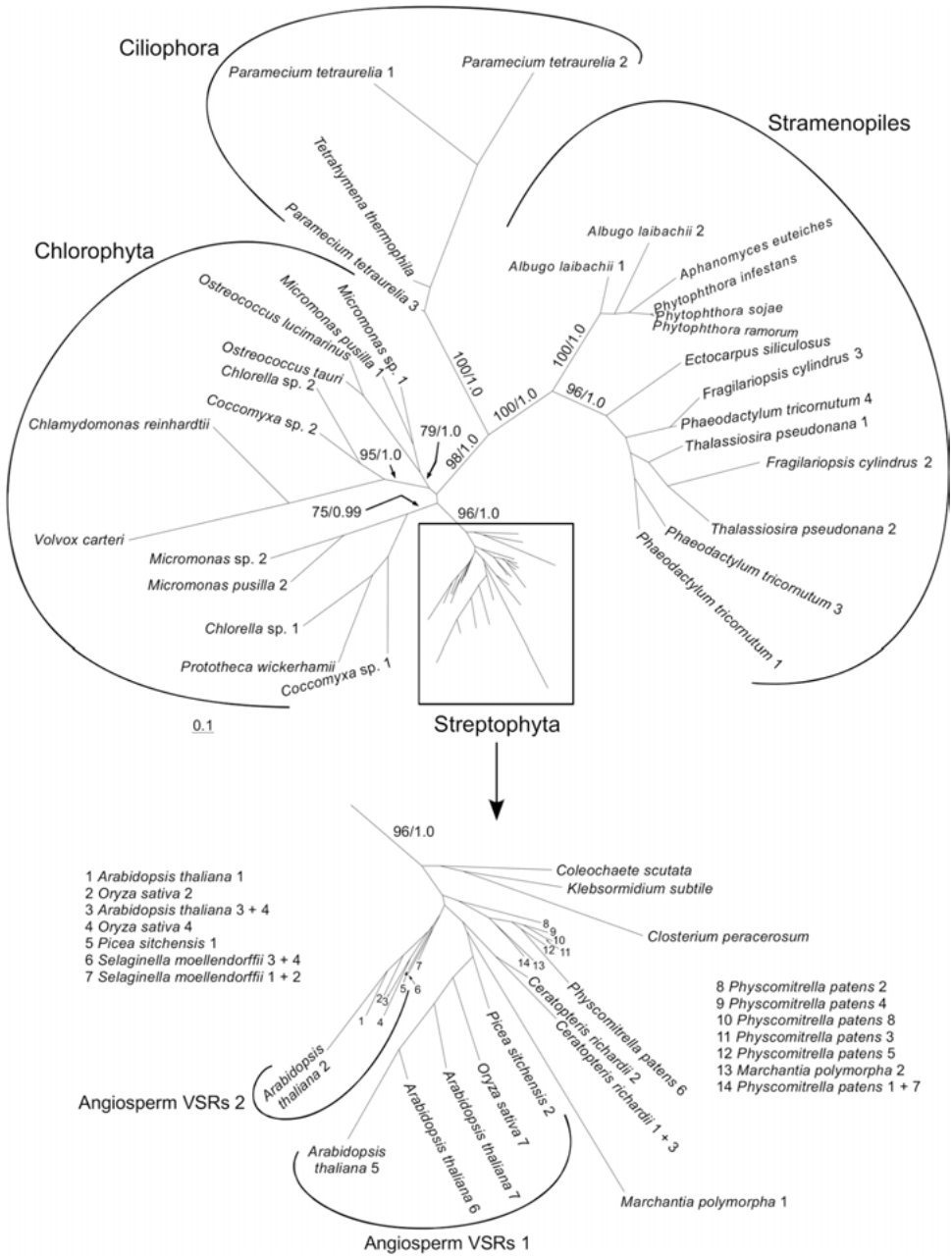

Figure 5.1 Unrooted maximum likelihood tree inferred from protein sequences of plant-type VSRs found in Viridiplantae (Chlorophyta and Streptophyta) and in Chromalveolata (Bacillariophyta, Ciliophora and Oomycetes). The extremely dense streptophyte clade has been excised and enlarged to demonstrate the branching pattern of VSR families among angiosperms, ferns and mosses. Only support values for internal branches and for gene duplications in chlorophyte and stramenopile sequences depicted (ML bootstrap, posterior probability). Evolutionary model: WAG+I+Γ; scale bar: substitutions per site.

aa, respectively, *Closterium peracerosum*: 191 aa, *Marchantia polymorpha*: 208 aa, *Prototheca wickerhamii*: 159 aa). This resulted in partial overlap of the sequences in the alignment and – in addition to some divergent sites in the sequences – may account for some long branches, e.g. of *Marchantia polymorpha.* These sequences most likely have also caused a decrease of resolution at internal branches.

Structure of putative VSRs from Protists

To test whether the putative VSRs from protists were indeed vacuolar-sorting receptors, we compared the structure of the putative VSRs with the structure of a member of each of the three angiosperm subfamilies (AtVSR1, AtVSR3 and AtVSR7) using several secondary structure and protein domain prediction programs. The results are summarized in Table 5.3.

All sequences contained an N-terminal PA domain and a trans-membrane domain at the C-terminus upstream from the nearly always present μ-adaptin binding motif YXXØ (Table 5.3). Most chromalveolate proteins comprised between 452 and 557 aa, whereas the viridiplant VSR proteins were a little bit longer than the majority of the chromalveolate sequences (around 100 to 200 aa longer). An exceptionally long putative VSR was found in *Phytophthora ramorum* (1457 aa). However, most likely this represents an artificial gene fusion, as the N-terminal part of the putative VSR from *Phytophthora ramorum* is very similar to hypothetical conserved proteins detected in the other two *Phytophthora* species and *Albugo laibachii*.

Modifications of the number of trans-membrane helices, of the μ-adaptin binding motif or of asx-hydroxyl sites or EGF signatures showed evolutionary patterns.

(i) In chlorophytes, 6 protein sequences have been predicted to contain an additional trans-membrane helix. Except for *Coccomyxa* sp. VSR 1, all VSRs containing two trans-membrane domains (TMDs) occur in the same subfamiliy, suggesting that the second TMD evolved immediately after the duplication event with subsequent loss in *Ostreococcus lucimarinus, Chlamydomonas reinhardtii* and *Volvox carteri*.
(ii) Whereas in nearly all viridiplant VSRs, the μ-adaptin binding motif was highly conserved (YMPL), it was highly modified in putative ciliate VSRs with only the tyrosine in the first position being conserved.
(iii) In the oomycetes, the conserved YMPL motif was found (except for one of the two isoforms of *Albugo albachii* VSRs) and no signal peptides could be detected for the VSR from *Phytophthora sojae*, however this sequence might represent an artificial gene fusion (see above).
(iv) In the diatom protein family, proteins with signal peptides and conserved YMPL were found and proteins with no detectable signal peptides and YXXØ motifs.
(v) In all chromalveolates, no asx-hydroxyl sites or EGF signature sequences could be detected.

It should be noted that after Prosite scans (Expasy server) and conserved domain search (NCBI) a complete EGF domain was only detected in *Ostreococcus lucimarinus, Ostreococcus tauri*, in *Micromonas pusilla* 2 and in one of the seven *A. thaliana* VSRs. In all other cases, only signature sequences representing parts of an EGF domain were detected.

Putative VSRs from Protists

Vacuolar (lysosomal) protein sorting is a fundamental feature of eukaryotic cells. However, the receptors used for sorting of soluble vacuolar proteins are not conserved. The mammalian receptor recognizes mannose-6-phosphate residues on N-linked oligosaccharides present on lysosomal proteins (Ghosh et al. 2003). In contrast, yeast and plant receptors bind to amino acid sequences although yeast vps10p and plant VSR receptors are structurally very different (Kirsch et al. 1994; Marcusson et al. 1994; Paris et al. 1997). These differences and the presence of a large number of different vacuolar sorting receptors in plants have been related to the increased complexity of the vacuolar system in plants, requiring several and new types of vacuolar sorting receptors compared to mammalian cells and yeast (Cao et al. 2000; Masclaux et al. 2005).

As shown by us, plant-type VSRs are also present in green algae and several chromalveolates, the latter representing plastid-containing (diatoms) as well as aplastidic lineages (oomycetes and ciliates). Comparison of the protein structure of protist VSRs with the three angiosperm-types of VSRs from *A. thaliana* supports the notion that these proteins are indeed vacuolar sorting receptors or relatives of VSRs. Most VSR-like proteins are predicted to be type 1 membrane proteins (single trans-membrane domain, C-terminus in the cytosol) as their *A. thaliana* counterparts.

As in *A. thaliana*, all putative chromalveolate and chlorophyte VSRs contain a luminal PA-domain, shown to be involved in ligand-binding in pea (Cao et al. 2000), and a cytoplasmic YXXØ-motif known to be required for binding of the adaptin 1 complex of clathrin-coated vesicles formed at the TGN (Happel et al. 2004). The trans-membrane domain and cytoplasmic domains are required for proper intracellular localization of plant VSRs (Paris et al. 1997). The YXXØ-motif (required for adaptin 1 binding) and the region between the trans-membrane domains and the YXXØ motifs were highly conserved across all VSR-like proteins suggesting a similar intracellular localization in Viridiplantae and chromalveolates. Therefore, from a structural perspective all these proteins are likely vacuolar sorting receptors or derivatives of VSRs.

A major difference between nearly all viridiplant and all chromalveolate VSRs is the presence of EGF domains or at least EGF signature sequences in the viridiplant receptors (Table 5.3), which are apparently completely absent in the chromalveolates (generally the chromalveolates lack this part of the protein completely). However, in viridiplants (angiosperms), the EGF domains and signature sequences are also not always well conserved, indicating that the evolutionary pressure to retain these signature sequences cannot be strong.

Origin of plant-type VSRs

The restricted distribution of plant-type VSRs to Viridiplantae and chromalveolates raises the question where this type of receptor originated. We consider two scenarios possible: (1) The plant-type VSR was an old eukaryotic invention and has been retained only in chromalveolates and viridiplants. (2) Plant-type VSRs have been present in the common ancestor of the Viridiplantae and the chromalveolates gained plant-type VSRs by horizontal or endocytotic gene transfer.

(i) Current classification schemes divide the eukaryotic superkingdom into five or six kingdoms or super-groups (Plantae [or Archaeplastida], Unikonta [Opisthokonta and Amoebozoa], Chromalveolata, Rhizaria, Excavata), although not all kingdoms have been sufficiently supported in phylogenetic analyses (Adl et al. 2005; Yoon et al. 2008). If a plant-type VSR was present in the common ancestor of all eukaryotes, this would imply four or five complete losses of this type of VSR in the common ancestors of these diverse kingdoms soon after split-up of the eukaryotes into different evolutionary lineages. Additionally, the genes for the plant-type VSRs must have been expunged later in two subkingdoms of the Plantae, the rhodophytes and the glaucophytes and one subkingdom in the chromalveolates, the Apicomplexa. This is not exactly the most parsimonious scenario and one would expect clear structural differences between viridiplant and chromalveolate VSRs that correlate with the taxon tree due to the long evolutionary time scale. The only feature supporting this idea is the presence of EGF signatures in the Viridiplantae and their complete lack in the Chromalveolata. This, however, could be equally well explained by one horizontal gene transfer followed by separate evolutionary pathways.

(ii) The notion of a horizontal or endocytotic gene transfer as the cause for presence of plant-type VSRs in chromalveolates is supported by several observations. In our phylogenetic tree, the branch of the chromalveolate VSRs emerged from chlorophyte sequences. Due to lack of resolution in this part of the tree, it is not possible to differentiate, whether the VSR gene originated from an early chlorophyte alga or from a viridiplant ancestor that lived before evolution of chlorophytes and streptophytes. Taking into consideration that the origin of the chromalveolates presumably predates the origin of the Streptophyta and the Chlorophyta, an ancestral viridiplant as a donor of a VSR gene seems to be more likely. A growing number of other studies provide further support for multiple horizontal or endocytotic gene transfer from the green lineage to chromists/chromalveolates (Armbrust et al. 2004; Becker et a. 2008; Hackett et al. 2007; Li et al. 2006; Montsant et al. 2005; Nosenko et al. 2006; Petersen et al. 2006; Tyler et al. 2006).

However, the origin of the plant-type VSRs remains elusive. No closely related proteins have been identified so far in other prokaryotic or eukaryotic organisms. Remarkably, also no relatives could be found in sister groups of the Viridiplantae, the red algae and the glaucophytes. Both completely sequenced red algae are extremophiles (Cyanidiphyta) with highly reduced genome sizes, and the glaucophyte and rhodophyte EST projects are far from representing complete genomes of glaucophytes and non-extremophile rhodophytes. Therefore, we cannot rule out that other rhodophytes and possibly the glaucophytes possess a plant-type VSR. If rhodophytes and glaucophytes indeed do not contain a plant-type VSR, the question arises, how these groups sort soluble vacuolar proteins. Homologues of the mannose-6-phosphate receptor and the yeast vps10p receptor are not present in the genome of *Cyanidioschyzon merolae* (unpublished results), suggesting that there might be still other types of vacuolar sorting receptors to discover.

Evolution of plant-type VSRs in chlorophytes and chromalveolates

The ancestral viridiplant VSR protein probably was a single-copy gene, had an N-terminal signal peptide for cotranslational import into the endomembrane system, a conserved C-terminal YMPL motif with an upstream trans-membrane domain, and perhaps one or several EGF domains. These features have been passed on to the offspring green lineages. Several gene duplication events resulted in VSR gene families. Mosses, ferns and spermatophytes evolved their VSR protein families independently. In the poorly sampled Chlorophyta, a gene duplication event was found in the *Micromonas* strains and in the *Chlorella* sp. and *Coccomyxa* sp. strain. The EGF domains seem to have degenerated in the various green lineages to different degrees. Our analysis included members of the classes Trebouxiophyceae (*Chlorella* sp., *Coccomyxa* sp. and *Prototheca wickerhamii*) and Chlorophyceae (*Volvox carteri* and *Chlamydomonas reinhardtii*) and scaly flagellates ("prasinophytes": two *Micromonas* and two *Ostreococcus* species). Given that a gene duplication was found in two trebouxiophyte genera and in scaly flagellates, it is tempting to speculate that the gene duplication may have preceded the evolution of the chlorophyte lineages followed by sequential loss in some lineages.

The ancestral chromalveolate genome probably obtained only one VSR gene together with other green algal genes from an engulfed/endocytotic green alga. The EGF domains of the VSR protein may have been lost either during the transfer process or later after establishment of the gene in the chromalveolate genome. The distinctive evolutionary pathways after separation of the chromalveolate lineages are reflected in their divergent features. In the ciliate plant-type VSRs, the YMPL motif diverged considerably. Almost none of the three positions following the tyrosine have been conserved. In contrast, in the oomycete plant-type VSRs, the YMPL motif has been maintained. As the genome of ciliates encodes also a putative vps10-type VSR, it might be possible that the plant-type VSR receptor lacking a YMPL motif serves other function in the highly developed endomembrane system of ciliates.

Signal peptides could not be detected in several organisms or were sometimes only present in one of the isoforms (e.g diatoms and oomycetes, Table 5.3). It may be possible that the signal peptides are highly derived and therefore not detectable using standard identification methods. However, in the diatoms, apparently gene duplication took place prior to separation into different species. The highly conserved protein probably is used as a VSR, whereas the more derived paralogue may serve a new function.

Angiosperms are characterized by the presence of different vacuole types in the same cell which would provide a possible explanation for requirement of different types of VSR. However, one can only speculate about the functions of the different VSR types in the *Micromonas* strains, in *Chlorella* sp., in *Coccomyxa* sp., in the diatoms and in *Paramecium tetraurelia.* Some of the duplicates acquired new domains indicating that they may serve a new currently unknown function (e.g. the additional trans-membrane domain in the *Micromonas* strains). In the case of diatoms, we may hypothesize (in analogy to land plants) that the evolution of a frustule which is formed in a special silica-deposition vesicle (Mayama and Kuriyama 2002) might require an additional level of protein sorting (silica-deposition vesicle and lysosomal compartment). In *Paramecium tetraurelia*, the different VSR types may be required to direct proteins specifically to food vacuoles,

contractile vacuoles or perhaps also alveoles, although in this case, the lack of a protein family of similar size in *Tetrahymena thermophila* is surprising.

Several interesting questions arise from this study: (1) Given the presence of plant-type VSRs in the chromalveolates, are the plant VSSs also conserved? (2) What is the function of the additional domains and paralogues in algae? (3) If rhodophytes and glaucophytes do not possess a plant-type VSR, how do these groups sort soluble vacuolar proteins? Currently, we do not know and comparative genomics alone cannot answer these questions. Cell biological work will be required to find answers to these questions.

Acknowledgements

We thank M. Melkonian for helpful comments.

References

Adl, S.M., A.G.B. Simpson, M.A. Farmer, R.A. Andersen, O.R. Anderson, J.R. Barta, et al. 2005. The new higher level classification of eukaryotes with emphasis on the taxonomy of protists. *J. Eukaryot. Microbiol. 52*: 399–451.

Armbrust, E.V., J.A. Berges, C. Bowler, B.R. Green, D. Martinez, N.H. Putnam, et al. 2004. The genome of the diatom *Thalassiosira pseudonana*: Ecology, evolution, and metabolism. *Science 306*: 79–86.

Becker, B. 2007. Function and evolution of the vacuolar compartment in green algae and land plants (Viridiplantae). *Int. Rev. Cytol. A – Surv. Cell Biol. 264*: 1–24.

Becker B., K. Hoef-Emden. 2009. Evolution of vacuolar targeting in algae. *Bot. Mar. 52*: 117–128.

Becker, B., K. Hoef-Emden and M. Melkonian. 2008. Chlamydial genes shed light on the evolution of photoautotrophic eukaryotes. *BMC Evol. Biol. 8*: 203.

Canuel, M., A. Korkidakis, Korkidakis, K. Konnyu, and C. R. Morales. 2008. Sortilin mediates the lysosomal targeting of cathepsins D and H. *Biochem. Biophys. Res. Com. 373*: 292–297.

Cao, X., S.W. Rogers, J. Butler, L. Beevers and J.C. Rogers. 2000. Structural requirements for ligand binding by a probable plant vacuolar sorting receptor. *Plant Cell 12*: 493–506.

Da Silva L.L.P., J.P. Taylor, J.L. Hadlington, S.L Hanton, C.J. Snowden, S.J. Fox, O. Foresti, F. Brandizzi, J. Denecke. 2005. Receptor salvage from the prevacuolar compartment is essential for efficient vacuolar protein targeting. *Plant Cell 17*: 132–148.

Domozych, D.S. 1991 The Golgi apparatus and membrane trafficking in green algae. *Int. Rev. Cytol.131*: 213–253.

Frigerio, L., G. Hinz, and D. G. Robinson. 2008. Multiple Vacuoles in Plant Cells: Rule or Exception? *Traffic 9*: 1564–1570.

Galtier, N., M. Gouy and C. Gautier. 1996. SEAVIEW and PHYLO_WIN: Two graphic tools for sequence alignment and molecular phylogeny. *Comput. Appl. Biosci. 12*: 543–548.

Ghosh, P., N.M. Dahms and S. Kornfeld. 2003. Mannose 6-phosphate receptors: new twists in the tale. *Nat. Rev. Mol. Cell Biol 4*: 202–212.

Hackett, J.D., H.S. Yoon, S. Li, A. Reyes-Prieto, S.E. Rummele and D. Bhattacharya. 2007. Phylogenomic analysis supports the monophyly of cryptophytes and haptophytes and the association of Rhizaria with chromalveolates. *Mol. Biol. Evol. 24*: 1702–1713.

Happel, N., S. Honing, J.M. Neuhaus, N. Paris, D.G Robinson and S.E.H. Holstein. 2004. *Arabidopsis* µA-adaptin interacts with the tyrosine motif of the vacuolar sorting receptor VSR-PS1. *Plant J. 37*: 678–693.

Hulo, N., A. Bairoch, V. Bulliard, L. Cerutti, B.A. Cuche, E. de Castro, C. Lachaize, P.S. Langendijk-Genevaux and C.J. Sigrist. 2008. The 20 years of PROSITE. *Nucleic Acids Res. 36*: D245–249.

Humair, D., D.H. Felipe, J.M. Neuhaus, N. Paris. 2001. Demonstration in yeast of the function of BP-80, a putative plant vacuolar sorting receptor. *Plant Cell 13*: 781–792.

Kirsch, T., N., Paris, J.M. Butler, L. Beevers and J.C. Rogers. 1994. Purification and initial characterization of a potential plant vacuolar targeting receptor. *Proc. Natl. Acad. Sci. USA 91*: 3403–3407.

Li, S.L., T. Nosenko, J.D. Hackett and D. Bhattacharya. 2006. Phylogenomic analysis identifies red algal genes of endosymbiotic origin in the chromalveolates. *Mol. Biol. Evol. 23*: 663–674.

Mahon, P. and A. Bateman. 2000. The PA domain: a protease-associated domain. *Protein Sci. 9*: 1930–1934.

Marcusson, E.G., B.F. Horazdovsky, J-L. CereghinoL, E. Gharakhanian and S.D. Emr. 1994. The sorting receptor for yeast vacuolar carboxypeptidase Y is encoded by the VPS10 gene. *Cell 77*: 579–586.

Marty, F. 1999. Plant vacuoles. *Plant Cell 11*: 587–599.

Masclaux, F.G, J.P. Galaud and R. Pont-Lezica. 2005. The riddle of the plant vacuolar sorting receptors. *Protoplasma 226*: 103–108.

Mayama, S and A. Kuriyama. 2002. Diversity of mineral cell coverings and their formation processes: a review focused on the siliceous cell coverings. *J. Plant Res. 115*: 289–295.

Montsant, A., K. Jabbari, U. Maheswari and C. Bowler. 2005. Comparative genomics of the pennate diatom *Phaeodactylum tricornutum. Plant Physiol. 137*: 500–513.

Neuhaus, J.M. and J.C. Rogers. 1998. Sorting of proteins to vacuoles in plant cells. *Plant Mol. Biol. 38*: 127–144.

Ni, X., M. Canuel, and C. R. Morales. 2006. The sorting and trafficking of lysosomal proteins. *Histology and Histopathology 21*: 899–913.

Nosenko, T., K.L. Lidie, F.M. Van Dolah, E. Lindquist, J.F. Cheng, D. Bhattacharya. 2006. Chimeric plastid proteome in the florida "red tide" dinoflagellate *Karenia brevis. Mol. Biol. Evol. 23*: 2026–2038.

Paris, N. and J.M. Neuhaus. 2002. BP-80 as a vacuolar sorting receptor. *Plant Mol. Biol. 50*: 903–914.

Paris, N., S.W. Rogers, L. Jiang, T. Kirsch, L. Beevers, T.E. Phillips and J.C. Rogers. 1997. Molecular cloning and further characterization of a probable plant vacuolar sorting receptor. *Plant Physiol. 115*: 29–39.

Park, J.H., M. Oufattole and J.C. Rogers. 2007. Golgi-mediated vacuolar sorting in plant cells: RMR proteins are sorting receptors for the protein aggregation/membrane internalization pathway. *Plant Sci. 172*: 728–745.

Park, M., S.J. Kim, A. Vitale and I. Hwang. 2004. Identification of the protein storage vacuole and protein targeting to the vacuole in leaf cells of three plant species. *Plant Physiol. 134*: 625–639.

Park, M., D. Lee, G.J. Lee and I. Hwang. 2005. AtRMR1 functions as a cargo receptor for protein trafficking to the protein storage vacuole. *J. Cell Biol. 170*: 757–767.

Petersen, C.M., M.S. Nielsen, A. Nykjaer, L. Jacobsen, N. Tommerup, H.H. Rasmussen, H. Roigaard, J. Gliemann, P. Madsen and S.K. Moestrup. 1997. Molecular identification of a novel candidate sorting receptor purified from human brain by receptor-associated protein affinity chromatography. *J. Biol. Chem. 272*: 3599–3605.

Petersen, J., R. Teich, H. Brinkmann and R. Cerff. 2006. A "green" phosphoribulokinase in complex algae with red plastids: Evidence for a single secondary endosymbiosis leading to haptophytes, cryptophytes, heterokonts, and dinoflagellates. *J. Mol. Evol. 62*: 143–157.

Rojo, E., C.S. Gillmor, V. Kovaleva, C.R. Somerville and N.V. Raikhel. 2001. VACUOLELESS1 is an essential gene required for vacuole formation and morphogenesis in *Arabidopsis. Dev. Cell 1*: 303–310.

Shimada,T., K. Fuji, K. Tamura, M. Kondo, M. Nishimura and I. Hara-Nishimura. 2003. Vacuolar sorting receptor for seed storage proteins in *Arabidopsis thaliana. Proc. Natl. Acad. Sci. USA 100*: 16095–16100.

Surpin, M. and N. Raikhel. 2004. Traffic jams affect plant development and signal transduction. *Nature Rev. Mol. Cell Biol. 5*: 100–109.

Tyler, B.M., S. Tripathy, X.M. Zhang, P. Dehal, R.H.Y. Jiang, A. Aerts, et al. 2006. *Phytophthora* genome sequences uncover evolutionary origins and mechanisms of pathogenesis. *Science 313*: 1261–1266.

Vitale, A. and N.V. Raikhel. 1999. What do proteins need to reach the plant vacuoles? *Trends Plant Sci. 4*: 149–155.

Vitale, A. and G. Galili. 2001. The endomembrane system and the problem of protein sorting. *Plant Physiol. 125*: 115–118.

Wang, H., J.C. Rogers JC and L.W. Jiang. 2011. Plant RMR proteins: unique vacuolar sorting receptors that couple ligand sorting with membrane internalization. *FEPS J. 278*: 59–68.

Yoon, H.S., J. Grant, J.I. Tekle, M. Wu, B.C. Chaon, J.C. Cole, J. M. Logsdon Jr., D.J. Patterson, D. Bhattacharya and L.A. Katz. 2008. Broadly sampled multigene trees from eukaryotes. *BMC Evol. Biol. 8*: 14.

Zouhar, J., A. Munoz and E. Rojo. 2010. Functional specialization within the vacuolar sorting receptor family: VSR1, VSR3 and VSR4 sort vacuolar storage cargo in seeds and vegetative tissues. *Plant J. 64*: 577–588.

6 Contractile vacuoles in green algae – structure and function

Karin Komsic-Buchmann and Burkhard Becker

Introduction

Fresh water organisms live in their natural environment under hypo-osmotic conditions. External water penetrates into the cell by osmosis. To sustain osmotic equilibrium many unicellular organisms expel water out of the cell by contractile vacuoles (CVs) (Kitching 1956; Patterson 1980).

Contractile vacuoles have fascinated microscopists since their discovery in the 18th century. According to Patterson (1980) the earliest report on contractile vacuoles was by Spallanzani (1776). In the second half of the 19th century, the relation of CVs to osmoregulation was discovered (Rossbach 1872; Hartog 1888; Degen 1905; Herfs 1922). Jennings (1904) was the first to demonstrate the discharge of contractile vacuoles in *Paramecium* using Indian ink. In the first half of the 20th century, Lloyd (1928a), Kitching (1938, 1952, and 1956) and Weatherby (1941) confirmed the role of CVs in osmoregulation. With the advent of electron microscopy, new insights into the ultrastructure of cells and CVs were achieved from the 1950th on (Rudzinska 1958; Schneider 1960; McKanna 1972 and 1973; Aaronson and Behrens 1974; Heywood 1978). Together with ion-physiological studies of that time (Dunham and Child 1961; Stoner and Dunham 1970; Dunham and Kropp 1973; Prusch 1977), a concept of the function of contractile vacuoles was developed: the CV is a discrete organelle, functionally distinct from other compartments and operating in osmoregulation respectively for cell volume regulation (Patterson 1980). More recently, the fast evolving molecular techniques have allowed the identification of proteins, which are involved in the function of CVs or osmoregulation in general (for example see Ulrich et al. 2011). In this review we will first describe the occurrence of CVs in general and analyse recent advances in our understanding of CV function in a few model systems. In the final part we will summarize our current knowledge on CV function in green algae.

Occurrence of contractile vacuoles

Contractile vacuoles are the most remarkable organelles in unicellular fresh water organisms due to their rhythmic activity. They are membrane-bound organelles, which periodically increase in volume (diastole) and finally expel their content out of the cell (systole). In general, they consist of the CV itself and associated vesicles and/or a tubular network. In Protozoa often microtubules are part of the CV complex (Patterson 1980; Allen 2000). Contractile vacuoles occur usually in protists and sponges which live in fresh water and possess no complete cell wall (Ettl 1961; Patterson 1980; Hausmann and Patterson 1984). In addition, they appear in some marine and parasitic organisms (Lloyd 1928a; Kitching 1956).

Many unicellular flagellated algae possess one or two CVs close to the basal bodies of their flagella: Cryptophyceae (Lucas 1970; Deane et al. 2002; Novarino 2003); Euglenophyceae (Hyman 1938; Leedale 1967; Shin and Boo 2001; Sánchez et al. 2004); Prasinophyceae (Suda et al. 2004; Becker and Hickisch 2005); Prymnesiophyceae (Mignot 1974; Green and Hibberd 1977), Chrysophyceae (Aaronson and Behrens 1974) and Chlorophyceae (Weiss et al. 1977; Gruber 1979; Luykx et al. 1997a). Some algae possesses more than two CVs e.g. *Mesostigma viride* (Buchmann and Becker 2009), the only known streptophyte flagellate, and *Haematococcus pluvialis* (Sineshchekov et al. 2001), a chlorophyte flagellate. Dinoflagellates possess typically no CVs, but they have a structure called pusule (Dodge 1972) which may function in osmoregulation. However, this structure is not only present in freshwater dinoflagellates; also marine species possess a pusule. CVs are not restricted to unicellular algae, multicellular algae possesses CVs at some stages of their life cycle too. Typically, they occur in phases where the cells have no rigid cell wall e.g. zoospores (e.g. *Stigeoclonium*, van den Hoek, Mann and Jahns 1995). Interestingly, gametes of the conjugating green algae *Cosmarium* and *Spirogyra* (Lloyd 1928b; van den Hoek, Mann and Jahns 1995) do contain CVs. However, in this case, CVs apparently do not function in osmoregulation; instead they are required for protoplast contraction after fusion of the gametes.

Heterotroph protists also possess a CV and have become important model systems regarding CV function. Examples are the kinetoplastids *Leishmania, Phytomonas* (Docampo et al. 2005), and *Trypanosoma cruzi*, the best examined parasite regarding the CV function (Allen and Naitoh 2002; Ulrich et al. 2011). Other well-known model systems requiring a CV for osmoregulation are *Dictyostelium discoideum* (Amoebozoa), and *Paramecium* (Ciliophora) (Allen and Naitoh 2002). The only known fungus possessing CVs are the biflagellate zoospores of the Oomycetes (Becket, Heath and McLaughlin 1974), which belong to the Chromalveolata.

Models systems: Recent advances of our understanding of general principles of CV function

Paramecium

The ciliate *Paramecium* possesses two highly structurally differentiated CVs. The CVs are located at fixed sites inside the cell. A permanent pore is present in the plasma membrane above each CV. Water is collected in the spongiome (see below) and transported via 5 to 10 "radial (collecting) canals" into the CV. The spongiome is a widely branched tubular membrane system and is divided into the smooth and the decorated spongiome. The smooth spongiome is directly connected to the collecting canals, while the decorated spongiome is located more peripherally and connected to the smooth spongiome. As the name suggests, the decorated spongiome carries electron microscopically visible particles, which have been shown to be part of the V-ATPase protein complex. The whole CV complex is reinforced by a system of microtubules. In the CV cycle the fluid continuously flows into the radial canals, channeled to the CV, and is released through the pore from the cell (Allen 2000; Allen and Naitoh 2002; Plattner 2010a). The major osmolytes of the CV are most likely K^+ and Cl^- (Stock et al. 2002a, b). The CV fluid

is always kept hypertonic to the cytosol (determined from K^+ and Cl^- activities only) ensuring water uptake into the CV irrespective of the ionic composition of the extracellular medium (Stock et al. 2002a). Remarkably, cells of *Paramecium* are able to change their internal osmotic potential. If the cells are cultured in iso-osmotic medium, CVs resume activity after some time (Stock et al. 2001). Whether CVs have an additional role in excretion is currently not clear (Iwamoto, Allen and Naitoh 2003).

In recent years, several proteins have been shown to be involved in the function of the CVs in *Paramecium tetraurelia* (for an overview see Table 6.1). One well studied example is the V-ATPase, which is located in the CV complex on the decorated spongiome. The V-ATPase transports protons from the cytosol into the CV using ATP hydrolysis as energy and produces an electrochemical gradient at the membrane. Grønlien et al. (2002) observed the electric potential of the CVs. As expected, during diastole the electric potential increased in a stepwise manner, most likely due to the re-attachment of the radial canals to the CV. The electrogenic sites are located at the radial arms. Interestingly, if cells from hypotonic medium were transferred to hypertonic medium, the fluid segregation was reduced and, in addition, the V-ATPase disappeared from the decorated spongiome (Grønlien et al. 2002). RNAi experiments showed, that the V-ATPase is necessary for CV

Table 6.1 Identified proteins and characteristics of the contractile vacuole complex in *Paramecium, Dictyostelium discoideum* and *Trypanosoma cruzi*. For references see text.

	Paramecium	***Dictyostelim discoideum***	***Trypanosoma cruzi***
Proton pumps	V-ATPase	V-ATPase	V-ATPase V-PPase
Other transporter	–	Rh50-like ammonium transporter	phosphate transporter polyamine transporter
Other ions	K^+, Cl^-	?	Polyamines, PO_4^{3-}
Aquaporin	?	?	+
Regulation by Calcium	+	+	+
Alkaline phosphatase	–	+	+
Clathrin-coated vesicles involved	–	+	+
Rab proteins	+	+	+
SNARE proteins	+	+	+
Exocyst complex involved	–	secA	–
Kinases	–	+	–
Actin/myosin microtubules	microtubules	actin	–
Pore detected	+	–	–

function and thought to be required for fluid segregation (Wassmer et al. 2005, 2006, 2009). Noteworthy, the pH of the CV fluid is only mildly acidic, pH 6.4 (Stock et al. 2002b). A putative inositol (1,4,5)-trisphosphate (Ins(1,4,5) P_3) receptor is located around the radial canals and the smooth spongiome of the CV complex. Although the exact function of this receptor is currently not clear, current evidence points to a role in Ca^{2+} homeostasis of the cell (Ladenburger et al. 2006). Similar to the V-ATPase, calmodulin (CaM) can be found in various intracellular locations including the CV complex. In the CV complex, it is concentrated at the CV pore and close to the decorated spongiome. Fok et al. (2008) speculated for a role for CaM in ion traffic. It is well known that SNAREs (soluble NSF attachment protein receptor; NSF = N-ethylmaleimide sensitive factor) from several subfamilies are present in the CV complex of *Paramecium*, indicating that membrane fusion events play a key role in CV function in *Paramecium* (Plattner, 2010a, b). R-SNAREs of the synaptobrevrin type (*Pt*Syb2, 6 and 9), Q-SNAREs of the syntaxin type (*Pt*Syx2, 14 and 15) and SNAP-25-LP were localized at the CV complex, with the exception of the decorated spongiome (Kissmehl et al. 2007; Schilde et al. 2006, 2008, 2010).

To summarize our current knowledge on CV function in *Paramecium*: V-ATPase is producing an electrochemical gradient which leads finally to water influx in the radial canals. The fluid is collected in the CV and then expelled into the medium through the CV pore. Ca^{2+} probably plays a role in CV regulation, as indicated by the presence of the (Ins(1,4,5)P_3)-receptor and calmodulin. In addition, numerous SNARE proteins are located at the membranes of the CV complex, indicating that the typical membrane fusion machinery is required for CV function.

Dictyostelium discoideum

In contrast to many other protists, the contractile vacuoles in the amoeba *Dictyostelium* occur not at a fixed position, instead they can move freely inside the cell (Patterson, 1980). They consist of a large main vacuole surrounded by numerous satellite vacuoles forming the spongiome (Nolta and Steck 1994).

An overview for proteins related to the CV function in *Dictyostelium discoideum* is given in Table 6.1. In *Dictyostelium,* 23 proteins have been confirmed to be located directly at the CV complex. Three of these CV-proteins are coding for transporters, respectively subunits of transporters. The gene rhgA (Rh50-like) encodes for a transmembrane ammonium transporter (Benghezal et al. 2001; Cornillon et al. 2002; and Mercanti et al. 2006). It is localized strictly to the CV compartment, but an Rh50-like-deficient mutant seems to show no phenotype related to osmoregulation. Mercanti et al. (2006) examined targeting of this protein to the CVs. Protein fusion constructs with the last 91 residues forming the Rh50 C-terminal cytoplasmic domain were successfully localized to the CV. The other two transporter genes are coding for the subunits A and M of the V-ATPase (vatA and vatM; Fok et al. 1993; Clarke et al. 2002). The latter subunit has several functions; it is involved in the targeting, the assembly of the enzyme complex and also in the proton translocation. A *GFP* fusion construct with *vatM* is a useful marker for observation of the CVs *in vivo*, the protein is apparently present at all membranes of the CV complex, both vacuolar and tubular elements, at any time of the CV cycle (Clarke et al. 2002).

Numerous proteins were identified which play a role in membrane traffic within the CVs. The clathrin assembly protein AP180 is localized at the CVs (clmA; Stavrou and O'Halloran 2006; Wen et al. 2009). Furthermore, two subunits of the adaptor-related protein complex 2 (ap2a1–1 and –2) are also present at the CVs (Wen et al. 2009). Epsins (epnA) plays important role in creating membrane curvature. In *Dictyostelium,* it is required for CV function and apparently involved in regulation of clathrin-coated vesicle (CCV) assembly, as it regulates the clathrin-associated protein Hip1r (Wen et al. 2009). So far, two SNAREs involved in CV function have been identified, vamp70B (vesicle associated membrane protein 70b), and vti1A (Vps10 tail interactor), a member of the v-SNARE family (Wen et al. 2009). Moreover, racH, a Rho GTPase, is involved in CV function, presumable by the delivery of vesicles carrying proton pumps, e.g. V-ATPase, to the early endosome. An indication for this is the altered distribution of the V-ATPase in racH knock-out cells (Somesh et al. 2006). Last but not least, the exocytic gene *sec*A (localized at the plasma membrane) is required for CV discharge. SecA mutants show an enlarged CV, suggesting that fusion of the CV membrane with the plasma membrane requires SecA. Fusion is believed to follow the 'kiss and run' mechanism with no intermingling of the CV and plasma membrane. Therefore, CVs are usually not involved in surface area regulation (Zanchi et al. 2010).

Some CV proteins identified are involved in osmotic stress response (Du et al. 2008). The Rab GTPase rab8a regulates CV discharging in response to osmotic stress. Further analysis revealed that rab8a itself is regulated by the rabGAP disgorgin (DDB_G0280955). Another putative rab GAP drainin (phgA) has also been shown to be involved in CV function in *Dictystelium*. In addition, a BEACH domain containing protein is located at the CV membrane, lvsA (Large Volume Sphere). This protein is involved in response to hypo-osmotic stress and required for cytokinesis (Gerald 2002).

Other proteins with a confirmed localization to the CVs are diverse. Two more Rab GTPases, the rab11A and the rab11C, are present at the CVs (Du et al. 2008). Some proteins where often used as markers for the CVs and are related to Ca^{2+}, Calmodulin (calA; Zhu and Clarke 1992 and Benghezal et al. 2001) and a glycoprotein gp100 called dajumin (Malchow et al. 2006). Another protein is golvesin (gol). This protein is distributed widely in the endomembrane system including the CV (Schneider et al. 2000). An alkaline phosphatase (alp) is also present in the CVs (Quiviger, de Chastellier, and Ryter 1978). An interesting CV protein is mpg1 (mental retardation GTPase activating Protein (MEGAP), member 1). MEGAP1^{-} cells empty their CVs less efficiently than normal and consequently have up to three times the usual number of CVs. A GFP fusion construct to mpg1 localizes to tubules of the CV network and when the systolic phase begins the tubules recruit cytosolic GFP-mpg1 (Heath and Insall 2008). To complete the list there are two more proteins confirmed to localize to CVs, vwkA a serin/threonin kinase (von Willebrand factor kinase A; Betapudi et al. 2005), and myoJ (Myosin 5b; Taft et al. 2008). Excitingly, *Dictyostelium* is the only known organism showing cooperation of actin/myosin in the CV complex.

Taken together, the structure of the CVs in *Dictyostelium* is not as ordered as in *Paramecium*, the system is more dynamic. But the proteins involved in CV function are similar.

Trypanosoma cruzi

Trypanosoma cruzi was one of the first organisms examined by transmission electron microscopy (Meyer and Porter 1954). Most of the studies on *Trypanosoma cruzi* were performed on the epimastigote type due to the availability of *in vitro* axenic cultures. The CV is present in each step of the *Trypanosoma* life cycle (Montalvetti, Rohloff and Docampo 2004) and is formed by the contractile vacuole itself (also called bladder) and the spongiome, composed of a series of numerous vesicles and tubules (Schoijet et al. 2010). The CV complex is located close to the flagellar pocket (de Souza 2009). The CV in *Trypanosoma* is described to operate in osmoregulation and cell volume regulation under hypo-osmotic stress (Regulatory Volume Decrease, RVD) (Montalvetti, Rohloff and Docampo 2004; Rohloff, Montalvetti and Docampo 2004; Rohloff and Docampo 2008). During RVD, cells exposed to a reduction in external osmolarity initially swell and then regain nearly normal cell volume (Rohloff and Docampo 2008). In addition to the contractile vacuole, acidocalcisomes are suggested to function in cell volume regulation, respectively osmoregulation in *Trypanosoma cruzi* (Rohloff, Montalvetti and Docampo 2004).

Several proteins were identified to be part of the contractile vacuoles or be related to in *Trypanosoma cruzi* (see Table 6.1). There are some transporters or subunits of transporters identified to localize to the CVs. The vacuolar proton pyrophosphatase (TcPPase or TcVP1) is not restricted to CVs, as acidocalcisomes also possess TcVP1 (Montalvetti, Rohloff and Docampo 2004). Aquaporin 1 mediates water transport through membranes and is also localized to the contractile vacuole complex and the acidocalcisomes (TcAQP1). Interestingly, if epimastigotes are transferred from iso- or hyperosmotic conditions to hypo-osmotic conditions, the aquaporin shifts from the acidocalcisomes to the CVs by fusion of these compartments (Montalvetti, Rohloff and Docampo 2004). Moreover, a polyamine transporter (TcPOT1) is also present in the CV membrane. If the medium is deficient in polyamines, this transporter can be transferred to the plasma membrane (Hasne et al. 2010). In the proteomic analysis of Ulrich et al. (2011) the subunits A, B, D and G of the V-ATPase were detected. Under hypo-osmotic conditions, the V-ATPase (observed by V-ATPase B-GFP fusion construct) is localized to the enlarged CV and additional smaller vacuoles, which might be acidocalsisomes (Ulrich et al. 2011). Furthermore, a phosphate transporter called Pho1was identified at the CV membranes and some granules in the cytosol. The orthologue in *S.cerevesia* Pho91 regulates phosphate and polyphosphate metabolism (Hurlimann et al. 2007) and the *Trypanosoma* protein is thought to be involved in the same functions. Interestingly, if the cell is exposed to hypo-osmotic stress, the localization of a TcPho1-GFP construct becomes more strongly associated with the CV (Ulrich et al. 2011).

Three proteins were confirmed to localize to the contractile vacuole complex, which are important for the function of the CVs. The first is calmodulin (CaM). This protein is present in the spongiome and in the cytosol (Ulrich et al. 2011). Calmodulin and the V-ATPase, respectively subunits of the V-ATPase, are often used as markers for identification of CVs in *Trypanosoma*. Calmodulin has been defined as a cytosolic Ca^{2+} receptor. It can stimulate the plasma membrane Ca^{2+}ATPase (Benaim et al. 1991) and the cyclic AMP phosphodiesterase (Tellez-Inon et al. 1985). The Ca^{2+}-ATPase Tca1 is located to the acidocalcisomes (Lu et al. 1998) and the cyclic AMP phophodiesterase C 2 (TcPDEC2)

localizes to the contractile vacuole complex, especially the spongiome. Cells treated with TcPDEC2 inhibitors showed an approximately 20 and 30% higher rate of volume recovery after exposure to hypo-osmotic conditions. The transgenic parasites overexpressing this enzyme are unaffected by the same inhibitors (Schoijet et al. 2010). Furthermore, the FYVE domain of TcPDEC2 recognizes specifically phosphatidylinositol 3-phosphate (PI 3-P) and recruits the protein to PI 3-P enriched membranes (Kutateladze 2007) of the CVs (Schooijet et al. 2011). It is noteworthy, that cAMP levels increase during hypo-osmotic stress (Rohloff et al. 2004), as does the expression level of TcPDEC2 (Schoijet et al. 2011). Interestingly, under iso-osmotic conditions, the CV of epimastigotes shows a cycle between 1 min and 1 min and 15 s (Clark 1959). Schoijet et al. (2011) speculated that TcPDEC2 could be an important mechanism to control cAMP oscillations responsible for the periodic function of the CV complex. The third protein is the alkaline phosphatase. This protein was detected by a cytochemical technique, which exhibits as dark precipitations using transmission electron microscopy. Precipitations were detected in the flagellar pocket, the contractile vacuole, in tubular structures around the CV – the spongiome –, and in the region between the CV and the flagella pocket (Rohloff, Montalvetti and Docampo 2004).

Six proteins involved in membrane fusion and trafficking were found in the CVs. The R-SNARE VAMP1 (vesicle associated membrane protein) is located in the CV of epimastigotes submitted to hypoosmotic stress (Ulrich et al. 2011). Interestingly, its orthologue in *Paramecium tetraurelia* PtSyb2–2 localizes to the entire contractile vacuole complex (Schilde et al. 2006). Moreover, two additional R-SNAREs are present in CV according to the proteome data of Ulrich et al. (2011). In agreement with the proteome data, GFP constructs (N-terminal) with TcSNARE2.1 and TcSNARE2.2 were detected on the CV membrane under hypo- and iso-osmotic conditions. Additionally, they co-localize with calmodulin in a region proximal to the CV. The adaptor associated protein AP180 is also localized to the CV (Ulrich et al. 2011). AP180 is involved in the assembly of the clathrin-coated vesicles. Two Rab GTPases are localized at the CV in *Trypanosoma* epimastigotes, Rab11 and Rab32, which are also localized to Golgi stacks. Furthermore, Rab11 shows a distinct localization distinguishable from the spongiome of the CV (Ulrich et al. 2011).

Rohloff, Montalvetti and Docampo (2004) identified four basic amino acids: valine, lysine, arginine and ornithine in a subcellular fraction containing most likely enriched contractile vacuoles. Furthermore, the fraction contained P_i, the hydrolysis product of PolyP. During hypo-osmotic or alkaline stress hydrolysis of short and long chain polyP occured in the acidocalcisomes, whereas the levels of short and long chain polyP increased after hyperosmotic stress. In addition, Ca^{2+} was released from the acidocalcisomes under osmotic or alkaline stress (Ruiz, Rodriguez and Docampo 2001). But, neither P_i nor basic amino acids were released to the extracellular medium. Possibly, basic amino acids and P_i are transferred from the acidocalcisomes to the contractile vacuole during hypoosmotic or alkaline stress by fusion of the compartments (Rohloff, Montalvetti and Docampo 2004).

To summarize this part, *Trypanosoma* is an organism which has to resist a broad range of osmotic conditions during its life cycle. The CV is not the only organelle with a function in osmoregulation; acidocalcisomes operate in this function, too. Likely, the regulatory mechanism is dependent on Ca^{2+} and phosphate (polyP and P_i). The system is supported

by a broad range of proteins involved in membrane trafficking and fusion. The general principle of water uptake seems to be the same as in other organisms; the development of an electrochemical gradient by hydrolysis of ATP by the V-ATPase and probably by the V-PPase is used to energize the process. In addition, *Trypanosoma cruzi* is the first organism where an aquaporin was demonstrated to be present in the CV membrane. cAMP seems to be an appropriate candidate for signaling of osmotic stress.

Taken together, the visible structure of the CVs in these three organisms is different. But, the general functions and processes are similar: (1) CVs contain a specific similar subset of proteins. (2) The proteins are transported to the CVs in vesicles which fuse with the CV membrane. (3) Proton pumps are generating an electrochemical gradient at the CV membranes but do not acidify the CV fluid. (4) The water can pass the CV membrane with the help of an aquaporin and an osmotic gradient. (5) Ca^{2+} and phosphate are important for the CV function. (6) The cell can sense osmotic changes in the extracellular environment and give an appropriate response. This is probably mediated by calcium and cAMP.

The contractile vacuole in green algae

Contractile vacuoles are present in fresh water green algae without a rigid cell wall to sustain osmotic pressure. This includes flagellated and non-flagellated gametes and vegetative cells. However, the function of the CV has been investigated recently in only three genera in some detail.

Mesostigma viride

Mesostigma viride is the only known flagellate within the Streptophyta (Marin and Melkonian 1999; Rodriguez-Ezpeleta et al. 2007). Impressively, the cells possess approximately 8 CVs surrounding the flagellar groove (see Figure 6.1). The system of CVs in *Mesostigma* is very dynamic, as the various CVs appear to connect for short time periods with each other. A CV cycle last about 24 s, whereby the systole takes only 10% of the time. At late diastole a CV shows a spherical shape with an average diameter of 1.5 µm. During systole, the CV associates with the membrane of the flagellar groove and forms contact zones of approximately 150 nm diameter and finally the CV collapses into smaller vacuoles. Probably, the CVs in *Mesostigma* do not expel all of their content out of the cell; it is possible that a part of the liquid remains in the cell as connections of collapsed CVs to CVs in diastolic phase occur. After systole, the smaller membrane compartments formed during the collapse start swelling and fuse with each other to form finally the large round vacuole at the end of diastole again. In this phase, connections between different CVs are also observable. In addition, coated vesicles are associated with the CVs. The density of clathrin-coated vesicles (CCV) and pits is correlated with the size of the CV. The bigger the CV is, the higher the density of coated vesicles and coated pits are. There are no cytoskeletal elements like microtubules associated to the system of CVs in *Mesostigma* (Buchmann and Becker 2009).

Brefeldin A (BFA) is a fungal macrolytic lactone and is an often used inhibitor of protein trafficking in endomembrane systems (Nebenführ, Ritzenthaler and Robinson 2002). A subset of Sec7-type GEFs (GTP exchange factors) is the molecular target for Brefeldin A.

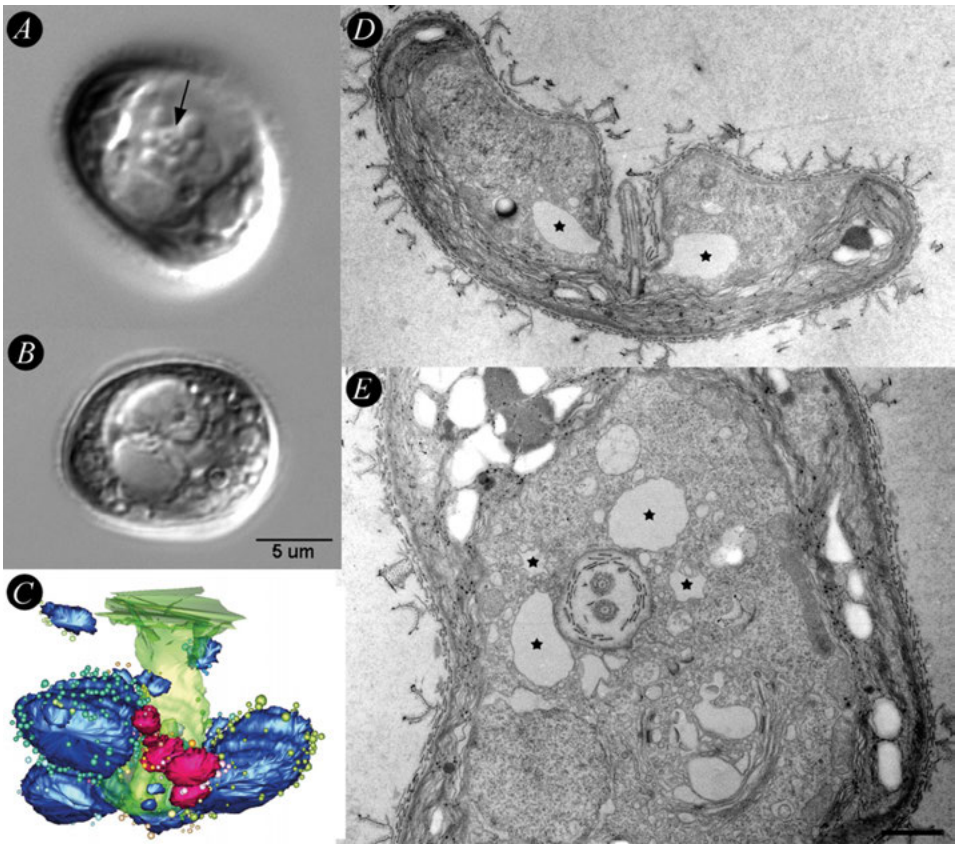

Figure 6.1 The contractile vacuoles in *Mesostigma viride*.
(A and B) DIC-images of *Mesostigma*. The CVs are surrounding the flagellar groove (arrow in A). The cell in B shows swollen CVs (25 min incubation with 4 µg Brefeldin A).
(C) 3-dimensional reconstructions of a 3.7 µm thick slice of a *Mesostigma* cell containing the system of CVs, for details see Buchmann and Becker (2009). The CVs (blue and purple) surround the flagella groove (green). Possibly, the vacuoles shown in purple are a developing CV. The colored round structures at the CVs are clathrin-coated vesicles (CCVs); CCVs associated with one CV are shown in the same color.
(D and E) Electron micrographs of cross sections of *Mesostigma*, horizontal and median, respectively. The CVs are marked with stars. The flagella groove penetrates deep into the cell and is encircled by CVs. Scale bar: 1 µm.
A and B and C unpublished own micrographs. D and E were taken from Buchmann and Becker (2009).

These GEFs catalyze the activation of Arf1p, an ADP ribosylation factor GTP-binding protein (Jackson and Casanova 2000). In turn, Arf1p is responsible for the recruitment of coat proteins (COPI and clathrin, via the adaptor complex AP-1) to membranes, resulting in the formation of transport vesicles (Scales et al. 2000; Nebenführ, Ritzenthaler and

Robinson 2002). Treatment of *M. viride* with Brefeldin A results in extreme swelling of the CVs, until the cells finally burst (see Figure 6.1B). It is likely that Brefeldin A-treated cells are performing a prolonged diastole and fail to terminate this phase (Becker and Hickisch 2005; Buchmann and Becker 2009).

Scherffelia dubia

The prasinophyte *Scherffelia dubia* possesses two contractile vacuoles, each on both sides of the flagellar groove at the anterior end (see Figure 6.2). A CV cycle lasts about 22 s, whereby contraction intervals as short as 9 s and as long as 30 s were also observed by Becker and Hickisch (2005). The maximum diameter of CVs in *S. dubia* at late diastole is about 1.4 µm. A so called scale reticulum (SR) is located in the region of the CV. It consists of a membranous reticulum with numerous coated pits, possibly clathrin-coated (Melkonian and Preisig 1986).

The following model for the CV cycle is assumed: During systole, the CV discharges its content into the flagellar groove. Adjacent, the scale reticulum starts swelling, likely due to osmotic uptake of water energized by the V-ATPase. At the end of the diastolic phase, the SR is disconnected from the large round CV. Membrane structures representing collapsed CVs have not been reported in *S. dubia* (Melkonian and Preisig 1986; Perasso et al. 2000; Becker and Hickisch 2005).

Concanamycin A is a well known inhibitor of the V-ATPase. *Scherffelia dubia* cells treated with Concanamycin A swell and finally burst. However, if Concanamycin A-treated cells were additionally incubated with 100 mM sucrose, the cells survive. Therefore, the V-ATPase is necessary for osmoregulation and CV function, respectively. Examination of the CVs with neutral red indicates that the CVs are not acidic (no staining).

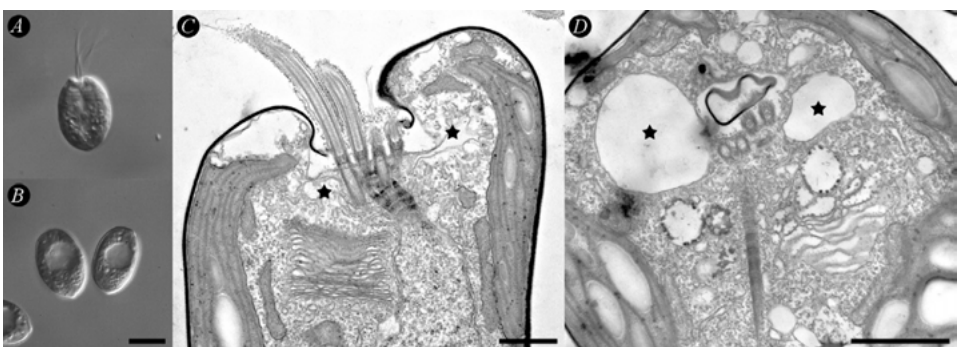

Figure 6.2 The contractile vacuoles in *Scherffelia dubia*.
(A and B) DIC-images of *Scherffelia dubia*. The CVs are located close to the basal bodies of the four flagella. The cell in B shows two swollen CVs (incubation with 1 µg Brefeldin A for 15 min). (C and D) Electron micrographs of cross sections of the region of CVs (marked with stars), horizontal and median, respectively. Unpublished own micrographs. Scale bar: 1 µm.

Furthermore, BFA affects the CVs in *S. dubia*. BFA-treated cells show two enlarged CVs, which fail to undergo systole (see Figure 6.2B). Hyperosmotic pressure decreases the volume of the swollen CVs, indicating that water uptake in the CVs is driven by osmosis. Exposure of the cells to both chemicals, Concanamycin A and BFA, for 5 or 10 minutes resulted in no large CVs. The cells lose their flagella, but the overall cell structure was not affected (Becker and Hickisch 2005).

Chlamydomonas

Cells of *Chlamydomonas reinhardtii* possess two CVs at the anterior end of the cell; close to the basal bodies of the two flagella (see Figure 6.3). The two CVs can contract and expand independently, but often they contract alternately. At the end of diastole, the CV rounds up. In the systole, the CV associates somehow with the plasma membrane, contracts, expels the content out of the cell and collapses into numerous smaller membrane compartments. At diastole, the vesicles start swelling and fuse with each other to form the large round vacuole again. This round vacuole continues to grow in diameter to form the single spherical CV at the end of diastole (Luykx et al. 1997a).

Luykx et al. (1997a) suggested a relation between the size of the CVs and the duration of CV cycles to the cell size and furthermore the expulsion rate (combined volume of both CVs at maximum diameter divided by the average CV cycle): the larger the cell, the greater the CV size, the CV cycle and respectively the expulsion rate. In additioin, Luykx et al. (1997a) observed a relationship between the osmotic strength of the media and the CV properties (size and cycle). When the medium is more hypotonic, the CVs become smaller and the contraction cycle decreases. Overall, this results in a higher efflux by the CVs. No CV activity was seen by Luykx et al. (1997a) at an osmotic strength of 120 mosM, indicating an iso-osmotic state. In addition, electron microscopy of cells

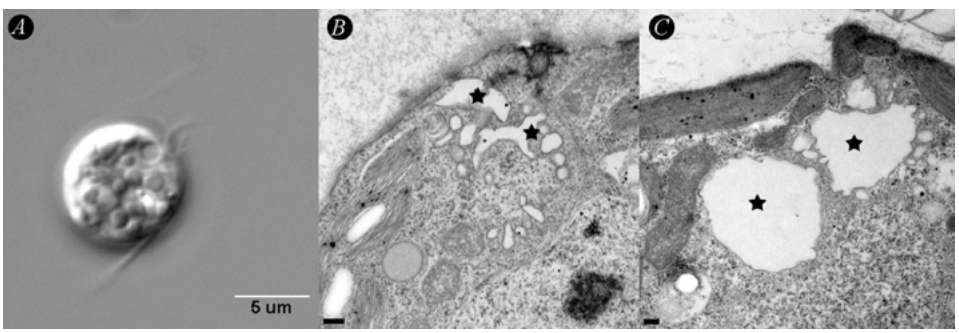

Figure 6.3 The contractile vacuoles in *Chlamydomonas reinhardtii*.
(A) DIC-image of a *Chlamydomonas*. In this light micrograph, one CV is visible close to the basal bodies of the two flagella. Scale bar: 10 µm.
(B and C) Electron micrographs of thin sections of the region of CVs (marked with stars) in *Chlamydomonas*. B and C show CVs in an early and later diastole phase, respectively. B and C Scale bar: 0.2 µm. Unpublished own micrographs.

under hyperosmotic conditions showed an aggregation of numerous small vesicles about 70–120 nm in diameter (Denning and Fulton 1989; Luykx et al. 1997a).

So far, no clear expulsion pore was observed in *C. reinhardtii* (Luykx et al. 1997a). Weiss et al. (1977) detected in a freeze-fracture study circular arrays of intramembrane particles in the two membranes, the CV and the overlaying plasma membrane. Furthermore, contact zones of approximately 200–400 nm were observed between the plasma and the CV membranes by Luykx et al. (1997a). This contact zone is marked by osmiophilic material in the narrow cytoplasmic space between the membranes. Only one observation made by Luykx et al. (1997b) showed a small pore between the two membranes, which seems unlikely to be an artifact.

Not much is known in *C. reinhardtii* regarding proteins involved in osmoregulation or CV function, respectively. Huber, Beyser and Fabry (1996) investigated the localization of Ypt/Rab proteins of the Ras superfamily in *C. reinhardtii*. One of the six proteins observed is located to the CVs, namely YptC1p. More specifically, the protein was associated with small vacuoles of the CV region, indicating that the protein is involved in the regulation of membrane fusion processes during early systole. Furthermore, a proton-pumping pyrophosphatase was localized to the CVs in *C. reinhardtii* (Robinson et al. 1997; Ruiz et al. 2001). But the localization is not restricted to the CVs; the protein was also found on the plasma membrane and other intracellular vacuoles (lytic vacuoles/acidocalcisomes). In addition, Ruiz et al. (2001) observed co-localization of the V-PPase with the V-ATPase at the CVs and the intracellular vacuoles. Moreover, they detected polyphosphate as a component of these two types of vacuoles using a DAPI staining technique. Two aquaporins are annotated in the *C. reinhardtii* genome. Aquaporins fascilitate passive transport of water and possibly some other polar molecules across membranes. Both putative aquaporins belong to the MIPD family which is divided into two groups. Probably, members of the one group transport glycerol and the other group glycerol and water cross membranes (Anderberg, Danielson and Johanson 2011). Unfortunately, the localization of these two proteins is still missing. Noteworthy, Denning and Fulton (1989) observed accumulation of large vacuoles around the nucleus in cells of *C. moewusii* after treatment with 2 mM EGTA, indicating a functional relation of CVs to calcium in green algae, too. Moreover, Meijer et al. (2001) observed a rapid generation of lyso-phosphatidic acid (LPA) when cells of *C. moewusii* were subjected to hyperosmotic stress. It is known, that LPA can act as an intracellular signaling molecule (Moolenar 2000). One function of LPA is the activation of phospholipase C and hence the mobilization of intracellular calcium. The cell reacts differentially to distinct hyperosmotic stresses, indicating several lipid-signaling pathways. However, *C. moewusii* has been shown to be only distantly related to *C. reinhardtii* (Pröschold et al. 2001).

Similarities, dissimilarities, general properties, evolutionary aspects

The CVs in *Mesostigma, Scherffelia* and *Chlamydomonas* are very similar in size and CV period (see Table 6.2 for an overview). The maximum diameter at the end of diastole is nearly the same and also the period is comparable. However, a major difference is in the number of CVs and therefore the efflux volume. *Scherffelia* and *Chlamydomonas* possess both two CVs, but *Mesostigma* has an average of eight CVs per cell and therefore a 3–4 times higher liquid efflux rates and assuming equilibrium water uptake rates. Interestingly,

Table 6.2 Comparison of the CVs in *Mesostigma, Scherffelia* and *Chlamydomonas*.

	Mesostigma	*Scherffelia*	*Chlamydomonas*
Diameter of vacuole at late diastole [µm]	1.5	1.4	1.4
Period [s]	24	22	15
Number of CVs/cell	ca. 8	2	2
Efflux [µm³/min]	51.3	11.7	15.3
Cytosolic osmolarity [mosM]	~85	~93	~125
Protonpumps	–	V-ATPase	V-ATPase V-PPase
Rab-Proteins	–	–	+
Clathrin-coated vesicles associated with CV	+	+	+
CV inhibited by BFA	+	+	–
Pore	contact zone	+ (n.d.)	+/contact zone
Osmotic strength of the medium [mosM]	10	5	0

n.d. not determined

Mesostigma shows the lowest cytosolic osmolarity compared to *Scherffelia* and *Chlamydomonas* (Table 6.2). But the differences are not very pronounced. Given the similar cell size, cytosolic osmolarity and the different efflux/influx volumes, it can be assumed that the membrane permeability of the plasma membrane is much higher in *Mesostigma* than in *Chlamydomonas* and *Scherffelia*. Therefore, it seems possible that *Scherffelia* and *Chlamydomonas* probably possess an aquaporin only in the CV membranes. In contrast, *Mesostigma* might possess an additional aquaporin in the plasma membrane, resulting in a higher influx of water into the cell and requiring more CVs for water homeostasis of the cell (compare Buchmann and Becker 2009). The presence of an aquaporin in a phospholipid bilayer increases the water permeability by one to two orders of magnitude (Baiges et al. 2002). In this way, *Scherffelia* and *Chlamydomonas*, would minimize water uptake in hypotonic environments and ensure the higher water permeability of the CV membrane (compared to the plasma membrane) required for efficient water transport into the CV.

The CVs of freshwater green flagellates investigated in detail are all characterized by the formation of clathrin-coated vesicles at the CVs. Furthermore, in the freshwater prasinophytes (*Scherffelia, Tetraselmis, Pyramimonas* and *Mesostigma*), CV function is inhibited by BFA (Becker and Hickisch 2005; Buchmann and Becker 2009), most likely due to BFA interference with the formation of clathrin-coated vesicles at the CV. The intracellular formation of clathrin-coated vesicles is a hallmark of the trans-Golgi network (TGN). Thus, it seems likely that the CV evolved from the TGN in green algae. Generally, it has been thought that chlorophytes evolved in a marine environment, whereas streptophytes evolved in a freshwater habitat (Falkowski et al. 2004; Simon et al. 2006).

However, the fact that the CVs in strepthophyte and chlorophyte algae evolved from the TGN is not easy to reconcile with this assumption.

Conclusion

Contractile vacuoles are found in every supergroup of eukaryotes. In every investigated system, the CV is involved in osmoregulation of the cell. Under hypo-osmotic conditions the CV complex is periodically collecting and expelling water out of the cell. Remarkably, given the current state of identification of proteins involved in CV function, every system seems to possess a similar set of proteins even in algae and in protozoa. Patterson (1980) described six structurally different types of CV complexes. This morphological complexity was always interpreted to indicate that CVs evolved independently in several organisms colonizing the freshwater environment as opposed to a marine source. Obviously, similar sets of proteins have been recruited by different protists.

References

Aaronson, S. and Behrens, U. 1974. Ultrastructure of an unusual contractile vacuole in several chrysomonad phytoflagellates. *J. Cell Sci. 14*: 1–9.

Allen, R.D. 2000. The contractile vacuoles and its membrane dynamic. *BioEssays 22*: 1035–1042.

Allen, R.D. and Naitoh, Y. 2002. Osmoregulation and Contractile Vacuoles of Protozoa. *Intl. Rev. Cytol. 215*: 351–394.

Anderberg, H.I., Danielson, J.Å.H., and Johanson, U. 2011. Algal MIPs, high diversity and conserved motifs. *BMC Evol. Biol. 11*: 110.

Anderca M.I., Suga, S., Furuichi, T., Shimogawara, K., Maeshima, M., and Muto, S. 2004. Functional identification of the glycerol transport activity of *Chlamydomonas reinhardtii* CrMIP1. *Plant Cell Physiol. 45*: 1313–1319.

Baiges, I., Schaffner, A.R., Affenzeller, M.J., and Mas, A. 2002. Plant aquaporins. *Physiol. Plant 115*: 175–182.

Becker, B. and Hickisch, A. 2005. Inhibition of contractile vacuole function by Brefeldin A. *Plant Cell Physiol. 46*: 201–212.

Becket, A., Heath, I.B., and McLaughlin, D.J. 1974. *An atlas of fungal ultrastructure*. Longman, London.

Benaim, G., Losada, S., Gadelha, F.R., and Docampo, R. 1991. A calmodulin-activated Ca^{2+}-Mg^{2+}-ATPase is involved in Ca^{2+} transport by plasma membrane vesicles from *Trypanosoma cruzi. Biochem. J. 280*: 715–720.

Benghezal, M., Gotthardt, D., Cornillon, S., and Cosson, P. 2001. Localization of the Rh50-like protein to the contractile vacuole in *Dictyostelium. Immunogenetics 52*: 284–288.

Betapudi, V., Mason, C., Licate, L., and Egelhoff, T.T. 2005. Identification and characterization of a novel alpha-kinase with a von Willebrand factor A-like motif localized to the contractile vacuole and Golgi complex in *Dictyostelium discoideum. Mol. Biol. Cell 16*: 2248–62.

Buchmann, K., and Becker, B. 2009. The system of contractile vacuoles in the green alga *Mesostigma viride* (Streptophyta). *Protist 160*: 427–443.

Clark, T.B. 1959. Comparative morphology of four genera of trypanosomatidae. *J. Protozool. 6*: 227–232.

Clarke, M., Köhler, J., Arana, Q., Liu, T., Heuser, J., and Gerisch, G. 2002. Dynamics of the vacuolar H^+-ATPase in the contractile vacuole complex and the endosomal pathway of *Dictyostelium* cells. *J. Cell Sci. 115*: 2893–2905.

Cornillon, S., Dubois, A., Bruckert, F., Lefkir, Y., Marchetti, A., Benghezal, M., De Lozanne, A., Letourneur, F., and Cosson, P. 2002. Two members of the beige/CHS (BEACH) family are involved at different stages in the organization of the endocytic pathway in *Dictyostelium. J. Cell Sci. 115*: 737–44.

De Souza, W. 2009. Structural organization of *Trypanosoma cruzi. Mem. Inst. Oswaldo Cruz 104, supl.I*: 89–100.

Deane, J.A., Strachan, I.M., Saunders, G.W., Hill, D.R.A., and McFadden, G.I. 2002. Cryptomonad evolution: Nuclear 18s rDNA Phylogeny versus Cell Morphology and Pigmentation. *J. Phycol. 38*: 1236–1244.

Degen, A. 1905. Untersuchungen über die kontraktile Vakuole und die Wabenstruktur des Protoplasmas. *Botanische Zeitung 63*: 163–202.

Denning, G.M., and Fulton, A.B. 1989. Electron microscopy of a contractile-vacuole mutant of *Chlamydomonas moewusii* (Chlorophyta) defective in the late stages of diastole. *J. Phycol. 25*: 667–672.

Docampo, R., de Souza, W., Miranda, K., Rohloff, P., and Moreno, S.N.J. 2005. Acidocalsisomes – conserved from bacteria to man. *Nat. Rev., Microbiol. 3*: 251–261.

Dodge, J.D. 1972. The ultrastructure of the dinoflagellate pusule: A unique osmo-regulatory organelle. *Protoplasma 75*: 285–302.

Du, F., Edwards, K., Shen, Z., Sun, B., De Lozanne, A., Briggs, S., and Firtel. R.A. 2008. Regulation of contractile vacuole formation and activity in *Dictyostelium. EMBO J. 6; 27, 15*: 2064–76.

Dunham, P.B. and Child, F.M. 1961. Ion regulation in *Tetrahymena. Biological Bulltein. Marin Biological Laboratory, Woods Hole, Mass. 121*: 129–140.

Dunham, P.B. and Kropp, D.L. 1973. Regulation of solutes in *Tetrahymena. In*: (Elliot, A.M.) *Biology of Tetrahymena*. Dowden, Hutchiinson and Ross, Pennsylvania. pp: 165–198.

Ettl, H. 1961. Über pulsierende Vakuolen bei Chlorophyceen. *Flora, Bd. 151, H. 1*: 88–98.

Falkowski, P.G, Katz, M.E., Knoll, A.H., Quigg, A., Raven, J.A., Schofield, O., and Taylor, F.J.R. 2004. The evolution of modern eukaryotic phytoplankton. *Science 305(5682)*: 354–360.

Fok, A.K., Aihara, M.S., Ishida, M., and Allen, R.D. 2008. Calmodulin Localization and its Effect on Endocytosis and Phagocyctic Membrane Trafficking in *Paramecium multimicronucleatum. J. Eukaryot. Microbiol. 55, 6*: 481–491.

Fok, A.K., Clarke, M., Ma, L., and Allen, R.D. 1993. Vacuolar H^+-ATPase of *Dictyostelium discoideum. J. Cell Sci. 106*: 1103–1113.

Gerald, N.J., Siano, M., De Lozanne, A. 2002. The *Dictyostelium* LvsA protein is localized on the contractile vacuole and is required for osmoregulation. *Traffic 3, 1*: 50–60.

Green, J.C. and Hibberd, D.J. 1977. The ultrastructure and taxonomy of *Diacronema vlkianum* (Prymnesiophyceae) with special reference to the haptonema and flagellar apparatus. *J. M. B. A. (United Kingdom) 57*: 1125–1136.

Grønlien, H.K., Stock, C., Aihara, M.S., Allen, R.D., and Naitoh, Y. 2002. Relationship between the membrane potential of the contractile vacuole complex and its osmoregulatory activity in *Paramecium multimicronucleatum. J. Exp. Biol. 205*: 3261–3270.

Gruber, H.E. 1979. Ultrastructure of the Golgi apparatus and contractile vacuole in *Chlamydomonas reinhardi. Cytologia 44*: 505–526.

Hartog, M.M. 1888. Preliminary note on the function and homologies of the contractile vacuole in plants and animals. *Report of the British Association for the Advancment of Science 58*: 714–716.

Hasne, M.P., Coppens, I., Soysa, R., and Ullman, B. 2010. A high-affinity putrescine – cadaverin transporter from *Trypanosoma cruzi. Mol Microbiol 76*: 78–91.

Hausmann, K. and Patterson, D.J. 1984. Contractile vacuole complexes in algae. *In:* (Wiesner, W., Robinson, D.G. und Starr, R.C.) *Compartments in Algal Cells and their Interaction*. Springer-Verlag, Berlin. pp. 140–145.

Heath, R.J., and Insall, R.H. 2008. *Dictyostelium* MEGAPs: F-BAR domain proteins that regulate motility and membrane tubulation in contractile vacuoles. *J. Cell Sci. 121(Pt 7)*:1054–64.

Herfs, A. 1922. Die pulsiernde Vakuole der Protozoen ein Schutzorgan gegen Aussüssung. *Arch. Protist. 44*: 227–260.

Heywood, P. 1978. Osmoregulation in the alga *Vacuolaria virescens*. Structure of the contractile vacuole and the nature of its association with the Golgi apparatus. *J. Cell Sci. 31*: 213–224.

Huber, H., Beyser, K., and Fabry, S. 1996. Small G proteins of two green algae are localized to exocytic compartments and to flagella. *Plant Mol. Biol. 31*: 279–293.

Hurlimann, H.C., Stadler-Waibel, M., Werner, T.P., and Freimoser, F.M. 2007. Pho91 is a vacuolar phosphate transporter that regulates phosphate and polyphosphate metabolism in *Saccharomyces cerevisiae. Mol. Biol. Cell 18*: 4438–4445.

Hyman, L.H. 1938. Observations on Protozoa. III. The vacuolar system of the Euglenida. *Beihefte zum Botanischen Zentralblatt 58*: 379–382.

Iwamoto, M., Allen, R.D., and Naitoh, Y. 2003. Hypo-osmotic or Ca^{2+}-rich external conditions trigger extra contractile vacuole complex generation in *Paramecium multimicronucleatum. J. Exp. Biol. 206*: 4467–4473.

Jackson, C.L., and Casanova, J.E. 2000. Turning on Arf: the Sec7-family of guanine-nucleotide exchange factors. *Trends Cell Biol. 10*: 60–67.

Jennings, H.S. 1904. A method of demonstrating the external discharge of the contractile vacuole. *Zool. Anz. 27*: 656–658.

Kissmehl, R., Schilde, C., Wassmer, T., Danzer, C., Nühse, K., and Plattner, H. 2007. Molecular identification of 26 syntaxin genes and their assignment to the different tracking pathways in *Paramecium. Traffic 8*: 523–542.

Kitching, J.A. 1956. Contractile Vacuoles of Protozoa. *Protoplasmatologia III*, D 3a: 1–45.

Kitching, J.A. 1938. Contractile vacuoles. *Biol. Rev. 13*: 403–444.

Kitching, J.A. 1952. Contractile vacuoles. *Symp. Soc. Exper. Biol. 6*: 145–165.

Kutateladze, T.G. 2007. Mechanistic similarities in docking of the FYVE and PX domains to Phosphatidylinositol 3-phosphate containing membranes. *Prog. Lipid Res. 46*: 315–327.

Ladenburger, E.-M., Korn, I., Kasielke, N., Wassmer, T., and Plattner, H. 2006. An Ins(1,4,5)P_3 receptor in *Paramecium* is associated with the osmoregulatory system. *J. Cell Sci. 119*: 3705–3717.

Leedale, G.F. 1967. *Euglenoid flagellates*. Prentice-Hall, New Jersey.

Lloyd, F.E. 1928a. The contractile vacuole. *Biol. Rev. Camb. phil. 3*: 329–358.

Lloyd, F.E. 1928b. Further observations on the behavior of gametes during maturation and conjugation in *Spirogyra. Protoplasma 3*: 45–66.

Lu, H.G., Zhong, L., de Souza, W., Benchimol, M., Moreno, S., and Docampo, R. 1998. Ca^{2+} content and expression of an acidocalcisomal calcium pump are elevated in intracellular forms of *Trypanosoma cruzi. Mol. Cell Biol. 18*: 2309–2323.

Lucas, I.A.N. 1970. Observations on the ultrastructure of representatives of the genera *Hemiselmis* and *Chroomonas* (Cryptophyceae). *Brit. Phycol. J. 5*: 29–37.

Luykx, P., Hoppenrath, M., and Robinson, D.G. 1997a. Structure and behavior of contractile vacuoles in *Chlamydomonas reinhardtii. Protoplasma 198*: 73–84.

Luykx, P., Hoppenrath, M., and Robinson, D.G. 1997b. Osmoregulatory mutants that affect the function of the contractile vacuoles in *Chlamydomonas reinhardtii. Protoplasma 200*: 99–111.

Malchow, D., Lusche, D.F., Schlatterer, C., De Lozanne, A., and Müller-Taubenberger, A. 2006. The contractile vacuole in Ca^{2+}-regulation in *Dictyostelium*: its essential function for cAMP-induced Ca^{2+}-influx. *BMC Dev. Biol. 6*: 31.

Marin B, Melkonian M (1999). "Mesostigmatophyceae, a new class of streptophyte green algae revealed by SSU rRNA sequence comparisons". *Protist 150*: 399–417.

McKanna, J.A. 1972. Contractile vacuoles in protozoans and sponges: comparative studies of fine structure and function in relation to the physical properties of membranes and water in biologic systems. *PhD thesis, University of Wisconsin*.

McKanna, J.A. 1973. Fine structure of the contractile vacuole pore in *Paramecium. J. Protozool. 20*: 631–638.

Meijer, H.J.G., Arisz, S.A., van Himbergen, J.A.J., Musgrave, A., and Munnik, T. 2001. Hyperosmotic stress rapidly generates lyso-phosphatidic acid in *Chlamydomonas. Plant J. 25*: 541–548.

Melkonian, M. and Preisig, H.R. 1986. A light and electron microscopy study of *Scherffelia dubia*, a new member of the scaly green flagellates (Prasinophyceae). *Nord. J. Bot. 6*: 235–256.

Mercanti, V., Blanc, C., Lefkir, Y., Cosson, P., and Letourneur, F. 2006. Acidic clusters target transmembrane proteins to the contractile vacuole in *Dictyostelium* cells. *J. Cell Sci. 119*: 837–45.

Meyer, H., and Porter, K.R. 1954. A study of *Trypanosoma cruzi* with the electron microscope. *Parasitology 44*: 16–23.

Mignot, J.P. 1974. Etude ultrastructurale d'un protiste flagellé incoloré: *Pseudodendromas Vlkii* Bourrelly. *Protistologica 10*: 397–412.

Montalvetti, A., Rohloff, P., and Docampo, R. 2004. A functional aquaporin colocalizes with the vacuolar proton pyrophosphatase to acidocalcisomes and the contractile vacuole complex of *Trypanosoma cruzi. J. Biol. Chem. 279*: 38673–38682.

Moolenar, W.H. 2000. Development of our current understanding of bioactive lysophospholipids. *Ann. NY Acad. Sci. 905*: 1–10.

Nebenführ, A., Ritzenthaler, C., and Robinson, D.G. 2002. Brefeldin A: deciphering an enigmatic inhibitor of secretion. *Plant Physiol. 130*: 1102–1108.

Nolta, K.V., and Steck, T.L. 1994. Isolation of the bipartite contractile vacuole complex from *Dictyostelium discoideum. J. Biol. Chem. 269, 3*: 2225–2233.

Novarino, G. 2003. A companion to the identification of cryptomonad flagellates (Cryptophyceae = Cryptomonadea). *Hydrobiologia 502*: 225–270.

Patterson,D.J. 1980. Contractile vacuoles and associated structures: their organization and function. *Biol. Rev. 55*: 1–46.

Perasso, L., Grunow, A. Brüntrup, I.M., Bölinger, B., Melkonian, M., and Becker, B. 2000. The Golgi apparatus of the scaly green flagellate *Scherffelia dubia*: uncoupling of glycoprotein and polysaccharide synthesis during flagellar regeneration. *Planta 210*: 551–62.

Plattner, H. 2010a. How to design a highly organized cell: An unexpectedly high number of widely diversified SNARE proteins positioned at strategic sites in the ciliate, *Paramecium tetraurelia. Protist 161, 4*: 497–516.

Plattner, H. 2010b. Membrane trafficking in Protozoa: SNARE Proteins, H^+-ATPase, actin and other key players in ciliates. *Int. Rev. Cell Mol. Biol. 280*: 79–184.

Pröschold, T., Marin, B., Schlösser, U.G., and Melkonian, M. 2001. Molecular phylogeny and taxonomic revision of *Chlamydomonas* (Chlorophyta). I. Emendation of *Chlamydomonas* Ehrenberg and *Chloromonas* Gobi, and description of *Oogamochlamys* gen. nov. and *Lobochlamys* gen. nov. *Protist 152*: 265–300.

Prusch, R.D. 1977. Protozoan osmotic and ionic regulation. *In*: (Gupta, B.L., Moreton, R.B., Oschman, J.L. and Wall, B.J.) *Transport of ions and water in animals*. Academic Press, London. pp: 363–377.

Quiviger, B., de Chastellier, C., and Ryter, A. 1978. Cytochemical demonstration of alkaline phosphatase in the contractile vacuole of *Dictyostelium discoideum. J. Ultrastruct. Res. 62, 3*: 228–36.

Robinson, D.G., Hoppenrath, M., Oberbeck, K., Luykx, P., and Ratajczak, R. 1997. Localization of pyrophosphatase and V-ATPase in *Chlamydomonas reinhardtii. Bot. Acta 111*: 108–122.

Rodriguez-Ezpeleta, N., Philippe, H., Brinkmann, H., Becker, B., and Melkonian, M. 2007. Phylogenetic analyses of nuclear, mitochondrial, and plastidic multigene data sets support the placement of *Mesostigma* in the Streptophyta. *Mol. Biol. Evol. 24*: 723–731.

Rohloff, P. and Docampo, R. 2008. A contractile vacuole complex is involved in osmoregulation in *Trypanosoma cruzi. Exp. Parasitol. 118*: 17–24.

Rohloff, P., Montalvetti, A., and Docampo, R. 2004. Acidocalsomes and the contractile vacuole complex are involved in osmoregulation in *Trypansomoa cruzi. J. Biol. Chem. 279*: 52270–52281.

Rossbach, M.J. 1872. Die rhythmischen Bewegungserscheinungen der einfachsten Organismen und ihr Verhalten gegen physikalische Agentien und Arzneimittel. *Arbeiten aus dem zoologisch – zootemischen Institut Würzburg 1*: 9–72.

Rudzinska, M.A. 1958. An electron microscopy study of the contractile vacuole in *Tokophyra infusiorum. J. Biophys. Biochem. Cytol. 4*: 195–201.

Ruiz, F., Rodriguez, C.O., and Docampo, R. 2001. Rapid changes in polyphosphate content within acidocalcisomes in response to cell growth, differentiation, and environmental stress in *Trypanosoma cruzi. J. Biol. Chem. 276, 28*: 26114–26121.

Ruiz, F.A., Marchesini, N., Seufferheld, M., Govindjee and Docampo, R. 2001. The polyphosphate bodies of *Chlamydomonas reinhardtii* possess a proton-pumping pyrophosphatase and are similar to acidocalcisomes. *J. Biol. Chem. 276, 49*: 46169–46203.

Sánchez, E., Vargas, M., Mora, M., Ortega, J.M., Serrano, A., Freer, E., and Sittenfeld, A. 2004. Descripción ultraestructural de *Euglena pailasensis* (Euglenozoa) del Volcán Rincón de la Vieja, Guanacaste, Costa Rica. *Rev. Biol. Trop. 52(1)*: 31–40.

Scales, S.J., Gomez, M., and Kreis, T.E. 2000. Coat proteins regulating membrane traffic. *Int. Rev. Cytol. 195*: 67–144.

Schilde, C., Lutter, K., and Kissmehl, R., and Plattner, H. 2008. Molecular identification of a SNAP-25-like protein in *Paramecium. Eucaryot. Cell 7*: 1397–1402.

Schilde, C., Schönemann, B., Sehring, I.M., and Plattner, H. 2010. Distinct subcellular localization of a group of synaptobrevin-like SNAREs in *Paramecium tetraurelia* and effects of silencing of the SNARE-specific chaperone NSF. *Eukaryot. Cell 9*: 288–305.

Schilde, C., Wassmer, T., Mansfeld, J., Plattner, H., and Kissmehl, R. 2006. A multigene family encoding R-SNAREs in ciliate *Paramecium tetraurelia. Traffic 7*: 440–455.

Schneider, L. 1960. Elektronenmikroskopische Untersuchungen über das Nephridialsystem von *Paramecium. J. Protozool. 7*: 75–90.

Schneider, N., Schwartz, J.M., Köhler, J., Becker, M., Schwarz, H., and Gerisch, G. 2000. Golvesin-GFP fusions as distinct markers for Golgi and post-Golgi vesicles in *Dictyostelium* cells. *Biol. Cell. 92, 7*: 495–511.

Schoijet, A.C., Miranda, K., Medeiros, L.C.S., de Souza, W., Flawiá, M.M., Torres, H.N., Pignataro, O.P., Docampo, R. and Alonso, G. D. 2011. Defining the role of a FYVE domain in the localization and activity of a cAMP phosphodiesterase implicated in osmoregulation in *Trypanosoma cruzi. Mol. Microbiol. 79*: 50–62.

Shin, W., and Boo, S.M. 2001. Ultrastructure of *Phacus trypanon* (Euglenophyceae) with an emphasis on striated fiber and microtubule arrangement. *J. Phycol. 37*: 95–105.

Simon, A., Glöckner, G., Felder, M., Melkonian, M., and Becker, B. 2006. EST analysis of the scaly green flagellate *Mesostigma viride* (Streptophyta): Implications for the evolution of green plants (Viridiplantae). *BMC Plant Biol. 6*: 2.

Sineshchekov, O.A., Sudnitsin, V.V., Govorunova, E.G., and Litvin, F.F. 2001. Rhythmic activity in the green flagellated alga *Haematococcus pluvialis* and its role in regulation of cell motility. *Biol. Membr. 18*: 83–91.

Somesh, B.P., Neffgen, C., Iijima, M., Devreotes, P. and Rivero, F. 2006. *Dictyostelium* RacH regulates endocytic vesicular trafficking and is required for localization of vacuolin. *Traffic, 7*: 1194–1212.

Spallanzani, L. 1776. *Opuscoli di fisica animale e vegetabile*. Presso la societa tipografica, Modena. pp. 64–75.

Stavrou, I., and O'Halloran, T.J. 2006. The monomeric clathrin assembly protein, AP180, regulates contractile vacuole size in *Dictyostelium discoideum. Mol. Biol. Cell 17, 12*: 5381–9.

Stock, C., Allen, R.D., Naitho, Y. 2001. How external osmolarity affects the activity of the contractile vacuole complex, the cytosolic osmolarity and the water permeability of the plasma membrane in *Paramecium multimicronucleatum. J. Exp. Biol. 204*: 291–304.

Stock, C., Grønlien, H.K., Allen, R.D., and Naitoh, Y. 2002a. Osmoregulation in *Paramecium*: in situ ion gradients permit water to cascade through the cytosol to the contractile vacuole. *J. Cell Sci. 115*: 2339–2348.

Stock, C., Grønlien, H.K., and Allen, R.D. 2002b. The ionic composition of the contractile vacuole fluid of *Paramecium* mirrors ion transport across the plasma membrane. *Eur. J. Cell Biol. 91*: 505–515.

Stoner, L.C. and Dunham, P.B. 1970. Regulation of cellular osmolarity and volume in *Tetrahymena. J. Exp. Biol. 53*: 391–399.

Suda, S., Watanabe, M.M., and Inouye, I. 2004. Electron microscopy of sexual reproduction in *Nephroselmis olivacea* (Prasinophyceae, Chlorophyta). *Phycol. Res. 52*: 273–283.

Taft, M.H., Hartmann, F.K., Rump, A., Keller, H., Chizhov, I., Manstein, D.J., and Tsiavaliaris, G. 2008. *Dictyostelium* myosin-5b is a conditional processive motor. *J. Biol. Chem. 283, 40*: 26902–10.

Tellez-Inon, M.T., Ulloa, R.M., Torruella, M., and Torres, H.N. 1985. Calmodulin and Ca^{2+}-dependent cyclic AMP phosphodiesterase activity in *Trypanosoma cruzi. Mol. Biochem. Parasitol. 17*: 143–153.

Ulrich, P.N., Jimenez, V., Park, M., Martins, V.P., Atwood, J., Moles, K., Collins, D., Rohloff, P., Tarleton, R., Moreno, S.N.J., Orlando, R., and Docampo, R. 2011. Identification of contractile proteins in *Trypanozoma cruzi. PLOS ONE 6, 3*: e18013.

Van den Hoek, C., Mann, D.G., and Jahns, H.M. 1995. *Algae, an introduction to phycology*. University Press, Cambridge. pp: 380–382, 463–466, 469–471.

Wassmer, T., Froissard, M., Plattner, H., Kissmehl, R., and Cohen, J. 2005. The vacuolar proton-ATPase plays a major role in several membrane-bounded organelles in *Paramecium. J. Cell Sci. 118*: 2813–2825.

Wassmer, T., Kissmehl, R., Cohen, J., and Plattner, H. 2006. Seventeen a-subunit isoforms of *Paramecium* V-ATPase provide high specialization in localization and function. *Mol. Biol. Cell 17*: 917–930.

Wassmer, T., Sehring, I.M., Kissmehl, R., and Plattner, H. 2009. The V-ATPase in *Paramecium*: functional specialization by multiple gene isoforms. *Eur. J. Phys. 457*: 599–607.

Weatherby, J.H. 1941. The contractile vacuole. *In:* (G.N. Calkins and F.M. Summers, eds) *Protozoa in biological research*. Columbia University Press. pp: 404–447.

Weiss, R.D., Goodenough, D.A., and Goodenough, U.W. 1977. Membrane particle arrays associated with the basal body and with contractile vacuole secretion in *Chlamydomonas. J. Cell Biol. 72*: 133–143.

Wen, Y., Stavrou, I., Bersuker, K., Brady, R.J., De Lozanne, A., and O'Halloran, T.J. 2009. AP180-mediated trafficking of Vamp7B limits homotypic fusion of *Dictyostelium* contractile vacuoles. *Mol. Biol. Cell. 20*: 4278–88.

Zanchi, R., Howard, G., Bretscher, M.S., and Kay, R.R. 2010. The exocytic gene secA is required for *Dictyostelium* cell motility and osmoregulation. *J. Cell Sci. 123*: 3226–3234.

Zhu, Q., and Clarke, M. 1992. Association of calmodulin and an unconventional myosin with the contractile vacuole complex of *Dictyostelium discoideum. J. Cell Biol. 118, 2*: 347–58.

7 Cytokinesis of brown algae

Christos Katsaros, Chikako Nagasato, Makoto Terauchi and Taizo Motomura

Introduction

Brown algae (Phaeophyceae) are complex photosynthetic organisms which have attracted the interest of phycologists for a number of reasons, ranging from their economic importance as a biological resource to their phylogenetic position within the eukaryotes. Particular points of interest, for example, include the independent evolution of complex multicellularity within this lineage, the secondary endosymbiosis event that produced chloroplasts and the production of unique biomolecules. Actually brown algae are one of only a small number of eukaryotic lineages that have evolved complex multicellularity. They have a very different evolutionary history compared to green plants, to which they are only distantly related. Recently, the 214 Mbp genome sequence of the filamentous seaweed *Ectocarpus siliculosus* (Dillwyn) Lyngbye, a model organism for brown algae, closely related to the kelps has been reported (Cock et al. 2010). The evolution of multicellularity in this lineage is correlated with the presence of a rich array of signal transduction genes. Of particular interest is the presence of a family of receptor kinases, as the independent evolution of related molecules has been linked with the emergence of multicellularity in both the animal and green plant lineages.

Apart from the recent data raised from molecular approaches, which emphasized the importance of brown algae, a number of particular structural features of this group have attracted the interest of biologists very early. Among these is the study of mitosis and cytokinesis. It is also interesting that neither unicellular nor simple, unbranched, uniseriate filamentous types occur among brown algae, the simplest morphological type being a branched uniseriate filament like *Ectocarpus*. Considering the great variety of forms of brown algae, from the simple filaments of *Ectocarpus* to the complex giant kelps like *Macrocystis* and *Alaria*, the importance of cell division is highly appreciated.

The study of cell division in brown algae has started very early by light microscopy (Swingle 1897; Strasburger 1897; Farmer and Williams 1898; Mottier 1900; Escoyez 1908; Yamanouchi 1909; Zimmermann 1923; Higgins 1931). As expected, the application of electron microscopy provided new insights in the study of these processes. Therefore, the first ultrastructural studies describing mitosis and cytokinesis in brown algal cells appeared during 70's and 80's. The pioneer ultrastructural studies during this time described two different patterns of cytokinesis in brown algal cells. In *Pylaiella littoralis* (Markey and Wilce 1975), *Fucus vesiculosus* (Brawley et al. 1977), *Cutleria cylindrica* (La Claire 1981), *Dictyota dichotoma* (Galatis et al. 1973) and *Sphacelaria tribuloides* (Katsaros et al. 1983), it was reported that cytokinesis progresses by furrowing of the plasma membrane, to which Golgi vesicles may fuse. On the other hand, Rawlence (1973) in a fine structural examination of *Ascophyllum nodosum*, reported that cytokinesis is accomplished by outgrowth of a partition membrane. The above controversy

showed that there were still open questions regarding the mechanism of cytokinesis in brown algae. As a result, a number of papers appeared later dealing with cell division in different brown algal species.

Brown algae have also particular cell features that make them quite interesting models for the study of cytoskeleton organization and the cell division process. The main peculiarities are the absence of cortical microtubules (MTs), preprophase MT band, phragmoplast and phycoplast, and the presence of centrosomes and a cortical AF cytoskeleton (reviewed by Katsaros et al. 2006). Moreover, an actomyosin contractile ring similar to that occurring in animals and yeasts has never been observed in brown algae. Therefore, a significant contribution to the study of brown algal cytokinesis was the application of immunofluorescence techniques, by which the organization of the fine cytoskeletal elements like MTs and actin filaments (AFs) was examined. In this way, combined immunofluorescence and transmission electron microscopy (TEM) studies have added new information contributing to elucidation of the brown algal cytokinetic mechanism (reviewed by Katsaros et al. 2006). However, there still exists a major question concerning the cytokinetic mechanism in brown algae, viz. how are the vesicles delivered to the equatorial plane, since there are no phragmoplast or phycoplast MTs? Although there is minor variability in the cytokinetic process of particular cell types in brown algae, e.g., zygotes or vegetative cells (Nagasato and Motomura 2002a; Bisgrove and Kropf 2004; Nagasato 2005; Varvarigos et al. 2005; Nagasato et al. 2010), a rough scheme was drawn up, which may be applied to all brown algae (Katsaros et al. 2006, 2009). Standard points of this schedule, with which all recent papers agree, are: (1) implication of MTs and AFs in cytokinesis, (2) absence of a phycoplast or a phragmoplast, (3) absence of a clear furrowing mechanism, and (4) assembly of the cytokinetic diaphragm by fusion of flat cisternae and Golgi-derived vesicles.

Cytoskeleton of brown algae and its role in cytokinesis and cell wall morphogenesis

Both cytoskeletal elements, i.e., MTs and AFs participate in mitosis and cytokinesis in higher plants and various algae (Chaffey and Barlow 2002; Bisgrove and Kropf 2004; Rogers 2005; Katsaros et al. 2006). In animals and yeasts, a contractile actomyosin ring pulls the plasma membrane inwards forming the furrow, thus cytokinesis initiates at the periphery of the cell (Simanis 2003; Piekny et al. 2005). In somatic cells of higher plants, a specific cytoskeletal array, the phragmoplast, consisting of two systems of overlapping MTs and AFs oriented transversely to the cytokinetic plane, delivers Golgi-derived vesicles to the plane of division forming the cell plate that expands centrifugally and finally fuses with the parent walls (Wick 1991; Assaad 2001; Smith 2001; Verma 2001).

Cytoskeleton of brown algal cells is drastically different from that of land plants, and it is mainly characterized by the continuous existence of a centrosome (MTOC: microtubule organizing center, Pickett-Heaps 1969) through the whole cell cycle.

The absence of cortical MTs, MT preprophase band and phragmoplast, as well as the presence of centrosomes in brown algal cells make them a quite interesting model for the study of MT organization during the cell cycle. The centrosome is composed of a pair of centrioles and pericentriolar materials (Brinkley 1985; Palazzo and Davis 2001). It is noteworthy that gamma-tubulin, which has a role in microtubule nucleation (Oakley and Oakley 1989; Stearns et al. 1991; Zheng et al. 1995), and centrin are always located

on centrosomes in brown algae (Katsaros and Galatis 1992; Karyophyllis et al. 2005). In brown algae, centrosomes always function as MTOCs during the whole cell cycle (Figure 7.1). No other microtubules occur in brown algal cells except those radiating out of the centrosomes. Only in one case microtubules have been determined in cortical sites in brown algal cells (Corellou et al. 2005). However, it should be noted that the

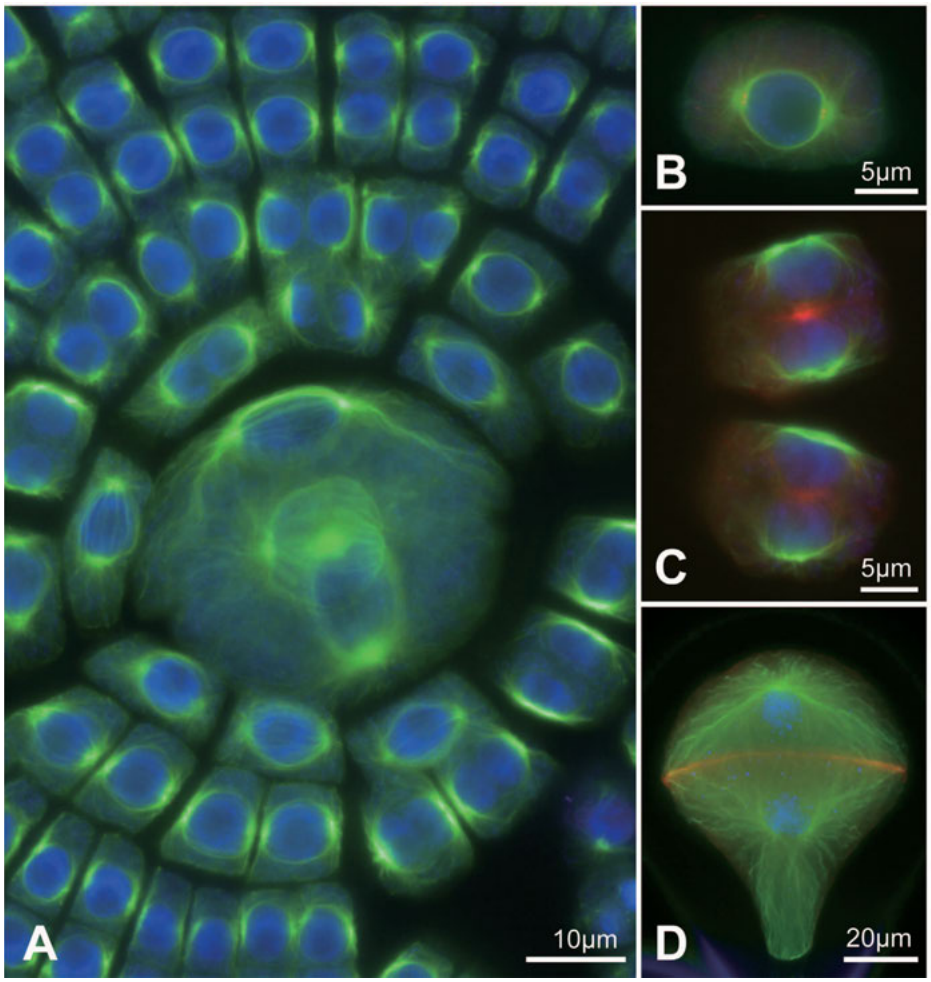

Figure 7.1 Immunofluorescence microscope images using anti-tubulin, anti-actin, and anti-γ-tubulin antibodies. Nuclei were stained with DAPI. A–C *Dictyota dichotoma*; D *Silvetia babingtonii*.
(A) Apical region of *D. dichotoma*. MTs (green) and nuclei (blue) in a large apical cell, sub-apical cells and cortical cells can be observed. It is noteworthy that almost all of MTs are radiating from two centrosomes in each cell.
(B) MTs radiate from two centrosomes. Two γ-tubulin dots can be detected in each one.
(C) MTs (green) and AFs (red) during early cyotokinesis. MTs radiate from centrosomes of two nuclei (blue) in telophase, and AFs begin to accumulate beween them.
(D) MTs (green) and AFs (red) during cyotokinesis of *S. babingtonii*. Actin plate (orange) can be detected at the cytokinetic plane, where MTs from both centrosomes intermingle.

re-organization of MT arrays during the development of *Fucus* zygotes and embryos found in this study, was followed *in vivo* after microinjection of fluorescent tubulin.

The role of microtubules in cytokinesis has been repeatedly underlined. In higher plants, cytokinetic mechanism involves phragmoplast, an assembly of MTs which control the formation of the cell plate. Cell plate consists of Golgi-derived vesicles and develops centrifugally, thus separating the daughter cells (Samuels et al. 1995). In brown algae interdigitating microtubules from the centrosomes associate with each nucleus to define the cytokinetic plane, where the actin disc is formed (Katsaros and Galatis 1992; Nagasato and Motomura 2002a, b; Bisgrove et al. 2003). Treatment with anti-MT agents inhibits cytokinesis, meaning that MTs are involved in this process (Katsaros et al. 2006, 2009). Cytokinesis was also inhibited by taxol treatment. The perinuclear and centrosome-associated MTs found in mitotic cells were gradually replaced by a MT system similar to that of interphase cells. In cells treated with taxol, in which the cytokinetic diaphragm had started, MTs were found on the cytokinetic plane, a phenomenon not observed in normal untreated cells (Dimitriadis et al. 2001).

Apart from MTs, AFs have been observed in brown algae using fluorescence microscopy following labelling with rhodamine-phalloidin or detection of actin molecules bound to special antibodies (Brawley and Robinson 1985; Kropf et al. 1989; Bouget et al. 1996; Alessa and Kropf 1999; Karyophyllis et al. 2000a; Hable et al. 2003; Bisgrove and Kropf 2004). Karyophyllis et al. (2000a) reported that the distribution of AFs changes during the cell cycle. At interphase, AFs are distributed at the surface of the cytoplasm forming a well organized cortical AF system, analogous to the cortical MT system occurring in higher plant cells. Combined studies using fluorescence microscopy, TEM and actin drugs, revealed that this cortical AF system is involved in cell wall morphogenesis by orienting cellulose microfibrils (Karyophyllis et al. 2000b). AFs colocalize with spindle MTs from metaphase to early telophase (Karyophyllis et al. 2000a; Nagasato and Motomura 2009). Just before cytokinesis, an actin plate is formed at the cytokinetic plane (Figure 7.1). This structure never constricts like the actin contractile ring in animal cells, and it remains present during the formation of the new cell partition. In zygotes of *Silvetia compressa*, the actin plate appears at the centre of the cell and then expands out toward the plasma membrane (Bisgrove and Kropf 2004). In *Fucus distichus*, this expansion was coincident with the outgrowth of the new cell partition membrane (Belanger and Quatrano 2000).

Recent advances on the study of the cytokinesis of brown algae

As already mentioned, in brown algae, two different patterns of cytokinesis have been reported from 1970s, using conventional chemical fixation (glutaraldehyde and osmium teroxide) and TEM; the first is that cytokinesis progresses by centripetal furrowing of the plasma membrane (Markey and Wilce 1975; Brawley et al. 1977; La Claire 1981; Katsaros et al. 1983) and the second one is that cytokinesis is accomplished by centrifugal outgrowth of a partition membrane (Rawlence 1973). Therefore, furrowing of the plasma membrane was a prominent feature in cytokinesis of brown algae at that time. However, chemical fixation is not adequate method for observations of cytokinesis, because rapid dynamic changes of fragile membranous structures can not be fixed by this method. Since 2000s, TEM observation using cryo-fixation and freeze substitution showed the

new images of cytokinesis of several brown algae, *Scytosiphon lomentaria* (Nagasato and Motomura 2002a), *Dictyota dichotoma, Halopteris congesta*, and *Sphacelaria rigidula* (Katsaros et al. 2009), and *Silvetia babingtonii* (Nagasato et al. 2010). From these studies, it was found that among these species, cytokinesis preferentially proceeded by furrowing of plasma membrane in vegetative cells of *S. rigidula*, while in vegetative cells of other species like *D. dichotoma* the diaphragm develops without a definite centrifugal or centripetal pattern (Katsaros et al. 2009). On the contrary, in zygotes of brown algae, *S. lomentaria* and *Silvetia babingtonii*, cytokinesis is mainly conducted by the outgrowth of the cell partition membrane (Nagasato and Motomura 2002a; Nagasato et al. 2010). The latter conclusion is also supported from observations on fucoid zygotes using FM4–64 (N-(3-triethylammoniumpropyl)-4-(6-(4-(diethylamino) phenyl) hexatrienyl) pyridinium dibromide), which is used to examine membrane trafficking of endocytosis and exocytosis (Belanger and Quatrano 2000; Bisgrove and Kropf 2004).

Cytokinesis in land plants progresses by centrifugal growth of a cell plate that is controlled by the phragmoplast (Schopfer and Hepler 1991) and the cell plate is formed by the fusion of Golgi-derived vesicles accumulated at the midpoint of the phragmoplast (Hepler 1982; Samuels et al. 1995). Therefore, cytokinetic processes in brown algae and land plants resemble in the outgrowth of the new cell partition membrane, the involvement of Golgi vesicles, and the transportation of Golgi vesicles by MTs (phragmoplast MTs in land plants *vs* MTs from both centrosomes in brown algae).

On the other hand, cytokinesis of brown algae has several characteristic features, not occurring in higher plants. First, as the initial sign, AFs accumulate at the cytokinetic plane and they make the actin plate (Karyophyllis et al. 2000a; Habble et al. 2003; Bisgrove and Kropf 2004). The actin plate initially appears at the center of the cell between the daughter nuclei and gradually expands towards the plasma membrane (Karyophyllis et al. 2000a; Bisgrove and Kropf 2004). As a different case, the organization of AFs and their role in cytokinesis was also studied in highly vacuolated cells of regenerating protoplasts and thallus of gametophytes of the brown alga *Macrocystis pyrifera* (Varvarigos et al. 2005). Before the onset of cytokinesis, a ring of AFs appeared on the putative cytokinetic plane just under the plasma membrane. Light and electron microscopy of cytokinetic cells revealed that large vacuoles occupy the space between the daughter nuclei, which very often are eccentrically positioned at the cell cortex. By the progress of cytokinesis, AF bundles emanating from the cytokinetic ring tend to form an actin plate that enters cytoplasmic pockets in which the cytokinetic diaphragm develops. The actin plate in cytokinesis of brown algae never constricts like the actin contractile ring in cytokinesis of animal cells. Dynamic changes of the actin plate, i.e. its first appearance at the central position of the cytokinetic plane and its following centripetal expansion, seem to be coincident with the outgrowth of the new cell partition membrane as mentioned above (Belanger and Quatrano 2000; Bisgrove and Kropf 2004; Nagasato and Motomura 2002a; Katsaros et al. 2009; Nagasato et al. 2010). Therefore, the actin plate must have a crucial role for centrifugal expansion of the partition membrane (Figure 7.1). Actually, pharmalogical studies using Latrunculin B and Cytochalasin B, and D, which disrupt actin filaments, showed that these reagents apparently inhibited cytokinesis (Allen and Kropf 1992; Karyophyllis et al. 2000a; Hable et al. 2003). In the cases of *D. dichotoma* and *S. rigidula*, as well as in particular

vacuolated cells like those of *M. pyrifera* protoplasts (Varvarigos et al. 2005), where the mode of development of the cytokinetic diaphragm is not centrifugal, the actin plate probably stabilizes the patches of the developing diaphragm. An alternative explanation is that the cytokinetic mechanism is not the same in all cell types of brown algae, depending on the particular cell features of each type.

Second unique feature in cytokinesis of brown algae is the involvement of flat cisternae and Golgi vesicles in the formation of the membranous diaphragm (Nagasato and Motomura 2002a; Katsaros et al. 2009; Nagasato et al. 2010). Flat cisternae can be detected only by rapid freezing fixation and freeze-substitution methods, not by chemical fixation (Figure 7.2). In vegetative cells of brown algae, they can be frequently observed just beneath the plasma membrane. During cytokinesis, Golgi vesicles and flat cisternae gather at the future cytokinetic plane, fuse to each other, and several membranous sacs are formed. Finally, these membranous sacs are connected together with additional fusion of Golgi vesicles and flat cisternae, and become a continuous new cell partition membrane (Figures 7.2, 7.3).

Recently, Nagasato et al. (2010) observed the process of cytokinesis of *Silvetia babingtonii.* The detailed stages of this process are: (1) fusion of Golgi vesicles to flat cisternae transform flat cisternae into expanded flat cisternae, and fucoidan is supplied to expanded flat cisternae from Golgi vesicles, (2) fusion of several expanded flat cisternae and supply of Golgi vesicles produce a membranous network, (3) the membranous network grows into membranous sacs without gaps by membrane recylcing via clathrin-coated pits, and membranous sacs line along the cytokinetic plane, (4) finally, membranous sacs become a continuous new cell partition membrane, and cell wall material deposits within it. These processes would be basically adapted to almost all cases of cytokinesis of brown algae (Figure 7.3). On the other hand, cytokinesis of land plants has been summarized as following (Samuels et al. 1995): (1) gathering of Golgi-derived vesicles at the equatorial plane by the phragmoplast, (2) elongation of thin tubes from each Golgi vesicle and fusion to each other to produce a continuous, interwoven, tubulo-vesicular network, (3) development of the tubulo-vesicular network into an interwoven smooth tubular network, then into a fenestrated plate-like structure, (4) formation of finger-like projections at the margins of the cell plate that fuse with the parent cell membrane, and (5) cell plate maturation that includes closing of the plate fenestrae. Therefore, common and characteristic aspects can be detected in cytokinesis of brown algae and land plants although these groups are phylogenetically different multicellular organisms. Future molecular approaches on crucial and characteristic proteins which participate to the brown algal cytokinesis will possess more drastic impact on the evolution of multicellular photosynthetic organisms.

Flat cisternae are unique membranous structures in brown algae. They were first found in *Scytosiphon lomentaria* zygotes using rapid-freezing fixation and freeze-substitution (Nagasato and Motomura 2002a). Afterwards, it has become clear that flat cisternae are ubiquitous in brown algal cells. Flat cisternae are characterized by the flat shape and the membrane thickness (650 nm in diameter and 20 nm in height on average in *Silvetia* zygotes) and density which are quite similar to the plasma membrane. In brown algal vegetative cells, flat cisternae can be frequently observed just beneath the plasma membrane and they participate to the membranous sac formation with Golgi vesicles during cytokinesis (Nagasato and Motomura 2002a, 2009; Nagasato et al. 2010).

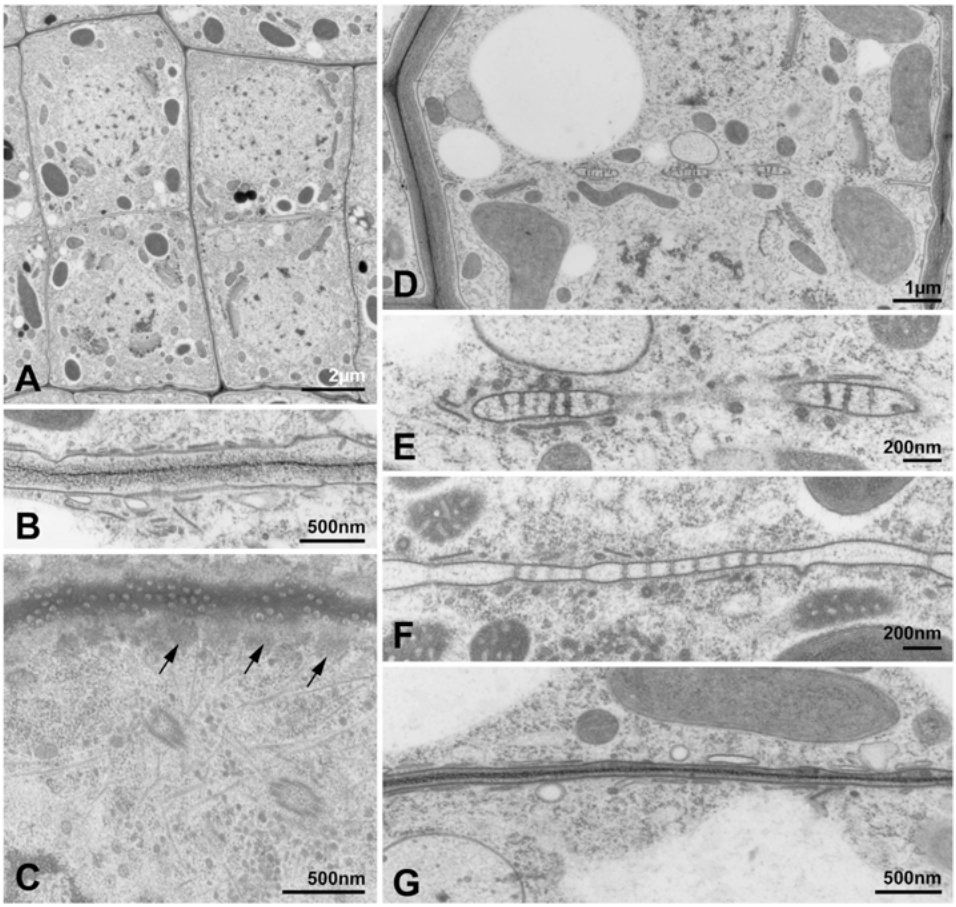

Figure 7.2 TEM images of cytokinesis of *Dictyota dichotoma* cortical cells using rapid freezing and freeze-substitution technique.
(A) Cortical cells, which have just finished cytokinesis.
(B) Flat cisternae are arranged just beneath the plasma membrane of vegetative cells.
(C) A pair of centrioles. Numerous MTs radiate nearby them. Plasmodesmata can be observed in the cell wall, and flat cisterae which are transversely cut are also detected beneath the cell wall (arrows).
(D) Initial stage of cytokinesis. Several membraneous sacs are located between daughter nuclei.
(E) Enlargement of D. It is noteworthy that pre-plasmodesmata appear in membraneous sacs.
(F) The membraneous sacs fuse and become continuous.
(G) After cytokinesis, cell wall material was deposited in the septum.

In *Silvetia babingtonii* zygotes, it was observed that flat citernae appeared at the mid region between daughter nuclei of telophase, where rough ER conspicuously developed (Nagasato et al. 2010). Therefore, at present, it is suggested that flat citernae originate from ER, not from Golgi body. Moreover, one of the functions of flat cisternae might be related to the cell wall formation of brown algae together with the secretion of the cell wall material through Golgi vesicles.

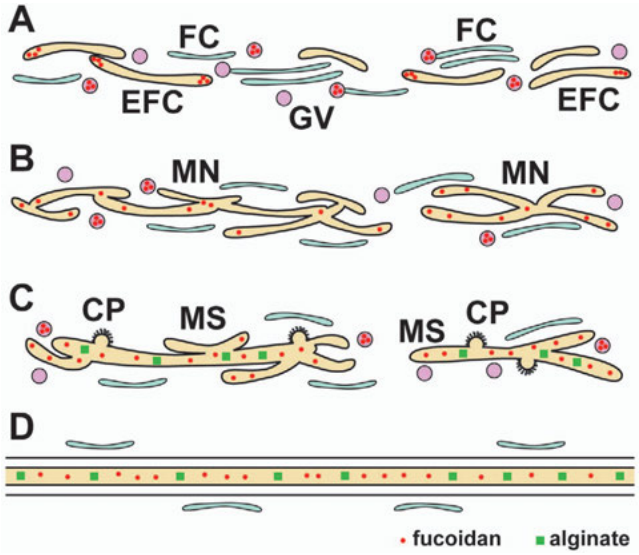

Figure 7.3 Schematic diagram of transitional membrane configuration during cytokinesis in brown algae.
(A) Fusion of GVs (Golgi vesicles) to FCs (flat cisternae) transforms FCs into EFCs (expanded flat cisternae). GVs put fucoidan into FCs.
(B) Fusion of EFCs and supply of GVs produces MN (membranous network).
(C) MN grows into MS (membranous sac) with disappearance of gaps in the MN. MSs appear in patches. CP (Clathrin-coated pits) are detected on the MS. Alginate starts accumulating.
(D) MSs become a continuous new cell partition membrane. Fibrous cell wall material deposits within it.

As mentioned above, pharmacological reagents that disrupt AFs, such as Latrunculin B and Cytochalasin B or D have been used to investigate the function of AFs in the progression of cytokinesis (Allen and Kropf 1992; Karyophyllis et al. 2000a; Hable et al. 2003). In the presence of these reagents, mitosis occurs, but not cytokinesis, indicating that AFs have an important function during the latter process. Moreover, the inhibition of Golgi-mediated secretion by Brefeldin A also prevents the progression of cytokinesis in zygotes of the brown alga *Fucus distichus* (Shaw and Quatrano 1996; Belanger and Quatrano 2000). Treatment with brefeldin A prevented rhizoid growth and cytokinesis but did not affect the progression of mitosis. Staining of Brefeldin-A treated zygotes with FM4–64 indicated that a new cell partition membrane was not formed with this treatment (Belanger and Quatrano 2000). However, these experiments have not revealed how the actin plate works for the formation of the new cell partition membrane and how the AFs function for the production and transportation of Golgi vesicles and flat cisternae in the cells at the ultrastructural level. Nagasato and Motomura (2009) observed in detail the effects of Latrunculin B and Brefeldin A to cytokinesis of *S. lomentaria* zygotes using electron microscopy. Latrunculin B inhibited the formation of flat cisternae,

only Golgi vesicles gathered at the cytokinetic plane, and fused with the plasma membrane there. However, a continuous partition membrane was not produced in cytokinesis. When Golgi vesicle secretion was prevented by Brefeldin A, flat cisternae appeared at the future cytokinetic plane, and a new cell partition membrane which was continuous to the plasma membrane was formed. However, normal cell wall deposition could not be observed. Inhibition of flat cisternae caused by treatment with Latrunculin A was also observed in *Silvetia babingtonii* zygotes (Nagasato et al. 2010). These results suggested that actin is involved in the formation of flat cisternae from ER, where it is necessary for completion of the new cell partition membrane, and actin plate at the cytokinetic plane will be necessary for fixing Golgi vesicles and flat cisternae and the following membraneous sacs (Katsaros et al. 2006, see also Figure 7.3).

Determination of the cytokinetic plane during cell division: The role of centrosome

In many organisms, position of cytokinesis is determined before actual cytokinesis starts (Barr and Gruneberg 2007; Bohnert and Gould 2011; Oliferenko et al. 2009). The position of the spindle primarily determines the final cytokinesis plane in animal cells (Rappaport 1986), which is mediated by the astral MTs and AFs at the cell cortex (Glotzer 2005). In fungi, division planes are determined before mitosis, e.g., by the position of the prophase nucleus in fission yeast and the previous bud site in budding yeast. Different from the case of animal cells, plant cells are embedded in a matrix of cell wall material and do not migrate. In land plants, mitotic spindle does not determine the future cytokinetic plane (Gunning and Wick 1985), instead, the future cell division planes are determined by a cortical array of MTs and AFs actin filaments, called preprophase band (Mineyuki 1999). Brown algal cells also do not divide by hit or miss fashion; they have a strict rule for determination of the future cytokinetic plane. A hint of it is from observations on mitosis and cytokinesis during zygote development of *Sargassum* (Tahara and Shimotomai 1926; Nagasato et al. 2001). In fertilization of *Sargassum*, sperm nucleus fuses to one of eight nuclei in egg which are positioned at the periphery of egg cytoplasm. The mitotic spindle is formed in a zygotic nucleus there, and afterwards, both the daughter nuclei migrate longitudinally to opposite sides of the egg, and cytokinesis occurs. From these observations on *Sargassum* zygote development, we can easily imagine that the cytokinetic plane is not determined by the position of mitotic spindle. To examine in more detail when and how the future cytokinetic plane is determined in brown algae, the cytokinesis of polyspermic zygotes of the isogamous brown alga *Scytosiphon lomentaria*, was studied (Nagasato and Motomura 2002b). When two male gametes fertilized one female gamete, three pairs of centrioles, from two male gametes and one female, existed in the zygote. Afterwards, the pair of centrioles derived from the female gamete selectively disappeared (Nagasato and Motomura 2004; Motomura et al. 2010) and two pairs of centrioles from the two male gametes remained in the polyspermic zygote. In the polyspermic zygotes, three kinds of mitotic spindle were formed at the center of the germlings; (1) the first case was that two bipolar spindles were formed, (2) the second was that a tripolar spindle was formed and two centrosomes existed together at one mitotic pole, and (3) the third was that a

tripolar spindle was formed and one centrosome was located far from the mitotic spindle. Cytokinesis in each case was observed as following: In the first case, four daughter cells were produced and each one contained a nucleus and a centrosome. In the second, three daughter cells were produced and each one contained a nucleus and a centrosome, and one of these daughter cells had two centrosomes which were adjacently located. In the third, four daughter cells were produced. Although one of the four cells did not have a nucleus, a centrosome was present in all four daughter cells. From these results, it becomes clear that the future cytokinetic plane of brown algae is determined by the centrosomal position after mitosis, and not the mitotic spindle orientation. In other words, MTs from centrosomes on both telophase nuclei determine the position of the cytokinetic plane on which MTs from both centrosomes interdigitate (Nagasato and Motomura 2002b; Bisgrove et al. 2003). It is speculated that a centrifugally expanding array of inter digitating MTs from both centrosomes defines a plane in which the cytokinetic machinery, including actin, assembles (Bisgrove et al. 2003; Bisgrove and Kropf 2004).

In vegetative cells of brown algae the organization of MTs during mitosis and cytokinesis has been studied by both immunofluorescence and TEM (La Claire 1982; Katsaros et al. 1983; Motomura and Sakai 1985; Katsaros and Galatis 1992). It was found that the developing partition membrane "bisects" the MT cage formed after telophase in pre-cytokinetic cells. This membrane is probably laid down when the overlapping MT systems and the respective nuclei have moved apart (Katsaros and Galatis 1992). The displacement of nuclei and large organelles forms a narrow cytoplasmic strand, not always continuous, in which an actin plate is probably organized (Karyophyllis et al. 2000a, b; Bisgrove et al. 2003; Bisgrove and Kropf 2004). It is possible that this actin plate is involved in the stabilization of the developing diaphragm (Katsaros et al. 2006, 2009). From the above it may be also suggested that the cytokinetic plane is determined by the centrosomal position, since the daughter centrosomes after telophase are positioned at the poles of the daughter nuclei (Figures 7.1, 7.4). However, the question "which is the factor determining the position of centrosomes" still remains.

Deposition of cell wall materials during cytokinesis

Cell wall materials of brown algae are unique compared to those occurring in land plants. Mabeau and Kloareg (1987) reported that cell walls accounted for one third to half of the thallus dry weight of *Fucus* and *Laminaria,* and about 80% of the isolated cell walls were water-soluble mucilages, namely alginates (50–65%) and sulfated fucan (9–18%). Therefore, cellulose content is quite low (below 20%) (see also Quatrano 1982).

Just after completion of cytokinesis, cell wall materials are deposited in the membranous sacs and the initial septum (Figure 7.3). Using anti-fucoidan and anti-alginate antibodies, and cellulase-gold probe, it was found that fucoidan was secreted by Golgi vesicles and firstly deposited in membranous sacs in the first cell division of *Silvetia* zygotes (Nagasato et al. 2010). Following it, alginate deposition started, while cellulose deposition occurred much later (Figure 7.3). Contrary to the detection of fucoidan in *trans*-face Golgi body, *trans* Golgi network and Golgi vesicles, alginate could not be detected in them, meaning that alginate synthesis occurs on membranes of the

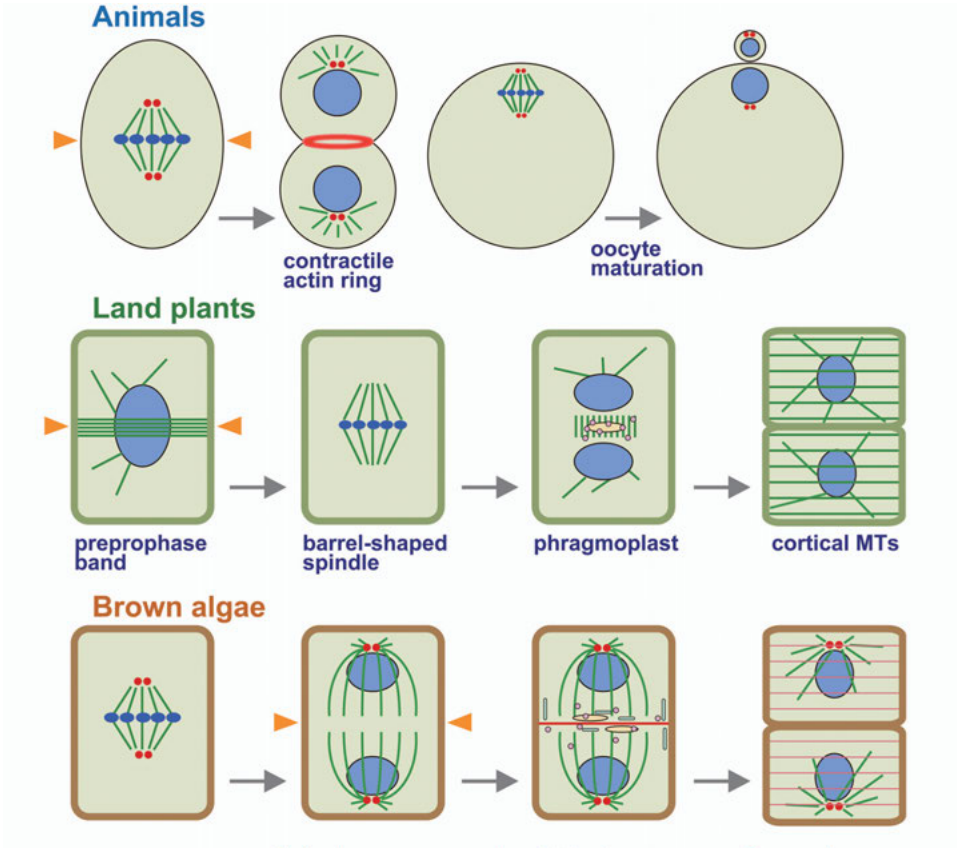

	Animals	Land plants	Brown algae
Centrioles	+	- Cortical microtubules	+ Cortical actin filaments
Determination of cytokinetic plane	Mitotic spindle	Preprophase band	Position of centrosomes after mitosis
Cell partition membrane	Centrifugally outgrowing	Centrifugally outgrowing	Patches and centrifugally outgrowing
Machinery of cytokinesis	Actin contractile ring	Phragmoplast (microtubules and actin filaments)	Actin plate
Membrane resource	Golgi vesicles	Golgi vesicles	Golgi vesicles and flat cisternae

Figure 7.4 Schematic summary of cytokinesis in animals, land plants and brown algae, showing the arrangement of MTs (green lines), AFs (red lines), centrosomes (red dots), nuclei and chromosomes (blue).

membranous sacs (namely future plasma membrane) and the plasma membrane of the initial septum. Recently, the whole genome information of a brown alga *Ectocarpus siliculosus* has been clarified (Cock et al. 2010), and Michel et al. (2010) deciphered the biosynthetic pathways of cellulose, alginate and sulphated fucans. They reported that enzymes on each step of alginate biosynthesis pathway from fructose 6-phosphase to mannuronan could be detected in genome of *E. siliculosus*, which are well known in

bacteria, *Pseudomonas* and *Azotobacter* (Rehm and Valla 1997; Ramsey and Wozniak 2005). The final step enzyme, mannuronate polymerase, which is estimated from the *Ectocarpus* genome information, does not have signal peptide, and instead of it, this enzyme has four transmembrane domains (Terauchi et al. unpublished data). Therefore, it might be speculated that alginate synthesis is conducted on plasma membrane. This hypothesis could be combined with the observation of special particle complexes, named "pentads", on the plasma membrane of a number of brown algae, *Ectocarpus siliculosus, Hincksia mitchelliae, Tilopteris mertensii, Sphacelaria rigidula, S. radicans* and *S. nana* by freeze fracture (Katsaros et al. 1996). It was reported that these particles were possibly enzyme complexes involved in synthesis of cell wall amorphous materials. Michel et al. (2010) also suggested candidate genes on biosynthetic pathway of sulfated fucans. The last enzymes, carbohydrate sulfotransferases, had signal peptides to ER (Terauchi et al. unpublished data), therefore, this supports the results that fucoidan can be firstly detected in Golgi vesicles during cytokinesis (Nagasato et al. 2010). Evans et al. (1973) and Callow et al. (1978) showed that sulfated polysaccharide synthesis occurred in Golgi bodies (and Golgi-rich perinuclear region) of *Fucus, Pelvetia*, and *Laminaria* by experiments using histochemistry and autoradiography.

Again, sulfated fucan is firstly detected in nascent septum during cytokinesis in brown algae. In the case of land plants, callose is firstly deposited into septum (Samuels et al. 1995; Thiele et al. 2009). Therefore, similar to the case of callose deposition in land plant cytokinesis, deposition of sulfated fucan in membranous sacs and nascent septum during the early stage of cytokinesis of brown algal cells guarantees the mechanical stabilization of nascent septum formation. Callose synthase in land plants has transmembrane regions and callose cannot be detected in Golgi bodies and Golgi vesicles (Samuels et al. 1995; Thiele et al. 2009). This means that pathway of initial polysaccharides into nascent septum in brown algae is different in the case of land plants. Concerning the existence of callose in brown algae, it was reported that callose exists at pores in the sieve plates of *Nereocystis lutkeana* (Schmitz and Srivastava 1976). However, immunoelectron microscopy using anti-β-1,3-linked glucan antibody showed no detection of these polysaccharides in the cell wall of *Scytosiphon lomentaria*; they can be detected in vacuoles and electron-lightly staining granules (lipid bodies), probably as laminaran (Nagasato and Motomura 2002c).

Plasmodesmata formation

Cell-to-cell communication plays a crucial function for regular development and morphogenesis in multicellular organisms. This communication system varies among organisms, for example, gap junctions are consisted of connexin proteins in animal cells (Makowski et al. 1984; Kumar and Gilula 1996), plugs in fungi (Trinci and Collinge 1973), pit plugs in red algae (Pueschel and Cole 1982; Scott et al. 1988; Pueschel 1989; Ueki et al. 2008), and plasmodesmata in green plants including land plants and some green algae (Robards and Lucas 1990; Ding et al. 1992a, b; Franceschi et al. 1994; Volk et al. 1996; Cook et al. 1997; Burch-Smith et al. 2011). By this communication system, metabolic products, proteins, RNA and viruses are transferred to neighboring cells (Kim 2005, Hyun et al. 2011; Niehl and Heinlein 2011) in land plants. Brown algae have

also plasmodesmata (Bisalputra 1966; Schmitz and Srivastava 1974, 1975; Marchant 1976; La Claire 1981; Schmitz and Kuhn 1982; Katsaros and Galatis 1988; see also Cook and Graham 1999). Contrary to plasmodesmata of land plants, in which ER is trapped (desmotubules), their structure in brown algae is quite simple, namely there is no ER penetration in them (La Claire 1981; Katsaros and Galatis 1988), although existence of desmotubules was reported in laminarialean plants (Schmitz and Srivastava 1975; Marchant 1976). Recent studies on cytokinesis of brown algae using rapid freezing and freeze substitution technique have provided new insights on plasmodesmata (Katsaros et al. 2009; Terauchi et al. 2012). In *Dictyota dichotoma* vegetative cells, plasmodesmata formation started from the early stage of cytokinesis (Figure 7.2). At first, tubular pre-plasmodesmata protruded in membranous sacs from the membrane, and these nascent plasmodesmata were locally gathered at places where a pit field will be formed. ER (desmotubules) did not exist in plasmodesmata.

Pit fields have been observed in *Laminaria hyperborea* and *L. saccharina* sporophytes (Schmitz and Kuhn 1982), especially in the cell wall of sieve tubes, however they could not be detected in *L. angustata* gametophytes (Motomura and Sakai 1984). Also, pit fields have not been reported in uniseriate brown algae, *Sphacelaria, Halopteris* and *Cutleria* (Katsaros et al. 1986, 2009; La Claire 1981). Existence of pit field, a characteristic conformation of a lot of plasmodesmata, may depend on thallus morphogenesis. In complicated parenchymatous thallus, pit fields frequently occur and function to transport actively and rapidly photosynthetic products and other signaling factors for cell-to-cell communications, while in simple pseudoparenchymatous filamentous thallus, this active transportation between neighboring cells is not necessary.

In land plants it has been reported that primary and secondary plasmodesmata occur (Maule 2008). In the case of cytokinesis of *Dictyota*, plasmodesmata formarion can be detected as pre-plasmodesmata in membranous sacs during cytokinesis, namely the primary plasmodesmata (Figures 7.2, 7.3). However, plasmodesmata formation was hardly detected in the first cell division of *Scytosiphon* and *Silvetia* zygotes (Nagasato and Motomura 2002a; Nagasato et al. 2010). Plasmodesmata, of course, exist in cross cell walls of mature thalli in these brown algae; therefore in this case, it is possible that they are secondarily produced during thallus development.

Despite the above, there are still unclear points in the mechanism of plasmodesmata formation in brown algae. For example, their relationship to the cell wall formation, involvement of cytoskeletons, and actual regulation of penetration of material through them. Additional studies will be necessary for a deeper understating from the view points of maintainance of cell-to-cell communication and elaborated morphogenesis of the brown algae.

References

Allen, V., and D. L. Kropf. 1992. Nuclear rotation and lineage specification in *Pelvetia* embryos. *Development 115*: 873–883.

Alessa, L., and D.L. Kropf. 1999. F-actin marks the rhizoid pole in living *Pelvetia* zygotes. *Development 126*: 201–209.

Assaad, F.F. 2001. Plant cytokinesis. Exploring the links. *Plant Physiol. 126*: 509–516.

Barr, F. A., and U. Gruneberg. 2007. Cytokinesis: placing and making the final cut. *Cell 131*: 847–860.

Belanger, K. D., and R.S. Quatrano. 2000. Membrane recycling occurs during asymmetric tip growth and cell plate formation in *Fucus distichus* zygotes. *Protoplasma 212*: 24–37.

Bisalputra T. 1966. Electron microscopic study of the protoplasmic continuity in certain brown algae. *Can. J. Bot. 44*: 89–93.

Bisgrove, S., and D.L. Kropf. 2004. Cytokinesis in brown algae: studies of asymmetric division in fucoid zygotes. *Protoplasma 223*: 163–173.

Bisgrove, S.R., D.C. Henderson, and D.L. Kropf. 2003. Asymmetric division in fucoid zygotes is positioned by telophase nuclei. *Plant Cell, 15*: 854–862.

Bohnert, K. A., and K.L. Gould. 2011. On the cutting edge: post-translational modifications in cytokinesis. *Trends Cell Biol. 21*: 283–292.

Bouget, F.-Y., S. Gerttula, S.L. Shaw, and R.S. Quatrano. 1996. Localization of actin mRNA during the establishment of cell polarity and early cell divisions in *Fucus* embryos. *Plant Cell 8*: 189–201.

Brawley, S. H., R.S. Quatrano, and R. Wetherbee. 1977. Fine structural stdies of the gametes and embryo of *Fucus vesiculosus* L. (Phaeophyta). III. Cytokinesis and the multicelular embryo. *J. Cell Sci. 24*: 275–294.

Brawley, S. H. and K.R. Robinson. 1985. Cytochalasin treatment disrupts the endogenous currents associated with cell polarization in fucoid zygotes: studies of the role of F-actin in embryogenesis. *J. Cell Biol. 100*: 1173–1184.

Brinkley, B. R. 1985. Microtubule organizing centers. *Annu. Rev. Cell Biol. 1*: 145–172.

Burch-Smith, T. M., S. Stonebloom, M. Xu, M, and P.C. Zambryski. 2011. Plasmodesmata during development: re-examination of the importance of primary, secondary, and branched plasmodesmata structure versus function. *Protoplasma 248*: 61–74.

Callow, M.E., S.J. Coughlan, and L.V. Evans. 1978. The role of Golgi bodies in polysaccharide sulphation in *Fucus* zygotes. *J. Cell. Sci. 32*: 337–356.

Chaffey, N. and P. Barlow. 2002. Myosin, microtubules, and microfilaments: cooperation between cytoskeletal components during cambial cell division and secondary vascular differentiation in trees. *Planta 214*: 526–536.

Cock, J.M. et al. 2010. The *Ectocarpus* genome and the independent evolution of multicellularity in brown algae. *Nature 465*: 617–621.

Cook, M.E. and L.E. Graham. 1999. Evolution of plasmodesmata. *In*: (A.J.E. Van Bel and W.J.P. Van Kesteren, eds) *Plasmodesmata: Structure, function, role in cell communication*. Springer, Berlin, Heidelberg. pp. 101–117.

Cook, M.E., L.E. Graham, C.E. Botha, and C.A. Lavin. 1997. Comparative ultrastructure of plasmodesmata of *Chara* and selected bryophytes: toward an elucidation of the evolutionary origin of plant plasmodesmata. *Amer. J. Bot. 84*: 1169–1178.

Corellou, F., S.M. Coelho, F.-Y. Bouget, and C. Brownlee. 2005. Spatial re-organization of cortical microtubules in vivo during polarization and asymmetric division of *Fucus* zygotes. *J. Cell Sci. 118*: 2723–2734.

Dimitriadis, I., C. Katsaros, and B. Galatis. 2001. The effect of taxol on centrosome function and microtubule organization in apical cells of *Sphacelaria rigidula* (Phaeophyceae). *Phycol. Res. 49*: 23–34.

Ding, B., J.S. Haudenshield, R.J. Hull, S. Wolf, R.N. Beachy, and W.J. Lucas. 1992a. Secondary plasmodesmata are specific sites of localization of the tobacco mosaic virus movement protein in transgenic tobacco plants. *Plant Cell 4*: 915–928.

Ding, B., R. Turgeon, and M.V. Parthasarathy. 1992b. Substructure of freeze-substituted plasmodesmata. *Protoplasma 169*: 28–41.

Escoyez E. 1908. Caryokinese, centrosome, et kinoplasme dans le *Stypocaulon scoparium. Cellule 25*: 181–203.

Evans, L.V., M. Simpson, and M.E. Callow. 1973. Sulphated polysaccharide synthesis in brown algae. *Planta 110*: 237–252.

Farmer, J.B., and J.L. Williams. 1898. Contribution to our knowledge of the Fucaceae: Their life history and cytology. *Phil. Trans. Roy. Soc. London* B *190*: 623–645.

Franceschi, V. R., B. Ding, and W.J. Lucas. 1994. Mechanism of plasmodesmata formation in characean algae in relation to evolution of intercellular communication in higher plants. *Planta 192*: 347–358.

Galatis B., C. Katsaros, and K. Mitrakos. 1973. Ultrastructure of the mitotic apparatus in *Dictyota dichotoma* (Lamour.). *Rap. Comm. Int. Mer Medit*. 22: 53–54.

Glotzer, M. 2005. The molecular requirement for cytokinesis. *Science 307*: 1735–1739.

Gunning, B. E. and S.M. Wick. 1985. Preprophase bands, phragmoplasts, and spatial control of cytokinesis. *J. Cell Sci. Suppl. 2*: 157–79.

Hable, W. E., N.R. Miller, and D.L. Kropf. 2003. Polarity establishment requires dynamic actin in fucoid zygotes. *Protoplasma 221*: 193–204.

Hepler, P.K. 1982. Endoplasmic reticulum in the formation of the cell plate and plasmodesmata. *Protoplasma 111*: 121–133.

Higgins M.E. 1931. A cytological investigation of *Stypocaulon scoparium* (L.) Kütz., with special reference to unilocular sporangia. *Ann. Bot. 45*: 345–353.

Hyun, T. K., M.N. Uddin, Y. Rim, and J.K. Jae-Yean Kim. 2011. Cell-to-cell trafficking of RNA and RNA silencing through plasmodesmata. *Protoplasma 248*: 101–116.

Karyophyllis, D., B. Galatis, and C. Katsaros. 2005. Gamma-tubulin localization during the cell cycle in *Sphacelaria rigidula* (Phaeophyceae, Sphacelariales). *J. Biol. Res. 4*: 151–156.

Karyophyllis, D., C. Katsaros, I. Dimitriadis, and B. Galatis. 2000a. F-Actin organization during the cell cycle of *Sphacelaria rigidula* (Phaeophyceae) *Eur. J. Phycol. 35*: 25–33.

Karyophyllis, D., C. Katsaros, and B. Galatis. 2000b. F-actin involvement in apical cell morphogenesis of *Sphacelaria rigidula* (Phaeophyceae): mutual alignment between cortical actin filaments and cellulose microfibrils. *Eur. J. Phycol. 35*: 195–203.

Katsaros, C., and B. Galatis. 1986. Ultrastructural studies on zoosporogenesis of *Halopteris filicina* (Sphacelariales, Phaeophyta). *Phycologia 25*: 358–370.

Katsaros. C, and B. Galatis. 1988. Thallus development in *Dictyopteris membranacea* (Phaeophyta, Dictyotales). *Br. Phycol. J. 23*: 71–88.

Katsaros, C., and B. Galatis. 1992. Immunofluorescence and electron microscope studies of microtubule organization during the cell cycle of *Dictyota dichotoma* (Phaeophyta, Dictyotales). *Protoplasma 169*: 75–84.

Katsaros, C., B. Galatis, and K. Mitrakos. 1983. Fine structural studies on the interphase and dividing apical cells of *Sphacelaria tribuloides* (Phaophyta). *J. Phycol. 19*: 16–30.

Katsaros, C., H.-D. Reiss, and E. Schnepf. 1996. Freeze-fracture studies in brown algae: putative cellulose synthesizing complexes on the plasma membrane. *Eur. J. Phycol. 31*: 41–48.

Katsaros, C., D. Karyophyllis, and B. Galatis. 2006. Cytoskeleton and morphogenesis in brown algae. *Ann. Bot. 97*: 679–693.

Katsaros, C., T. Motomura, C. Nagasato, and B. Galatis. 2009. Diaphragm development in cytokinetic vegetative cells of brown algae. *Bot. Mar. 52*: 150–161.

Kim, J. Y. 2005. Regulation of short-distance transport of RNA and protein. *Curr. Opin. Plant Biol*. 8: 45–52.

Kropf, D.L., S.K. Berge, and R.S. Quatrano. 1989. Actin localization during *Fucus* embyogenesis. *The Plant Cell 1*: 191–200.

Kumar, N.M., and N.B. Gilula. 1996. The gap junction communication channel. *Cell 84*: 381–388.

La Claire, J. W. II. 1981. Occurrence of plasmodesmata during infurrowing in a brown alga. *Biol. Cell 40*: 139–142.

La Claire, J. W. II. 1982. Light and electron microscopic studies on growth and reproduction in *Cutteria* (Phaeophyta). III. Nuclear division in the tricbothalic meristem of *C. cytindrica. Phycologia 21*: 273–287.

Mabeau, S. and B. Kloareg. 1987. Isolation and analysis of the cell walls of brown algae: *Fucus spiralis, F. Ceranoides, F. vesiculosus, F. serratus, Bifurcaria bifurcata* and *Laminaria digitata. J. Exp. Bot. 38*: 1573–1580.

Makowski, L., D.L. Caspar, W.C. Phillips, T.S. Baker, and D.A. Goodenough. 1984. Gap junction structures. VI. Variation and conservation in connexon conformation and packing. *Biophysical J. 45*: 208–218.

Marchant, H.J. 1976. Plasmodesmata in algae and fungi. *In*: (B.E.S. Gunning and A.W. Robards, eds) *Intercellular communication in plants: Studies on plasmodesmata*. Springer-Verlag, Heidelberg, New York. pp. 59–80.

Markey, D.R. and R.T. Wilce. 1975. The ultrastructure of reproduction in the brown alga *Pylaiella littoralis* I: mitosis and cytokinesis in the plurilocular gametangia. *Protoplasma 85*: 219–241.

Maule, A. J. 2008. Plasmodesmata: structure, function and biogenesis. *Curr. Opin. Plant Biol. 11*: 680–686.

Michel. G., T. Tonon, D. Scornet, J.M. Cock, and B. Kloareg, B. 2010. The cell wall polysaccharide metabolism of the brown alga *Ectocarpus siliculosus*. Insights into the evolution of extracellular matrix polysaccharides in Eukaryotes. *New Phytol. 188*: 82–97.

Mineyuki, Y. 1999. The preprophase band of microtubules: its function as a cytokinetic apparatus in higher plants. *Int. Rev. Cytol. 187*: 1–49.

Mottier D.M. 1900. Nuclear and cell division in *Dictyota dichotoma. Ann. Bot. 14*: 163–192.

Motomura, T. and Y. Sakai. 1984. Ultrastructural studies of gametogenesis in *Laminaria angustata* (Laminariales, Phaeophyta) regulated by iron concentration in the medium. *Phycologia 23*: 331–343.

Motomura, T. and Y. Sakai. 1985. Ultrastructural studies on nuclear division in *Carpomitra cabrerae* (Curemente) Kützing (Phaeophyta, Sporochnales). *Jpn. J. Phycol. 33*: 21–31.

Motomura, T., C. Nagasato, and K. Kimura. 2010. Cytoplasmic inheritance of organelles in brown algae. *J. Plant Res. 123*: 185–192.

Nagasato, C. 2005. Behavior and function of paternally inherited centrioles in brown algal zygotes. *J. Plant Res. 118*: 361–369.

Nagasato, C., T. Motomura, and T. Ichimura. 2001. Degeneration and extrusion of nuclei during oogenesis in *Silvetia babingtonii, Cystoseira hakodatenis* and *Sargassum confusum* (Fucales, Phaeophyceae). *Phycologia 40*: 411–420.

Nagasato, C. and T. Motomura. 2002a. Ultrastructural study on mitosis and cytokinesis in *Scytosiphon lomentaria* zygotes (Scytosiphonales, Phaeophyceae) by freeze-substitution *Protoplasma 219*: 140–149.

Nagasato, C. and T. Motomura. 2002b. Influence of the centrosome in cytokinesis of brown algae: polyspermic zygotes of *Scytosiphon lomentaria* (Scytosiphonales, Phaeophyceae). *J. Cell Sci. 115*: 2541–2548.

Nagasato, C. and T. Motomura. 2002c. New pyrenoid formation in the brown alga, Scytosiphon lomentaria (Scytosiphonales, Phaeophyceae). *J. Phycol 38*: 800–806.

Nagasato, C. and T. Motomura. 2004. Destruction of maternal centrioles during fertilization of the brown alga, *Scytosiphon lomentaria* (Scytosiphonales, Phaeophyceae). *Cell Motil. Cytoskel. 59*: 109–118.

Nagasato, C. and T. Motomura. 2009. Effect of latrunculin B and brefeldin A on cytokinesis in the brown alga Scytosiphon lomentaria (Scytosiphonales, Phaseophyceae). *J. Phycol. 45*: 404–412.

Nagasato, C., A. Inoue, M. Mizuno, K. Kanazawa, T. Ojima, K. Okuda, and T. Motomura. 2010. Membrane fusion process and assembly of cell wall during cytokinesis in the brown alga, *Silvetia babingtonii* (Fucales, Phaeophyceae). *Planta 232*: 287–298.

Niehl, A. and M. Heinlein. 2011. Cellular pathways for viral transport through plasmodesmata. *Protoplasma 248*: 75–99.

Oakley, C.E., and B.R. Oakley. 1989. Identification of γ-tubulin, a new member of the tubulin superfamily encoded by mipA gene of *Aspergilus nidulans*. *Nature 338*: 662–664.

Oliferenko, S., T.G. Chew, and M.K. Balasubramanian. 2009. Positioning cytokinesis. *Genes Dev. 23*: 660–74.

Palazzo, R.E., and T. Davis 2001. *Centrosomes and spindle pole bodies.* Academic Press, London.

Pickett-Heaps, J. D. 1969. The evolution of the mitotic apparatus: an attempt at comparative ultrastructural cytology in dividing plant cells. *Cytobios 3*: 257–280.

Piekny, A., M. Werner and M. Glotzer. 2005. Cytokinesis: welcome to the Rho zone. *Trends Cell Biol. 15*: 651–658.

Pueschel, C. M. 1989. An expanded survey of the ultrastructure of red algal pit plugs. *J. Phycol. 25*: 625–636.

Pueschel, C. M. and K.M. Cole. 1982. Rhodophycean pit plugs: an ultrastructural survey with taxonomic implications. *Am. J. Bot. 69*: 703–20.

Quatrano, R.S. 1982. Cell-wall formation in *Fucus* zygotes: A model system to study the assembly and localization of wall polymers. *In*: (R.M. Brown Jr., ed) *Cellulose and other natural polymer systems. Biogenesis, structure and degradation*. Plenum Press, New York, London. pp. 45–59.

Ramsey, D. M., and D.J. Wozniak. 2005. Understanding the control of *Pseudomonas aeruginosa* alginate synthesis and the prospects for management of chronic infections in cystic fibrosis. *Mol. Microbiol. 56*: 309–322.

Rappaport, R. 1986. Establishment of the mechanism of cytokinesis in animal cells. *Int. Rev. Cytol. 105*: 245–81.

Rawlence, D. J. 1973. Some aspects of the ultrastructure of Ascophyllum nodosum (L.) Le Jolis (Phaeophyceae, Fucales) including obserbation on cell plate formation. *Phycologia 12*: 17–28.

Rehm, B. H. A., and S. Valla. 1997. Bacterial alginates: biosynthesis and applications. *Appl. Microbiol. Biotech. 48*: 281–288.

Robards, A. W., and W.J. Lucas. 1990. Plasmodesmata. *Ann. Rev. Plant Physiol. Plant Mol. Biol. 41*: 369–419.

Rogers H.J. 2005. Cytoskeletal regulation of the plane of cell division: An essential component of plant development and reproduction. *Adv. Bot. Res. 42*: 69–111.

Samuels, A. L., T.H. Giddings Jr, and L.A. Staehelin. 1995. Cytokinesis in tobacco BY–2 and root tip cells: a new model of cell plate formation in higher plants. *J. Cell Biol. 130*: 1345–1357.

Schmitz, K., and L.M. Srivastava. 1974. Fine structure and development of sieve tubes in *Laminaria groenlandica* Rosenv. *Cytobiologie 10*: 66–87.

Schmitz, K. and L.M. Srivastava. 1975. On the fine structure of sieve tubes and the physiology of assimilate transport in *Alaria marginata. Can. J. Bot. 53*: 861–876.

Schmitz, K. and L.M. Srivastava. 1976. The fine structure of sieve elements of *Nereocystis lutkeana. Amer. J. Bot. 63*: 679–693.

Schmitz, K., and R. Kuhn. 1982. Fine structure, distribution and frequency of plasmodesmata and pits in the cortex of *Laminaria hyperborea* and *L. saccharina. Planta 154*: 385–392.

Schopfer, C.R., and P.K. Hepler. 1991. Distribution of membranes and the cytoskeleton during cell plate formation in pollen mother cells of *Tradescantia. J Cell Sci 100*: 717–728.

Scott, J., J. Thomas, and B. Saunders. 1988. Primary pit connections in *Compsopogon coeruleus* (Balbis) Montagne (Compsopogonales, Rhodophyta). *Phycologia 27*: 327–333.

Shaw, S. L. and R.S. Quatrano. 1996. The role of targeted secretion in the establishment of cell polarity and the orientation of the division plane in *Fucus* zygotes. *Development 122*: 2623–2630.

Simanis, V. 2003. Events at the end of mitosis in the budding and fission yeasts. *J. Cell Sci. 116*: 4263–4275.

Smith, L.G. 2001. Plant cell division: building walls in the right places. *Nat. Rev. Mol. Cell Biol. 2*: 33–39.

Stearns, T., L. Evans, and M. Kirschner. 1991. γ-tubulin is a highly conserved component of the centrosome. *Cell 65*: 825–836.

Strasburger E. 1897. Kernteilung und Befruchtung bei *Fucus. Jb. wiss. Bot. 30*, 351–374.

Swingle W.T. 1897. Zur Kenntnis der kern- und Zelltheilung bei den Sphacelariaceen. *Jb. wiss. Bot. 30*, 297–350.

Tahara, M., and N. Shimotomai. 1926. Mitosen bei *Sargassum. Sci. Rep. Tohoku Imper. Univ. 1*: 189–192.

Terauchi, M., Nagasato C., Kajimura, N., Mineyuki Y., Okuda K., Katsaros C., Motomura T. 2012. Ultrastructural study on plasmodesmata in the brown alga *Dictyota dichotoma* (Dictyotales, Phaeophyta). *Planta 236 (4)*: 1013–1026, DOI 10.1007/s00425-012-1656-4.

Thiele, K., G. Wanner, V. Kindzierski, G. Jürgens, U. Mayer, F. Pachl, and F. F. Assaad. 2009. The timely deposition of callose is essential for cytokinesis in *Arabidopsis. Plant J. 58*:13–26.

Trinci, A. P. J., and A.J. Collinge. 1973. Structure and plugging of septa of wild type and spreading colonial mutants of *Neurospora crassa. Arch. Mikrobiol. 91*: 355–364.

Ueki, C., C. Nagasato, T. Motomura, and N. Saga. 2008. Reexamination of the pit plugs and the characteristic membranous structures in *Porphyra yezoensis* (Bangiales, Rhodophyta). *Phycologia 47*: 5–11.

Varvarigos, V., B. Galatis and C. Katsaros. 2005. A unique pattern of F-actin organization supports cytokinesis in vacuolated cells of *Macrocystis pyrifera* (Phaeophyceae) gametophytes. *Protoplasma 226*: 241–245.

Verma, D.P.S. 2001. Cytokinesis and building of the cell plate in plants. *Ann. Rev. Plant Physiol. Plant Mol. Biol. 52*: 751–784.

Volk, G. M., R. Turgeon, and D.U. Beebe. 1996. Secondary plasmodesmata formation in the minor-veinphloem of *Cucumis melo* L. and *Cucurbita pepo* L. *Planta 199*: 425–432.

Wick, S.M. 1991. Spatial aspects of cytokinesis in plant cells. *Curr. Opin. Cell Biol. 3*: 253–260.

Yamanuchi S. 1909. Mitosis in *Fucus. Bot. Gaz. 47*: 173–197.

Zheng, Y., M.L. Wong, B.M. Alberts, and T. Mitchison. 1995. Nucleation of microtubule assembly by a γ-tubulin containing ring complex. *Nature, 378*: 578–583.

Zimmermann, W. 1923. Zytologische Untersuchungen an *Sphacelaria fusca*. Ein Beitrag zur entwicklungsphysiologie der Zelle. *Z. Bot. 15*: 113–175.

8 Development of antheridial filaments and spermatozoid release in *Chara contraria*

Qiaojun Jin and Karl H. Hasenstein

Introduction

The green alga *Chara* is thought to be the closest relative of land plants (Karol et al. 2001; Delwiche et al. 2002; Turmel et al. 2003). Despite many advanced features like oogamous sexual reproduction and phragmoplastic cell division (Graham 1993) this alga has retained several ancestral features not found in higher land plants, such as zygotic meiosis. One of the evolutionarily interesting aspects, shared with bryophytes and ferns, is the formation of motile spermatozoids, which are produced in the antheridium, the male reproductive organ. Formed by mitosis of a node cell, the antheridium is a bright orange, multi-cellular, spherical organ of about 0.5 mm in diameter. The outer layer is comprised of interlocked shield cells that contain a mass of antheridial filaments, which are attached to the central mother cells (Pickett-Heaps 1967). The antheridial filaments are derived by division of the second capitulum, and cells in the filaments are arranged as individual threads. Each cell in the filaments develops into a spermatozoid (Pickett-Heaps 1968). At maturity, the shield cells rupture and the spermatozoids are released from the antheridial filaments through liberation pores of unknown nature (Kwiatkowska and Poplonska 2002). The mature spermatozoids of *Chara* have two flagella that originate at the lateral anterior end, contain little cytoplasm, and coil for about 2½ turns within the cell wall. The anterior part contains approximately 30 linearly arranged mitochondria, followed by the dense, narrow, and cylindrical nucleus. The posterior part of the cell contains six starch-filled plastids linearly arranged with associated mitochondria (Duncan et al. 1997).

Although spermatogenesis and ultrastructure of spermatozoids are known, their release process has not been studied. The swimming pattern suggests that microtubules (MT) and microfilaments play a prominent role for spermatozoid development and motility but the function of these cytoskeletal elements in the activation (onset of motility) and release of spematozoids is unknown.

The functionality of the cytoskeleton is commonly studied by utilizing drugs that disrupt or stabilize the cytoskeleton such that the dynamic rearrangement of cytoskeletal elements is inhibited. The dinitroaniline herbicide Oryzalin binds to tubulin dimers and induces MT depolymerization (Hugdahl and Morejohn 1993; Morejohn et al. 1987) and has been used to study microtubule-dependent cellular processes (Bartels and Hilton 1973; Morejohn 1991). Latrunculin, a drug purified from the marine sponge *Latrunculia magnifica* (Keller), was shown to depolymerize F-actin *in vivo* and *in vitro* (Kashman et al. 1980; Spector et al. 1983). It binds to the actin monomer and alters the interface

to prevent polymerization (Walter et al. 2000). The oxime derivative 2,3-butanedione monoxime (BDM) is a myosin ATPase inhibitor in eukaryotic cells and uncompetitively inhibits myosin and myofibril ATPase activity by increasing the equilibrium constant of the cleavage step and delaying the release of inorganic phosphate (Herrmann et al. 1992). In maize root tips, BDM treatment altered the distribution pattern of plant myosin VIII and a putative homologue of myosin II. It caused the disappearance of endoplasmic MTs and cortical MTs assemblies with an increased amount at the plasmodesmata and pit fields (Samaj et al. 2000). Here we describe the effect of the drugs Oryzalin, Latrunculin B (LatB) and BDM on spermatozoid release process in *Chara contraria* A. Braun *ex* Kützing and discuss the relationship between the cytoskeleton and spermatozoid release.

Experimental set up and manipulations

Chara contraria (Characeae) was cultured in 20 L glass tanks containing soil from a local pond under a 3 cm layer of sand. The tanks were filled with tap water and kept at room temperature (22–25°C) under natural window illumination. Mature antheridia were taken from thalli, and placed into artificial pond water (Kiss, 1994) containing 0.01, 0.1, 1 or 5 µM LatB, 10 or 50 µM Oryzalin and 1, 10 or 20 mM BDM on glass slides. Then the antheridia were cut open and spermatozoid release was observed by video-microscopy using an Olympus DP71 digital camera (Olympus, Center Valley, PA, USA) mounted on a Nikon Eclipse E600FN microscope (Melville, NY, USA). Because the tested compounds were dissolved in methanol, all treatments were compared with otherwise untreated controls immersed in 0.05% (v/v) methanol in culture medium. Spermatozoid release was observed for about 30 minutes or until most spermatozoid had been released. All experiments were repeated at least three times.

Data evaluation

The videos were examined for the duration between cutting of the antheridia and beginning of spermatozoid release, movement of the spermatozoid inside the cell before release, time between spermatozoid release and onset of motility of individual spermatozoids, and average spermatozoid release rate. In addition, the size of released spermatozoids was measured from single frames using Image J (version 1.3, NIH, Bethesda, MD, USA). The size of the spermatozoid was defined as the ratio of the length of the expanded spermatozoid over the diameter of the spermatozoid coil (L/D). The spermatozoid release dynamics were expressed as percentage and described by a special case of the logistic function $F = 1/(1 + \exp[-(t - a)b])$, where a corresponds to the time t when 50% of the spermatozoids were released and b determines the slope of the linear release rate (see Figure 8.7). The average release was calculated from minimized sums of squares of the distribution of the released spermatozoid over time. Statistical analyses were performed with Proc GLM with Tukey-Kramer adjustments for multiple comparisons (SAS version 9.1, SAS Institute, Cary, NC, USA).

Cytoskeletal studies

Mature antheridia were cut into halves. One half of each antheridium was placed into 1 μM LatB or 50 μM Oryzalin for about 1 hour before fixing in 1.5% formaldehyde in PHEM buffer with 5% (v/v) DMSO (PHEMD) (Brown and Lemon 1995) for 2 hr at room temperature. The second half was used as control. MTs, F-actin, and nuclei were stained after digestion of the cell wall with [incubation in 1% (w/v) cellulase Y-O and 0.1% (w/v) pectolyase Y-23 (both Koamicho Corporation, Tokyo, Japan) containing 1% BSA for 30 min]. MTs were stained with monoclonal antibody YOL 1/34 (Accurate Chemical & Scientific Corp., Westbury, NY) followed by Alexa 488-conjugated secondary anti-rat antibody (Molecular Probes (Invitrogen), CA, USA).

F-actin was visualized by incubation in Alexa-phalloidin 488 for 5 h after cellulase and pectolyase treatment as above and additional washing with 5% glycerol in PHEMD buffer for 10 min and 0.1% Triton X-100 in PHEMD buffer for 30 min. The nuclei were stained with 0.005% (w/v) propidium iodide in phosphate buffered saline pH 7 for two minutes. Images were taken with a confocal laser scanning microscope (MRC-1024, BioRad, Hercules, CA) with Lasersharp 2000 software (v. 5.1). Individual experiments were repeated at least three times.

Liberation pore identification

The cell walls of mature antheridial filaments were stained with 0.02% (w/v) calcofluor white in artificial pond water for 10 min. Fluorescence images were taken using an Olympus DP71 digital camera (Olympus, Center Valley, PA, USA) mounted on a Nikon Eclipse E600FN microscope (Melville, NY, USA).

Results

The development of spermatozoids

The antheridia in various stages of development allow an examination of the progression of the cytoskeletal organization during the development of the antheridial filaments. The mitotic events lead to progressively denser packaging of nuclei (Figure 8.1), before the nuclei develop into coiled spermatozoids. The mature spermatozoids have two lateral anterior flagella, show little cytoplasm but a discrete distribution of nuclei and microtubules that remain straight during the release process of the filamentous cell (Figure 8.2) before changing their shape to the motile coiled form of free-swimming spermatozoids. The posterior part of the spermatozoid is characterized by thick microtubular material.

The process of spermatozoid release

After opening the antheridia, the coiled spermatozoids remained inside the antheridial filaments for about 12–20 min. The release process began with the movement of the flagella inside the cell for about 1–2 minutes before expulsion through the liberation pore.

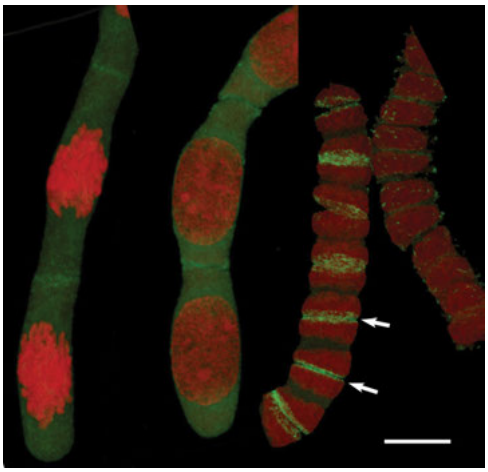

Figure 8.1 The development of antheridial filaments of *Chara contraria* is characterized by cell divisions that lead to increasingly smaller volumes of cytoplasm. While the diameter of the filaments does not change, the volume per cell decreases and the nuclear material (red) occupies a larger proportion (1). The symmetry of the cell divisions is illustrated by the alternating zones of bright microtubule staining (arrows). Filaments that have completed cell mitosis no longer contain cytoplasmic material. Bar = 10 μm.

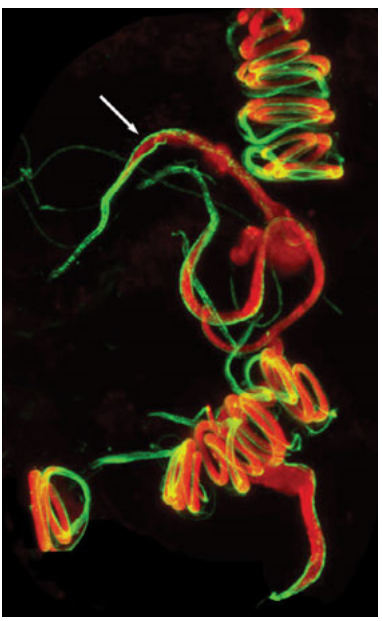

Figure 8.2 Mature spermatozoids in antheridial filaments before and after passage through the liberation pore have microtubules that align with the coiled nucleus. Spermatozoids that were just released (arrow) are elongated and exhibit microtubules concentrated at the tail end. All magnifications are similar. Bar = 10 μm.

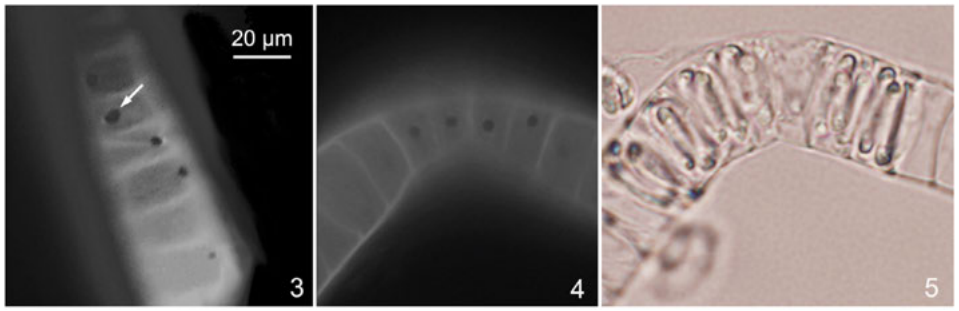

Figures 8.3–8.5 *Chara contraria*: The liberation pores of antheridial filaments. Calcofluor white-stained filaments (3) show pores as dark, round areas on the cell wall (arrow). Comparing calcofluor white stained filaments (4) and a transmission light micrograph (5) of the same region shows liberation pores on empty and spermatozoid containing cells. All magnifications are similar.

The typical release process took less than one second and started with the plastid-rich posterior end, followed by the nuclear zone, and lastly the flagella. In about 15% of the observed cells, the flagella remained trapped inside the cell while the bulk of the sperm had escaped. After some time (a few seconds to a minute), the flagella were pulled out by a quick contraction of the nuclear region. During the passage through the liberation pore (Figures 8.3, 8.4, this paper; Kwiatkowska and Poplonska 2002), the spermatozoid uncoiled, but regained its spiral form immediately thereafter. The liberation pores were not aligned among different cells within the antheridial filament, leading to omnidirectional release. After the release, the spermatozoids remained immobile for about one minute before gradually developing their motility. A small portion of spermatozoids (about 5%) moved extensively inside the cell prior to the release process. These spermatozoids rapidly rotated inside the cell, their release time was markedly extended, and often the spermatozoid emerged in reversed order with the flagella appearing first. After the spermatozoid was released, there were some particles moving inside the cell wall, which could be stained by propidium iodide.

The liberation pore

Spermatozoids were released through liberation pores in the cell walls of antheridial filaments (Figure 8.3). Both empty and spermatozoid-containing cells had a single liberation pore (Figures 8.4, 8.5) with an average diameter about 2.9 µm. The pores were arranged in a zigzag pattern at the filament surface. When and how the liberation pores develop is unknown but there is evidence that the formation of pores at least transiently is outlined by F-actin (data not shown).

LatB, Oryzalin and BDM effects on release, activation, and motility

The time period between opening of antheridia and the onset of spermatozoid release determined the “delay of spermatozoid release” and the time of the spermatozoid

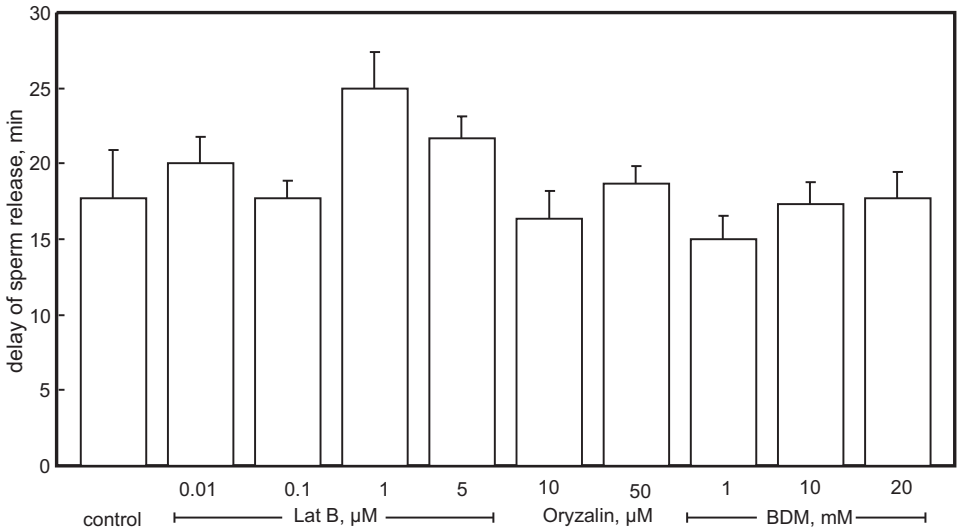

Figure 8.6 *Chara contraria*: Delay of spermatozoid release from antheridial filaments after exposure to various concentrations of LatB, Oryzalin or BDM showed no concentration-dependent effects. However, LatB reduced the average release time ($p = 0.02$, Proc GLM with Tukey-Kramer adjustments). Averages of three experiments with more than 60 released spermatozoids each ± SE.

moving inside the cell before the release event was measured as "activation time". The time between the release and onset of motility was measured as "movement lag time".

The average time between opening of antheridia and the release of spermatozoid from exposed antheridial filaments for controls was about 20 min (Figure 8.6). LatB, Oryzalin and BDM did not change the delay of spermatozoid release (Figure 8.6). The delay of release may have been a function of the maturation of the antheridium rather than a direct effect of LatB. Larger, more intensely colored and therefore likely to be more mature antheridia had shorter delays (data not shown).

The activation time in controls was ca. 132 ± 21 seconds (Avg ± SE). LatB (1 µM) increased the activation time to about 267 ± 22 seconds (Avg ± SE). BDM (1 mM) significantly decreased the activation to about 4 seconds. Higher concentrations of BDM (10 or 20 mM) completely inhibited the movement of spermatozoids inside the cells. The spermatozoids in these solutions were released without activation. LatB at other concentrations (0.01, 0.1 and 5 µM), and Oryzalin (10 and 50 µM) had no significant effects on the activation time (Figure 8.7). Because the effect of the drugs was observed at different concentrations, penetration or diffusion of the compounds into the antheridial cells was not a limiting factor.

LatB and BDM decreased the spermatozoid mobility lag time by about 50%, and Oryzalin (10 µM) by 60%; 50 µM Oryzalin had no effect on the mobility lag time. Spermatozoids released into 10 or 20 mM BDM were immobile (Figure 8.8).

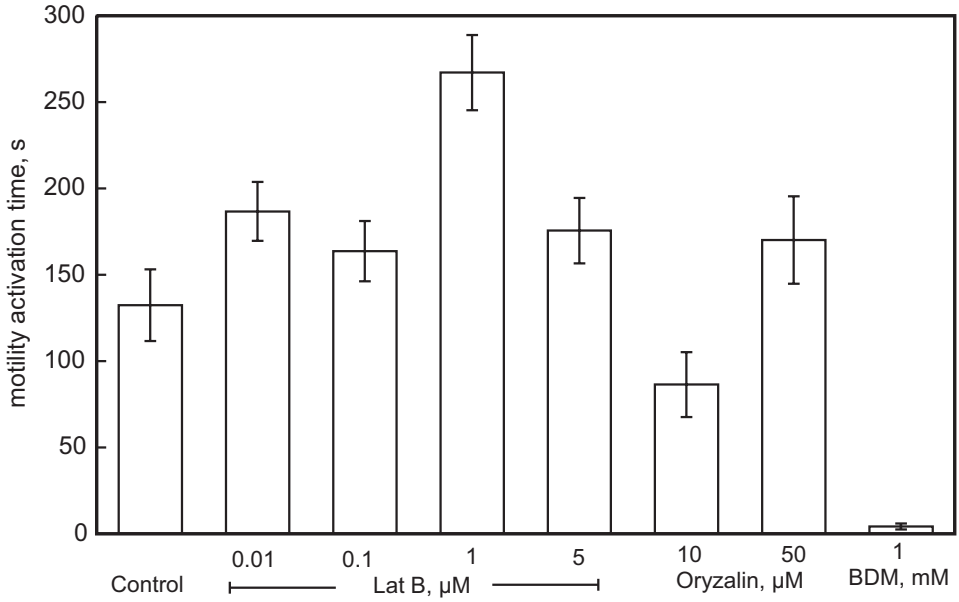

Figure 8.7 *Chara contraria*: Activation time of spermatozoid cells of *Chara contraria* before release from the antheridial filaments in the presence of Oryzalin, LatB, or the ATPase inhibitor BDM. LatB (1 µM) increased the motility activation time, the time that the spermatozoid moves inside the cell before release ($p < 0.0001$). BDM (1 mM) dramatically decreased the activation time ($p < 0.0001$, Proc GLM with Tukey-Kramer adjustments), and at higher concentrations (10, 20 mM) completely inhibited the movement of flagella inside the cell wall. Oryzalin and LatB at other concentrations had no significant effect on the activation time; $n \geq 17$.

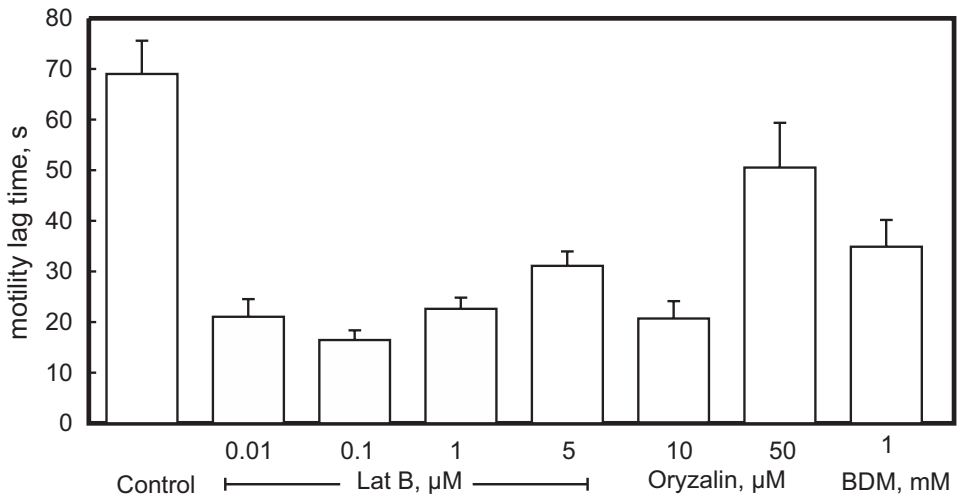

Figure 8.8 *Chara contraria*: The lag time for spermatozoid mobility in the presence of Oryzalin, LatB, or the ATPase inhibitor BDM. LatB, Oryzalin (10 µM) and 1 mM BDM significantly decreased the lag time for spermatozoid movement, the time between the spermatozoid was released and becoming motile ($p \leq 0.0001$, Proc GLM with Tukey-Kramer adjustments). Oryzalin (50 µM) had no effect; $n \geq 20$.

Effects of LatB, Oryzalin and BDM on the dynamics of spermatozoid release by the antheridial filaments

The typical spermatozoid release process produces a sigmoid curve over time (Figure 8.9). The expression as percentage normalizes data and allows description of release time and extent of synchronization by a logistic function. The release process was defined by beginning, massive release (from ca 10 to 90% of the spermatozoids are released during this period), and completion. The beginning of release was slow, and intervals between release events extended to minutes; after a few minutes, massive release began and several release events occurred simultaneously. After about 6–7 minutes, few spermatozoids were left inside the filaments and most of that sub-population gained motility inside the filament cell.

The duration of the beginning stage depended on the degree of maturity of the antheridium. More mature antheridia spent shorter time at the beginning stage. The duration of the massive release period was similar despite different degrees of maturity.

Some antheridia contained spirally shaped spermatozoids inside the maternal filament cell, but the spermatozoids were not released. From such antheridia, a smaller proportion

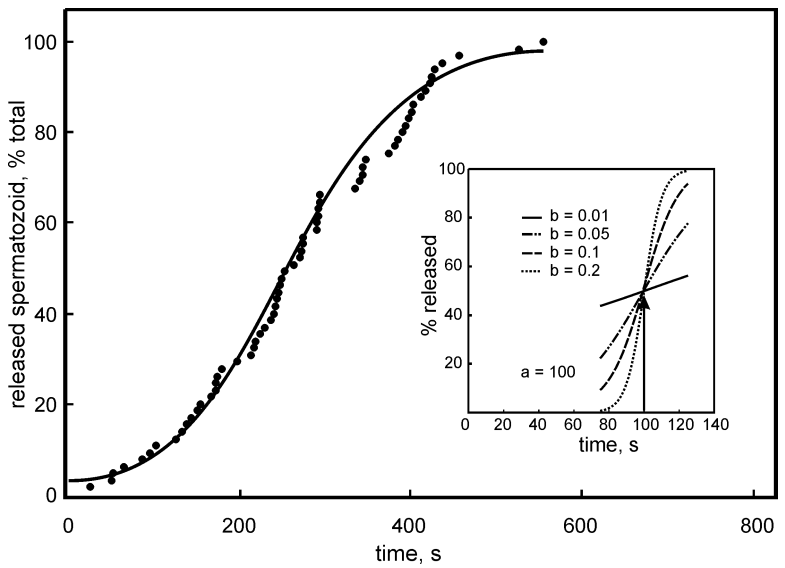

Figure 8.9 *Chara contraria*: The typical time course of spermatozoid release from the antheridial filaments follows a sigmoidal distribution. Normalizing release data as percent total allows comparison between different treatments using the same regression analysis. In this example, each dot represents an actual release event and the solid curve shows an optimized regression (minimal sums of squares) of the logistic function $F = 1/(1 + \exp[-(t - a)b])$, where a determines the offset of experimental time t, at which 50% of the release events has occurred and the factor b determines the slope. Inset panel shows a series of curves with identical a (100 s), but different values for b.

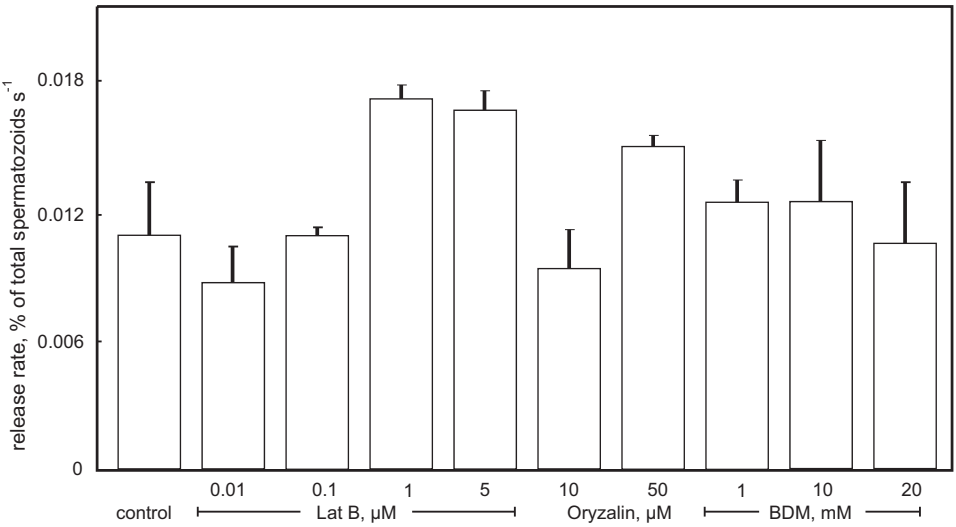

Figure 8.10 *Chara contraria*: The mean spermatozoid release rate of antheridial filaments in the presence of LatB, Oryzalin and BDM. The drugs had no effects on the mean spermatozoid release rate, but decreased the variation among individuals from about 22% of the mean in controls to an average of 12% in LatB-treated, 10% in Oryzalin and 7% in BDM-treated filaments. The release rate was expressed as the percentage of spermatozoids released in one second and was calculated as the coefficient b of the function $F = 1/(1 + \exp[-(t - a)b])$. N =3, means ± SE.

of spermatozoids was released during the initial phase and a larger number of spermatozoids than usual developed motility inside the cell. However, these spermatozoids were not released, even after several hours and a massive release stage could not be determined. The average spermatozoid release rate (factor b in the logistic function) was not affected by LatB, Oryzalin, or BDM. However, these drugs decreased the variation of the release rate from about 22% of the mean in controls to an average of 12% in LatB-treated, 10% in Oryzalin and 7% in BDM-treated filaments (Figure 8.10). Some spermatozoids in the 10 and 20 mM BDM solution were never released and lost their tightly wound organization inside the cells (data not shown).

LatB, Oryzalin and BDM effects on the relaxation of released spermatozoids

The spiraled spermatozoids were typically coiled around the axis of the filament. The length to width ratio of the cells was about 1:3 and the spermatozoid occupied the inner space of the filamentous cell, which represents a cylinder of about 9 µm length by 23 µm diameter. After the spermatozoid was released from the filament, it resumed its spiral shape immediately as a tightly wound helix with a length to diameter ratio of less than 0.5. As the spermatozoid gained mobility, the spiral extended, and both length and diameter of the helix increased over time. LatB did not affect the relaxation rate of spermatozoids in a concentration dependent manner (Figure 8.11); 0.1 µM LatB was

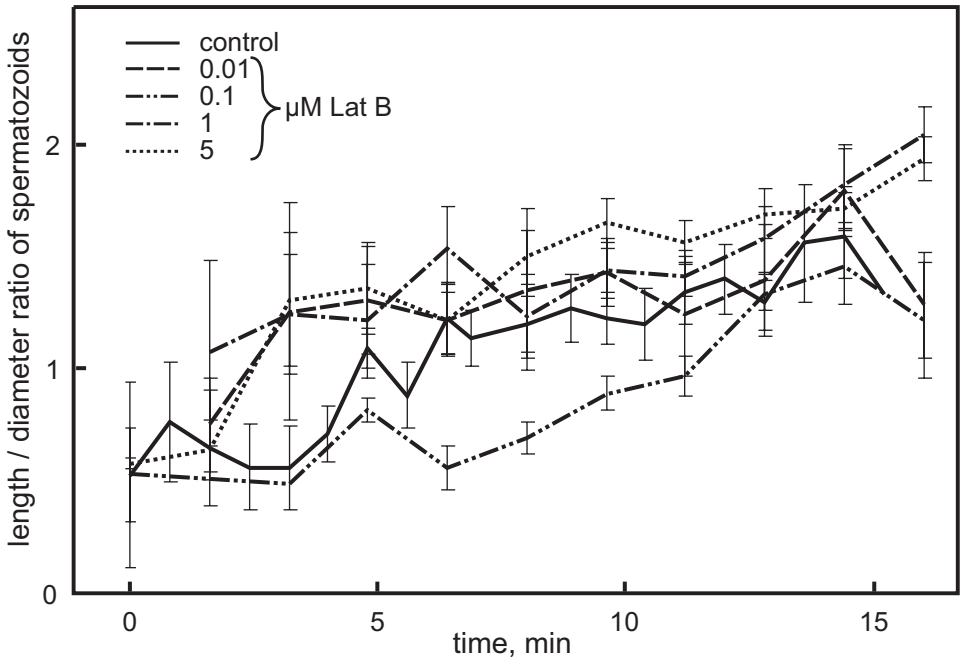

Figure 8.11 *Chara contraria*: Size increase of spermatozoids over time after release into solutions with different concentrations of LatB. For the first 6 min, the size increase for the spermatozoids in 0.01, 1 and 5 µM LatB treated media was larger than in controls. 0.1 µM LatB had no effect. Between 6 to 13 min, 0.1 µM LatB inhibited the relaxation process (size increase), while other LatB concentrations had no effect. The change in spermatozoid size is defined as ratio of length by diameter of the spermatozoid helix. Statistical analysis (Prog GLM) indicated significant increase over time as indicated by positive slopes of regression lines ± standard error (0.01 µM LatB: 0.02930 ± 0.01946, 0.1 µM LatB: 0.07438 ± 0.01075, 1 µM LatB: 0.05738 ± 0.01342 and 5 µM LatB: 0.06060 ± 0.01006, Control: 0.06294 ± 0.00822); $n \geq 14$.

most inhibitory for the relaxation process. Higher concentrations of LatB prevented a small number of spermatozoids from regaining their spiral form right after release; these spermatozoids remained elongated before slowly assuming a helical shape. This phenomenon was never observed in other treatments. Oryzalin (50 µM) and BDM (1 mM) inhibited the relaxation of spermatozoid coils over time, but 10 µM Oryzalin had no effect (Figure 8.12). Spermatozoids in 10 µM Oryzalin and 1 mM BDM took longer to gain full motility than in other treatments. Although the flagella of spermatozoids immersed in either 10 µM Oryzalin or 1 mM BDM exhibited flagellar mobility, they were not able to swim directionally. Spermatozoids released into 10 or 20 mM BDM remained immobile and had irregular shapes. A statistical comparison among all treatments showed that the relaxation rate of released spermatozoids (corresponding to the slope of a linear regression line) did not differ significantly ($p = 0.0576$; SAS, Proc MIXED).

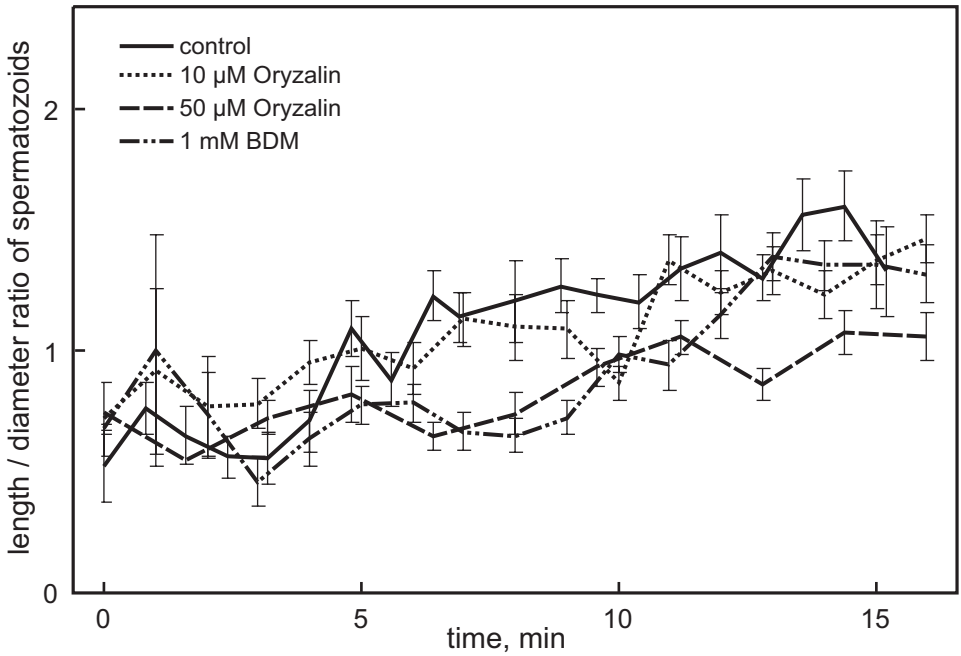

Figure 8.12 *Chara contraria*: Size increase of spermatozoids over time after release into solutions of Oryzalin and BDM. Oryzalin (50 µM), and BDM (1 mM) inhibited size increase. However, the inhibitory effects decreased after 10 min. The lower concentration of Oryzalin (10 µM) had no effect. The change in spermatozoid size is defined as ratio of length by diameter of the spermatozoid helix. Statistical analysis (Prog GLM) indicated significant increase over time as indicated by positive slopes of regression lines ± standard error (10 µM Ory 0.04235 ± 0.00692, 50 µM Ory 0.03146 ± 0.00762 and 1 mM BDM 0.06154 ± 0.00701, Control: 0.06294 ± 0.00822); $n \geq 14$.

Response of microtubules and F-actin to Oryzalin and LatB

Both released (Figures 8.13, 8.14) and unreleased (Figures 8.15, 8.16) spermatozoids showed normal MTs in controls (Figures 8.13, 8.15) but enhanced MT staining 1 h after application of 50 µM Oryzalin (Figures 8.14, 8.16), despite the normal effect of Oryzalin to depolymerize MTs of spermatozoids at 5 µM concentration (Figure 8.17). In contrast, F-actin in released (Figures 8.18, 8.19) and unreleased spermatozoids (Figures 8.20, 8.21) appeared fragmented but not completely dissolved after 1 h treatment of 1 µM of LatB (Figures 8.19, 8.21) compared to controls (Figures 8.18, 8.20).

Implications of results

The spermatozoid release process and the effects of cytoskeletal drugs on that process were studied for the first time. In nature, the antheridial shield cells open into a rosette, exposing the antheridial filaments to the environment. After the filaments become exposed to the external medium, changes of turgor pressure and the removal of unidentified inhibitors are possibly involved in triggering spermatozoid release. The opening of possibly slightly immature antheridia triggered spermatozoid in much the same kinetics as the release

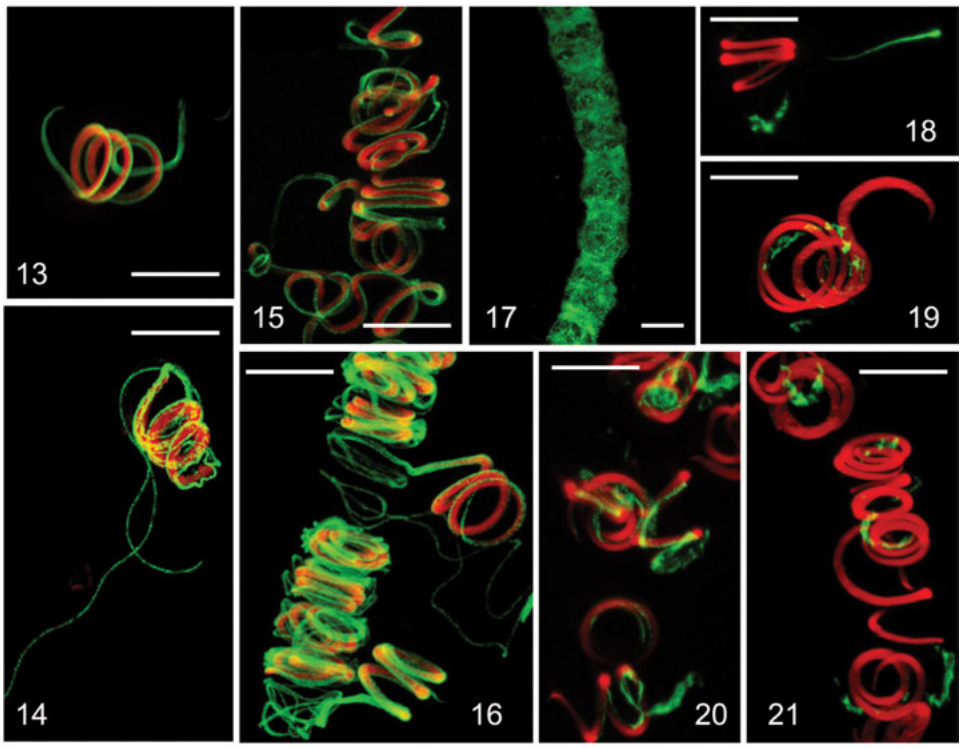

Figures 8.13–8.21 *Chara contraria*: MT (green, 13–17) and F-actin (green, 18–21) organizations of developing spermatozoids in the presence of Oryzalin and LatB. Both released (13, 14) and unreleased (15, 16) spermatozoids showed normal MTs in controls (13, 15) but enhanced MT staining 1 h after application of 50 μM Oryzalin (14, 16). However, application of 5 μM Oryzalin for 1 h depolymerized MTs (17). F-actin in released (18, 19) and unreleased spermatozoids (20, 21) appeared fragmented and, compared to controls (18, 20), did not completely dissolve after 1 h incubation in 1 μM of LatB (19, 21). Red: nuclei; bars = 10 μm.

from mature antheridia. Although the liberation pores as reported by Kwiatkowska and Poplonska (2002) were detected in empty and occupied cells (Figures 8.4, 8.5), it is uncertain as to whether these pores are predetermined or develop as a result of digestive (cellulase) activity of the maturing spermatozoid. Their formation may be related to late developmental changes in the cell wall composition that, unlike generic pectic and cellulosic elements, may be restricted to specific zones (Domozych et al. 2009). The "unplugging" of the pore could also be facilitated by turgor pressure differences resulting from the release of osmotic compounds from the antheridial cavity.

The typical release process begins with the posterior part of the spermatozoid and suggests that a signal is involved in the recognition of the pore and proper orientation of the spermatozoid. This concept is supported by the much longer release time for spermatozoids that started to move inside the cell and extended times to complete the release of inverted spermatozoid cells. The fast movement inside the maternal cell of non-released spermatozoid may represent a search strategy to complete the release event.

Calcofluor white is a fluorescent dye that binds strongly to cellulose, carboxylated polysaccharides, callose, and chitin (Hughes and McCully 1975). Using calcofluor white as a stain, the liberation pore became visible as a dark spot in the cell wall both in empty and spermatozoid-containing cells (Figures 8.4, 8.5). This visibility in cells still occupied suggests that the pores are plugged by material that is not stained by Calcofluor white. Thus, this material is likely different from cellulose, carboxylated polysaccharides, or callose. Although it is possible that pores are unplugged prior to release of the spermatozoids, their rapid release suggests that the cell contents are flushed out of the maternal cell. Whether plug removal is a mechanical or enzymatic process is not known. The previously mentioned pressure change could activate hydrolytic enzymes or disrupt mechanical connections and lead to unplugging of the pores.

The delay in spermatozoid release was not affected by the drugs tested (Figure 8.6). The lack of effectiveness may be related to low membrane or wall permeability of the drugs. After the liberation pore is unplugged, the drugs could enter through the liberation pore and diffuse to other cells in the same filament through plasmodesmata. This concept is supported by observations with propidium iodide (PI). Pre-release antheridial filaments did not show nuclear staining by propidium iodide for at least 20 min (data not shown). Unplugging of the liberation pores permitted propidium iodide into the cell and staining of the nucleus. Relative impermeability of cell wall and/or membrane is also supported by observations that the cytoskeletal drugs did affect the behavior of released but not pre-release spermatozoid.

Before release, the spermatozoids move inside the cell for about 130 seconds (Figure 8.7). The myosin ATPase inhibitor BDM completely blocked this movement, which indicates that the movement is dependent upon ATPase activity. However, spermatozoids in 10 and 20 mM BDM could still be released, which suggests that the movement inside the cell is not essential for the release event and that ATPase activity is not required for the release event. LatB and Oryzalin did not affect the duration of movement inside the cell except for 1 μM LatB (Figure 8.7). This concentration extended the activation time to 1.5 times the control value. The consequence and significance of this extension is unknown.

LatB and Oryzalin decreased the duration of spermatozoid movement lag time (Figure 8.8), which implies that both intact MT and F-actin are required to establish proper motility. Disruption of either cytoskeletal element shortened the lag time and promoted spermatozoid motility; however, Oryzalin was effective only at concentration less than 10 μM. Surprisingly, 50 μM Oryzalin enhanced MT stability instead of depolymerizing MTs (Figures 8.15, 8.16). High concentrations of LatB lead to fragmentation of F-actin but not to complete depolymerization (Figures 8.19, 8.20). Application of supraoptimal concentrations of Oryzalin may stabilize unidentified proteins or inhibit processes that control the MT organization in motile spermatozoids, therefore changing the dynamic equilibrium of MTs. The observation that spermatozoids in BDM completely lost their mobility after release indicates that the mobility of the spermatozoid after release relies on conventional myosin/ATP interactions.

Although LatB, Oryzalin, and BDM did not affect the average release rate, they synchronized it among individual antheridia (Figure 8.10). For all treatments the duration for a release event was similar to controls except after BDM treatments. Although BDM did not affect the average release rate, it altered the release event itself; some spermatozoids

incubated in BDM were never released and showed irregularly shaped nuclei. The sensitivity of spermatozoid release to BDM indicates that the release is an acto-myosin dependent process. Similar to BDM-induced changes of the organization of F-actin and MTs in the maize root apex (Samaj et al. 2000), higher concentrations of BDM (e.g., 20 mM) may disrupt both MT and F-actin networks. This disruption may contribute to the non-release of spermatozoids.

LatB caused expansion of the spiral spermatozoid beyond the dimensions of controls (Figure 8.11). In contrast, MT dynamics disruption by Oryzalin caused compression of the spiral spermatozoid (Figure 8.12). These observations support the "tensegrity" concept proposed by Ingber and colleagues (Ingber 1993, 1998; Ingber et al. 1994), which describes the cell as a "tensegral" unit whose cytoskeleton is organized by tension elements like F-actin extended over compression resistant MTs (for review see Pickett-Heaps et al. 1999).

The manchette MTs in the ostrich spermatozoid are responsible for the formation and maintenance of the shape of the nucleus (Soley 1997). Abnormal manchette MT development in spermatozoid of mice mutants resulted in abnormally shaped nuclei (Meistrich et al. 2005). BDM disorganized MTs and F-actins in *Saccharomyces cerevisiae* Meyen (Chon et al. 2001) and thus may have caused a change in the organization of MTs and F-actins in nuclei of released and non-released *Chara* spermatozoids, which may have caused deformed nuclei after BDM exposure.

In conclusion, this study shows that MTs and F-actin are involved in spermatozoid release and spermatozoid mobility in *Chara contraria*; the shape of nucleus of the spermatozoid is sensitive to MTs and F-actin altering drugs.

References

Bartels, P.S. and J.L. Hilton. 1973. Comparison of trifluralin, oryzalin, pronamide, propham and colchicine treatments on microtubules. *Pesticide Biochem Physiol 3*: 462–472.

Chon, K., H.S. Hwang, J.H. Lee and K. Song. 2001. The myosin ATPase inhibitor 2,3-butanedione-2-monoxime disorganizes microtubules as well as F-actin in *Saccharomyces cerevisiae. Cell Biol Toxicol 17*: 383–93.

Delwiche, C.F., K.G., Karol and M.T. Cimino. 2002. Phylogeny of the genus *Coleochaete* (coleochaetales, Charophyta) and related taxa inferred by analysis of the chloroplast gene rbcL. *J Phycol 38*: 394–403.

Domozych, D.S., I. Sorensen, and W.G.T. Willats. 2009. The distribution of cell wall polymers during antheridium development and spermatogenesis in the Charophycean green alga, *Chara corallina*. *Ann Bot 104*: 1045–1056.

Duncan, T.M., K.S. Renzaglia and D.J. Garbary. 1997. Ultrastructure and phylogeny of the spermatozoid of *Chara vulgaris* (Charophyceae). *Plant Syst Evol 204*: 125–140.

Graham, L.E. 1993. *The* Origin *of Land Plants*. Wiley, NewYork, pp 304.

Herrmann C, J. Wray, F. Travers and T. Barman. 1992. Effect of 2,3-butanedione monoxime on myosin and myofibrillar ATPases. An example of an uncompetitive inhibitor. *Biochem 31*: 12227–32.

Hugdahl, J.D. and L.C. Morejohn 1993. Rapid and reversible high-affinity binding of the dinitroaniline herbicide oryzalin to tubulin from *Zea mays* L. *Plant Physiol 102*: 725–740.

Hughes J. and M.E. McCully 1975. The use of an optical brightener in the study of plant structure. *Stain Technol 50*: 319–29.

Ingber, D.E. 1993 Cellular tensegrity: defining new rules of biology design that govern the cytoskeleton. *J Cell Science 104*: 613–627.

Ingber, D.E. 1998. The architecture of life. *Scientific American 178*: 30–39.

Ingber, D.E., L. Dike, L. Hansen, S. Karp, H. Liley, A. Maniotis, H. McNamee, D. Mooney, G. Plopper, J. Sims and N. Wang. 1994. Cellular tensegrity: exploring how mechanical changes in the cytoskeleton regulate cell growth, migration, and tissue pattern during morphogenesis. *Int Rev Cytol 150*: 173–224.

Kwiatkowska, M. and K. Poplonska 2002. Further ultrastructural research of *Chara vulgaris* spermiogenesis: endoplasmic reticulum, structure of chromatin, 3H-lysine and 3H-arginine incorporation. *Folia Histochem Cytobiol 40*: 85–97.

Karol, K.G., R.M. Mccourt, M.T. Cimino and C.F. Delwiche. 2001. The closest living relatives of land plants. *Science 294*: 2351–2353.

Kiss, J.Z. 1994. The response to gravity is correlated with the number of statoliths in *Chara* rhizoids. *Plant Physiol 105*: 937–940.

Kashman, Y., A. Groweiss and U. Shmueli. 1980. Latrunculin, a new 2-thiazolidinone macrolide from the marine sponge *Latrunculia magnifica. Tetrahedron Let 21*: 3629– 32.

Meistrich, M.L., P.K. Trostle-Weige and L.D. Russell. 2005. Abnormal manchette development in spermatids of azh/azh mutant mice. *Am J Anat 188*: 74–86.

Morejohn, L.C., 1991. The molecular pharmacology of plant tubulin and microtubules. In C Lloyd, ed, *The Cytoskeletal Basis of Plant Growth and Form*. Academic Press, London, UK, pp 29–43.

Morejohn, L.C., T.E. Bureau, J. MoleBajer, A.S. Bajer and Fosket D.E. 1987. Oryzalin, a dinitroaniline herbicide, binds to plant tubulin and inhibits microtubule polymerization in vitro. *Planta 172*: 252–64.

Pickett-Heaps, J.D., B.E.S. Gunning, R.C. Brown, B.E. Lemmon and A.L. Cleary. 1999. The cytoplast concept in dividing plant cells: cytoplasmic domains and the evolutions of spatially organized cell division. *Am J Bot 86*: 153–172.

Pickett-Heaps, J.D. 1967. Ultrastructure and differentiation in *Chara* sp. III. Formation of the antheridium. *Aust J Biol Sci 21*: 255–74.

Pickett-Heaps, J.D. 1968. Ultrastructure and differentiation in *Chara*. IV. Spermatogenesis. *C. fibrosa. Aust J Biol Sci 21*: 655–90.

Samaj J., M. Peters, D. Volkmann and F. Baluška. 2000. Effects of myosin ATPase inhibitor 2,3-butanedione 2-monoxime on distributions of myosins, F-actin, microtubules, and cortical endoplasmic reticulum in maize root apices. *Plant Cell Physiol 41*: 571–82.

Soley, J.T. 1997. Nuclear morphogenesis and the role of the manchette during spermiogenesis in the ostrich (*Struthio camelus*). *J Anat 190*: 563–576.

Spector, I., N.R. Shochet, Y. Kashman and A. Groweiss. 1983. Latrunculins: novel marine toxins that disrupt microfilament organization in cultured cells. *Science 219*: 493–95.

Turmel, M., C. Otis and C. Lemieux. 2003. The mitochondrial genome of *Chara vulgaris*: Insights into the mitochondrial DNA architecture of the last common ancestor of green algae and land plants. *Plant Cell 15*: 1888–1903.

Walter, M.M., R.A. Kathryn and J.M. Paul. 2000. Latrunculin alters the actin-monomer subunit interface to prevent polymerization. *Nature Cell Biol 2*: 376–8.

9 Dinoflagellate bioluminescence – a key concept for studying organelle movement

Kirsten Heimann, Paul L. Klerks and Karl H. Hasenstein

Chapter overview

Bioluminescence in *Pyrocystis lunula* depends on circadian movement of scintillons and chloroplasts between active and inactive locations. The involvement of the cytoskeleton in these transport processes was investigated using cytoskeleton-specific drugs. Chloroplast movements were visualized by chlorophyll autofluorescence and confocal laser scanning microscopy. Latrunculin B and Oryzalin prevented translocation of chloroplasts. Four hours after transition to the night phase, mechanically inducible bioluminescence was inhibited by Latrunculin B, the myosin inhibitor 2,3 butanedione monoxime (BDM), and Oryzalin in dose-dependent fashions. The actin stabilizer Jasplakinolide slightly enhanced bioluminescence but abolished Latrunculin B effects. The microtubule depolymerizer Colchicine had no effect on bioluminescence. These results suggest that F-actin and microtubules are involved in the movements of chloroplasts and scintillons. Although the tested drugs affected bioluminescence, further experiments are needed to determine if effects on bioluminescence were mediated by drug-induced failed translocations of scintillons or chloroplasts.

Mechanisms of circadian-controlled establishment and down regulation of bioluminescence in dinoflagellates

In photosynthetic bioluminescent dinoflagellates, light emission is under circadian control. Bioluminescence is down-regulated during the day and re-established at night. In *Pyrocystis lunula* and other members of this genus, establishment and down-regulation of bioluminescence are characterized by reciprocal movements of chloroplasts and scintillons (non-membranous "flashing units"; (Nicolas et al. 1987a)) between active and inactive positions (Swift and Reynolds 1968, Nicolas et al. 1987b). Chloroplasts are positioned at the cell periphery during the day and occupy a central location at night. The diurnal distribution of scintillons has proven harder to elucidate. The peripheral position of night phase scintillons has long been known (Swift and Reynolds 1968, Nicolas et al. 1987b) and recent ultrastructural analyses provided unambiguous evidence of the central location of scintillons in day phase cells (Seo and Fritz 2000). In addition, Western blot analysis showed the presence of luciferase, the enzyme responsible for the bioluminescent reaction, in both day- and night phase cells of *P. lunula* (Knaust et al. 1998), indicating that *P. lunula* does not depend on diurnal scintillon reassembly as many other bioluminescent dinoflagellates. These and earlier results using scintillon luminescence combined with image intensification for *P. fusiformis* and *P. noctiluca* (Widder and

Case 1982) suggest that circadian control of mechanically induced bioluminescence by diurnal translocation of scintillons may be common in the genus *Pyrocystis* (Sweeney 1981, Colepicolo et al. 1993, Seo and Fritz 2000).

In contrast to the complex diurnal movements of chloroplasts and scintillons in the genus *Pyrocystis*, circadian bioluminescence in *Lingulodinium polyedrum* (formerly *Gonyaulax polyedra* (Steidinger and Tangen 1997)) depends on the diurnal dis- and reassembly of scintillons. However, bioluminescence still depends on some movement because the pre-scintillons are formed in the cell centre near the Golgi apparatus and are translocated to the cell periphery at the onset of the night phase (Nicolas et al. 1987a).

Mechanically inducible bioluminescence in dinoflagellates requires association of the scintillons with the vacuole. This association is described in the "proton trigger" model, where a mechanical stimulus leads to action potentials at the tonoplast (Nicolas et al. 1987a, Nicolas et al. 1991). Depolarization of the tonoplast acidifies the scintillon lumen through the influx of protons originating from the acidic vacuole (Nicolas et al. 1987a, Nicolas et al. 1991). The acidification of the scintillons activates the enzyme luciferase (an oxygenase with an acidic pH optimum), which oxidizes the substrate luciferin and leads to the emission of light (Knaust et al. 1998). Thus, in addition to the potential role of the cytoskeleton in diurnal scintillon translocation processes, it may also tether the scintillons to the vacuolar membrane.

Involvement and mechanism of the cytoskeleton in organelle movement

A role for filamentous actin (F-actin) in organelle trafficking events has been well established. Actin filaments participate in endocytotic vesicle trafficking in animal, plant and fungal cells (Heuser 1989, Hill et al. 1996, Santos and Snyder 1997, Walch-Solimena et al. 1997, Shurety et al. 1998, Baluska et al. 2004, Ovecka et al. 2005, Samaj et al. 2005). The cytoskeletal drugs Latrunculin B, Oryzalin and Colchicine have been used to study the involvement of cytoskeletal components in chloroplast movements (Pickett Heaps 1991, Tanaka 1991, Kadota and Wada 1992, Kandasamy and Meagher 1999, Foissner and Wasteneys 2007). These drugs have been shown to be highly specific because they bind to monomeric G-actin (Latrunculin B) or tubulin dimers (Colchicine and Oryzalin) thus shifting the equilibrium from polymerized to monomeric components. This shift in equilibrium leads to the disintegration of the respective cytoskeletal component (Spector et al. 1983, Morejohn et al. 1987a, Morejohn et al. 1987b, Spector et al. 1989, Hugdahl and Morejohn 1993).

Although F-actin and microtubules have been implicated in the transport of various membranous organelles, their involvement in translocation of non-membranous particles is less certain. However, a role for F-actin in the movement of non-membranous subnuclear organelles was recently shown in *Xenopus* oocytes (Kiseleva et al. 2004).

Using cytoskeletal drugs in combination with confocal microscopy and bioluminescence measurements, our study aimed to unravel the role of the cytoskeleton in the diurnal translocation of scintillons and chloroplasts in the marine dinoflagellate *Pyrocystis lunula*. Results suggest that F-actin and microtubules are involved in circadian chloroplast movements and that both cytoskeletal components participate in the translocation of scintillons and/or their tethering to the tonoplast.

Experimental design and set up

Cell cultivation and preparation for drug treatments and measurement of bioluminescence

Pyrocystis lunula (Schütt) was obtained from Lumitox® Gulf L.C. (Slidell, LA, USA) and maintained in a Percival® environmental growth chamber at 20°C, on a 12:12 h light:dark cycle in synthetic dinoflagellate medium and an irradiance of 65 μmol photons m^{-2} s^{-1} (Heimann et al. 2002).

To ensure uniform organelle distributions, cultures at the end of the exponential growth phase (4 weeks) were used for all experiments. The effect of cytoskeletal drugs on diurnal chloroplast translocations was analyzed using chlorophyll autofluorescence and confocal laser scanning microscopy (MRC-1024 BioRad). The effect of cytoskeletal drugs on bioluminescence was measured for mechanically inducible bioluminescence following the set-up, conditions, instrumentation, and procedures described in Heimann et al. (2002).

Briefly, cells were homogenously suspended by stirring on a magnetic stirrer for 15 min, 2 h prior to the onset of the night phase. Cell concentration of the cultures was established by counting in a Sedgewick Rafter counting chamber and cultures were diluted to 100 cells mL^{-1} with artificial seawater. Assays were conducted with 3 mL volumes at a density of 100 cells mL^{-1} incubated in the presence and absence of cytoskeletal drugs prior to photoperiod transitions from day to night. The following drugs were used: Latrunculin B (Calbiochem, EMD Biosciences Inc., 10394 Pacific Center Court, San Diego, CA 92121), Jasplakinolide (Molecular Probes, Invitrogen Corporation, 1600 Faraday Avenue, Carlsbad, CA 92008), 2,3 butanedione monoxime (BDM; Sigma), Oryzalin (ChemService, 660 Tower Lane, West Chester, PA 19381), and Colchicine (Sigma). Stock solutions of all drugs were prepared using DMSO as a solvent, except for BDM, which was prepared in sterile artificial seawater. The amount of DMSO in treatments did not exceed 1% and controls were therefore tested in the presence of 1% DMSO without drugs. Incubation times (time prior to photoperiod transition from day to night) and final concentrations of drugs used, are summarized in Table 9.1. Measurements were performed in a room illuminated with light at 550 nm (a wavelength the organism does not detect) to avoid downregulation of bioluminescence during the cells' night phase. Bioluminescence was measured 4 h after the transition of photoperiods using a custom-built bioluminometer designed for measuring cumulative, mechanically activated bioluminescence over 1 min (Tox-Box®, Lumitox Gulf L.L.C., Slidell, LA, USA). To verify that the cytoskeletal drugs did not exhibit a general physiological effect, bioluminescence was quantified in controls and treatments by stimulating total bioluminescence with 0.5% acetic acid in the presence of the drugs (treatments) or DMSO (controls). Washout experiments, where the drugs were removed after the incubation period and cells were allowed to recover for 24 h in uncontaminated artificial seawater under culturing conditions (recovery experiments as per Heimann et al. 2002), were performed to eliminate that effects on bioluminescence were due to cytotoxic effects. The effect of cytoskeletal drugs is expressed as percent bioluminescence relative to controls. Results were analyzed using actual bioluminescence emissions (relative units) via one-way ANOVA using Statistica 7 (StatSoft, Inc., Tulsa, OK 74104).

Table 9.1 Summary of cytoskeletal drug treatment regimes for bioluminescence experiments in *Pyrocystis lunula*

Drug	Concentration	Incubation time[a]
Latrunculin B	0, 0.5, 1, 10 μM	1 h
Jasplakinolide	0, 1, 2 μM	2 h
Jasplakinolide followed by	2 μM	1 h
Latrunculin B	10 μM	1 h
2,3 butanedione monoxime	0, 2, 4, 8, 10, 20 mM	1 h
Oryzalin	0, 5, 10, 50 μM	1 h
Colchicine	1 mM	2 h

[a]Cells of *P. lunula* were treated with cytoskeletal drugs for the times indicated prior to photoperiod transition from day to night.

Cytoskeletal drug treatment and quantification of chloroplast movements

To investigate the effect of cytoskeletal drugs on diurnal chloroplast translocation, cells were incubated in 10 μM Latrunculin B for 2 h or 50 μM orzyalin for 1 h before photo period transitions from day to night or from night to day. Effective concentrations of cytoskeletal drugs were derived from the bioluminescence assays. Micrographs were taken 4 h after photo period transitions. A total of 50 cells were analyzed per treatment. Differential interference contrast was used to document cell morphology after Oryzalin treatment.

The effect of Latrunculin B on the actin cytoskeleton was examined in cells fixed with methanol:acetic acid (3:1/v:v) at −20ºC for 15 min, washed three times with PHEM/DMSO buffer (Brown and Lemmon 1995) and labeled with FITC-phalloidin (Invitrogen, Carisbad, CA 92008) following the manufacturer's instructions. Fluorescence was documented by confocal laser scanning microscopy (LaserSharp 2000, v. 5.1.).

Results

Circadian distribution and locations of scintillons and chloroplasts

In *Pyrocystis lunula* grown under a 12:12 h light:dark photoperiod, chloroplasts were distributed evenly throughout the cytosol during the day phase (Figure 9.1) and aggregated in the cell centre during the night phase (Figure 9.2). Upon transition from night to day, bioluminescence was down-regulated within 20 min. In contrast, the establishment of full bioluminescence required 2 h after day to night transition (Figure 9.3). Bioluminescence was stable in mid-night cells for the 2 h measured. If no light was provided at the onset of the day phase, bioluminescence declined to 50% of the normal night emission and remained constant over the 1 h measured (Figure 9.4). In contrast, photoperiod transition from night to day accompanied by the onset of light led to complete down-regulation of bioluminescence within 20 min of receiving light (Figure 9.4, arrow). These observations demonstrate that bioluminescent cells grown in 12:12 light: dark cycles were capable to respond to changes in illumination.

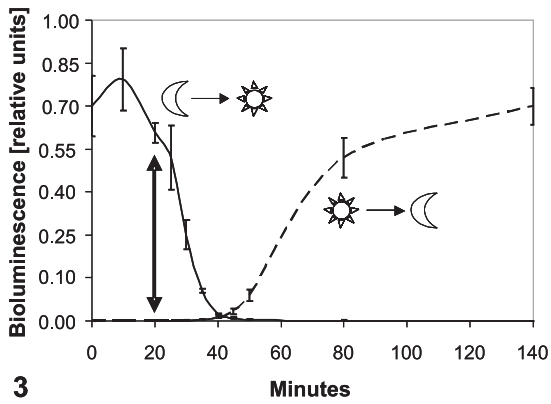

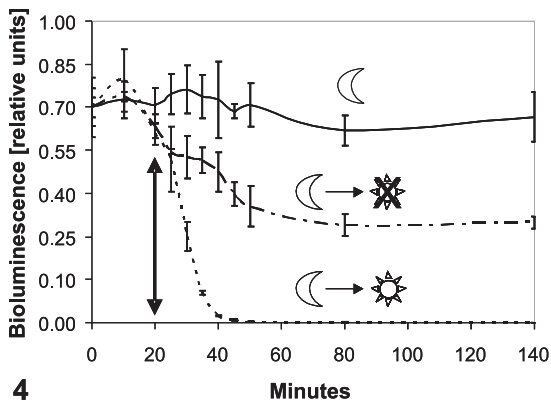

Figures 9.1–9.4 Diurnal morphologies and bioluminescent profiles of *Pyrocystis lunula*.
Figure 9.1 Nomarski micrograph of a day phase cell with chloroplasts extended throughout the cytosol.
Figure 9.2 Nomarski micrograph of a night phase cell with centrally located chloroplasts. Scale bars for Figures 9.1–9.2 represent 20 µm.
Figure 9.3 Bioluminescence profiles at transition of photo periods (occurring at t20; vertical arrow) from night to day (solid line) and day to night (broken line). Bioluminescence for times 0–20 min on the y-axis represents measurements taken for the last 20 min of the previous photoperiod, i.e. before photoperiod transitions. Lighting conditions were synchronized with the circadian rhythm expressed in relative units. ☾→☼ = photo period transition night to day; ☼→☾ = photo period transition day to night; n = 3 ± SD.
Figure 9.4 Bioluminescent profile of cells maintained in the dark (solid line; ☾), maintained in the dark at a time when normal phase transition occurred (line with long and short dashes; ☾→✸) or undergoing normal night-day transition (hatched line; ☾→☼). For the latter, transition occurred at t20; vertical arrow). Values are mean ± SD (n = 3), with bioluminescence expressed in relative units.

Effects of cytoskeletal drugs on diurnal scintillon and chloroplast translocations

The actin network in control cells was concentrated in the cell centre and radiated out to the median cell periphery in thick bundles, with less dense branches present along the longitudinal axis of the cell (Figure 9.5). Latrunculin B depolymerized most peripheral

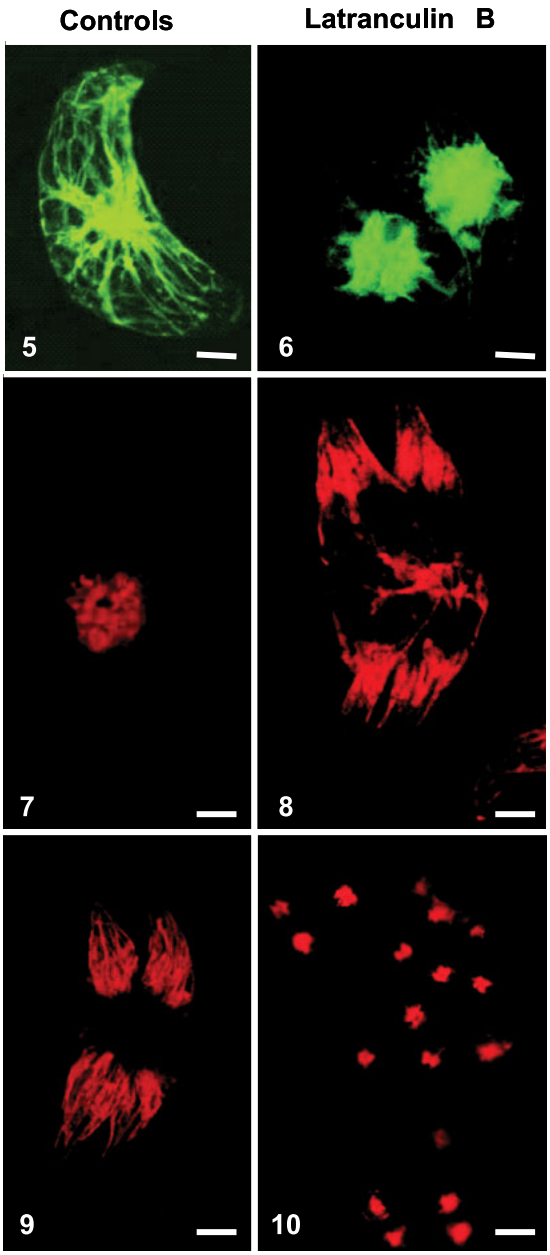

Figures 9.5–9.10 Distribution of the actin cytoskeleton and chloroplasts in controls (left column) and 10 µM Latrunculin-treated cells of *Pyrocystis lunula* (right column). Figures 9.5 and 9.6 depict the actin cytoskeleton of night phase cells, while Figures 9.7–9.10 show the location of the chloroplasts (chlorophyll autofluorescence). The actin cytoskeleton was documented in methanol:acetic acid fixed cells (Figures 9.5 and 9.6). The controls show actin bundles radiating from the cell centre (Figure 9.5). Latrunculin B-treated night phase cells (10 µM, 2 h, Figure 9.6) show reduced fluorescence, lack F-actin bundles, and show diffuse actin staining in the cell centre. Chloroplasts in controls were centrally located in night phase cells (Figure 9.7) and peripherally distributed in day phase cells (Figure 9.9). Latrunculin B application two hours before day-to-night transition prevented translocation of chloroplasts to the cell centre (Figure 9.8) and application to night phase cells prevented the movement of chloroplasts from their central night positions to the cell periphery (Figure 9.10). Micrographs were taken 4 h after photo period transitions. Scale bars represent: 20 µm (Figures 9.5–9.9) and 100 µm (Figure 9.10).

actin filaments and only diffuse actin labeling was observed in the central regions of the cells (Figure 9.6).

Chloroplasts of control cells of *Pyrocystis lunula* were located in the cell centre 1 h after transition from day to night (Figure 9.7). Treatment with 10 µm Latrunculin B 2 h prior to the transition from day to night inhibited chloroplast migration to the cell centre

(Figure 9.8), resulting in chlorophyll autofluorescence pattern typical of control day-phase cells (Figure 9.9) and a small amount of chlorophyll autofluorescence in the cell centre (Figure 9.8). Similarly, cells treated with Latrunculin B at photoperiod transition from night to day showed chlorophyll autofluorescence only close to the cell centre (Figure 9.10) after transition to the day phase and chloroplasts never reached their typical day phase distribution (see Figure 9.9). This observation indicates that chloroplast migration was strongly inhibited (compare to Figure 9.7).

When day phase cells of *Pyrocystis lunula* were treated with Latrunculin B, the mechanically-inducible bioluminescence was inhibited in a dose-dependent manner, with 0.5 μM of the drug reducing bioluminescence to 50% and 10 μM of Latrunculin B reducing bioluminescence to 10% (Figure 9.11). In contrast, 1 μM Jasplakinolide enhanced bioluminescence by an average of 17% ($F_{(2, 27)} = 7{,}351$; $p = 0.003$), and no further enhancement was observed in treatments with 2 μM Jasplakinolide (Tukey's post hoc, $p = 0.997$; Figure 9.11). When Jasplakinolide was applied for 1 h prior to the addition of Latrunculin B during the day phase, bioluminescence was no longer affected by the Latrunculin B (data not shown). The myosin inhibitor BDM inhibited mechanically-inducible bioluminescence in a dose-dependent manner (Figure 9.12). Treatment with 8 mM BDM resulted in 50% reduction of bioluminescence and 20 mM BDM abolished mechanically-inducible bioluminescence. Reduction of bioluminescence was not due to cytotoxic or general physiological effects of the cytoskeletal drugs, as cells fully regained their bioluminescence after washout and a 24h recovery period and no difference in the total bioluminescent potential (acetic-acid stimulatable bioluminescence) between controls and treatments was observed (data not shown). These data suggest that myosin activity is needed for mechanically-inducible bioluminescence.

The F-actin depolymerizing drug Latrunculin B inhibited bioluminescence in a dose-dependent manner (Figure 9.11). Treatment with the F-actin stabilizing drug Jasplakinolide slightly promoted bioluminescence (Figure 9.11). The myosin inhibitor BDM inhibited bioluminescence in a dose-dependent manner (Figure 9.12). $n = 10$; averages ± SE.

Within 4 h of day to night transition, chloroplasts in untreated cells reached their central night phase location (Figure 9.13). Treatment of day phase cells with 50 μM Oryzalin prevented chloroplast relocation to their night phase position (Figure 9.14). The differential interference contrast micrograph of the same cell pair showed typical day phase morphology (Figure 9.15), and suggests that the diffuse chlorophyll autofluorescence pattern of Oryzalin-treated cells (compare Figure 9.14 to Figures 9.9 and 9.16) is not the result of general adverse effects of the drug on cell morphology but specific for microtubule depolymerization. Oryzalin-treated night phase cells of *Pyrocystis lunula* did not show typical day or night phase chlorophyll autofluorescence patterns, but exhibited random chloroplast distributions (Figure 9.17). Controls showed normal, well resolved day phase chloroplast distributions (Figure 9.16).

Oryzalin inhibited mechanically-inducible bioluminescence in a dose-dependent manner with 10 μM inhibiting bioluminescence by 50% and 50 μM abolishing mechanically-inducible bioluminescence (Figure 9.18). In contrast, incubation with 1 mM Colchicine, another microtubule depolymerizing drug, did not significantly reduce bioluminescence ($F_{(1, 18)} = 1.6156$, $p = 0.22$; data not shown).

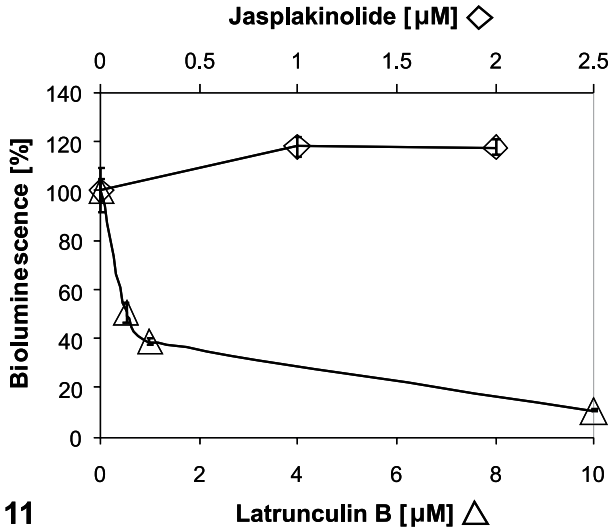

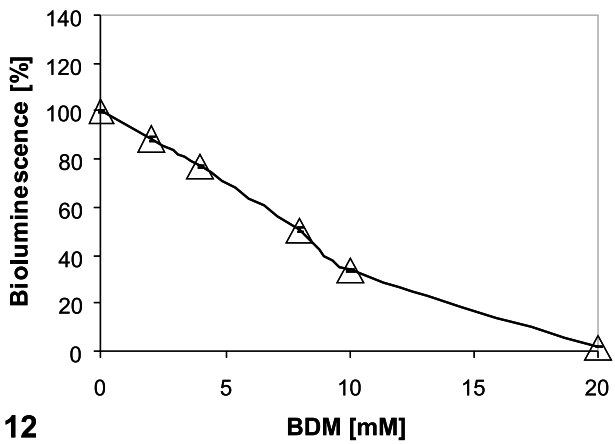

Figures 9.11–9.12 Effect of Jasplakinolide, Latrunculin B, and 2,3 butanedione monoxime (BDM) on mechanically triggered bioluminescence in *Pyrocystis lunula*. Assays were conducted in the presence and absence of cytoskeletal drugs applied prior to photoperiod transitions from day to night. Stock solutions of drugs were added to medium to establish concentrations shown. Bioluminescence was measured 4 h after the transition of photoperiods and is expressed relative to that of untreated controls.

Synthesis of results

Diurnal chloroplast movement

Chloroplasts of *Pyrocystis lunula* exhibit distinct day- and night phase distributions. During the day, the chloroplasts extend throughout the cytosol. At night the chloroplasts move and are centrally located. The observed diurnal changes in chloroplast distribution correspond to previously documented changes in *P. lunula* (Swift and Taylor 1967,

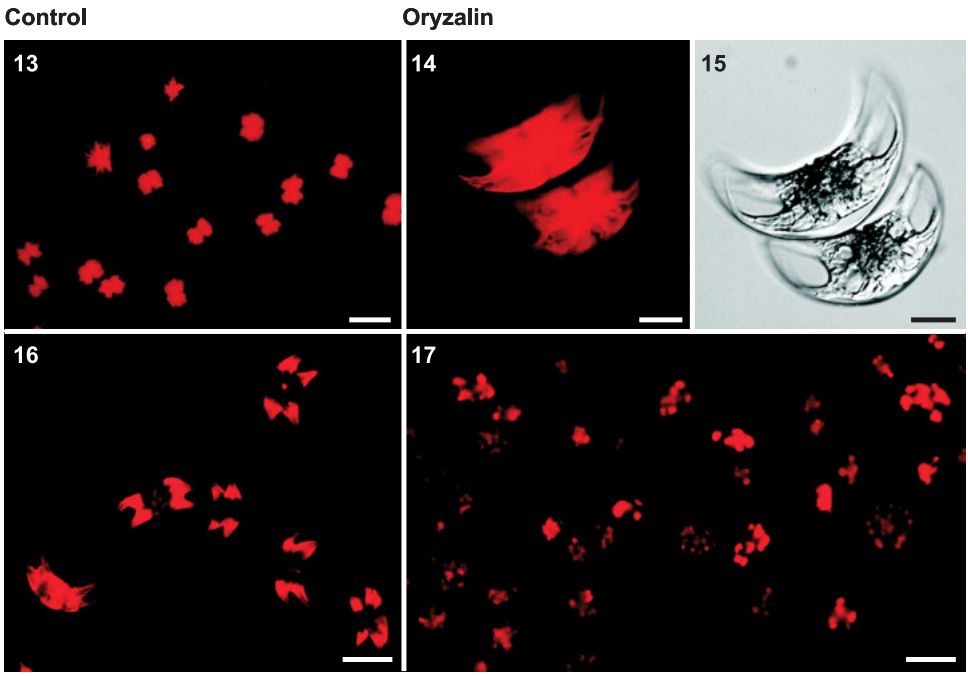

Figures 9.13–9.17 The microtubule depolymerizing drug Oryzalin inhibited chloroplast movements in *Pyrocystis lunula* when incubated in 50 μM orzyalin for 1 h before photoperiod transitions from day to night (Figures 9.13–9.15) and from night to day (Figures 9.16–9.17). Micrographs were taken 4 h after photo period transitions. A total of 50 cells were analyzed per treatment. Untreated controls show chloroplast distributions expected after photoperiod transitions (Figure 9.13 day to night control, central location of chloroplasts; Figure 9.16 night to day control, peripheral location of chloroplasts). Treatment with 50 μM Oryzalin inhibited chloroplast migration to the cell centre after day to night transitions (Figure 9.14) and the cells resemble day-phase cells (Figure 9.15, compare with Figure 9.1). Oryzalin treatment partially inhibited chloroplast migration after night to day transition. Chlorophyll autofluorescence pattern did not match typical day- or night phase locations (Figure 9.17). Scale bars = 50 μm (Figures 9.13, 9.16–9.17) and 20 μm (Figures 9.14–9.15).

Topperwien and Hardeland 1980, Seo and Fritz 2000) and other species of this genus (Sweeney 1981, Hardeland 1982, Hardeland and Nord 1984). However, the mechanism(s) of chloroplast movement remain(s) unknown. Ultrastructural analyses by Seo and Fritz (2000) provided evidence for a chloroplast reticulum, which expands in day phase cells and contracts in night phase cells. Night phase cells contain extensively stacked thylakoids as opposed to the more typical dinoflagellate 2–3 thylakoid stacks of day phase cells. Chlorophyll autofluorescence patterns in day phase cells of our study also support the concept of a chloroplast reticulum.

Effects of cytoskeletal drugs on chloroplast movements

Latrunculin B depolymerization of F-actin inhibited the diurnal translocation of chloroplasts (Figures 9.8 and 9.10). These results are in line with the reported abnormal

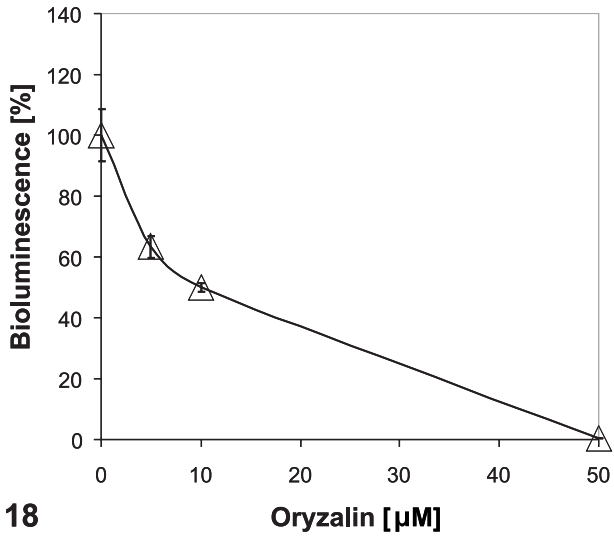

Figure 9.18 The microtubule depolymerizing drug Oryzalin (triangles) inhibited mechanically triggered bioluminescence in *Pyrocystis lunula*. Cells were tested in the presence and absence of cytoskeletal drug or 1% DMSO (solvent controls). Incubation times (time prior to photoperiod transition from day to night) and final concentrations of drugs are summarized in Table 9.1. Bioluminescence was measured 4 h after the transition of photoperiods. Bioluminescence is expressed relative to that of controls. n = 10, average ± SE.

chloroplast aggregation in *Arabidopsis* following Latrunculin B treatment (Kandasamy and Meagher 1999). Oryzalin did not affect chloroplast movements in *Arabidopsis* (Kandasamy and Meagher 1999), but prevented chloroplast movement in day phase cells of *Pyrocystis lunula*. Thus chloroplast translocation toward the cell centre was at least partially dependent on microtubules.

Diurnal chloroplast translocations in *Pyrocystis lunula* were F-actin- and microtubule-dependent similar to light-induced chloroplast movements in the moss *Physcomitrella patens* (Sato et al. 2001). Light-induced F-actin-dependent chloroplast migration was also documented in protonema of the fern *Adiantum* (Kadota and Wada 1992), but the lack of an effect of Colchicine led these authors to conclude that chloroplast translocations in *Adiantum* are not microtubule-dependent. Our studies also showed no effect of Colchicine on mechanically-inducible bioluminescence (see below) but convincing results were obtained with Oryzalin. The distribution of chloroplasts after treatment of night phase cells with Oryzalin resembled neither day- nor night phase arrangements (Figure 9.17). The observed punctate fluorescence pattern suggests microtubule dependence of the expansion of the proposed chloroplast reticulum (Seo and Fritz 2000). Upon microtubule depolymerization, non-expanded chloroplast units might relocate to proxy day phase positions potentially using the actin cytoskeleton. This hypothesis is supported by the complete inhibition of chloroplast migration in night phase cells of *P. lunula* treated with Latrunculin B prior to transition to the day phase.

Effects of cytoskeletal drugs on scintillon movements

The mechanism of scintillon movement was not investigated in any of the studies describing the position of scintillons in the genus *Pyrocystis* (Swift and Reynolds 1968, Sweeney 1980, Sweeney 1982, Widder and Case 1982, Nicolas et al. 1987b, Seo and Fritz 2000). Since bioluminescence in *Pyrocystis lunula* is restricted to the night phase, the dependence of bioluminescence on cytoskeletal properties can be tested only by treating day phase cells prior to the onset of the night phase. Depolymerisation of F-actin reduced bioluminescence in a dose-dependent manner, and F-actin stabilization somewhat enhanced bioluminescence. These results indicate that the scintillons operate under the control of F-actin, but do not clarify whether F-actin is involved in the movement of scintillons or whether it tethers the scintillons to the vacuolar membrane, an association necessary for mechanically-inducible bioluminescence (Nicolas et al. 1987a).

Although dose-dependent inhibition of bioluminescence by BDM supports active scintillon transport, the dependency of bioluminescence on some bridge between vacuole and scintillons via the acto-myosin system cannot be ruled out. F-actin and myosin could also play some role in the deformation of the tonoplast necessary for enveloping the scintillons. Such close tonoplast-scintillon association has been reported in other bioluminescent dinoflagellates (Nicolas et al. 1987a, Nicolas et al. 1987b). Support for a combination of tethering and transport could be derived from observations in *Lingulodinium polyedrum*, where the scintillons are destroyed at the onset of the day phase and rebuilt (as "pre-scintillons") at the onset of the night phase at ribosomes located pericentrally in the vicinity of the Golgi bodies (Nicolas et al. 1987a). These authors suggested that these "pre-scintillons" associate with and then translocate along the vacuolar membrane to their active location at early night phase. Our observations that mechanically-inducible bioluminescence in *Pyrocystis lunula* requires at least 2 h after transition to the night phase, in contrast to the rapid (20 min) down-regulation after transition to the day phase, may be an indication of similarly complex connection and transport interactions between the scintillons and the vacuolar membrane.

Pretreatment of cells with the F-actin-stabilizing drug Jasplakinolide abolished the Latrunculin B effect but treatment with Jasplakinolide alone had a slight promotive effect. These results suggest that scintillon migration is F-actin dependent, while bioluminescence *per se* may be F-actin independent and are supported by studies on the effect of Jasplakinolide on vesicle transport in species ranging from plants to fruit flies (Shurety et al. 1998, Tilney et al. 2000, Desnos et al. 2003, Baluska et al. 2004).

Interpretation of cytoskeletal drug effects on scintillon and chloroplast movements

Our study suggests that F-actin and microtubules are involved in the movements of chloroplasts and scintillons. The inhibition of bioluminescence in *Pyrocystis lunula* by Oryzalin suggests microtubule-based translocation of scintillons from their day phase distribution to vacuole-associated peripheral night phase position. However, since translocation of both organelles occurs simultaneously albeit in opposite directions, the inhibitory effect of cytoskeletal drugs on the establishment of mechanically-inducible bioluminescence could result from chloroplasts blocking the association of scintillons with the vacuole, which is necessary for mechanically-inducible bioluminescence. The

latter possibility is supported by high resolution ultramicrographs of *Lingulodinium polyedrum*, where no association of scintillons with cytoskeletal elements was detected (Nicolas et al. 1987a). However, proving scintillon/cytoskeletal association would require three-dimensional reconstruction of cytoskeletal elements, tonoplast and chloroplast arrangements.

Unlike Oryzalin, Colchicine did not inhibit mechanically-inducible bioluminescence, which may indicate that Colchicine is either not taken up as readily as Oryzalin or that some other factor reduced its effectiveness. This notion is supported by similar, seemingly contradictory results between Colchicine and other microtubule depolymerizing drugs on microtubule involvement in stomatal movements (Assmann and Baskin 1998) and recent studies on varying potency of F-actin depolymerizing drugs (Foissner and Wasteneys 2007). Thus conclusions based on drug treatments that stomatal movements are independent of microtubules (Assmann and Baskin 1998) are inconclusive at best because the microtubule disruptor propyzamide and the microtubule stabilizer taxol demonstrated a clear involvement of microtubules in stomatal movements (Fukuda et al. 1998). The different effectiveness of Oryzalin and Colchicine could depend on stronger affinity of Oryzalin for tubulin dimers (Morejohn et al. 1987b, Hugdahl and Morejohn 1993) or differing mechanisms between Oryzalin and Colchicine interactions with microtubules (Lahav et al. 2004).

Summary

In summary, we have shown that F-actin and microtubule depolymerizing drugs interfered with diurnal movement of chloroplast and/or the chloroplast reticulum in *Pyrocystis lunula*. Although Oyrzalin and Latrunculin B inhibited bioluminescence in a dose-dependent manner, their effect does not distinguish between roles of these cystoskeletal elements in scintillon translocation and/or tonoplast – scintillon interactions. Biochemical analyses of isolated scintillons will be required to unambiguously resolve the function of the cytoskeleton in trafficking or tethering of scintillons.

Acknowledgements

This research was funded by grants from the US Department of Energy (DE-FG02–97-ER12220) to PLK and James Cook University (Merit Research Grant) to KH. We are also grateful to Krista DeMattio, who performed part of the BDM study as a special research component of her BSc at James Cook University.

References

Assmann, S.M. and T.I. Baskin. 1998. The function of guard cells does not require an intact array of cortical microtubules. *J. Exp. Bot. 49*: 163–170.

Baluska, F., J. Samaj, A. Hlavacka, J. Kendrick-Jones and D. Volkmann. 2004. Actin-dependent fluid-phase endocytosis in inner cortex cells of maize root apices. *J. Exp. Bot. 55*: 463–473.

Brown, R.C. and B.E. Lemmon. 1995. Methods in plant immunolight microscopy. *In*: (D. Galbraith, D. Bourque and H. Bohnert, eds) *Methods in plant cell biology. Part A*. Academic Press, London. pp 85–107.

Colepicolo, P., T. Roenneberg, D. Morse, W.R. Taylor and J.W. Hastings. 1993. Circadian regulation of bioluminescence in the dinoflagellate *Pyrocystis lunula. J. Phycol. 29*: 173–179.

Desnos, C., J.S. Schonn, S. Huet, V.S. Tran, A. El-Amraoui, G.A. Raposo, I. Fanget, C. Chapuis, G. Menasche, G. de saint Basile, C. Petit, S. Cribier, J.P. Henry and F. Darchen. 2003. Rab27A and its effector MyRIP link secretory granules to F-actin and control their motion towards release sites. *J. Cell Biol. 163*: 559–570.

Foissner, I. and G.O. Wasteneys. 2007. Wide-ranging effects of eight cytochalasins and latrunculin A and B on intracellular motility and actin filament reorganization in characean internodal cells. *Plant Cell Physiol. 48*: 585–597.

Fukuda, M., S. Hasezawa, N. Asai, N. Nakajima and N. Kondo. 1998. Dynamic organization of microtubules in guard cells of *Vicia faba* L. with diurnal cycle. *Plant Cell Physiol. 39*: 80–86.

Hardeland, R. 1982. Circadian-rhythms of bioluminescence in 2 species of *Pyrocystis* (Dinophyta). Measurements in cell-populations and in single cells. *J. Interdisc. Cycle Res. 13*: 49–54.

Hardeland, R. and P. Nord. 1984. Visualization of free-running circadian-rhythms in the dinoflagellate *Pyrocystis noctiluca. Mar. Behav. Physiol. 11*: 199–207.

Heimann, K., J.M. Matuszewski and P.L. Klerks. 2002. Effects of metals and organic contaminants on the recovery of bioluminescence in the marine dinoflagellate *Pyrocystis lunula* (Dinophyceae). *J. Phycol. 38*: 482–492.

Heuser, J. 1989. The role of coated vesicles in recycling of synaptic vesicle membrane. *Cell Biol. Int. Rep. 13*: 1063–1076.

Hill, K.L., N.L. Catlett and L.S. Weisman. 1996. Actin and myosin function in directed vacuole movement during cell division in *Saccharomyces cerevisiae*. *J. Cell Biol. 135*: 1535–1549.

Hugdahl, J.D. and L.C. Morejohn. 1993. Rapid and reversible high-affinity binding of the dinitroaniline herbicide oryzalin to tubulin from *Zea mays* L. *Plant Physiol. 102*: 725–740.

Kadota, A. and M. Wada. 1992. Photoorientation of chloroplasts in protonemal cells of the fern *Adiantum* as analyzed by use of a video-tracking system. *Bot. Magazine-Tokyo 105*: 265–279.

Kandasamy, M.K. and R.B. Meagher. 1999. Actin-organelle interaction: Association with chloroplast in *Arabidopsis* leaf mesophyll cells. *Cell Motil. Cytoskel. 44*: 110–118.

Kiseleva, E., S.P. Drummond, M.W. Goldberg, S.A. Rutherford, T.D. Allen and K.L. Wilson. 2004. Actin- and protein-4.1-containing filaments link nuclear pore complexes to subnuclear organelles in *Xenopus* oocyte nuclei. *J. Cell Sci. 117*: 2481–2490.

Knaust, R., T. Urbig, L.M. Li, W. Taylor and J.W. Hastings. 1998. The circadian rhythm of bioluminescence in *Pyrocystis* is not due to differences in the amount of luciferase: A comparative study of three bioluminescent marine dinoflagellates. *J. Phycol. 34*: 167–172.

Lahav, M., M. Abu-Abied, E. Belausov, A. Schwartz and E. Sadot. 2004. Microtubules of guard cells are light sensitive. *Plant Cell Physiol. 45*: 573–582.

Morejohn, L.C., T.E. Bureau, J. Molebajer, A.S. Bajer and D.E. Fosket. 1987a. Oryzalin, a dinitroaniline herbicide, binds to plant tubulin and inhibits microtubule polymerization *in vitro*. *Planta 172*: 252–264.

Morejohn, L.C., T.E. Bureau, L.P. Tocchi and D.E. Fosket. 1987b. Resistance of rosa microtubule polymerization to colchicine: Results from a low-affinity interaction of colchicine and tubulin. *Planta 170*: 230–241.

Nicolas, M.T., D. Morse, J.M. Bassot and J.W. Hastings. 1991. Colocalization of luciferin binding-protein and luciferase to the scintillons of *Gonyaulax polyedra* revealed by double immunolabeling after fast-freeze fixation. *Protoplasma 160*: 159–166.

Nicolas, M.T., G. Nicolas, C.H. Johnson, J.M. Bassot and J.W. Hastings. 1987a. Characterization of the bioluminescent organelles in *Gonyaulax polyedra* (Dinoflagellates) after fast-freeze fixation and antiluciferase immunogold staining. *J. Cell Biol. 105*: 723–735.

Nicolas, M.T., B.M. Sweeney and J.W. Hastings. 1987b. The ultrastructural localization of luciferase in 3 bioluminescent dinoflagellates, 2 species of *Pyrocystis*, and *Noctiluca*, using antiluciferase and immunogold labeling. *J. Cell Sci. 87*: 189–196.

Ovecka, M., I. Lang, F. Baluska, A. Ismail, P. Illes and I.K. Lichtscheidl. 2005. Endocytosis and vesicle trafficking during tip growth of root hairs. *Protoplasma 226*: 39–54.

Pickett, Heaps J.D. 1991. Postmitotic cellular reorganization in the diatom *Cymatopleura solea* – the role of microtubules and the microtubule center. *Cell Motil. Cytoskel. 18*: 279–292.

Samaj, J., N.D. Read, D. Volkmann, D. Menzel and F. Baluska. 2005. The endocytic network in plants. *Trends Cell Biol. 15*: 425–433.

Santos, B. and M. Snyder. 1997. Targeting of chitin synthase 3 to polarized growth sites in yeast requires Chs5p and Myo2p. *J. Cell Biol. 136*: 95–110.

Sato, Y., M. Wada and A. Kadota. 2001. Choice of tracks, microtubules and/or actin filaments for chloroplast photo-movement is differentially controlled by phytochrome and a blue light receptor. *J. Cell Sci. 114*: 269–279.

Seo, K.S. and L. Fritz. 2000. Cell ultrastructural changes correlate with circadian rhythms in *Pyrocystis lunula* (Pyrrophyta). *J. Phycol. 36*: 351–358.

Shurety, W., N.L. Stewart and J.L. Stow. 1998. Fluid-phase markers in the basolateral endocytic pathway accumulate in response to the actin assembly-promoting drug Jasplakinolide. *Mol. Biol. Cell 9*: 957–975.

Spector, I., N.R. Shochet, D. Blasberger and Y. Kashman. 1989. Latrunculins – novel marine macrolides that disrupt microfilament organization and affect cell-growth. 1. Comparison with Cytochalasin-D. *Cell Motil. Cytoskel. 13*: 127–144.

Spector, I., N.R. Shochet, Y. Kashman and A. Groweiss. 1983. Latrunculins – novel marine toxins that disrupt microfilament organization in cultured-cells. *Science 219*: 493–495.

Steidinger, K.A. and K. Tangen. 1997. Dinoflagellates. *In*: (C.R. Tomas, ed) *Identifying marine phytoplankton*. Academic Press, San Diego. pp 387–584.

Sweeney, B.M. 1980. The circadian rhythms in bioluminescence and organellar movements in the large dinoflagellate, *Pyrocystis fusiformis. Eur. J. Cell Biol. 22*: 495–495.

Sweeney, B.M. 1981. Control of the cell-cycle in *Pyrocystis fusiformis* by a circadian oscillator. *J. Cell Biol. 91*: A1-A1.

Sweeney, B.M. 1982. Microsources of bioluminescence in *Pyrocystis fusiformis* (Pyrrophyta). *J. Phycol. 18*: 412–416.

Swift, E. and G.T. Reynolds. 1968. Localization of bioluminescence in marine dinoflagellate *Pyrocystis lunula* Schütt using an image intensifier. *Biol. Bull. 135*: 439-&.

Swift, E. and W.R. Taylor. 1967. Bioluminescence and chloroplast movement in the dinoflagellate *Pyrocystis lunula. J. Phycol. 3*: 77–81.

Tanaka, I. 1991. Microtubule-determined plastid distribution during microsporogenesis in *Lilium longiflorum*. *J. Cell Sci. 99*: 21–31.

Tilney, L.G., P.S. Connelly, K.A. Vranich, M.K. Shaw and G.M. Guild. 2000. Actin filaments and microtubules play different roles during bristle elongation in *Drosophila*. *J. Cell Sci. 113*: 1255–1265.

Topperwien, F. and R. Hardeland. 1980. Free-running circadian-rhythm of plastid movements in individual cells of *Pyrocystis lunula* (Dinophyta). *J. Interdisc. Cycle Res. 11*: 325–329.

Walch-Solimena, C., R.N. Collins and P.J. Novick. 1997. Sec2p mediates nucleotide exchange on Sec4p and is involved in polarized delivery of post-Golgi vesicles. *J. Cell Biol. 137*: 1495–1509.

Widder, E.A. and J.F. Case. 1982. Distribution of sub-cellular bioluminescent sources in a dinoflagellate, *Pyrocystis fusiformis. Biol. Bull. 162*: 423–448.

10 Algal cell biology – important tools to understand metal and herbicide toxicity

Kirsten Heimann

Introduction

Light emission is an easily quantifiable parameter which enables quantification of effects of photosystem II inhibiting herbicides using PAM (pulse amplitude modulated) fluorometry e.g. (Magnusson et al. 2008) or metal and other pollutants (including herbicides) effects on the bioluminescent response system of marine dinoflagellates and bacteria (*Vibrio* spp) (Craig et al. 2003; Heimann et al. 2002; Okamoto et al. 1999; Parvez et al. 2006). Therefore, and because the assays fulfill the criteria of toxicity tests, such as ease of handling, rapid and reliable data acquisition and cost saving, both methodologies are being used increasingly in environmental monitoring and in ecotoxicology as toxicity tests (Heimann et al. 2002; Parvez et al. 2006). Toxicity of photosynthesis inhibiting pollutants is recorded as an increase in chlorophyll fluorescence and a decrease in effective quantum yield when using PAM fluorometry (Magnusson et al. 2008), while pollutants that inhibit the bioluminescent reaction are recorded as a decrease in luminescent light output (Craig et al. 2003; Heimann et al. 2002). This chapter will not report on or summarise ecotoxicolgical experiments using either PAM or bioluminescence, rather the intent is to elucidate how knowledge of bioluminescent pathways and the regulation thereof can be used to make inferences of the mechanism of action of pollutants. For this purpose the bioluminescent system of the marine dinoflagellate *Pyrocystis lunula* will be used as a model and its bioluminescent system as well as its regulation is briefly described below.

The bioluminescent system of *Pyrocystis lunula*

Bioluminescence is under circadian control in photosynthetic dinoflagellates (see Chapter 9), with bioluminescence being down-regulated upon exposure to light and re-established at night. Bioluminescence of *Pyrocystis lunula* and other bioluminescent dinoflagellates require vacuolar association of the scintillons (non-membranous "flashing units"; (Nicolas et al. 1987)) at the cell periphery in night phase cells (Figure 10.1).

Mechanically-inducible bioluminescence in dinoflagellates requires association of the scintillons with the vacuole (Figure 10.1). This association is described in the "proton trigger" model, where a mechanical stimulus leads to action potentials at the tonoplast (Nicolas et al. 1991; Nicolas et al. 1987) (see also Chapter 9). Briefly, a stimulus, such as for example mechanical (touch) or shear stress, is received at the plasma membrane, which is then transmitted to the cell's interior and ultimately the tonoplast of the acidic vacuole *via* yet to be identified receptors and signal transductions pathways. For bioluminescence to occur, it is essential that scintillons, which contain the vital

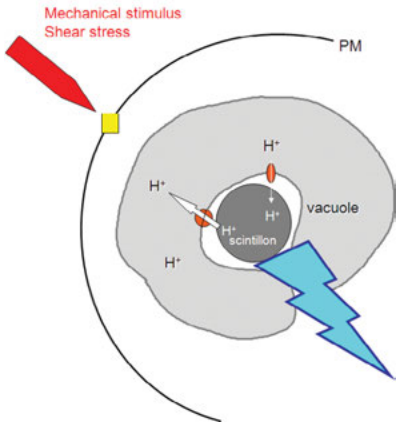

Figure 10.1 Schematic presentation of the bioluminescent mechanism (proton trigger model) in *Pyrocystis lunula*.

components for the bioluminescent reaction (the enzyme luciferase and the substrate (luciferin)), are in close proximity to the acidic vacuole, almost completely enveloped by the tonoplast, which is only the case in night phase cells (see Chapter 9). Transduction of the stimulus leads to acidification of the scintillon via proton channels allowing protons to flow from the higher concentration in the vacuole to the lower concentration in the scintillon, activating the scintillon-associated enzyme luciferase (an oxygenase with an acidic pH optimum). The luciferase oxidizes the substrate luciferin which leads to the emission of light (Knaust et al. 1998). The bioluminescent light is emitted in the blue spectrum of the visible light in marine dinoflagellates (Figure 10.2), as blue light penetrates the furthest in the ocean (Hastings and Johnson 2003). The bioluminescent reaction is terminated when the scintillon pH is returned to neutral or slightly basic conditions through actively pumping protons against the concentration gradient back into the vacuole. The return to neutral or basic conditions renders the enzyme luciferase inactive and terminates the bioluminescent light output.

Dissecting the signal transduction pathway for mechanically-activated bioluminescence in *Pyrocystis lunula*

Signaling molecules

Calcium

Calcium has been shown to act as a second messenger in diverse signal transduction cascades from microaglae to mankind (Bogeski et al. 2011; Ganesan and Zhang 2012; Hashimoto and Kudla 2011; Mazars et al. 2011; Rudolf et al. 2012; Thurley et al. 2012 and references therein). Calcium signaling is also involved in many and varied responses to touch. For example, calcium mediates wound and touch responses in maize through interacting with calcium-dependent kinases (CDKs), which are part of the signaling

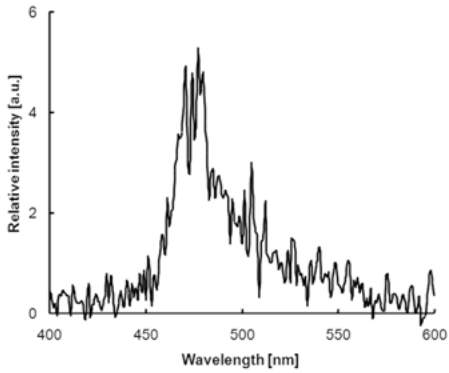

Figure 10.2 Wavelength (nm) scan of bioluminescence in *Pyrocystis lunula*. Bioluminescence was activated with 1% acetic acid and the wavelength scan was conducted in a 1 cm cuevette using a luminometer (Varian Eclipse) from 400 to 600 nm. Luminescence is reported as relative intensity in arbitrary units (a.u.).

cascade in the jasmonate signaling pathway (Szczegielniak et al. 2012). In general, calcium-mediated cell signaling has been exceptionally well studied in plants, particularly with regards to touch responses (for recent reviews see Braam 2005; Chehab et al. 2009; Fasano et al. 2002; Gillespie and Muller 2009; Li and Gong 2011; Monshausen and Gilroy 2009; Sachs 1991). In contrast, calcium signaling in algae has been poorly investigated, mainly in the context of negative and positive phototactic responses (e.g. Alvarez et al. 2012; McLachlan et al. 2012; Wakabayashi et al. 2011), flagellar excision (e.g. Goedhart and Gadella 2004; Wheeler et al. 2008), gravity sensing and polarized growth (e.g. Braun and Limbach 2005; Braun and Limbach 2006), exudates secretion (Quesada et al. 2006), action potential generation (Beilby 2007) and binding to calcium-binding proteins, for example the basal body connector associated protein centrin (Radu et al. 2010). There are very few publications for touch-induced calcium signaling in algae. For example, touch elicited an avoidance reaction in the green flagellate *Spermatozopsis similis*. Here touch induced an anterior inflow of calcium which changed the flagella-driven forward directed breast stroke and pulling motility to an undulating beat pattern resulting also in flagella reorientation through calcium interaction with the striated basal body connector, resulting in flagella now pushing the cell in the opposite direction (Kreimer and Witman 1994). Calcium has been shown to enter cells *via* voltage-gated calcium channels in response to touch in zebrafish (Low et al. 2012) and many other plant and animal systems (for recent reviews see Bhatla and Kalra 2004; Blatt 2000; Casamassima et al. 2010; Johannes et al. 1991; Krol and Trebacz 2000; Obermair et al. 2008; Pottosin and Schnknecht 2007; Verret et al. 2010; Walter and Messing 1999; Weiergraber et al. 2008; Weiergraber et al. 2006) and in algae e.g. (Verret et al. 2010; Wheeler and Brownlee 2008).

Protein kinase C

Protein kinase C (PKC) is a family of various isoforms and PKC is known to be an important signal transducer (for recent review see Silva et al. 2012). Conventional PKC isoforms (α, $ß_I$, $ß_{II}$, and γ) are activated by calcium, diaacylglycerol (DAG) and

phospholipids, e.g. phosphatidylserine, while novel PKCs (δ, ε, η, θ) are activated by DAG but not calcium and atypical PKCs (ι, λ and PKM ζ) are neither activated by calcium nor DAG (Silva et al. 2012). It has been suggested that PKCs are recruited to the plasma membrane *via* RACK proteins (Adams et al. 2011) and that conventional PKCs remain active after the initial signal, the calcium wave, has subsided. The signal is prolonged and amplified by PKCs presumably through production of DAG from phosphatidylinositol by phospholipase C (Silva et al. 2012). PKCs exert their regulatory action by phosphorylating hydroxyl groups of the amino acids serine and threonine and the have been implicated in a wide array of functions, such as receptor desensitization, modulation of plasma membrane structure and regulations of transcription and cell growth (Silva et al. 2012), all of which could play a role in the regulation of bioluminescence in *Pyrocystis lunula*.

G proteins

Monomeric and heteromeric G-proteins (GTPases) are also known to participate in signal amplification and transmission (for recent reviews see Gloerich and Bos 2011; Hewavitharana and Wedegaertner 2012). Importantly, it has been shown that Mastoparan treatment can activate phopholipase C in *Chlamydomonas* (Arisz et al. 2003; Kuin et al. 2000; van Himbergen et al. 1999) and therefore treatment of *Pyrocystis lunula* with Mastoparan could enhance the bioluminescent signal via the PKC-PLC signaling pathway (Kukkonen 2011; Li 2011) see above, particularly since some G-proteins have been shown to participate in signaling cascades for chemotaxis (Wang et al. 2011b).

Signal enhancing and interrupting drugs

Calcium ionophores, calcium channel blockers, competing ions and calcium chelators

Several drugs have a known and specific interaction with components of signal transduction cascades (for recent reviews see Doering and Zamponi 2003; Kania 2005). The antibiotic calcimycin, A23187, a calcium ionophore has long been used to document calcium signaling in diverse biological systems (Entman et al. 1972; Reed and Lardy 1972; Wong et al. 1973). While A23187 also transports magnesium, which is another bivalent ion involved in cell signaling (Alatossava 1988; Hand et al. 1977; Jeacocke 1993; Marinetti et al. 1993; Tissier et al. 1993; Zhang et al. 1995), its affinity for calcium is an order of magnitude greater. The calcium channel blocker Verapamil has been used extensively to study calcium channel mediated responses in algae (Alexandrov et al. 1990; Ermilova et al. 1998; Harz and Hegemann 1991; Love et al. 1997; Maier and Calenberg 1994) and Lanthanum, a cation that interferes with calcium binding through competitive interactions with calcium (Jencks and Fujimori 1990; Weiss 1973) have also been used extensively to delineate calcium-mediated processes from other ion-regulated ones (Weiss 1973). In addition, EGTA (ethylene glycol tetraacetic acid) is a bivalent cation chelator with a higher affinity for calcium over magnesium (Bett and Rasmusson 2002) and is therefore well suited to validate results obtained with calcium ionophores and voltage-gated calcium channel inhibitors.

G-protein and protein kinase C activity modulators

In attempting to dissect the signal transduction cascade, several drugs were used that interfere specifically with calcium-mediated signaling, G protein involvement and protein kinase C (PKC) mediated pathways. All of these components have been described to be able to interact with each other in specific cell signaling events (Kukkonen 2011; Li 2011).

Mastoparan is a toxin present in wasp venom, which interferes with G-protein (GTPases) mediated signaling and regulatory pathways (Higashijima et al. 1988). Mastoparan also interacts with the monomeric G-proteins Rho and Rac (Koch et al. 1991), which are part of the Ras G-protein family (Bustelo et al. 2007). Rho and Rac are known to regulate actin dynamics and they have been found to occur in all eukaryotic systems, including plants and algae (Boureux et al. 2007; Bustelo et al. 2007), which is of interest with regard to the actin dependence of scintillon movement (see Chapter 9). In particular, since establishment and likely down-regulation of bioluminescence in *Pyrocystis lunula* involves the actin cytoskeleton (see Chapter 9), effects of Mastoparan on bioluminescence would shed a light on the involvement of the monomeric G-proteins Rac and Rho.

Bisindolylmaleimide (BIM) is a well-known inhibitor of protein-kinase C (PKC) regulated pathways (Cartee et al. 2002; Komander et al. 2004) and inhibits PKC activity through competitive binding at the ATP binding site required for phosphorylating downstream proteins (Baldo et al. 1995). However, given the various PKC isoforms, it is difficult to select a specific inhibitor for a specific isoform (Nakamura et al. 2000; Son et al. 2011; Sridhar and Pattabiraman 2005). The PKC inhibitor BIM was chosen, as it is highly specific for conventional PKCs and has an inhibitory concentration of these PKCs of only 14 nM (Toullec et al. 1991). Furthermore, BIM inhibits conventional PKCs (Toullec et al. 1991), which are regulated by calcium (see above), an ion suspected to be first in line for transducing the mechanical stimulus that elicits the bioluminescent response. In contrast, phorbol 12-myristate 13-acetate (PMA) is a potent and specific protein activator of PKC (Baldo et al. 1995) and was used to ascertain conventional PKC involvement in transducing the mechanical stimulus to elicit the bioluminescence response in *P. lunula*.

Effects of calcium, G-protein and PKC modulating drugs on the bioluminescent output of *Pyrocystis lunula*

Calcium modulating drugs

Bioluminescence-competent night phase cells of *Pyrocystis lunula* were incubated in 12.5 to 50 µM of the calcium ionophore A23187 or 0.25–1% of DMSO (dimethylsulfoxide), the carrier solvent for the ionophore (Figure 10.3A). The maximal bioluminescent response was recorded immediately over the time course of 10 min. To investigate the effects of calcium signal interfering drugs, day phase cells of *P. lunula* were incubated with the voltage-gated calcium channel blocker Verapamil, the calcium-competing ion Lanthanum and EGTA at concentrations of 0–50 mM and 0–40 mM, respectively (Figure 10.3B) and 2.5 mM EGTA, 2.5 mM calcium – 2.5 mM EGTA and 5 mM calcium – 5 mM EGTA (Figure 10.3C) four hours prior to the transition to the night phase. For these

experiments, bioluminescence was mechanically-induced and recorded for 1 min. All experiments were independently repeated three times and standard error (SE) is shown.

The calcium ionophore A23187 stimulated bioluminescent output without mechanical activation in a dose-dependent manner and almost to the full potential of mechanically-inducible bioluminescence (Figure 10.3A) suggesting that calcium could be involved

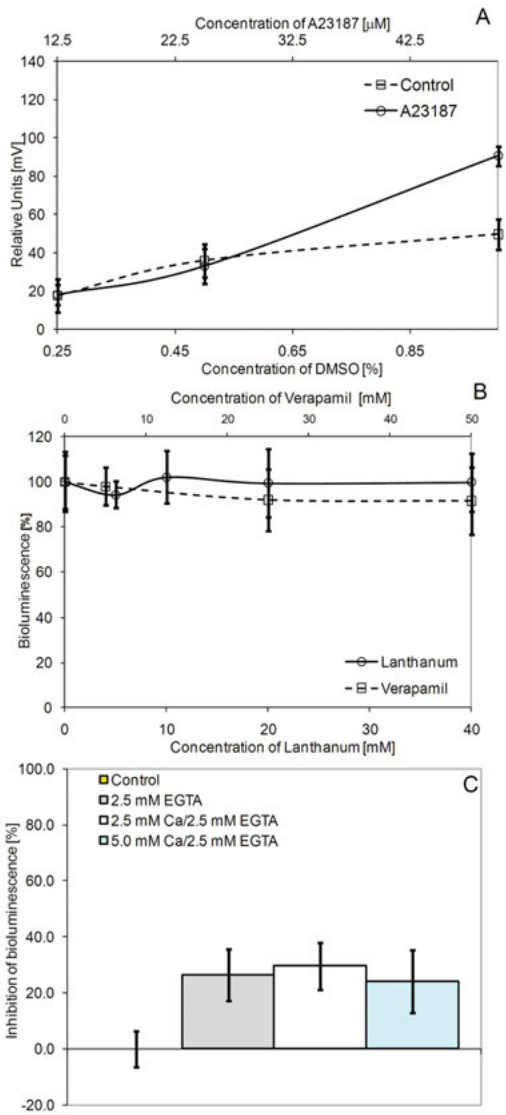

Figure 10.3 Effect of calcium signaling modulating drugs on bioluminescence in *Pyrocystis lunula*. A. Dose-response effects of the calcium ionophore A23187 and the carrier solvent DMSO (dimethyl sulfoxide); B. Dose-response effects of calcium channel blockers Verapamil and Lanthanum; C. Dose-response effect of the bivalent cation chelaator EGTA; n = 3 ± SE.

in transducing the mechanical stimulus that leads to the bioluminescent response in *P. lunula*. However, far higher concentrations than those reported in the literature were required to elicit this response, which could be the result of the cell wall acting as a barrier and preventing efficient interaction. For example, it was shown that nano molar concentrations of A23187 increased the calcium permeability in rabbit mesenteric arteries (Itoh et al. 1985). The same study also demonstrated that intracellular calcium stores were more sensitive to A23187 than the surface of the artery, as higher calcium permeability was recorded. Few studies have used the ionophore A23187 to investigate calcium-mediated cell signaling in algae. It was shown in the green alga *Micrasterias* that A23187 treatment led to detectable calcium gradients within the cells (Holzinger et al. 1995), hence sterical hindrance by the presence of a cellulose wall seems unlikely. In addition, using A23187 it was demonstrated that calcium is involved in photomovement of the cyanobacterium *Synechocystis* (Moon et al. 2004) and treatment of *Lemna* with A23187 in the dark under high external calcium did mimic blue light-induced chloroplast movements (Tlalka and Fricker 1999).

The carrier solvent DMSO, used for dissolving the ionophore, only stimulated bioluminescence by maximally 30% at the highest dosage (1%) used (Figure 10.3A). This stimulation was most likely due to permeabilising effects on the plasma membrane of *P. lunula*, allowing for either calcium influx from the medium or for acidification of the scintillons from either internal or external sources. This may be unlikely though, as it has been shown that concentrations of DMSO as used here did not change plasma membrane permeability in cell suspension cultures of *Taxus cuspidatus* (Wang et al. 2011a) and in contrast to these suspension cells, *P. lunula* is protected by a thick cellulose wall, which is hard to penetrate (Swift and Remsen 1970). It is equally possible that the slight reduction of the bioluminescent output in cells treated with DMSO is independent of the solvent, as spontaneous bioluminescent flashes without the need for mechanical activation have been reported in marine dinoflagellates including *P. lunula* (Biggley et al. 1969).

In contrast to the positive response of bioluminescence to treatment with A23187, the calcium channel blocker Verapamil, the calcium-competing ion Lanthanum and the bivalent cation chelator EGTA exhibited little effect on mechanically-inducible bioluminescence in *P. lunula*, inhbiting bioluminescence by only 10%, not at all, or by 20%, respectively (Figures 10.3B–C). In addition, only a weak dose-response was recorded for the Verapamil treatment and none was evident for Lanthanum (Figure 10.3B) and no effect of calcium in the calcium/EGTA treatments was observed (Figure 10.3C). These data seem to suggest that calcium is likely to play a minor role in transducing the mechanical stimulus and that results obtained for treatment with A23187 may be due to unspecific interactions. It was, however, reported that Verapamil binds to membrane fractions of the green algal flagellate *Chlamydomonas rheinhardtii* (Dolle and Nultsch 1988). It is interesting to note that membrane fractions were used to study the binding of calcium channel blockers, which might suggest that these drugs could have problems diffusing through the cell walls, which is required for interaction with the calcium channels in the plasma membrane. While it is also potentially possible that algal calcium channels may differ from mammalian ones (calcium channel blockers were developed for animal cells to study the prevention of illness and disease), the binding study on *Chlamydomonas* would suggest that sufficient similarity remained for specific binding to occur. Indeed calcium channels have been detected in algae and plants and it has been demonstrated that they do not differ significantly from animal ones (Johannes et al. 1991).

Effects of G-protein and protein kinase C modulators

Bioluminescent-competent night phase cells were treated with Mastoparan, a G-protein binding wasp venom, the PKC inhibitor BIM and the PKC activator PMA (Figure 10.4). Mastoparan stimulated bioluminescence in *P. lunula* by almost 100% over control bioluminescence up to a concentration of 20 mM, while higher concentrations were less effective (Figure 10.4A). In contrast, the conventional PKC inhibitor BIM showed only a modest dose-dependent effect with inhibition of maximally 20% (Figure 10.4A). Similarly, activation of conventional PKC with PMA only increased bioluminescence by 20% (Figure 10.4B).

Other than interacting specifically with heteromeric and monomeric G-proteins, Mastoparan also has an effect on calcium- and calcium/potassium regulated events (Glavinovic et al. 1992; Yule and Williams 1991), phosphoinositide-regulated cellular events (Nakahata et al. 1990) and inositol phospholipid metabolism, the latter resulting in flagella abscission in *Chlamydomonas rheinhardtii* (Quarmby et al. 1992). Futhermore, release of arachidonic acid via phosphoinositide-independent pathways upon Mastoparan treatments have also been observed (Gil et al. 1991), as have been effects that are known to

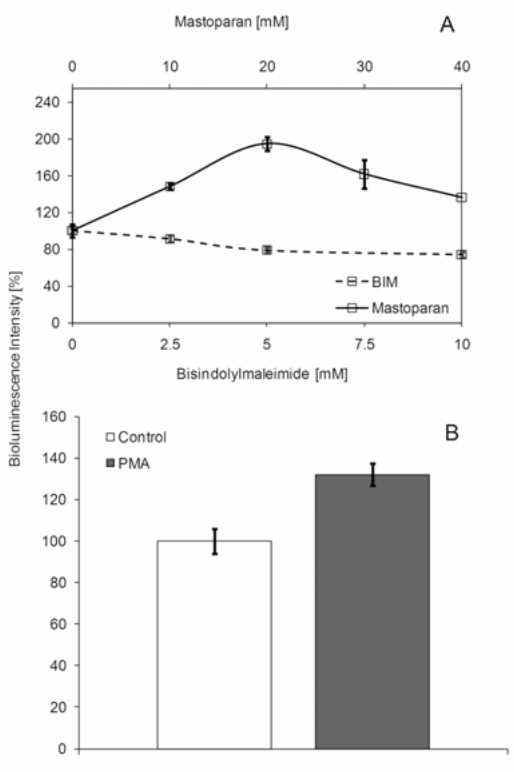

Figure 10.4 Effects of G-protein and protein kinase C modulating drugs on bioluminescence in *Pyrocystis lunula*. A. Dose-reponse effects of the G-protein binding drug Mastoparan and the conventional PKC inhibitor bisindolylmaleimide (BIM); B. Effect of the PKC activator phorbol 12-myristate 13-acetate (PMA); n = 3 ± SE.

be G-protein-independent by simply increasing membrane permeability (Tanimura et al. 1991). Few studies have actually used Mastoparan to dissect signaling pathways in algae and all have been carried out using *Chlamydomonas*. In *Chlamydomonas*, Mastoparan treatment activates the phospholipases C and D (Arisz et al. 2003; Kuin et al. 2000; van Himbergen et al. 1999) and phospholipasee C activity has been shown to mobilize intracellular calcium stores (Kuin et al. 2000).

In the context of the tight linkage of phospholipase C and protein kinase C activity (Kukkonen 2011; Li 2011), it is interesting to note that a stronger response to either the PKC inhibitor BIM or the activator PMA would have been expected, at least to similar effects as Mastoparan, as these signaling cascades can be tightly linked. Given the multitude of interactions of Mastoparan with independent and/or different aspects of signaling pathways, results obtained with Mastoparan cannot pinpoint to a specific component of a signaling pathway and its specific effect on G-protein mediated pathways need to be further corroborated using other drugs that target another part of signaling cascades.

In conclusion, the effects of the calcium ionophore A23187 and Matoparan suggest that the mechanical stimulus which elicits bioluminescence in *Pyrocystis lunula* is calcium-mediated and amplified by G-proteins. However, the relatively minimal response to the calcium channel blocker Verapamil and EGTA, as well as the lack of effect of Lanthanum casts doubt on the involvement of calcium as a signal transducer in mechanically-stimulated bioluminescence in *P. lunula*. Similarly, Mastoparan has been shown to have a plethora of interactions with multitudes of different signaling cascades, essentially all those which are at least in one aspect regulated by G-proteins, and hence the positively stimulating effect on bioluminescence requires further investigation. Caution in interpreting the Mastoparan result is warranted, as the conventional PKC inhibitor BIM and activator PMA had only little effects. As G-protein signaling is often coupled with protein kinase and/or phospholipase regulation/signal amplification, an equally strong bioluminescent response to BIM and PMA compared to Mastoparan would have been more convincing. In addition, the low response to treatment with BIM and PMA does not suggest that conventional protein kinase C and/or phospholipases are involved in transducing the mechanical stimulus in the bioluminescent *P. lunula*.

Use of heavy metals and spontaneous bioluminescent flash responses to elucidate regulation and signal transduction of the mechanical stimulus in *Pyrocystis lunula*

Two modes of bioluminescence exist in *Pyrocystis lunula*: (1) a mechanical stimulus induced bioluminescent response and (2) random spontaneous flashes that occur without mechanical activation (Biggley et al. 1969). Previous dose-response and time-course experiments established that the heavy metals cadmium, copper, lead and nickel (Heimann et al. 2002) and the detergent reference toxicant sodium dodecyl suphate (SDS) (Craig et al. 2003) inhibit mechanically-inducible bioluminescence in *Pyrocystis lunula*. To investigate the potential reason for the inhibition of mechanically-inducible bioluminescence, previously established IC_{50} concentrations (concentration that leads to 50% inhibition) (Table 10.1) were used and the effect on spontaneous bioluminescence was investigated by measuring flash intensity and frequency using a Varian Eclipse bioluminometer and bioluminescent-competent night phase cells of *Pyrocystis lunula*.

Table 10.1 Four hour inhibitory concentrations [μM] of 50% (IC_{50}) of metal pollutants and the reference toxicant SDS.

Pollutant	4 h IC_{50}
Cadmium	1.18 ± 0.07
Copper	0.96 ± 0.08
Lead	12.8 ± 5.83
Nickel	73.1 ± 6.73
SDS	15.6 ± 0.058

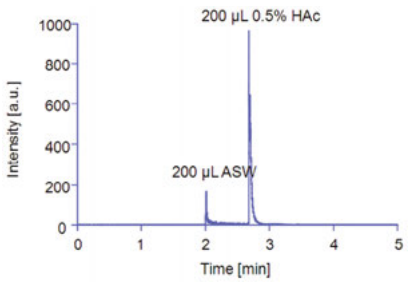

Figure 10.5 Effect of addition of artificially filtered seawater (ASW) and 0.5% acetic acid (HAc) on bioluminescent flash responses in *Pyrocystis lunula*.

To account for the possible excitation of bioluminescence through addition of liquids to bioluminescent-competent night phase cells of *P. lunula* and to distinguish between mechanical and spontaneous bioluminescence, filtered seawater was added to 1000 cells as controls and 0.5% acetic acid (HAc) was added as the maximally inducible bioluminescence (Figure 10.5). In a ten minute time course, the addition of filtered seawater elicited a single bioluminescent flash, as did the addition of HAc, albeit with a 5 times increased amplitude and no changes in flash frequency (Figure 10.5). These results indicate that it was possible to differentiate between spontaneous and mechanically-induced bioluminescence in time-course experiments.

Filtered seawater was added to bioluminescent-competent night phase cells to serve as random flash controls (Figures 10.6A–E) and with copper, cadmium, lead, nickel and SDS (Figures 10.6F–J) as per Table 10.1 and the spontaneous bioluminescence was recorded for 10 min measuring amplitude and flash frequency. Spontaneous bioluminescent flashes were rare to evenly spaced with a moderate amplitude in controls (Figures 10.6A–E), while heavy metal and SDS treatment resulted in a dramatic increase in flash frequency with amplitudes being at least two times in the case of copper (Figure 10.6G) to three times higher for all other treatments (Figures 10.6G–J) compared to controls. This indicates that reduction in spontaneous bioluminescence due to toxicant treatment could be the result of exhaustion of the bioluminescent potential of *P. lunula*, which is feasible, given that cells are being incubated for 4 h prior to photoperiod transition and need to establish their bioluminescent potential in the presence of these toxicants (Heimann et al. 2002).

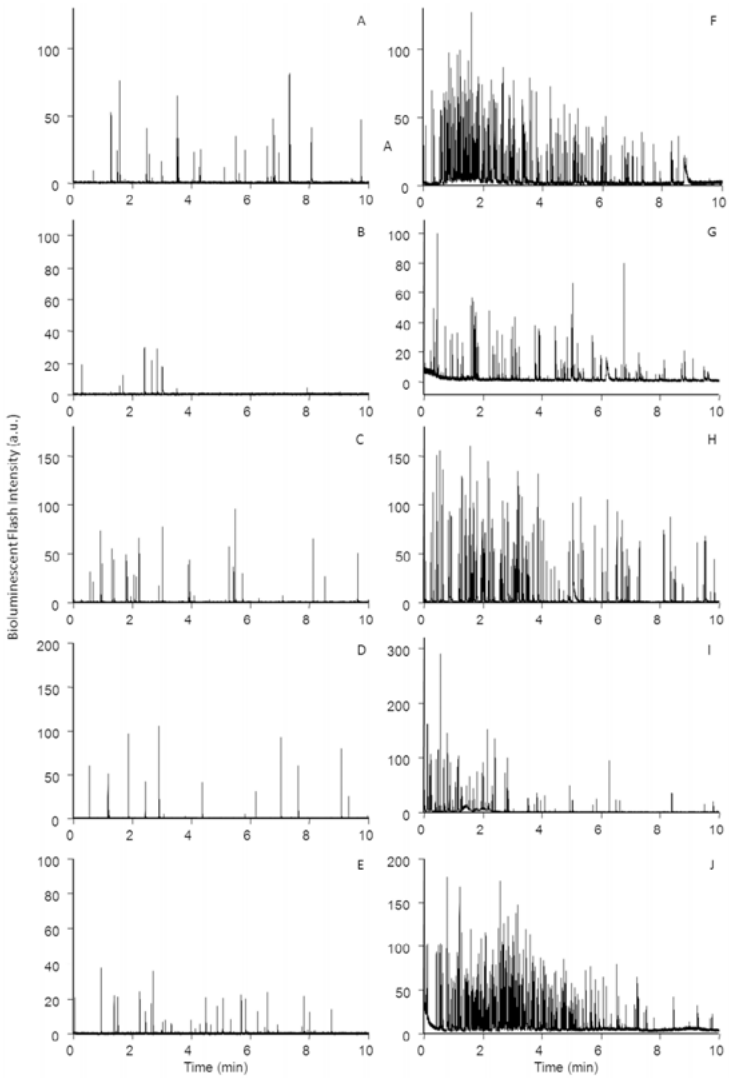

Figure 10.6 Effects of filtered seawater, heavy metals and sodium dodecyl sulfate (SDS) on spontaneous bioluminescence in *Pyrocystis lunula*. (A–E) Bioluminescent flash frequency and amplitude in controls treated with the addition of filtered seawater; (F–J) Bioluminescent flash frequency and amplitude in heavy metal and SDS treatments as per Table 10.1; F: copper, G: cadmium, H: lead, I: nickel and J: SDS. These time-course experiments shown are representative effects of five independent replicates.

Cellular mechanisms for metal toxicity are relatively well studied. In general, many metals in particular lead have been shown to elicit genotoxic effects, through either replacing zinc or other essential cofactors in important proteins or through directly intercalating with DNA causing DNA-defects and bulging for recent review see (Lima et al. 2011). However, genotoxic effects, although demonstrated for *Pyrocystis lunula* for

lead and nickel, as mechanically-inducible bioluminescence did not recover within 72 h (Heimann et al. 2002), cannot explain the immediate and dramatic increase in spontaneous bioluminescent flashes, as shown here, as DNA damage is a function of metal exposure and time. Furthermore, some metals, such as zinc, have been shown to interact with voltage-gated monomeric and dimeric proton channels (Musset et al. 2010), resulting in their inactivation. If such proton channels were present in the tonoplast (Figure 10.1), however, metal treatment should result in a decrease in spontaneous bioluminescent flashes. Many heavy metals have also been shown to form reactive oxygen species (ROS) and redox signaling functions of these highly reactive ROS (hROS) have been demonstrated (for recent review see Freinbichler et al. 2011). The potential for metal ions to induce fast redox signaling would fit with the spontaneous bioluminescent time response observed here. Also, the enzyme luciferase is a rather unspecific oxygenase (Hastings and Johnson 2003) and the interaction of this enzyme with ROS should be further investigated. In any case, metal treatment must change the pH in the vicinity of the scintillons to a pH below 7 for the enzyme luciferase to be activated. The strong response to SDS treatment demonstrates fully active luciferase, as the detergent breaks down membranes enabling the acidification of the scintillons. It is hence not surprising that highest spontaneous bioluminescence was recorded in SDS treatments.

Can the biosynthetic origin of *Pyrocystis lunula* luciferin be unraveled using a herbicide that interferes with the chlorophyll biosynthetic pathway?

Anecdotal evidence based on the similarity between the tetrapyrrole head of chlorophyll and the open tetrapyrrole of dinoflagellate luciferin (Schultz et al. 2005) (Figure 10.7) suggests that dinoflagellate luciferins are a degradation product of chlorophylls. The herbicide oxyfluorfen (a diphenyl ether) has a history in commercial use for controlling of certain annual broadleaf and grassy weeds in farmlands (Samtani et al. 2012). Oxyfluorfen inhibits protoporphyrinogen IX oxidase (Figure 10.8), the enzyme that catalyses the last common step in the tetrapyrrole synthesis pathway before differentiating into separate chlorophyll and haem pathways (Jung 2011; Lermontova and Grimm 2000). The inhibition of this step potentially results in an accumulation of protoporphyrinogen IX (as occurred in *Chlamydomonas reinhardtii* (Hallahan et al. 1992)) and blocks all subsequent steps in the branching pathways, resulting in inhibition of chlorophyll and haem synthesis (Lermontova and Grimm 2000).

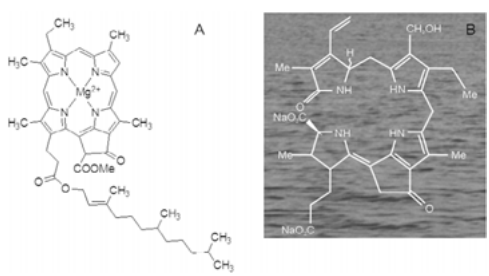

Figure 10.7 Structural similarity between chlorophyll (A) and the luciferase substrate luciferin (B).

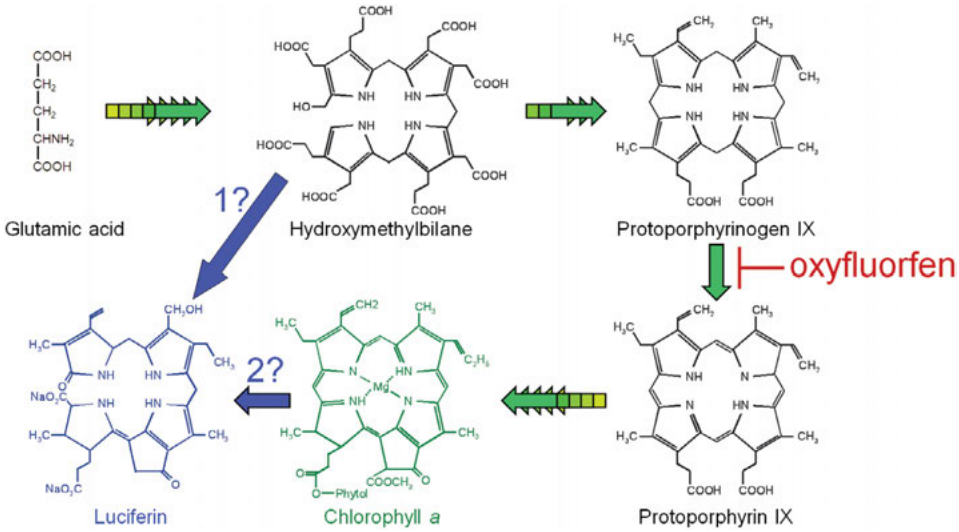

Figure 10.8 Two conceptual pathways for the origin of luciferin from the chlorophyll biosynthetic pathway. Number of arrow heads indicates number of steps omitted in the synthesis pathway. The location of action of oxyfluorfen is indicated.

To investigate the anecdotal evidence that dinoflagellate luciferin is a degradation product of chlorophyll, dose-response, time-course and recovery experiments were conducted to evaluate the effect of oxyfluorfen on mechanically-inducible bioluminescence in *Pyrocystis lunula*.

Oxyfluorfen concentrations (0–2,400 µg L^{-1}) were prepared in DMSO as a carrier solvent and concentrations of DMSO did not exceed 1% (see above). Four hours before photoperiod transition to the night phase, 100 cells of *P. lunula* were treated with oxyfluorfen while controls received the carrier solvent DMSO. Mechanically-inducible bioluminescence was measured 4, 28, 52 and 172 h after dosing with the herbicide. Mechanically-inducible bioluminescence of *P. lunula* was inhibited in a dose- and time-dependent manner exhibiting the classical sigmoidal curve fit (Figure 10.9) and treatments after 52 h of exposure did only recover slightly after exchange with uncontaminated medium after 172 h (Figure 10.10). IC_{50} concentrations were 378 ± 37, 242 ± 30.4 and 102 ± 56.9 µg oxyfluorfen L^{-1} ± SE and an IC_{50} could not be calculated for 4 h incubations, as insufficient inhibition was attained (Figure 10.9). To evaluate whether the inhibition of mechanically-inducible bioluminescence could be due to luciferin limitation, luciferin autofluorescence was measured with an excitation of 300 nm and an emission of 482 nm (Figure 10.11), as was chlorophyll autofluorescence (excitation 430 nm, emission 685 nm (data not shown)) on a Varian Eclipse fluorometer. There was no difference in either luciferin or chlorophyll autofluorescence between controls and treatments of *P. lunula* at 2,400 µg oxyfluorfen L^{-1}, suggesting that the inhibition of bioluminescence is not mediated by blocking the chlorophyll biosynthetic pathway or through chlorophyll degradation (Figure 10.8).

In conclusion, the herbicide oxyfluorfen is highly toxic to *Pyrocystis lunula*, but the mechanism of cytotoxicity does not appear to be mediated through blocking of

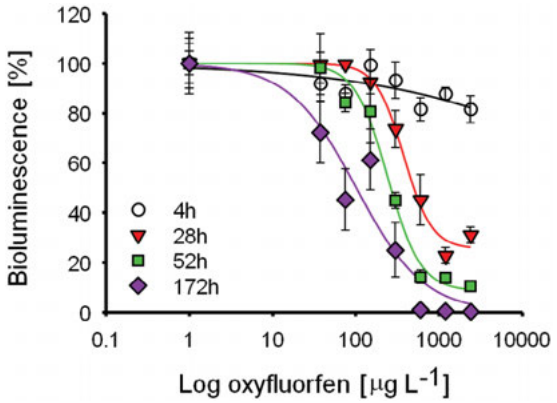

Figure 10.9 Dose-response and time-course results on the effect of oxyfluorfen on mechanically-induced bioluminescence in *Pyrocystis lunula*.

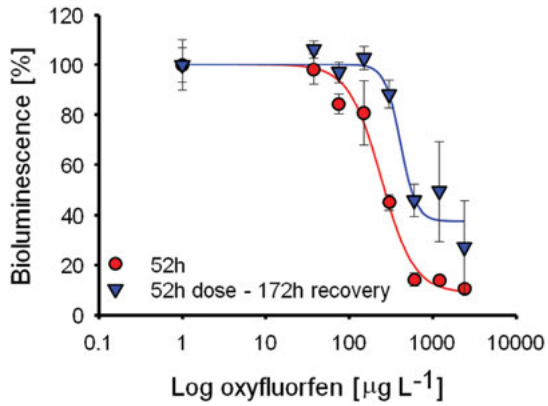

Figure 10.10 Effect of 52 h-oxyfluorfen treatment and 172 h recovery on mechanically-induced bioluminescence in *Pyrocystis lunula*.

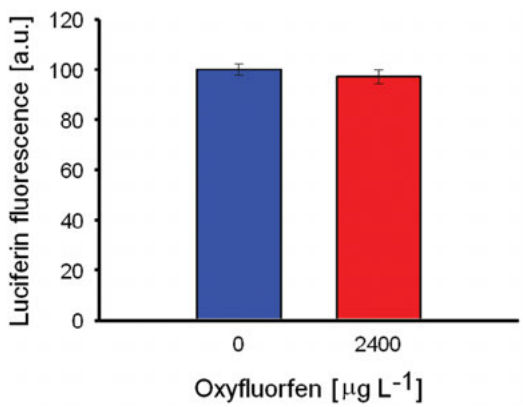

Figure 10.11 *Pyrocystis lunula* luciferin autofluorescence in control and 172 h oxyfluorfen treatment.

the chlorophyll biosynthetic pathway, as no difference in chlorophyll or luciferin autofluorescence was evident. No other mechanism for oxyfluorfen toxicity has been described to date, thus to unravel the mechanism by which oxyfluorfen inhibits mechanically-inducible bioluminescence remains to be elucidated. The origin of luciferin could not be established using oxyfluorfen, as its extreme cytotoxicity in *P. lunula* did not allow for longer experiments. Such experiments would be required to be able to correlate chlorophyll degradation with luciferin increase and *vice versa* (Figure 10.8, option 2). It is equally possible that luciferin is the result of an overproduction of a component in the chlorophyll biosynthetic pathway, if other enzymes downstream are rate limiting (Figure 10.8, option 1), a hypothesis that cannot be ruled out at present.

Acknowledgements

This research was funded by grants from James Cook University (Merit Research Grant) to KH. I am also grateful to Laura Smith, who performed part of the oxyfluorphen toxicity study as a special research component of her BSc at James Cook University.

References

Adams, D.R., D. Ron and P.A. Kiely. 2011. RACK1, A multifaceted scaffolding protein: Structure and function. *Cell Com. Signal. 9*.

Alatossava, T. 1988. Effects of cellular calcium and magnesium content on growth of ionophore A23187-treated *Lactobacillus lactis. Agri. Biol. Chem. 52*: 1275–1276.

Alexandrov, A.A., L.A. Alexandrova and G.N. Berestovsky. 1990. Bock of Ca^{2+} channel from algae cells reconstituted in planar lipid bilayer by Verapamil. *Studia Biophys. 138*: 127–130.

Alvarez, L., L. Dai, B.M. Friedrich, N.D. Kashikar, I. Gregor, R. Pascal and U.B. Kaupp. 2012. The rate of change in Ca^{2+} concentration controls sperm chemotaxis. *J. Cell Biol. 196*: 653–663.

Arisz, S.A., F. Valianpour, A.H. van Gennip and T. Munnik. 2003. Substrate preference of stress-activated phospholipase D in *Chlamydomonas* and its contribution to PA formation. *Plant J. 34*: 595–604.

Baldo, A., A. Sniderman, S. St. Luce, X.-J. Zhang and K. Cianflone. 1995. Signal transduction pathway of acylation stimulating protein: involvement of protein kinase C. *J. Lipid Res. 36*: 1415–1426.

Beilby, M.J. 2007. Action potential in charophytes. *In* Jeon K.W., editor. *Int. Rev. Cytol. – a Survey Cell Biol., Vol 257*. 43–82.

Bett, G. and R. Rasmusson. 2002. Computer Models of Ion Channels *In* (Cabo C. and D. Rosenbaum, editors). *Quantitative Cardiac Electrophysiology*. Marcel Dekker. 48.

Bhatla, S.C. and G. Kalra. 2004. Imaging of calcium channels during polarity induction in plant cells. *Biologia Plantarum 48*: 327–332.

Biggley, W.H., E. Swift, R.J. Buchanan and H.H. Seliger. 1969. Stimulable and spontaneous bioluminescence in marine dinoflagellates, *Pyrodinium bahamense, Gonyaulax polyedra*, and *Pyrocystis lunula. J. Gen. Physiol. 54*: 96-&.

Blatt, M.R. 2000. Cellular signaling and volume control in stomatal movements in plants. *Ann. Rev. Cell Developmental Biol. 16*: 221–241.

Bogeski, I., R. Kappl, C. Kummerow, R. Gulaboski, M. Hoth and B.A. Niemeyer. 2011. Redox regulation of calcium ion channels: Chemical and physiological aspects. *Cell Calcium 50*: 407–423.

Boureux, A., E. Vignal, S. Faure and P. Fort. 2007. Evolution of the Rho family of ras-like GTPases in eukaryotes. *Mol. Biol. Evol. 24*: 203–216.

Braam, J. 2005. In touch: plant responses to mechanical stimuli. *New Phytologist. 165*: 373–389.
Braun, M. and C. Limbach. 2005. Actin-based gravity-sensing mechanisms in unicellular plant model systems. *17th ESA Symposium on European Rocket and Balloon Programmes and Related Research. Vol. 590.* 41–45.
Braun, M. and C. Limbach. 2006. Rhizoids and protonemata of characean algae: model cells for research on polarized growth and plant gravity sensing. *Protoplasma. 229*: 133–142.
Bustelo, X., V. Sauzeau and I. Berenjeno. 2007. GTP-binding proteins of the Rho/Rac family: regulation, effectors and functions *in vivo. Bioessays 28*: 356–370.
Cartee, L., R. Smith, Y. Dai, M. Rahmani, R. Rosato, J. Almenara, P. Dent and S. Grant. 2002. Synergistic induction of apoptosis in human myeloid leukemia cells by phorbol 12-myristate 13-acetate and flavopiridol proceeds via activation of both the intrinsic and tumor necrosis factor-mediated extrinsic cell death pathways. *Mol. Pharmacol. 61*: 1313–1321.
Casamassima, F., A.C. Hay, A. Benedetti, L. Lattanzi, G.B. Cassano and R.H. Perlis. 2010. L-type calcium channels and psychiatric disorders: a brief review. *Am. J. Med. Gen. Part B-Neuropsych. Gen. 153B*: 1373–1390.
Chehab, E.W., E. Eich and J. Braam. 2009. Thigmomorphogenesis: a complex plant response to mechano-stimulation. *J. Exp. Bot. 60*: 43–56.
Craig, J.M., P.L. Klerks, K. Heimann and J.L. Waits. 2003. Effects of salinity, pH and temperature on the re-establishment of bioluminescence and copper or SDS toxicity in the marine dinoflagellate *Pyrocystis lunula* using bioluminescence as an endpoint. *Environm. Poll. 125*: 267–275.
Doering, C.J. and G.W. Zamponi. 2003. Molecular pharmacology of high voltage-activated calcium channels. *J. Bioenerg. Biomembr. 35*: 491–505.
Dolle, R. and W. Nultsch. 1988. Specific binding of the calcium channel blocker [H^3] Verapamil to membrane fractions of *Chlamydomonas rheinhardtii*. *Arch. Microbiol. 149*: 451–458.
Entman, M.L., J.C. Allen, E.P. Bornet, P.C. Gillette, E.T. Wallick and A. Schwartz. 1972. Mechanisms of calcium accumulation and transport in cardiac relaxing system (sarcoplasmic reticuculum membranes) – effects of Verapamil, D-6000, X537A and A23187. *J. Mol. Cell. Cardiol. 4*: 681–687.
Ermilova, E., Z. Zalutskaya, T. Munnik, H. van den Ende and B. Gromov. 1998. Calcium in the control of chemotaxis in *Chlamydomonas. Biologia. 53*: 577–581.
Fasano, J.M., G.D. Massa and S. Gilroy. 2002. Ionic signaling in plant responses to gravity and touch. *J. Plant Growth Reg. 21*: 71–88.
Freinbichler, W., M.A. Colivicchi, C. Stefanini, L. Bianchi, C. Ballini, B. Misini, P. Weinberger, W. Linert, D. Vareslija, K.F. Tipton and L. Della Corte. 2011. Highly reactive oxygen species: detection, formation, and possible functions. *Cell. Mol. Life Sci. 68*: 2067–2079.
Ganesan, A. and J. Zhang. 2012. How cells process information: Quantification of spatiotemporal signaling dynamics. *Protein Science 21*: 918–928.
Gil, J., T. Higgins and E. Rozengurt. 1991. Mastoparan, a novel mitogen for Swiss 3T3 cells, stimulates pertussis toxin-sensitive arachidonic-acid release without inositol phosphate accumulation. *J. Cell Biol. 113*: 943–950.
Gillespie, P.G. and U. Muller. 2009. Mechanotransduction by hair cells: models, molecules, and mechanisms. *Cell 139*: 33–44.
Glavinovic, M.I., A. Joshi and J.M. Trifaro. 1992. Mastoparan blockade of currents through Ca2+-activated K+ channels in bovine chromaffin cells. *Neuroscience 50*: 675–684.
Gloerich, M. and J.L. Bos. 2011. Regulating Rap small G-proteins in time and space. *Trends Cell Biol. 21*: 615–623.
Goedhart, J. and T.W.J. Gadella. 2004. Photolysis of caged phosphatidic acid induces flagellar excision in *Chlamydomonas. Biochem. 43*: 4263–4271.
Hallahan, B.J., P. Camilleri, A. Smith and J.R. Bowyer. 1992. Mode of action studies on a chiral diphenyl ether peroxidizing herbicide – correlation between differential inhibition of protoporphyrinogen-IX oxidase activity and induction of tetrapyrrole accumulation by the enantiomers. *Plant Physiol. 100*: 1211–1216.

Hand, W.L., N.L. King, J.D. Johnson and D.A. Lowe. 1977. Requirement for magnesium influx in activation of alveolar macrophages mediated by ionophore A23187. *Nature. 265*: 543–544.

Harz, H. and P. Hegemann. 1991. Rhodopsin-regulated calcium currents in *Chlamydomonas. Nature 351*: 489–491.

Hashimoto, K. and J. Kudla. 2011. Calcium decoding mechanisms in plants. *Biochimie 93*: 2054–2059.

Hastings, J.W. and C.H. Johnson. 2003. Bioluminescence and chemiluminescence. *Biophotonics, Pt A. 360*: 75–104.

Heimann, K., J.M. Matuszewski and P.L. Klerks. 2002. Effects of metals and organic contaminants on the recovery of bioluminescence in the marine dinoflagellate *Pyrocystis lunula* (Dinophyceae). *J. Phycol. 38*: 482–492.

Hewavitharana, T. and P.B. Wedegaertner. 2012. Non-canonical signaling and localizations of heterotrimeric G proteins. *Cellular Signalling. 24*: 25–34.

Higashijima, T., S. Uzu, T. Nakajima and E.M. Ross. 1988. Mastoparan, a peptide toxin from wasp venom, mimiccs receptors by activating GTP-binding regulatory proteins (G-proteins). *J. Biol. Chem. 263*: 6491–6494.

Holzinger, A., D.A. Callaham, P.K. Hepler and U. Meindl. 1995. Free calcium in *Micrasterias* – local grandients are not detected in growing lobes. *Eur. J. Cell Biol. 67*: 363–371.

Itoh, T., Y. Kanmura and H. Kuriyama. 1985. A23187 increases calcium permeability of store sites more than of surface membranes in the rabbit mesenteric artery. *J. Physiol. 359*: 467–484.

Jeacocke, R.E. 1993. The concentration of free magnesium and free calcium ions both increase in skeletal muscle fibres entering rigor mortis. *Meat Science 35*: 27–45.

Jencks, W.P. and T. Fujimori. 1990. Mechanism of the inhibition of the SR calcium ATPase by Lanthanum. *Biophys J. 57*: A204–A204.

Johannes, E., J.M. Brosnan and D. Sanders. 1991. Calcium channels and signal transduction in plant cells. *Bioessays 13*: 331–336.

Jung, S. 2011. Level of protoporphyrinogen oxidase activity tightly correlates with photodynamic and defense responses in oxyfluorfen-treated transgenic rice. *J. Pesticide Sci. 36*: 16–21.

Kania, B.F. 2005. Voltage-gated calcium channel blockers as potential analgesics for humans and animals. *Medycyna Weterynaryjna 61*: 976–979.

Knaust, R., T. Urbig, L.M. Li, W. Taylor and J.W. Hastings. 1998. The circadian rhythm of bioluminescence in *Pyrocystis* is not due to differences in the amount of luciferase: A comparative study of three bioluminescent marine dinoflagellates. *J. Phycol. 34*: 167–172.

Koch, G., B. Haberman, C. Mohr, I. Just and K. Aktories. 1991. Interactions of Mastoparan with the low-molecular mass GTP-binding protein-Rho and Protein-Rac. *FEBS Lett. 291*: 336–340.

Komander, D., G. Kular, A. Schüttelkopf, M. Deak, K. Prakash, J. Bain, M. Elliott, M. Garrido-Franco, A. Kozikowski, D. Alessi and D. van Aalten. 2004. Interactions of LY333531 and other bisindolyl maleimide inhibitors with PDK1. *Structure 12*: 215–226.

Kreimer, G. and G.B. Witman. 1994. Novel touch-induced, Ca^{2+} dependent phobic response in a flagellate green-alga. *Cell Motil. Cytoskel. 29*: 97–109.

Krol, E. and K. Trebacz. 2000. Ways of ion channel gating in plant cells. *Ann. Bot. 86*: 449–469.

Kuin, H., H. Koerten, W. Ghijsen, T. Munnik, H. van den Ende and A. Musgrave. 2000. *Chlamydomonas* contains calcium stores that are mobilized when phospholipase C is activated. *Planta 210*: 286–294.

Kukkonen, J.P. 2011. A menage a trois made in heaven: G-protein-coupled receptors, lipids and TRP channels. *Cell Calcium 50*: 9–26.

Lermontova, I. and B. Grimm. 2000. Overexpression of plastidic protoporphyrinogen IX oxidase leads to resistance to the diphenyl-ether herbicide acifluorfen. *Plant Physiol. 122*: 75–83.

Li, X.H. 2011. Phosphorylation, protein kinases and ADPKD. *Biochim. Biophys. Acta-Mol. Basis of Disease 1812*: 1219–1224.

Li, Z.G. and M. Gong. 2011. Mechanical stimulation-induced cross-adaptation in plants: an overview. *J. Plant Biol. 54*: 358–364.

Lima, P.D.L., M.C. Vasconcellos, R.C. Montenegro, M.O. Bahia, E.T. Costa, L.M.G. Antunes and R.R. Burbano. 2011. Genotoxic effects of aluminum, iron and manganese in human cells and experimental systems: A review of the literature. *Human Exp Toxicol. 30*: 1435–1444.

Love, J., C. Brownlee and A.J. Trewavas. 1997. Ca2+ and calmodulin dynamics during photopolarization in *Fucus serratus* zygotes. *Plant Physiology. 115*: 249–261.

Low, S.E., I.G. Woods, M. Lachance, J. Ryan, A.F. Schier and L. Saint-Amant. 2012. Touch responsiveness in zebrafish requires voltage-gated calcium channel 2.1b. *J. Neurophysiol. 108*: 148–159.

Magnusson, M., K. Heimann and A.P. Negri. 2008. Comparative effects of herbicides on photosynthesis and growth of tropical estuarine microalgae. *Mar. Poll. Bull. 56*: 1545–1552.

Maier, I. and M. Calenberg. 1994. Effect of extracellular Ca^{2+} and Ca^{2+}-antagonists on the movement and chemoorientation aof male gamets of *Ectocarpus siliculosis* (Phaeophyceae). *Bot. Acta 107*: 451–460.

Marinetti, G.V., T.W. Morris and P. Leaky. 1993. Effects of Ca^{2+}, Mg^{2+} and depolarizing agents on the PI-32-labeling and degradation of phophatidylinositols in rat-brain-synaptosomes. *Neurochem. Res. 18*: 345–351.

Mazars, C., C. Briere, S. Bourque and P. Thuleau. 2011. Nuclear calcium signaling: An emerging topic in plants. *Biochimie 93*: 2068–2074.

McLachlan, D.H., G.J.C. Underwood, A.R. Taylor and C. Brownlee. 2012. Calcium release from intracellular stores is necessary for the photophobic response in the benthic diatom *Navicula perminuta* (Bacillariophyceae). *J. Phycol. 48*: 675–681.

Monshausen, G.B. and S. Gilroy. 2009. Feeling green: mechanosensing in plants. *Trends Cell Biol. 19*: 228–235.

Moon, Y.J., Y.M. Park, Y.H. Chung and J.S. Choi. 2004. Calcium is involved in photomovement of cyanobacterium *Synechocystis* sp PCC 6803. *Photochem. Photobiol. 79*: 114–119.

Musset, B., S.M.E. Smith, S. Rajan, V.V. Cherny, S. Sujai, D. Morgan and T.E. DeCoursey. 2010. Zinc inhibition of monomeric and dimeric proton channels suggests cooperative gating. *J. Physiol.-London 588*: 1435–1449.

Nakahata, N., M.T. Abe, I. Matsuoka and H. Nakanishi. 1990. Mastoparan inhibits phosphoinositde hydrolysis via pertussins toxin-sensitive G-proeint in human astrocytoma cells. *FEBS Lett. 260*: 91–94.

Nakamura, K., K. Shinozuka and M. Kunitomo. 2000. Suppressive effect of protein kinase C inhibitors on tumor cell function via phosphorylation of p53 protein in mice. *Yakugaku Zasshi-J. Pharmaceut. Soc. Japan. 120*: 1387–1394.

Nicolas, M.T., D. Morse, J.M. Bassot and J.W. Hastings. 1991. Colocalization of luciferin binding-protein and luciferase to the scintillons of *Gonyaulax polyedra* revealed by double immunolabeling after fast-freeze fixation. *Protoplasma 160*: 159–166.

Nicolas, M.T., G. Nicolas, C.H. Johnson, J.M. Bassot and J.W. Hastings. 1987. Characterization of the bioluminescent organelles in *Gonyaulax polyedra* (Dinoflagellates) after fast-freeze fixation and antiluciferase immunogold staining. *J. Cell Biol. 105*: 723–735.

Obermair, G.J., P. Tuluc and B.E. Flucher. 2008. Auxiliary Ca(2+) channel subunits: lessons learned from muscle. *Cur. Opin. Pharmacol. 8*: 311–318.

Okamoto, O.K., L.M. Shao, J.W. Hastings and P. Colepicolo. 1999. Acute and chronic effects of toxic metals on viability, encystment and bioluminescence in the dinoflagellate *Gonyaulax polyedra*. *Comp. Biochem. Physiol. C-Pharmacol. Toxicol. Endocrinol. 123*: 75–83.

Parvez, S., C. Venkataraman and S. Mukherji. 2006. A review on advantages of implementing luminescence inhibition test (*Vibrio fisheri*) for acute toxicity prediction of chemicals. *Environ. Internat. 32*: 265–268.

Pottosin, II and G. Schnknecht. 2007. Vacuolar calcium channels. *J. Exp. Bot. 58*: 1559–1569.

Quarmby, L.M., Y.G. Yueh, J.L. Cheshire, L.R. Keller, W.J. Snell and R.C. Crain. 1992. Inositol phospholipid-metabolism may trigger flagellar excission in *Chlamydomonas rheinhardtii. J. Cell Biol. 116*: 737–744.

Quesada, I., W.C. Chin and P. Verdugo. 2006. Mechanisms of signal transduction in photo-stimulated secretion in *Phaeocystis globosa. Febs Lett. 580*: 2201–2206.

Radu, L., I. Durusse, L. Assairi, Y. Blouquit, S. Miron, J.A. Cox and C.T. Craescu. 2010. *Scherffelia dubia* centrin exhibits a specific mechanism for Ca^{2+}-controlled target binding. *Biochem. 49*: 4383–4394.

Reed, P.W. and H.A. Lardy. 1972. A23187 – divalent cation ionophore. *J. Biol. Chem. 247*: 6970-&.

Rudolf, R., M. Hafner and M. Mongillo. 2012. Investigating second messenger signalling *in vivo. In* Conn P.M., editor. *Methods in Enzymology, Vol 505: Imaging and Spectroscopic Analysis of Living Cells: Live Cell Imaging of Cellular Elements and Functions*. Vol. 505. 363–382.

Sachs, F. 1991. Mechanical transduction by membrane ion channels – a mini review. *Mol. Cell. Biochem. 104*: 57–60.

Samtani, J.B., J. Ben Weber and S.A. Fennimore. 2012. Tolerance of strawberry cultivars to Oxyfluorfen and Flumioxazin herbicides. *Hortscience 47*: 848–851.

Schultz, L.W., L.Y. Liu, M. Cegielski and J.W. Hastings. 2005. Crystal structure of a pH-regulated luciferase catalyzing the bioluminescent oxidation of an open tetrapyrrole. *Proc. Nat. Acad. Sci. U. S. A. 102*: 1378–1383.

Silva, R.D., L. Saraiva, I. Coutinho, J. Goncalves and M. Corte-Real. 2012. Yeast as a powerful model system for the study of apoptosis regulation by Protein Kinase C Isoforms. *Cur. Pharmaceut. Design 18*: 2492–2500.

Son, Y.K., D.H. Hong, D.J. Kim, A.L. Firth and W.S. Park. 2011. Direct effect of protein kinase C inhibitors on cardiovascular ion channels. *BMB Reports 44*: 559–565.

Sridhar, J. and N. Pattabiraman. 2005. Synthesis and isozyme selectivity of small molecule protein kinase C inhibitors: a review of patents. *Expert Opin. Therap. Patents 15*: 1691–1701.

Swift, E. and C.C. Remsen. 1970. The cell wall of *Pyrocystis* spp. (Dinococcales). *J. Phycol. 6*: 79–86.

Szczegielniak, J., L. Borkiewicz, B. Szurmak, W. Lewandowska-Gnatowska, M. Statkiewicz, M. Klimecka, J. Ciesla and G. Muszynska. 2012. Maize calcium-dependent protein kinase (ZmCPK11): local and systemic response to wounding, regulation by touch and components of jasmonate signaling. *Physiol. Plant. 146*: 1–14.

Tanimura, A., Y. Matsumoto and Y. Tojyo. 1991. Mastoparan increases membrane permeability in rat parotid cells independently of action on G-proetins. *Biochem. Biophys. Res. Com. 177*: 802–808.

Thurley, K., A. Skupin, R. Thul and M. Falcke. 2012. Fundamental properties of Ca^{2+} signals. *Biochim. Biophys. Acta-Gen. Subj. 1820*: 1185–1194.

Tissier, M., A. Ouahabi, G. Jeminet and J. Juillard. 1993. Mode of action of calcimysin (A-23187). 6. Complexation of transition and heavy metal divalent cations in methanol. *J. Chim. Phys. Physico-Chim Biol. 90*: 595–608.

Tlalka, M. and M. Fricker. 1999. The role of calcium in blue-light-dependent chloroplast movement in *Lemna trisulca* L. *Plant J. 20*: 461–473.

Toullec, D., P. Pianetti, H. Coste, P. Bellevergue, T. Grandperret, M. Ajakane, V. Baudet, P. Boissin, E. Boursier, F. Loriolle, L. Duhamel, D. Charon and J. Kirilovsky. 1991. The bisindolylmaleimide GF-109203X is a potent and selective inhibitor of protein kinase C. *J. Biol. Chem. 266*: 15771–15781.

van Himbergen, J.A.J., B. ter Riet, H.J.G. Meijer, H. van den Ende, A. Musgrave and T. Munnik. 1999. Mastoparan analogues stimulate phospholipase C- and phospholipase D-activity in *Chlamydomonas*: a comparative study. *J. Exp. Bot. 50*: 1735–1742.

Verret, F., G. Wheeler, A.R. Taylor, G. Farnham and C. Brownlee. 2010. Calcium channels in photosynthetic eukaryotes: implications for evolution of calcium-based signalling. *New Phytologist. 187*: 23–43.

Wakabayashi, K., Y. Misawa, S. Mochiji and R. Kamiya. 2011. Reduction-oxidation poise regulates the sign of phototaxis in *Chlamydomonas reinhardtii. Proc. Nat. Acad. Sci. U. S. A. 108*: 11280–11284.

Walter, H.J. and R.O. Messing. 1999. Regulation of neuronal voltage-gated calcium channels by ethanol. *Neurochem. Int. 35*: 95–101.

Wang, X.Q., Y.J. Yuan, J.C. Li and C. Chen. 2011a. Changes of cell membrane permeability induced by DMSO and ethanol in suspension cultures of *Taxus cuspidata*. *In* (Cao Z., Y.H. He, L. Sun and X.Q. Cao, editors). *Appl. Chem. Eng. Pts 1–3*. Vol. 236–238. 942–948.

Wang, Y., C.L. Chen and M. Iijima. 2011b. Signaling mechanisms for chemotaxis. *Develop. Growth Diff. 53*: 495–502.

Weiergraber, M., J. Hescheler and T. Schneider. 2008. Human calcium channelopathies. Voltage-gated Ca2+ channels in etiology, pathogenesis, and pharmacotherapy of neurologic disorders. *Nervenarzt. 79*: 426–+.

Weiergraber, M., M.A. Kamp, K. Radhakrishnan, R. Hescheler and T. Schneider. 2006. The Ca(v)2.3 voltage-gated calcium channel in epileptogenesis – Shedding new light on an enigmatic channel. *Neurosci. Biobehav. Rev. 30*: 1122–1144.

Weiss, G.B. 1973. Use of Lanthanum to delineate mechanisms of calcium-dependent actions in diffrent isolated muscle systems. *Acta Physiol. Scand.*: 127–127.

Wheeler, G.L. and C. Brownlee. 2008. Ca^{2+} signalling in plants and green algae – changing channels. *Trends Plant Sci. 13*: 506–514.

Wheeler, G.L., I. Joint and C. Brownlee. 2008. Rapid spatiotemporal patterning of cytosolic Ca^{2+} underlies flagellar excision in *Chlamydomonas reinhardtii. Plant J. 53*: 401–413.

Wong, D.T., Wilkinso.Jr, R.L. Hamill and J.S. Horng. 1973. Effects of antibiotic ionophore, A23187, on oxidative phosphorylation and calcium transport of liver-mitochondria. *Arch. Biochem. Biophys. 156*: 578–585.

Yule, D.I. and J.A. Williams. 1991. Mastoparan induces oscillations of cytosolic Ca^{2+} in rat pancreatic acinar cells. *Biochem. Biophys. Res. Com. 177*: 159–165.

Zhang, G., C.M. Williams, M.K. Campenot, L.E. McGann, A.J. Cutler and D.D. Cass. 1995. Effects of calcium, magnesium, potassium and boron on sperm cells isolated from pollen of *Zea mays* L. *Sex. Plant Reprod. 8*: 113–122.

Index